



Application of Advanced Cementitious Materials in Infrastructure

I. Shalom

Delft University of Technology

Cover phot:

Strain-Hardening Cementitious Concrete (SHCC) design by Ductal® with unique properties as ultra-high strength, stiffness, ductility, and durability

Application of Advanced Cementitious Materials in Infrastructure

by

I.Shalom

in partial fulfillment of the requirements for the degree of

Master of Science
in Civil Engineering

at the Delft University of Technology,

Thesis committee:

Prof.dr.ir. D.A. Hordijk	TU Delft
Dr.ir. C. van der Veen	TU Delft
Dr. M.H. Kolstein	TU Delft
Ir. A.D. Reitsema	TU Delft
Ir. H. de Waardt	Witteveen+Bos

An electronic version of this thesis is available at <http://repository.tudelft.nl/>.

PREFACE

This document presents the master thesis within Structural Engineering with a specialization in Concrete Structures. The research was carried out in cooperation with the Faculty of Civil Engineering & Geosciences at the Delft University of Technology and the engineering consulting company Witteveen+Bos. The study focuses on the application of Advanced Cementitious Materials in Infrastructure emphasis the ability to replace traditional concrete in bridges superstructure.

Completing this thesis wouldn't have been possible without the members of my committee. I would like to thank my gratitude to Professor Dick Hordijk, dr. ir. C. van der Veen, Dr. M.H. Kolstein, and ir. A.D. Reitsema for their assistance and inspiring ideas.

Secondly, I would like to thank Huig de Waardt, my supervisor at Witteveen+Bos, for the time and effort he dedicated to my work. His engineering insights and attention to details were valuable for the final results of this research, his engineering expertise in the field of concrete structures challenged me to bring the research to a higher level.

I would like to express my gratitude to Witteveen+Bos providing me the resources to work on my research.

At lastly, I would like to thank my parents for their support, my girlfriend for her interest and patience, and to my friends.

Izick Shalom

Amsterdam, February 2016

ABSTRACT

Advanced Cementitious Materials (ACM's) are products with materials found in conventional concrete (cement, silica fume, sand, superplasticizer, and water) plus distinctive materials like fibers (steel, carbon) and quartz. The superiority of ACM's in terms of strength, ductility, and durability marks it as high potential replacement of traditional concrete.

The growing expansion of ACM applications and technical experience gained in the last two decades in countries including Japan, Germany, Austria, Australia, USA, Denmark, Canada, France, and the Netherlands results in new frontier of cement materials used in infrastructure. The economic feasibility of ACM's has been demonstrated in footbridges, outstanding bridges, and large pre-cast series. Furthermore safety and durability of ACM's, especially of Ultra-high performance concrete (UHPC) has been proven encouraging further research efforts. This research is one part of an ongoing research under the supervision of Professor D.A. Hordijk at the Technical University of Delft on the application of ACM's in infrastructure.

The biggest potential for new infrastructure with ACM's is in precast girders and thin plates. Throughout utilizing the excellent properties of ACM's like UHPC, a new lighter-weight, durable, efficient, and adaptable superstructure has been developed in this study to replace the existing traditional design of bridges in the nearby future. One example of the approach taken in this thesis is the benefit of long life-cycle. Due to dense matrix, which prevents the ingress of detrimental substances apply UHPC selectively in the superstructure where it required to sustain high level of durability. Another example of the mindset of this thesis is lightweight design, means material distribution follows the forces distribution.

In this thesis the outcome of an extensive material study was an overview of the ACM's properties, time depended behavior, non-linear behavior, design standards, and field of application. Based on the material study different parameters are analyzed to enhance

the understanding of the behavior of structure with ACM. It has been found that structural elements from UHPC are far more efficient than their corresponded traditional concrete structures. The maximum crack size is significantly lower, the slenderness is much higher which result in higher efficiency and reduction of the dead loads. Also the shrinkage and creep of ACM's is studied. The time-dependend imposed deformation of UHPC elements (plate, flange, truss member) with different sizes cause stresses in the model ends up as transverse cracks when the deformation is restrained.

Based on the drawn conclusion of the parametric study, the design stage of the new ACM superstructure was initiated complying with requirements & boundaries according to the NEN norms and SETRA (French recommendation for UHPC). The new superstructure is 35% lighter than traditional solution, with efficient material distribution, built only from concrete, with elegant simple solutions. The low reliability of the fibers as replacement for reinforcement well-thought-out in the design.

Some suggestion for future research in the field of modular adaptable superstructure have promising potential as far as applying ACM's.

CONTENT

1. Introduction	1
1.1 Problem definition	1
1.2 Research strategy	4
1.3 Scope.....	5
1.4 Research Objective's	9
1.5 Research questions Main question	9
1.6 Thesis outline.....	11
2. Candidate materials	13
2.1 Advanced Cementitious Material.....	14
2.2 Design codes.....	16
2.3 Mechanical properties	18
2.4 Creep.....	27
2.5 Shrinkage	29
2.6 Durability.....	30
2.7 Workability	31
2.8 Affordability.....	33
3. Durability of Bridges	35
3.1 Degradation	35
3.2 Design service life.....	39
3.3 Deterioration assessment.....	42
3.4 Strategies for combating deterioration	44
3.5 Durability of ACM's	44

4. Design input.....	47
4.1 Goal of case study.....	47
4.2 Case description.....	48
4.3 Object description KW110.....	49
4.4 Requirement & conditions new design.....	52
4.5 Actions.....	54
5. Parametric analysis girder.....	67
4.6 Parametric study.....	68
4.7 Structural concepts.....	81
4.8 Design alternatives.....	95
4.9 Iterative analysis.....	130
4.10 Recommendation.....	161
6. Preliminary design girder.....	166
4.1 T-girder.....	166
4.2 3D – dimensioning.....	167
4.3 Finite element analysis.....	169
4.4 The Warren T-Girder.....	176
4.5 Global design.....	198
4.6 Overview design.....	236
4.7 Remarks & Suggestions.....	239
7. Conclusions.....	241
7.1 Part I – literature study.....	241
7.2 Part III – Design study.....	245
7.3 Future research.....	248
A. References.....	252
B. List of Tables.....	258
C. List of figures.....	262

D. Innovative concrete	274
E. Stress-strain relationship.....	333
F. Simplified ULS Calculation	346
G. Engineering report SCIA.....	371

ACRONYMS

ACM	Advanced Cementitious Materials
UHPC	Ultra-High Performance Concrete
SHCC	Strain Hardening Cementitious Concrete
NSC	Normal Strength Concrete
CC	Conventional Concrete
FRC	Fiber Reinforced Concrete
HSFRC	High Strength Fiber Reinforced Concrete
RPC	Reactive Powder Concrete
LWC	Lightweight Concrete
HVFC	High Volume Fly-ash Concrete
SCC	Self Compacting Concrete
FC	Foamed Concrete
PMC	Polymer Modified Concrete
TRUHPC	Textile Reinforced Ultra-High Performance Concrete
GC	Geopolymer Concrete
POT	Post-Tensioned
PRT	Pre-Tensioned

1 • Introduction

1.1 Problem definition

In the Nederland, as in most countries of the western world, motorized transportation increased from half a million to seven million within a decade after 1960, after which the growth stabilised towards ten million vehicles nowadays [Centraal Bureau voor de Statistiek, 2013]. The rapid increase in traffic instigated the expansion of roads world-wide and a substantial amount of bridge structures. The Conventional concrete bridges are the majority of the concrete bridges nowadays, they suffer from several sustainability problems such as: Carbonation, salt attack and Chloride attack. Consequently these structures suffer from high maintenance and repair costs. [Ed. K. van Breugel].



Figure 1.1: Little Cedar Creek bridge USA 2011, Ductal UHPC waffle deck, girders and joints

The use of innovative concrete like Ultra high performance concrete, Fibers reinforced high strength concrete or Fly-ash concrete has reached a level of technological maturity that is demonstrated by many applications of these new materials. For example (Figure 1.2) hybrid bridge deck with light-weight concrete core, fibre reinforced polymer as tensile reinforcement and Ultra high strength concrete compression layer.

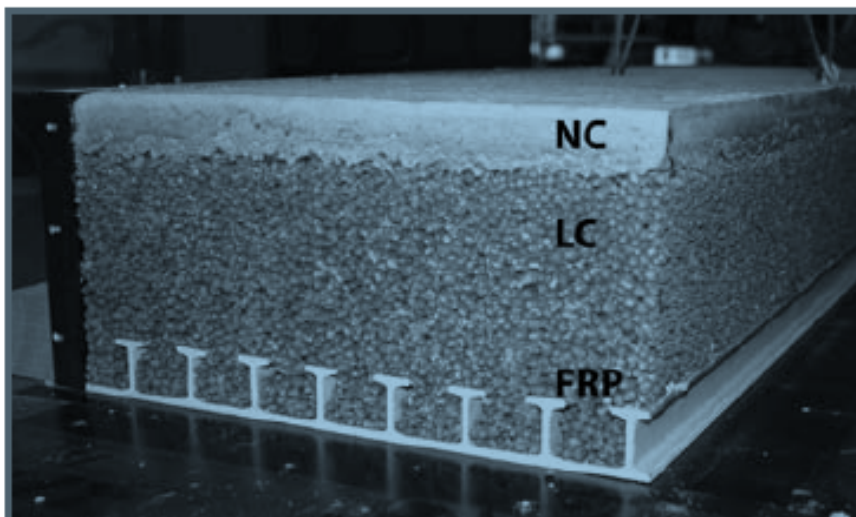


Figure 1.2: Hybrid bridge deck with sandwich structure

Nevertheless the scale of application is however limited by high costs, lack of practical knowledge, uncertainty long term behavior, and lack of design codes. Highway bridges design with new materials have to comply with SLS and ULS design, fatigue, and dynamic loads just like traditional concrete. Engineers naturally prefer to use the familiar traditional concrete, supplied with design tools like the Eurocode on new material without design tools and with uncertainties regarding its strength, durability, workability, affordability.

It can be said that the high costs coupled with the lack of engineering design tools is the largest impediment to the widespread use of innovative concrete in bridges. One possible way of overcoming the drawbacks is the implementation of hybrid construction that is the use of ACM (Advanced Cementitious Material) in combination with traditional materials, especially concrete.

Research for bridge applications with innovative concrete such as Ultra-high performance concrete (UHPC) on precast, prestressed girders, waffle panels for bridge decks; and as a jointing material, is underway at several universities around the world. Structural regulations for the usage of ACM will enter into force soon but several aspects about the usage of different high strength concrete require further research: Aesthetics, durability, economic considerations, sustainability and risk of production, which also have to be quantified. The ACM is an advanced construction material whose mechanical and durability properties far surpass those of conventional material. By the use of ACM's as an alternative for the CC amount of steel reinforcement may be reduced bars as less concrete material can be used.

Designing the future infrastructure will require a different approach comparing with the conventional design approach. Due to the extremely high strength and durability of ACM. It is basically a new material and its application should not follow the path of regular concrete. With time new structural concepts will be developed that can better utilize the superb properties of the ACM [Man-Chung Tang]. Recent research of T.J.P.M. de Goede shows that HSC bridge with a span of 42m can be optimized regarding the structural safety, material usage, durability and reducing maintenance costs. Therefore innovative application of ACM for infrastructure will need to show improvement in the following main properties: Strength, Workability, Durability and Affordability.

1.2 Research strategy

Previous to dealing with the research main questions [1.5] it is necessary to determine the approach to this research. It will begin with the flexible research by collecting knowledge and quantify it: Literature study [2]. Afterwards design input will be determined by picking suitable case study [4] followed by Design study [5] which is the largest part of this thesis.

- Part I - Literature study
- Part II - Design Input
- Part III - Parametric analysis
- Part IV - Design study hybrid girder

1.3 Scope

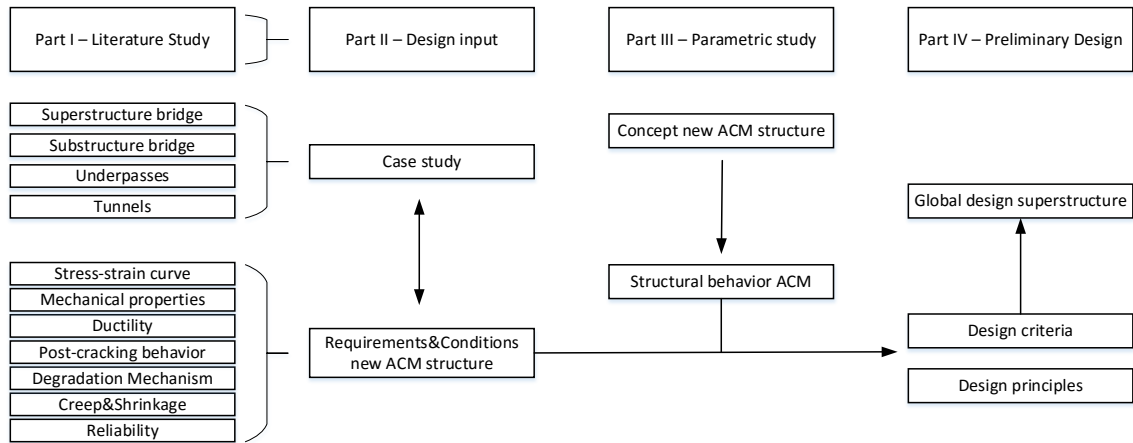


Figure 1.3: Illustration of thesis scope

This master thesis will try to take the challenge of designing a bridge using the latest innovative concrete materials by looking at the fundamental mechanics of structures and materials. Taking this challenge without predefining the scope may lead to inefficient progress of the research and to overloaded research. In order to manage the size of the research project and to be able to come to a satisfying answer to the main research questions, the scope of the project is limited. The focus will remain on the research objective and the irrelevant issues will be removed. The following restrictions apply:

1.3.1 Choice of material

ACM are belong to the building materials with higher performance than CC in terms of mechanical properties, durability, workability and costs. The development of these materials are not yet resulted in an acceptable number of applications. Based on literature study different innovative materials are chosen other than traditional vibrated concrete (C70/85) which meet one or more of the following requirements:

- Material already used in structural elements in existing reference project

- Material mechanical properties and long-term behavior are defined in laboratories of known institutions
- Material mechanical properties and long-term behavior are known by the structural behavior of existing structures built with this material

Furthermore the ACM should show be applicable in infrastructural elements subjected to high loads levels..

<i>Acronym</i>	<i>Concrete type</i>	<i>Acronym</i>	<i>Concrete type</i>
NSC/CC	Normal strength concrete/Conventional concrete	SCC	Self-compacting concrete
HSC	High strength concrete	FC	Foamed concrete
UHPC	Ultra high performance concrete	PMC	Polymer modified concrete
LWC	Light weight concrete	TRC	Textile reinforced concrete
HVFA	High volume fly ash concrete	RPC	Reactive powder concrete
SHCC	Strain-hardening cementitious composites	GC	Geopolymer cement

Table 1.1: Material choice

1.3.2 Choice of structure

Applications of ACM in infrastructure sector is possible in different structures due to the improve of durability, mechanical properties and reduce of weight. Typical constructions are bridges, tunnels, slurry walls, open tunnels pit, underpasses, lock gates and foundations piles. Applying this complex ACM into each of these structures requires years of experimental research and years of experience until the behavior of the new design may declared as safe to use. The different between successful implementation of ACM and failure lies on the reliability of the product but also on the interaction of ACM with other material as steel and other ACM types. One way to motivate successful implantation of ACM is to increase production from small quantities for special solutions to market-oriented large quantities with high repetition.

In the civil infrastructure sector the bridges industry have high potential of application of ACM in comparison with the other structures. Particularly in Netherland there are 3206 highway bridges with total area of 4,663,903 m² [Table 1.2] [Rijkswaterstaat, 2012]

<i>Type object</i>	<i>Quantity</i>	<i>Total area [m²]</i>	<i>Maintenance (Million €)</i>	<i>Replacement (billion €)</i>
Viaduct highway	2762	2,932,811	59	10.4
Small concrete bridge	606	531,550	-	-
Large concrete bridge	49	567,443	8	2.0
Steel bridge	34	193,792	7	0.6
Movable bridge	57	438,307	15	1.4
Total bridges	3208	4,663,903	89	14.4
Tunnels	22	716,483	70	2.8
Aqueduct	12	191346	3	0.4
Mooring	17	21326	2	0.2
Underpassage	547	454412	-	-
Culvert	619	118,071	-	-

Table 1.2: Infrastructure objects in main road network Netherland 2012 [Rijkswaterstaat, 2012]

The majority of the bridges in Netherland are constructed in the 60's and 70's with a current service time of 50 years these infrastructure's the safty level of these assets should be managed. Figure 1.4], . The Annual maintenance costs of 89 million Euro is required for keeping service levels. The estimated replacement costs are 14.40 billion euro. But this is not a solution, new build bridges will increase the maintenance costs and the high number of bridges will make inspection of the assets too expansive.

The development of new type of bridges with ACM , emphasizing high durability with market-oriented costs and with suitable design for replacement of existing bridges and reconstruction of existing bridges with possible large scale production (prefabrication) might be the optimal solution for the future bridges industry.

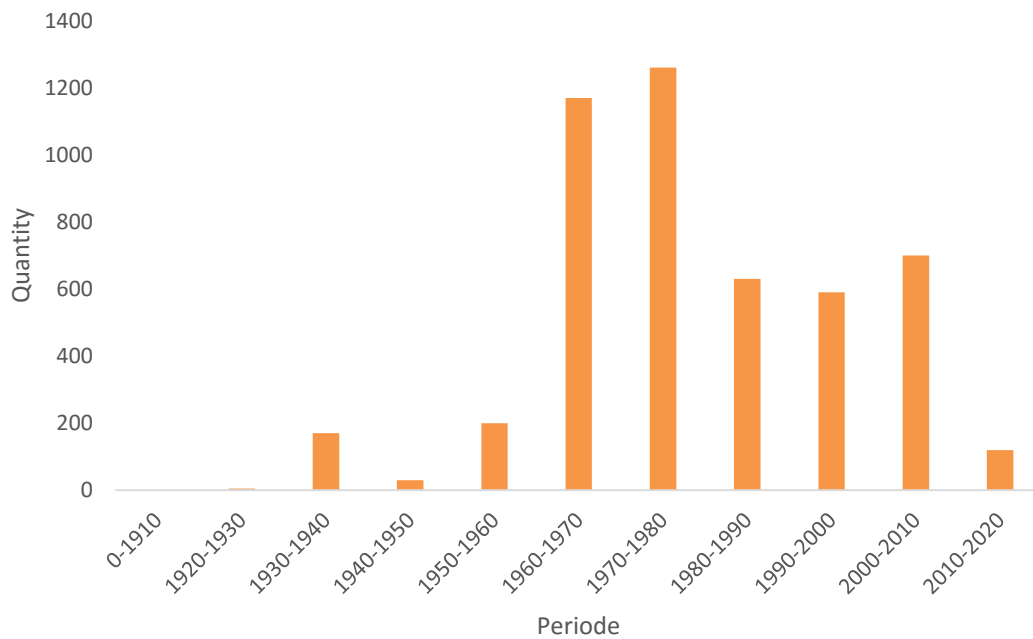


Figure 1.4: Realization concrete bridges in Netherland

Within the scope of this research the bridge geometry, boundary conditions, requirements, substructure and foundations are defined in a case study. These properties will be imposed on the new bridge design. The reference bridge is constructed with conventional reinforced concrete or/and prestressed concrete with common dimensions for the Dutch highways.

1.3.3 Structural safety

The structural behavior of the new bridge design will be checked with the existing Eurocode and with other norms and standards. The ULS and SLS checks will be done according the Eurocode. Safety margins will be added to the calculations by introducing safety factors derived from statistical analysis of the material behavior.

1.3.4 Actions

The actions on the bridge structure are in compliance with the provisions in the Eurocode structural regulations. Calculations will deal with limited amount of load cases. The governing cases will be used.

1.4 Research Objective's

This master thesis research is part of a much larger research group investigating applications of ACM in concrete structures. There are many possibilities for research within this subject as there are many possibilities for ACM application, for example: connections, piers, foundation, literature study, pedestrian bridge, traffic bridge, tunnels ext. Accounting the scope of the thesis [1.3] result in the following goals:

- Potential of ACM in civil infrastructure
- Replacing traditional bridge design
- Innovative use of materials
- Weighting design criteria

This large group of master graduation thesis is part of different PHD thesis about application of ACM. The chairman of this thesis Prof. Hordijk is the supervisor of the entire research project.

1.5 Research questions Main question

The research objectives can be translated into the main question of this research:

“Can advanced cementitious materials be used to develop technically and economically feasible heavy-traffic bridge as a realistic alternatives for the existing conventional bridges? “

1.5.1 Sub-questions

The sub-questions dividing the thesis into two parts. With the compliance of the first part the question of the second part can be answered. Each part is characterised with different approach and results, which are linked together. The intention is to consider small pieces of the objective rather than main objective which makes the work on this research substantially easier. The questions are:

Part I - Preliminary research

What is the actual state-of-the-art on application of ACM in (traffic) bridges?

Which types of ACM can be used for heavy traffic bridge? And consequently what is the geometry of the objects?

What are the material-specific challenges regarding the design, production and costs of hybrid structures, and how they addressed in practice?

Which design concept for hybrid ACM bridge is feasible based on the given constraints and cost?

For which ACM norms and standards can be used to design the bridge? How reliable these are?

How can ACM be applied with no existing norms and standards?

Part II – Design study

What are the required structural demands for road-traffic ACM bridges?

What are the boundary conditions? (Case study)

Which design practice is suitable for the given structural requirements and boundary conditions?

How can design parameters can be optimized by simple hand-calculations?

Which design principles are need to be considered to develop Hybrid Bridge?

Which design computer design tools can be used to analyse the bridge and how can the bridge be modelled in this computer design tool?

1.6 Thesis outline

The thesis can be divided into 4 parts:

Part I - Literature study

- Candidate materials
- Durability of bridges

Part II – Design Input

- Case study
- Boundary conditions
- Actions

Part III – Design study hybrid girder

- Parametric analysis
- Preliminary design

Part IV – Design study hybrid deck

- Parametric analysis deck
- Execution aspects

The research begins with introduction [1] describing the aim and the scope of the research followed by the literature study. This is a very broad study consist of the search for candidate materials [2] where mechanical properties, durability, workability and affordability of typical ACM are discussed, the principle of durability of bridges [3], and the design input [4]. The second part of the thesis begins with parametric analysis of the girder [5] followed by the Preliminary design [6.]

Part I

Literature study

2. Candidate materials

Construction materials have been developed over the time bringing design concepts that used to be a dream to reality. Scientists are constantly busy with the search for new innovative construction material. In the recent decades various of tests in the laboratories tried to improve the mechanical properties of the conventional concrete as we know it. Concrete has kept evolving to satisfy more demanding design requirement for improvement in performance. The concrete industry took the challenge of developing new material addressing issues like environmental concerns, economic factors, durability and strength.

The development of ACM is conducted in universities and companies around the globe in Italy, China, USA, France, UK, Japan, The Netherland and Spain. There are hundreds of articles and papers specifying intensive work in defining the capabilities and properties of the new concrete material. In this chapter the conventional and the ACM will be pointed. The focus in this chapter will be on type of concrete which is currently in use within the infrastructure sector or concrete material which potentially may be used in the infrastructure sector.



Figure 2.1: Current practice of mixing concrete [Erix Schlangen, 2012]

For today's structures, we look for materials with four distinctive properties [Man-Chung Tang]. These properties will be the guideline of this chapter:

1. Strength
2. Workability
3. Durability
4. Affordability

As a start, the following criteria will be studied for each type of concrete in relations with their performance. These are called the performance criteria and are derived from laboratory tests and experience during the service time. The performance criteria will be shortly introduce.

2.1 Advanced Cementitious Material

In this literature study creative concrete types will be associate with the mentioned performance parameters. These parameters will be indication factors for the concrete long-term performance and sustainability through creative application in construction. In [Table 2.1] the most relevant concrete types and their abbreviation are presented.

<i>Acronyms</i>	<i>Concrete type</i>	<i>Acronyms</i>	<i>Concrete type</i>
NSC (ref)	Normal strength concrete	SCC	Self-compacting concrete
HSC	High strength concrete	FC	Foamed concrete
UHPC	Ultra high performance concrete	PMC	Polymer modified concrete
LWC	Light weight concrete	TRC	Textile reinforced concrete
HVFA	High volume fly ash concrete	RPC	Reactive powder concrete
SHCC	strain hardening Cementitious composites	GC	Geopolymer cement

Table 2.1: Innovative concrete material

Sustainable:	HVFA, GC
High performance:	HSC, UHPC, RPC, SHCC, SCC
State-of-the-art:	TRC, PMC
Conventional:	NSC, LWC

The performance criteria of concrete according to [United-States Federal Highway Administration] there are 8 performance characteristics. In this study the following characteristic will be addressed:

<i>Index</i>	<i>Criteria</i>	<i>Index</i>	<i>Criteria</i>
1	Mechanical properties	6	Compaction
2	Stress-strain	7	Curing and finishing
3	Creep	8	Durability
4	Shrinkage	9	Crack behaviour
5	Freeze-thaw	10	Costs

Table 2.2: Performance criteria concrete

In the appendix [D] an extensive study is conducted for each concrete type as part of the literature study. There are a lot of experiments, papers and thesis available. In the

following section the collected data will be transformed into a complete simplified overview of the available materials with which an ACM hybrid bridge will be design.

2.2 Design codes

The goal of this section is to explore the characteristic values of different ACM with high potential to be applied in heavy traffic concrete bridge . Currently the mechanical properties of the concrete represents the ultimate limit state value (ULS) which can never be exceeded by the combination of the live loads, dead loads and variable loads [Eurocode]. Although this Eurocode is supplied with very structured method to determine the design load, and the resistance it is not yet clear how to use the existing codes to find the ULS values for ACM.

In [Table 2.3] an overview is given on the current design codes for concrete structures and calculations methods for concrete structures. When the design code is not exist or not cover the application of the material, a full-scale laboratory test for local response and numerical investigation is required. Please note, the French code and the Japanese code are general recommendation for UHPC not developed specifically for highway bridge structures.

<i>Name</i>	<i>Region</i>	<i>Documents</i>	<i>Description document</i>	<i>Application</i>
EC2	Europe	1992-1-1	Design of concrete structures	Concrete classes up to C90/105 without fibers
		1992-2	Design of concrete Bridges	
		1991-1	Actions on structures	
VBC	Netherland	NEN 6720	Regulations for concrete – Structural requirements and calculation methods	Concrete classes up to C90/105 without fibers
		*CUR-111	Guidelines fibre reinforced concrete	Thin NSFRC
AFGC-SETRA	French	AFG 02	Recommendation for UHPC General design recommendations for the use of UHPFRC in reinforced and prestressed concrete structures	General Design code UHPFRC
ACI	USA	ACI 318	Building code requirements for RC	
Jap 06	Japan	JAP	Modifications compared to the earlier French recommendations	HSC, UHPC concrete bridges
CAN	Canada	CAN 06	Canadian Highway Bridge Design Code	UHPC concrete bridges
		CAN 96	Canadian Prestressed Concrete Institute	
SCH	Germany	SCH 08		UHPC
		*DAfStb	Guidelines FRC	NSFRC

Table 2.3: Existing standards and recommendations ACM (*guidelines)

2.3 Mechanical properties

The designer of the concrete mix-design defines during the design process criteria which will determine the mechanical properties of the hardened concrete. These are the compressive strength, tensile strength and elasticity.

Higher strengths offers savings in material weight and consequently it result in less dead load. The compressive strength of NSC is around 50 MPa. The diverse area of application and strength classes is expressed by adjusting the mix-design of the concrete specimen. The strength of the various concrete materials will be most influence design parameter during the firsts design cycles. The compressive strength, tensile strength, elasticity and ductile/brittle behavior will be represented in the stress-strain relationship given in [Figure 2.3] for each of the concrete types listed in [Table 2.1].

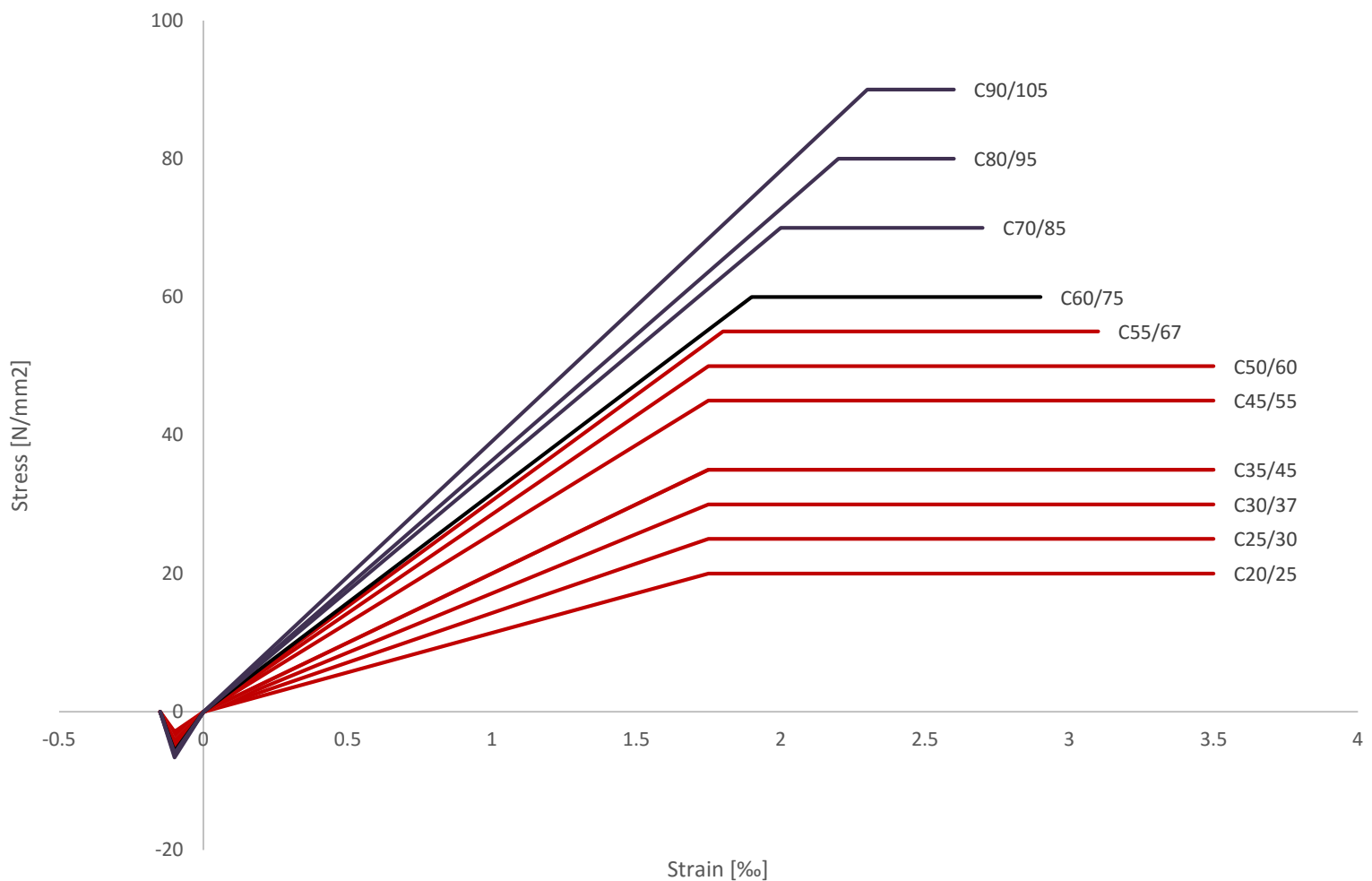
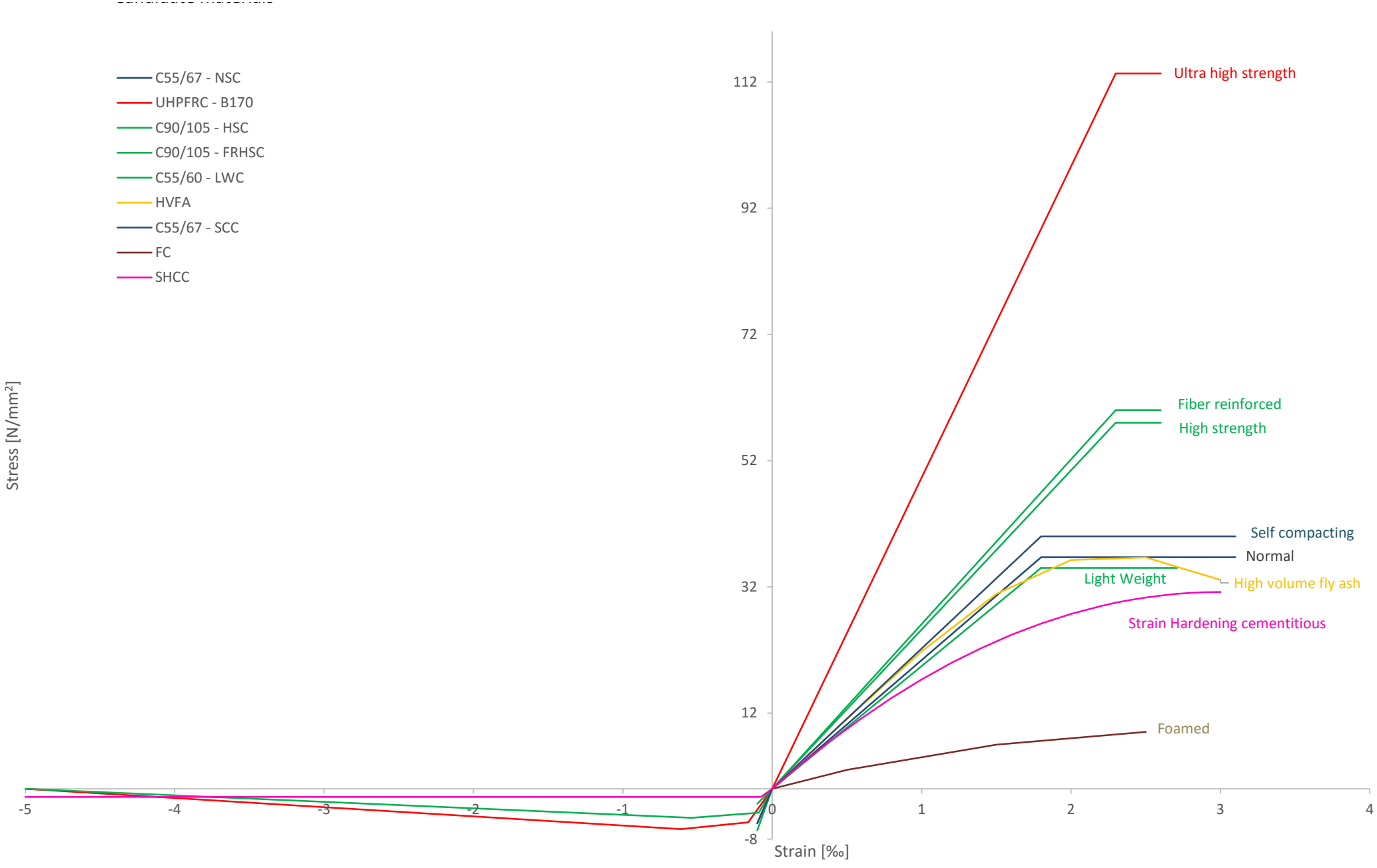


Figure 2.2: Bi-linear stress-strain diagram for compression and tension [conform EC2]

Figure 2.3: Bi- linear and parabolic stress-strain diagram for compression and tension conform different design codes and experiments



The presented stress-strain diagram presented is derived with different norms and design codes [Table 2.3], the values seen in [Figure 2.3] are the ultimate limit state values. Which means that the characteristic stresses are reduced with partial safety factor as part of the probabilistic design.

<i>Type ACM</i>	<i>Calculation method</i>
Normal Strength Concrete	EN-NEN 1992
High Strength Concrete	EN-NEN 1992
Ultra High Performance Concrete	AFGC-SETRA
Light Weight Concrete	EN-NEN 1992
High Volume Fly Ash Concrete	Hardjito and Rangan Research
Strain Hardening Cementitious Composites	Recommendations for Design and Construction of High Performance Fiber Reinforced Cement Composites with Multiply Fine Cracks (HPFRCC) [Japanese]
Self-Compacting Concrete	EN-NEN 1992
Foamed Concrete	Research Daniel Caduff, Jan G.M. Van Mier
Fibre Reinforced High Strength Concrete	Canadian Highway bridge design code (CAN-06), Japanese code (JAP 06), CUR – Aanbeveling 111, and the French AFGC-SETRA

Table 2.4: Calculation methods used to plot the stress-strain diagram

2.3.1 Compressive stress-strain limit state

The experimental values of the concrete compressive strength may vary from the empirical values when applying the Eurocode expressions into other types of concrete not defined in this code. For concrete class of C90/105 the compression strength is related to the characteristics 5% cylinder strength (f_{ck}) and the cube strength ($f_{ck,cube}$) [NEN-EN1992-1-1 art. 3.1]. The values are determined at 28 days with uniaxial compressive test and are used as qualitative comparison of the compressive strengths. Unless mentioned all compressive strength values in this research follows this definition. The design value is: $f_{cd} = \frac{\alpha_{cc} f_{ck}}{\gamma_c}$. In [Figure 2.5] the different ACM are distinguished in agreement with the compressive strength, Young's modulus and ultimate strain.

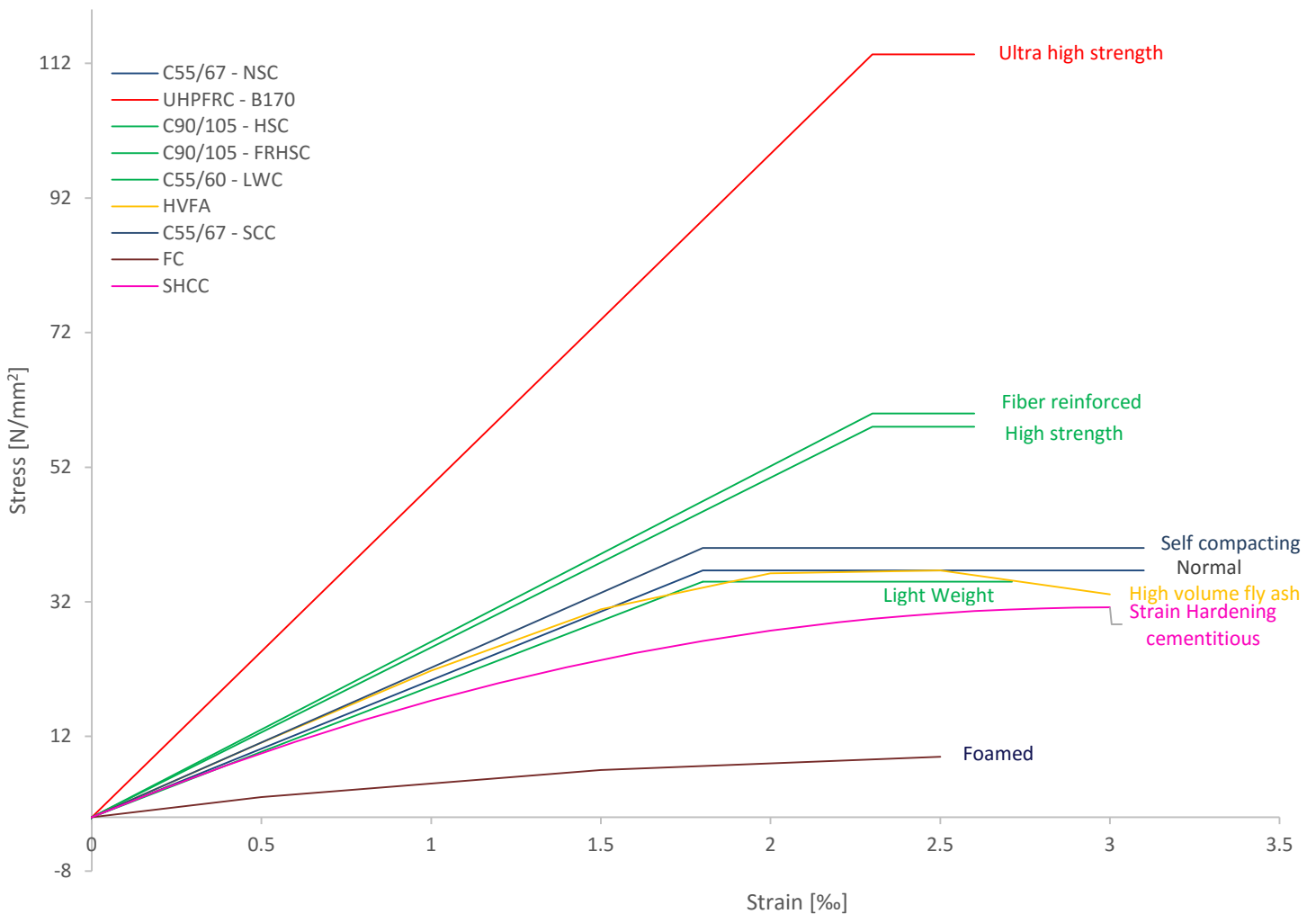


Figure 2.4: Compressive stress-strain diagram

2.3.2 Tensile stress-strain limit state

The tensile strength of the concrete is by far smaller than the compressive strength. Few concrete types such as UHPFRC, RPC, SHCC and TRC with volumic fibers content of 6%, 7%, 2.5% and 3% respectively result in ductile behavior under tension. The tensile strength is measured by uniaxial test at 28-days. Please note, by some ACM thermal treatment is applied which accelerate the curing process.

There are two more concrete types not mentioned in [Figure 2.6] . These have very high tensile strength comparable to tensile strength of steel:

- The RPC have tensile strength in the order of 40-100 N/mm² achieved by applying very fine materials and low w/c ratio, thermal treatment and higher curing temperature.
- The PMC is can be considered to some extent as the perfect material for tension with values between 800-1400 N/mm².

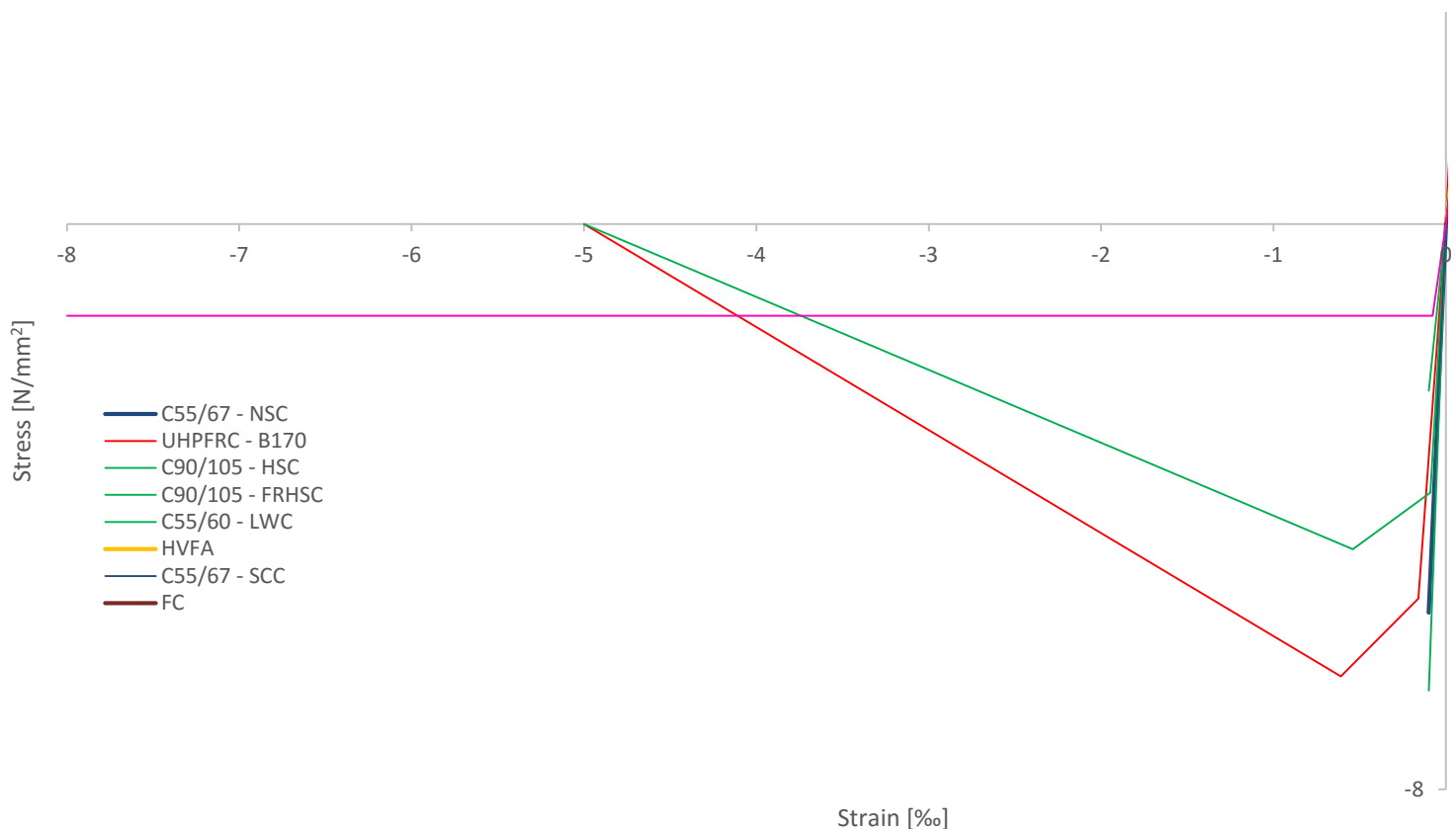


Figure 2.6: Tensile stress-strain relationship ACM

2.3.3 Shear strength

Deriving the shear capacity of concrete according to the EC2 and the Dutch code (NEN 6720 art. 8.2.5) can be accomplished with empirical expressions. The shear capacity of concrete members is expressed by these expression as function of the material characteristics and the shape of cross-section. The shear strength is depended on the compressive strength and in particularly on the tensile strength. However, for several of state-of-the-art concrete materials there are not yet empirical expressions found. In this case the shear strength is based on experimental results.

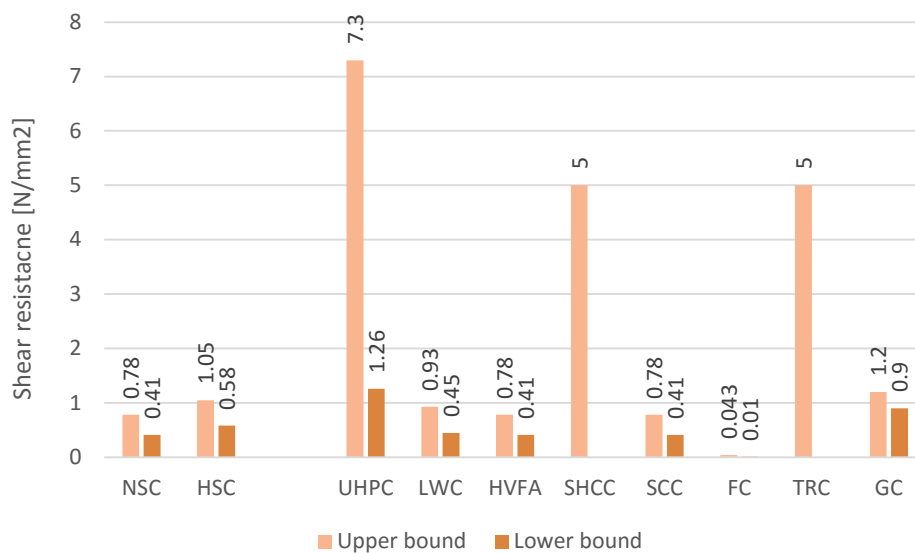


Figure 2.7: Upper boundary shear strengths of different concrete types

The high values of UHPC, SHCC and TRC is due to the added steel fibers. The other concrete types are without any fibers.

<i>Acronyms</i>	<i>Compressive strength</i>
NSC (ref)	40 N/mm ²
HSC	90 N/mm ²
UHPC	170 N/mm ²
LWC	40 N/mm ²
HVFA	40 N/mm ²
SHCC	40 N/mm ²
SCC	40 N/mm ²
TRC	-
FC	-
GC	-

Table 2.5

2.3.4 Modulus of Elasticity

The modulus of elasticity is an indication of the rigidity of the concrete member or structure. It is defined as the ratio between the stress and strain. The modulus of elasticity of concrete is influenced by the stiffness of the aggregate and the paste volume fraction.

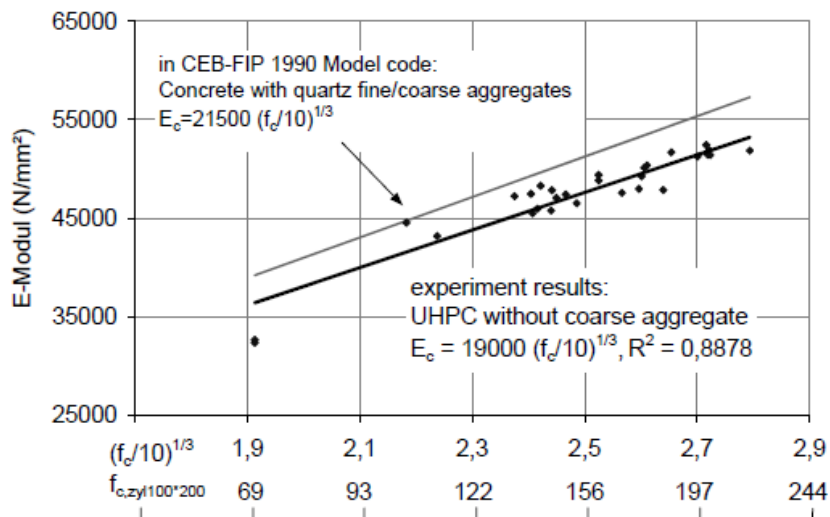


Figure 2.8: Relationship between modulus of elasticity and compressive strength of UHPC according to the CEB-FIP Model Code 1990 [P02, p209]

High values of elasticity are important to the serviceability limit state where the mid-span deflection are limited to ca. $L/300 - L/500$. In concrete bridges this resistance against deflection is crucial design value together with the load-bearing capacity. However members with very high E-modulus will tend to be more brittle unless fibers are added to the mix-design.

One important feature of the E-modulus is the distribution of stress. The stress distribution of Hybrid Bridge (non-homogenous cross-sections) will be proportional to E-modulus values of the different material within the linear-elastic behavior. A good example of stresses distribution in the field of infrastructures is orthotropic plates where stiffness values differ in two mutually perpendicular directions due to different E-modulus values.

Think about the longitudinal stiffness of this beam compound from different types of concrete types with possible fibers, prestressed cables, reinforcement bars and with possible longitudinal variation of the cross-sectional shape. Understanding the behavior of such a structure is a key for the design stage since it cannot be calculated with conventional methods. This will be possible using the information assembled in this section [2.3].

2.3.5 Mechanical properties summary

<i>Concrete</i>	<i>Compression</i> [N/mm ²]	<i>Tension</i> [N/mm ²]	<i>Shear</i> [N/mm ²]	<i>E – modulus</i> 10 ³ *[N/mm ²]	<i>Stress-strain</i> <i>curve</i>
NSC	0 - 65	1.6 - 4.1	0.41 – 0.78	27 - 37	Parabolic-linear
HSC	65 - 105	4.2 – 5.5	0.58 – 1.05	37 - 44	Linear branch steeper, less ductile
VHSC	105 - 150	4.2 – 5.5	1.05-1.26	39 - 47	Linear branch steeper, less ductile
UHPC	150 - 200	11.7	1.26 – 7.3	40 - 70	Strain-softening, brittle failure without fibers
RPC	200 - 800	40 - 100	60	60 - 75	very rigid and brittle without fibers
LWC	7 - 80	2.1 – 3.2	0.45 – 0.93	27 - 37	Lower elasticity
SCC	0 - 65	1.6 – 4.1	0.41 – 0.78	27 - 37	No chance
SHCC	32 - 39	3 - 8	5	16 - 20	Strain hardening under direct tension load
PMC	Inapplicable	800 - 1400	No data	40 – 130	Brittle failure under tension
FC	0.5 - 10	0.5 – 1.6	0.01 – 0.043	23 - 37	Brittle materials
TRC	74 - 86	4.4 - 8	5	21 - 35	brittle fracture behavior without fibers
HVFA	27 - 45	2 – 4.2	0.41 – 0.78	23 - 30	Similar to CC
GC	30 - 50	4 – 5.5	0.9 – 1.2	22 - 29	Similar to CC

Table 2.6: Mechanical properties matrix

2.4 Creep

Creep and relaxation of concrete are viscoelastic behavior of material. It stands for the strain response to a stress that is constant with time. The creep and shrinkage of the concrete depend on the ambient humidity, the dimensions of the element and the composition of the concrete. Creep is also influenced by the maturity of the concrete and the magnitude and duration of the load. [EN 1992-1-1 2004].

The long term deflections of concrete member due to creep have to be determined within the serviceability limit state with the quasi-permanent load combination. The Eurocode provides rules for calculation of deflections [EC2-1-1 art. 7.4.1], but limits for the deflection are not given [C01]. Therefore, the old Dutch limitations for the deflections are used. These are stated in [NEN 6723:2009 art. 6.2.1.1] and demand that the deflection is less than 1/300 times the span (concrete classes up to C95/105).

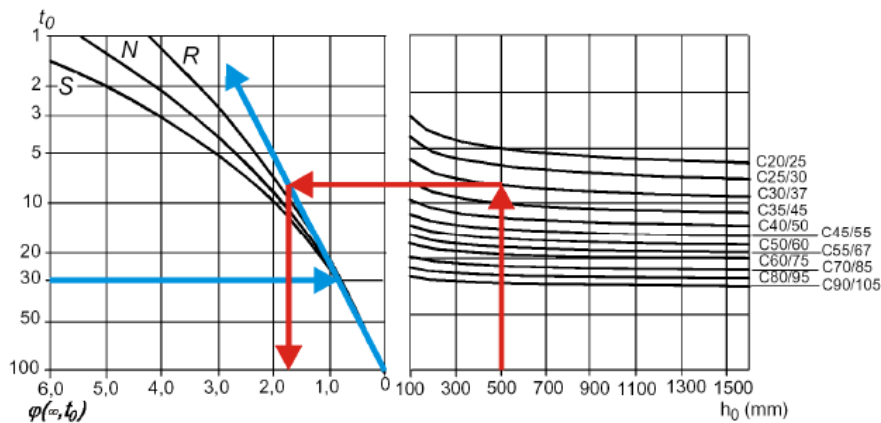


Figure 2.9: Example of finding the creep factor for RH=80% [Walraven, 2012]

Some innovative concrete types suffer from lack of data about their creep behaviour. This is related to short experience engineers have with these new materials compared with conventional concrete. The long-term behavior is still under investigation in laboratories trying to derive an analytical expressions for the calculations of creep.

Creep coefficient is defined as the ratio between the mean young's modulus and the actual value of young modulus minus 1: $E_{cm}/E_c - 1$.

<i>Concrete</i>	<i>Creep coefficient</i> [-]	<i>Creep Behavior</i>
NSC	1.4 - 1.5	
HSC	0.5 - 1	
UHPC	0.78	
RPC	1.05 - 1.2	
LWC	1.4 - 1.5	Similar to NSC
SCC	1.4 - 1.5	Similar to NSC
SHCC		
PMC	Inapplicable	Creep is dominated by the matrix behavior There are a lot of matrix factors and environmental factors influencing creep Composite reinforcement can be highly creep resistant in the fiber direction Fiber alignment is therefore important for creep reduction
FC	1.4 - 1.5	Similar to NSC
TRC	1.4 - 4.5	Similar to NSC
HVFA	Inapplicable	lower than Portland cement concrete of the same strength
GC	0.4 - 0.8	

Table 2.7: Summary creep

2.5 Shrinkage

There are different types of shrinkage: plastic, chemical, autogenous and drying shrinkage. The first three are active in the hardening phase. Drying shrinkage however is attributed to an exchange of moisture with the environment and can go on for many years for structures with large dimensions. Autogenous shrinkage is caused by lack of water during the hydration process so it reaches its final value after a relatively short period of time. Concrete mix-design with low w/c (such as UHPC) will be therefore more affected by autogenous shrinkage which will cause unwanted cracks. This is typically solved by using Superplasticizer, fine grana size and thermal treatment.

The calculation of shrinkage of concrete [conform the EN 1992-1-1] is possible for concrete classes up to C90/105.

<i>Concrete</i>	<i>Shrinkage</i> <i>[mm/m]</i>	<i>Shrinkage description</i>
NSC	0.2	
HSC	0.25 - 0.3	Higher autogenous shrinkage Negligible small drying shrinkage
UHPC	0.7	Higher autogenous shrinkage 0.55 mm/m Small drying shrinkage 0.15 mm/m
RPC	No data	High autogenous shrinkage
LWC	0.3-0.35	Negligible autogenous High drying shrinkage
SCC	0.2	Similar values of shrinkage to NSC
SHCC	0.3	Drying shrinkage 0.17 - 0.25 mm/m Autogenous shrinkage 0.03 mm/m
PMC	No data	Very low shrinkage
FC	No data	Up to 10 times higher than NSC due to absent of aggregate
TRC	0.84 – 1.88	
HVFA	No data	Drying shrinkage of fly-ash concrete is generally less than CC
GC	0.1	Drying shrinkage

Table 2.8: Shrinkage matrix

2.6 Durability

Probably the most costly aspect in degradation processes are related to repair and maintenance costs, approximately 50% from new build [ED. K van Breugel, 2013]. The common degradation mechanism in the Netherland are Carbonation which caused by consumption of $\text{Ca}(\text{OH})_2$ by the CO_2 through cracks, leading to drop of PH and corrosion of the rebar and chloride penetration which leads to corrosion and cracking. Important concrete design- parameters which focuses on prevention are the concrete cover and the tightness (porosity) of the cement paste. This subchapter will cover the durability aspects of the different types of concrete.

2.6.1 Freeze and thaw

While freezing, the volume of water increases and can create strong pressures and high tensions into the concrete. According to the concrete strength, these forces are the subject of an elastic absorption or can give place to weakening in the structure even a complete destruction of the concrete. Concrete mix-design have a significant role in taking Freeze-thaw into account. Adding admixtures as air entrainer have a positive effect.

<i>Concrete</i>	<i>Freeze-Thaw resistance</i>
HSC	Due high density → influence of freeze-thaw is smaller resist the freeze-thaw effects better than CC
UHPC	Higher resistance against mechanical abrasions and freeze and thaw stresses as well as a greater impermeability for fluids and gasses
RPC	Low air entrance → Very high resistance
LWC	Adequate freeze -thaw resistance
SCC	Air entraining admixtures improve freeze-thaw durability
SHCC	10 times higher resistance to freeze-thaw
PMC	Better resistance to freeze-thaw cycles than CC
FC	High air-content → good resistance
TRC	No data
HVFA	May be less resistant to scaling when subjected to freeze-thaw
GC	Good resistance

Table 2.9: Freeze-Thaw

2.6.2 Aggressive environmental -attacks

<i>Concrete</i>	<i>Resistance to aggressive chemical attacks</i>
HSC	Better resistance against environmental attacks such as chloride attack, carbonation, alkali-silica reaction.
UHPC	Low permeability → durable material
RPC	Very high resistance against carbonation, chloride attack, erosion and air permeability
LWC	Average resistance
SCC	Better durability than CC due to homogenous material
SHCC	Archive his durability through crack width limitation. Good resistance against all environmental agents
PMC	Corrosion-resistance is remarkably better. Resistance to environmental agents still under investigation
FC	Good resistance to aggressive chemical attack however low density may cause higher rate of carbonation.
TRC	Textile have no risk of corrosion, ingress of chloride of carbonation.
HVFA	Two times more permeable for chloride after 28 days After 180 days chloride resistance comparable to CC Alkali-silica reaction can be controlled with Fly-ash class Sulphate resistance of HVFA however do not meet the requirements Carbonation at a similar rate
GC	Durable material with excellent resistance to chemical attack

Table 2.10: Resistance to aggressive chemical attacks

2.7 Workability

Proper compaction is a critical success factor to obtain a reliable and durable structure. Compaction reduces voids, increase density and a good embedment of reinforcement. The consistency classes dividing the concrete into five classes: [NEN 8005]: Dry, semi-dty, semi plastic, plastic and flowable. The influencing factors for are the Particle grading of aggregate, the maximum diameter, percentage fine material ($<250\mu\text{m}$) and super

plasticizers. The consistency tests are developed to verify the consistency class before concrete is poured. Design procedure for concrete classes up to C95/105 can be used. The freshly placed concrete should be given circumstances to develop into good quality concrete. A major factor is the undistributed reaction between cement and water (hydration). As soon as concrete exposed to its environment, moisture exchange will take place (evaporation) until equilibrium is established. Curing techniques will prevent these moisture losses and maintain proper conditions for hydration.

<i>Concrete</i>	<i>Compaction</i>	<i>Curing</i>
HSC	Large density require more vibration	Thermal treatment applied Higher temperature peek
UHPC	Flows extremely well due to the good lubricating effect of the binder	Heat curing is required Higher temperature peek
RPC		Heat curing is required
LWC	Similar to NSC	More complicated than CC
SCC	Not require any additional compaction	Important for the top-surface of elements made with SCC.
SHCC		More heat of hydration leading to crack formation
PMC	Not required	Curing process in a controlled environment (prefabrication)
FC	Not required	Allows controlled discharge into narrow openings
TRC		
HVFA	Same workability	Same workability
GC	Precasting is recommended.	Precasting is recommended.

Table 2.11

2.8 Affordability

Affordability defined as the production costs and the construction costs of the new material. However, maintenance of the structure during the serviceability life cycle of the structure is considered as well. We may look at the initial costs and the capitalized costs for maintenance as net present value over the entire service time of the structure (Design & Construct & Maintenance) or we may consider as mentioned the production and construction costs.

Costs is a determining factor for comparison of construction materials. In this respect, it looks like a 'chicken and egg' question. A potentially good but expensive material may become affordable when its application is more widespread due to mass production, while its application can only get widespread if its cost is sufficiently low. Stainless steel, for example, is good for many applications in construction. However, the higher price of stainless steel is a hindrance to its widespread use.

<i>Concrete</i>	<i>Cost [€/m³]</i>	<i>Description</i>
NSC	282.8	Without formwork costs, including rebar, batching plant and casting
HSC	Few percent of saving	Slender design → Saving in material usage
UHPC	700	-
RPC		Least costly components of CC are replaced by expensive elements which results in a substantial increase in cost over and above that of CC (5 to 10 times higher than HSC).
LWC		Forecasted and delivered cost about 21% more than CC Cast in-place concrete including formwork, reinforcement, conveying, finishing and curing the LWC will cost 4% than CC.
SCC	310	Some producers may add a surcharge as high as €30/m ³
SHCC		Total economic costs are reduced by 15% as result of less maintenance and lower construction traffic congestion High performance and exceptional raw material requirements demand double energy consumption per cubic meter SHCC compared with CC.
PMC		Very expansive raw materials
FC		Reduced labour and supervision costs, cost compares favourably with other fill materials
TRC		Raw material costs and the prefabrication costs are higher than conventional reinforced concrete.
HVFA		Less expensive than CC thanks to the usage of by-product the fly-ash as a replacement of the expansive cement powder.
GC		Comparable cost with CC

Table 2.12: Costs overview

3. Durability of Bridges

Durability relates to the length of time a structural material remain intact and fully functional. The durability of any material in relation to its structural purpose greatly depends on the environmental conditions of the construction are. A bridge is particularly fully exposed to the elements, great care is needed to ensure material resistance to decay. The durability of the materials can be effected by such a conditions as: Temperature humidity, rainfall, degree of exposure, pollution, salty air, and abrasion from wind-borne sand and de-icing salts which sprayed during the winter.

3.1 Degradation

How simple the qualitative approach for the determination of the durability of concrete structure, how complex the quantitative formation. This is due to complexity of understanding the degradation processes but also due to the unknown porosity and pore distribution of concrete and the variability of the climate. The governing degradation mechanism are:

- Exposure to hazardous environmental conditions
 - Acids
 - Sulphates

- Carbon dioxide
- Internal degradation over time
 - Reactive aggregates (ASR => expansion, deterioration), chlorides (corrosion)
- External loads
 - Cracks or worse (more exposure or even failure)

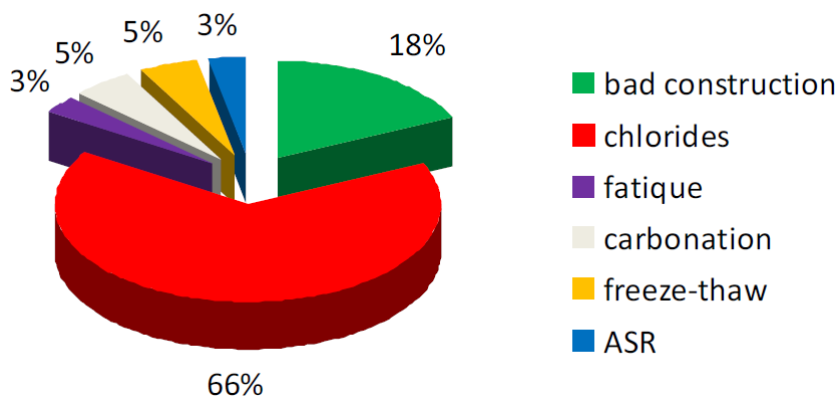


Figure 3.1: Degradation causes concrete [CIE5127]

3.1.1 Bad construction

Owing to poor design of the bridge and poor concrete quality with unsatisfying permeability, porosity, cover thickness and crackwidth the corrosion process (H_2O and O_2 access) may be accelerated over time.



Figure 3.2: Uncovered rebar [CIE5127]

3.1.2 Chloride ingress

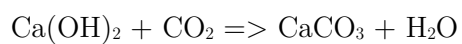
Chlorides locally depassivate rebars and initiate corrosion, the permeability determines ingress speed. Chlorides are not harmful for the concrete but to the steel rebars. Once the PH-value in the concrete reaches values smaller 9 corrosion will initiate.



Figure 3.3: Chlorides as accelerator [CIE5127]

3.1.3 Carbonation

The ingress of carbon dioxide caused by the consumption of Calcium-hydroxide in the pores by the outside air leads to drop of PH and corrosion.



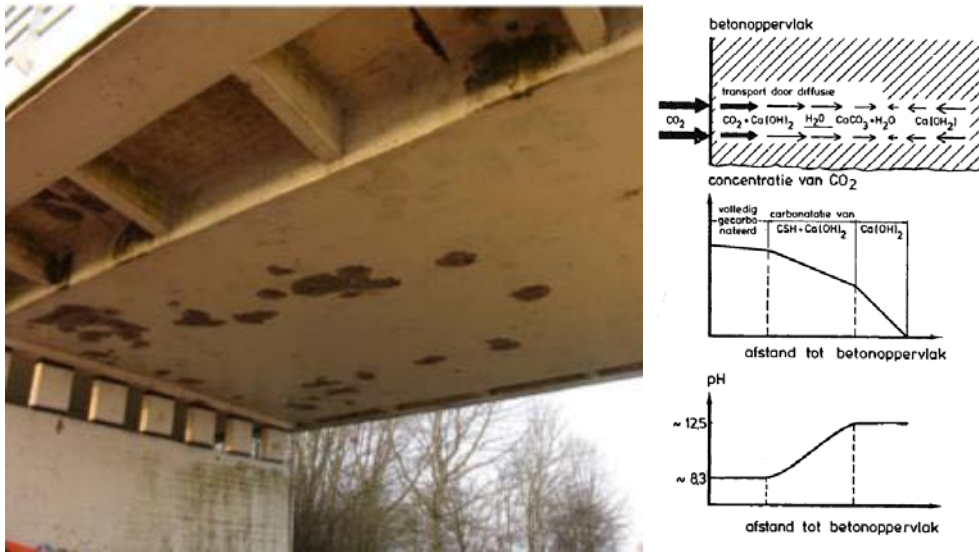


Figure 3.4: Carbonation of concrete [CIE5127] [CIE5110]

3.1.4 Alkali-Silica Reaction

The Alkali from the cement react with the Silica from the aggregate producing Alkali-Silica gel which attracts water resulting in the expansion of the reaction product causing multiple cracks.



Figure 3.5: Alkali-Silica reaction [CIE5127]

3.2 Design service life

According to the Eurocode, the design service life of common civil engineering structure should be between 50 - 100 years [C04, Table 2.1]. Under normal conditions, only minor repairs and maintenance required during the service life. Because of the inhomogeneous properties of concrete material factors (γ_m) are introduced to the Resistance side to account for the uncertainties in the derivation of section characteristics. In addition a conversion factor (η) is applied taking into account degradation of material properties over time.

The classification of the environmental actions correlates with the mix-design parameters such as W/C ratio, aggregate size, admixtures content and slump [NEN-EN 206 Art. 4]. The Eurocode will be used as guideline for the service-life design of ACM. In [Figure 3.6] overview of the environmental actions is given.

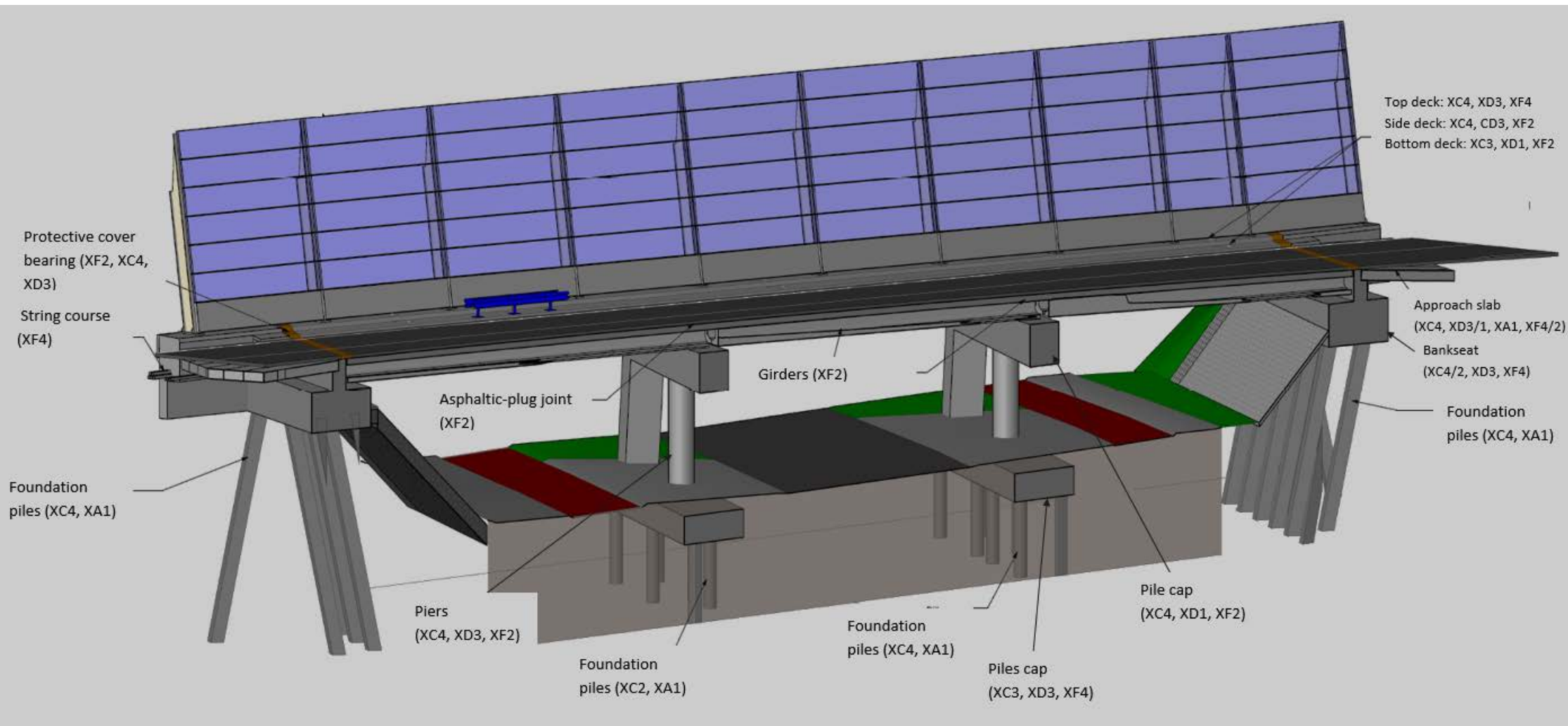


Figure 3.6: Environmental classes of sub and superstructure for typical traffic bridge in the Netherland

The environment actions [Table 3.1] are governing for the determination of the concrete cover, steel bars diameter and maximum allowable crack width for conventional concrete. Applying higher quality of concrete will resist the these actions which may result in slender structures. The difference bridge components [Table 3.1] will be extensive explained in [3.3].

<i>Bridge component</i>	<i>Degradation mechanism</i>
Top deck	Carbonation initiated corrosion Chloride induced corrosion, not from sea water Freeze-thaw attack, with and without de-icing salts
Girders	Freeze-thaw attack, with de-icing salts, Fatigue
Asphaltic plug-joint	Freeze-thaw attack, with de-icing salts, Fatigue
Piers	Carbonation initiated corrosion Chemical Attack Freeze-thaw attack with de-icing salt
Foundation piles	Carbonation initiated corrosion Chemical Attack
Piles cap	Carbonation initiated corrosion Chloride induced corrosion, not from sea water (De-icing) Freeze-thaw attack, with de-icing salts,
Bankseat	Carbonation initiated corrosion Chloride induced corrosion, not from sea water (De-icing) Chemical Attack
Approach slab	Carbonation initiated corrosion Chloride induced corrosion, not from sea water (De-icing) Freeze-thaw attack, with de-icing salts,
Protective cover bearing	Freeze-thaw attack, with de-icing salts Carbonation initiated corrosion Chloride induced corrosion, not from sea water (De-icing)
String course	Freeze-thaw attack with de-icing salt

Table 3.1: Degradation mechanism of bridge components

3.3 Deterioration assessment



Figure 3.7: Concrete Bridge [B09, p574]]

The deterioration of bridge structures occurs primarily through one of the three reasons:

1. Chemical reactions between the material from which the structure is constructed and the environment to which it is exposed: Iron will oxidise to Iron (II) Oxide and Calcium hydroxide in the PC react with carbon dioxide and sulphates.
2. Physical processes that results from the interaction between the structure and some vector within the environment resulting in either direct loss of serviceability or producing conditions which allow other deleterious processes to be initiated. For example Fatigue cracks.
3. Extreme events which impose transient forces and/or displacements that lie outside of the normal design envelope. For example: earthquakes.

The most common deterioration for each bridge component is specified.

3.3.1 Bridge deck

In a typical highway, the long-term effect of salt spray from passing traffic may lead to early corrosion of the front face reinforcement. The biggest issues causing durability problems are inadequate cover and faulty drainage.

3.3.2 Bearing and Asphaltic plug-joint

Bearings and expansion joints have proved to be among the most troublesome components of bridges. In particular, deterioration of substructures due to water leaking through expansion joints has been common especially in bridges carrying roads where de-icing salt is used. The durability of the waterproofing system is satisfactory for at least 20 years.

Elastomeric bearing grow old, wear out or deteriorate. Their main defects are corrosion for metal, cracking and spalling for concrete and, for laminated rubber, sheet corrosion and relative slip with rubber cracks. The problem is that bearing have not been designed to be replaced without impeding the flow of traffic

3.3.3 Piers

High splash water rate caused by passing water may lead to corrosion of the steel reinforcement and spalling of the concrete cover.

3.3.4 Abutment

One of the primary areas of concern in all types of abutment walls is the top of the bearing shelf. Water running from the carriageway surfaces above will normally flow onto the bearing shelf and every effort should be made at the design stage to drain this water away from the abutment wall. Nevertheless, the majority of existing abutment walls suffers from water staining and chloride induced corrosion

3.3.5 String course section

The introduction of a horizontal joint immediately below the stringcourse on a wing wall can have serious consequences. Differential shrinkage stresses will probably initiate a regular pattern of vertical cracks running completely through the string course section. Traffic passing over the structure will splash road salts directly onto the string course and there will be a high risk of corrosion in the parapet reinforcement.

3.4 Strategies for combating deterioration

Protecting the bridge structure from deterioration is possible through identification of number of different strategies. According to [B09, p576] there are three main approaches that may be adopted.

1. Remove the environment: Main chemical reaction and physical interaction which leads to the degradation of the bridge require the present of water. If water exposure and/or rapid drying can take place then deterioration will be kept minimum (Water management).
2. Alter the material or the structure: Select appropriate material for the particular environment, avoid complicated detailed design of the structure and finally ensure safe access to critical parts of the structure.
3. Protect the structure from the environment: Use surface coating to the exclusion of the environment. For example use of silane and siloxane surface treatments to protect concrete or cathodic protection for steel.

3.5 Durability of ACM's

The superiority of ACM's as durable material holds the excellent resistance the common degradation mechanism in concrete structures as carbonation, chloride attack and bad construction (insufficient cover). In most cased (89%) these mechanism will be reasonable for demolishing or repair of the bridge structure. A new structure is designed according to the new standards wishing to extend the service life of the bridge and to minimize the maintenance costs should use ACM's as UHPC, SHCC or HSFRC.

In ordinary concrete, the ratio of w/b is in the order of 0.4-0.6. To obtain high performance the w/b ratio is reduced to below 0.2. This is by increasing the amount of binder (cement), and adding silica fume (20% of the mass). The aggregate of UHPC are very small. The result is extremely compact material.

3.5.1 Creep & Shrinkage

UHPC exhibit a relative high autogenous shrinkage with low creep. This time depended deflection may be a disadvantage to the durability in case of restrained shrinkage and creep cause tensile stresses and cracks.

SHCC have a higher tensile strain capacity due to the ability to restrain the crack opening by occurrence of multiple fine micro cracks. The creep and shrinkage of the material is rather high.

The data obtained in [2.3.5] regarding durability is summarized in the following table:

<i>Durability parameter</i>	<i>NSC</i>	<i>UHPC</i>	<i>SHCC</i>
Creep coefficient [-]	1.4-1.5	0.6-0.8	1.2-1.4
Shrinkage [$\mu\text{m}/\text{m}$]	200	500-1000	720-1400
Strain hardening [%]	-	0.05-0.50	1.0-5.00
Crack width [mm]	0.3	0.050-0.100	0.050-0.065
Water porosity	12-16	6-9	21-28
Air permeability [10^6]		0.003-0.0046	0.1-0.5

Table 3.2: Overview durability

It is can be concluded that the common durability mechanism can be efficiency eliminated by applying ACM's with improved properties. However it requires specialized techniques to apply it in bridge construction.

Part II

Design Input

4. Design input

Concrete bridges are designed with multidiscipline team of engineers. Previous to the designed phase presented in Part III and Part IV of this thesis the input parameters are discussed. This is possible by means of reference project picked carefully for which optimization and improvement are necessary. The first reference project is of in-situ casted reinforced concrete bridge. The second is prefabricated prestressed concrete bridge. Both projects are design in conventional concrete and constructed in traditional construction method. The design phase and the execution phase are inseparable, but strongly interacted in a Design/Construct contract (referred as D/C). This interaction appears to be a critical success factor for innovative projects, where elements are beyond the state-of-the-art.

4.1 Goal of case study

In order to limit the scope of this research and to be able to compare the traditional bridges with AMC bridge, it was decided to select a case study for which the optimisation would be carried out. The case study will provide the required references for the load cases, boundary conditions and geometry of the bridge substructure and superstructure. Moreover it will provide the indication of the costs efficiency of the proposed new innovative bridge design.

4.2 Case description

As mentioned, two objects will be introduced. Both are located at the Kethelplein interchange in the municipality of Schiedam, South – Holland province [Figure 4.1].



Figure 4.1: Location of objects KW110 and KW160 , interchange Kethelplein in Schiedam [W01]

The construction of these objects is already completed. Both bridges are designed to carry the same loads with similar environmental classes, clearance gauge and soil conditions. However the critical design points for which special attention was required are not similar. This will be further explained.

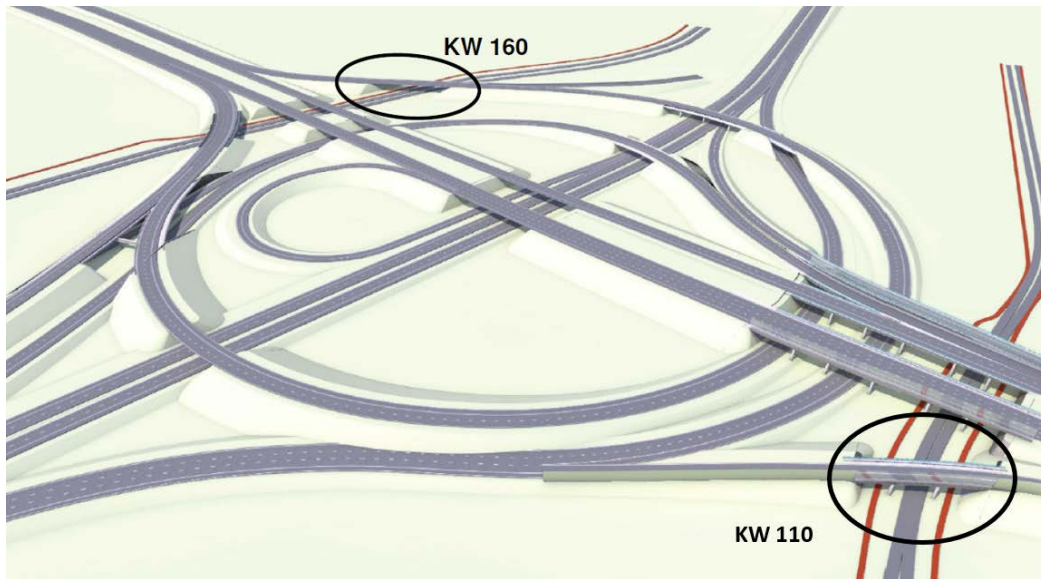


Figure 4.2: Impression Interchange Kethelplein with objects KW110 and KW160 [W01]

4.3 Object description KW110

This bridge is constructed together with the realisations of two soil bodies at both sides of the bridge. The substructure includes two abutments and three intermediate piers supporting the bridge superstructure. The viaduct consist of three fields [Figure 4.3] of 17.0m, 16.3m and 15.1m from the left to the right. Between the fields there are semi-rigid joints which means that this viaduct can be seen as statically determined system. The width of the bridge including the asphalt road, safety rail, and service lane and noise shields is in total 12m. At the boundaries of the bridge are the abutments which transfers the vertical and horizontal forces to the soil with foundations piles of 50mm. The beams are located on bearings and can rotate in the longitudinal direction. The intermediate supporting points designed with cross-beam (the piers) . The prefabricated ZIP-500 beams are prestressed with FeP1860 strands of 12.9mm.

<i>Concrete</i>	<i>Class</i>	<i>Comments</i>
Prefab beams	C55/67	Prestressed
Cast in-situ	C30/37	Substructure and compression layer
Density	25 kN/m ³	

Table 4.1: General design specifications KW110 [W01]

<i>Parameter</i>	<i>Unit</i>	<i>Value</i>
Width	m	12
Total length	m	48.4
Spans	m	17, 16.3, 15.1
Beams height (ZIP-500)	mm	600
Compressive layer	mm	230

Table 4.2: General design specifications KW110 [W01]

<i>Steel</i>	<i>Class</i>
Reinforcement bars	B500B
Prestressed steel	FeP1860

Table 4.3 General design specification KW110 [W01]

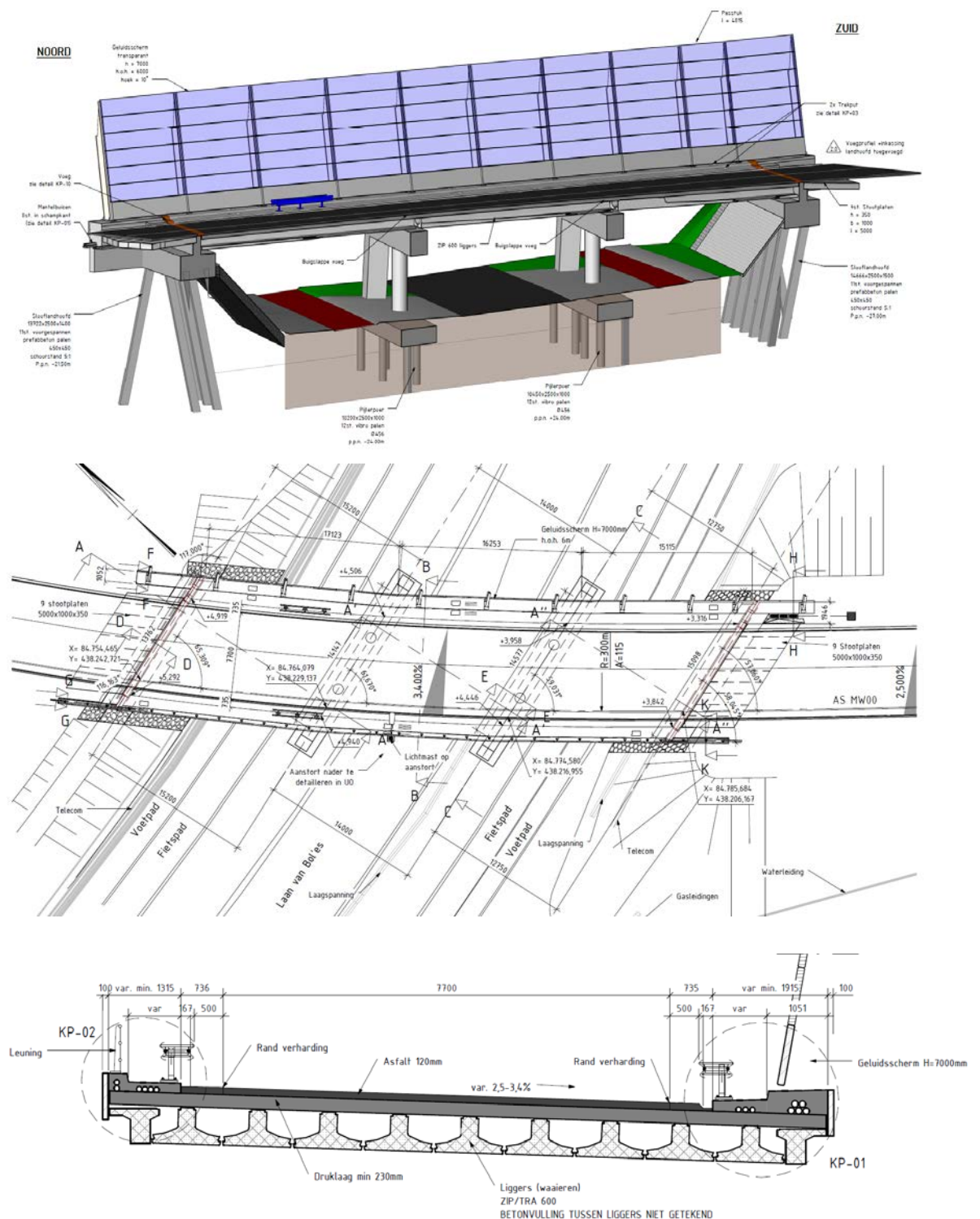


Figure 4.3: From top to bottom: Longitudinal cross-section, Top-view and lateral cross-section KW110 [W01]

4.4 Requirement & conditions new design

Norms and standards are developed to meet minimum safety and reliability levels of structures. During the design phase engineers must prove their design meet these requirements. In the case of innovative materials these norms are often absence. Instead the design has to comply with a number of conditions in order to sustain a representative comparison between the conventional design and the new design. Furthermore, the durability and serviceability requirements will stay identical to ensure the benefits of the new design.

The boundary conditions are retained and used for the new concept design. These boundary conditions are imposed from the substructure of the bridge. Which means the global geometry of the bridge is retained, the span and width of the bridge are fixed. However the span-to-depth ratio is parameter which will definitely optimized. The forces introduced in the substructure by the new bridge will probably be different so special attention will be required.

The requirements from the new design are partially derived from the specifications of the reference projects and from the literature study [2]. The requirements can be divided into 3 levels simplifying it for the entire bridge:

- Material level: Concrete science and technology, design aspects
- Cross-sectional level: Critical cross-sections, ULS and SLS design
- Structural level: Structural liability comparable with reference project

<i>Index</i>	<i>Material level</i>
M.	Apply innovative material
M.1	Concrete quality for infrastructure application must be proven
M.2	The material must be durable with minimal 100 years life – cycles
M.3	The materials must
M.4	Design must be suitable for prefabrication and/or cast in-situ
M.5	Mechanical properties must be genuine, therefore verifications with the producers is required
M.6	Design must consider execution aspects as mentioned in the reference projects

Table 4.4: Material level requirements for bridge design

<i>Index</i>	<i>Cross-sectional level requirements</i>
C.	The design must safe
C.1	Sufficient resistance
C.2	Sufficient torsion capacity
C.3	Sufficient shear capacity
C.4	Sufficient rotation capacity
C.5	Cross-section height will be variable
C.6	If fibers are applied take it into account in the capacity calculation with sufficient safety factors

Table 4.5: Cross-sectional level requirements for bridge design

<i>Index</i>	<i>Structural level requirements</i>
S.1	Structure must comply with the Eurocode regulations
S.1.1	Unity checks according to EC1 and EC2 must be made
5.1.2	The structure must be design according to the durability classes correspond with the reference bridge
S.1.3	Design should not deflect more than $L/300$
S.1.4	Fully prestressed design KW110
S.1.5	Shear reinforcement
S.1.6	Actions are considered according NEN-EN1991-1-5
S.2	Structure specification must comply with the reference project
S.2.1	Absent of prestressing for KW160
S.2.2	Absent of reinforcement bars in KW110
S.2.3	Bridge width and length dimensions according to the reference project
S.2.4	Similar geotechnical principles
S.2.5	Substructure are identical

Table 4.6: Structural level requirements for bridge design

4.5 Actions

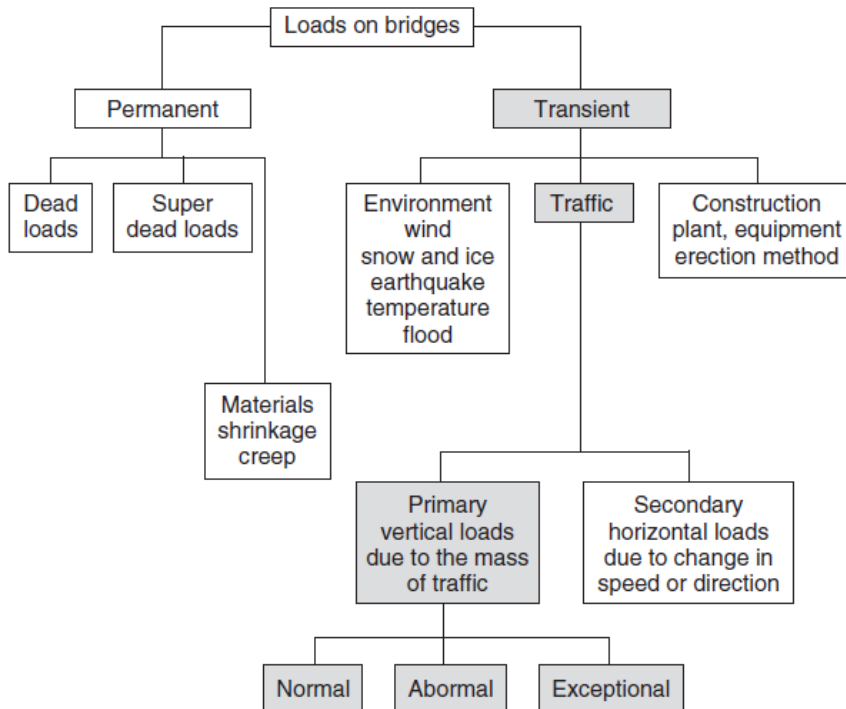


Figure 4.4: Action on bridges [CIE5127]

This section deals with the loads act on the structure. The different loads are actions which are classified by their variation in time as follows: [C04]

- Permanents actions (G)– e.g. self-weight, fixed equipment and actions by shrinkage and settlements
- Variable actions (Q)– e.g. imposed loads, wind/snow/temperature loads
- Accidental actions (A) - e.g. impact from vehicles, explosions

These actions, on concrete bridges are mentioned in EC1. In order to design the hybrid bridge and carry full structural analysis it is important to derive the exact actions. Men may derive these exact values acting on the reference bridges since these are quantified according to the EC1 and use these values to design the new hybrid bridge. Hence every

new design of concrete bridge will have to comply with the EC1 standards in the determination of the actions.

In concrete bridges the self-weight tends to be high, this is also in most cases the dominant load. The permanent, variable and accidental actions on the bridge will be multiply with partial load factors (γ_f) depend on favourable/unfavourable situations, uncertainty in the calculation model and deviation from the characteristic value. The norm defined as well the combination factor ($\Psi_{0,i}, \xi$), structure must withstand most unfavourable combination of actions. [NEN 6720] [NEN-EN 1991] [NEN-EN 1990].

4.5.1 Permanent load

The main component in terms of action is the self-weight of the concrete. For concrete bridge the permanent load includes the following cases:

- Deck and beams
- Asphalt layer
- Soil pressure
- Dead loads:
 - Compression layer
 - Safety rail
 - Wingwalls abutment
 - Hand rail
 - Pedestrian guardrail
 - Noise barrier
 - Splayed kerb
- Imposed deformation:
 - Shrinkage: Mainly autogenous shrinkage for CC.
 - Creep

The permanent loads may also include weight components of fiber, prestressing steel, steel reinforcement bars. There are no standard methods to determine the self-weight of the composite bridge, this aspect will be explained later on in this research.

4.5.2 Traffic

The first step in the determination of the variable vertical traffic loads is the carriageway division, the divisions of the carriageway into traffic lanes. For virtual width $w \geq 6.0 m$ with notional lane width of 3m will give number of virtual lanes [NEN-EN 1991-2 art.4.2.3]. Carriageway with two-way traffic with separation will be treated as one carriageway for the entire virtual width.

The Eurocode define the traffic loads due to road traffic by four characteristics load models applied on the individual lanes. The first load model covers most of the effects of the traffic by Lorries and cars. The second load model cover the dynamic effects by normal traffic. The third and the fourth load models represents exceptional vehicles and crowd loading. In the scope of this thesis the only the first two load models will be considered applicable for bridges with span up to 200m.

Load model 1

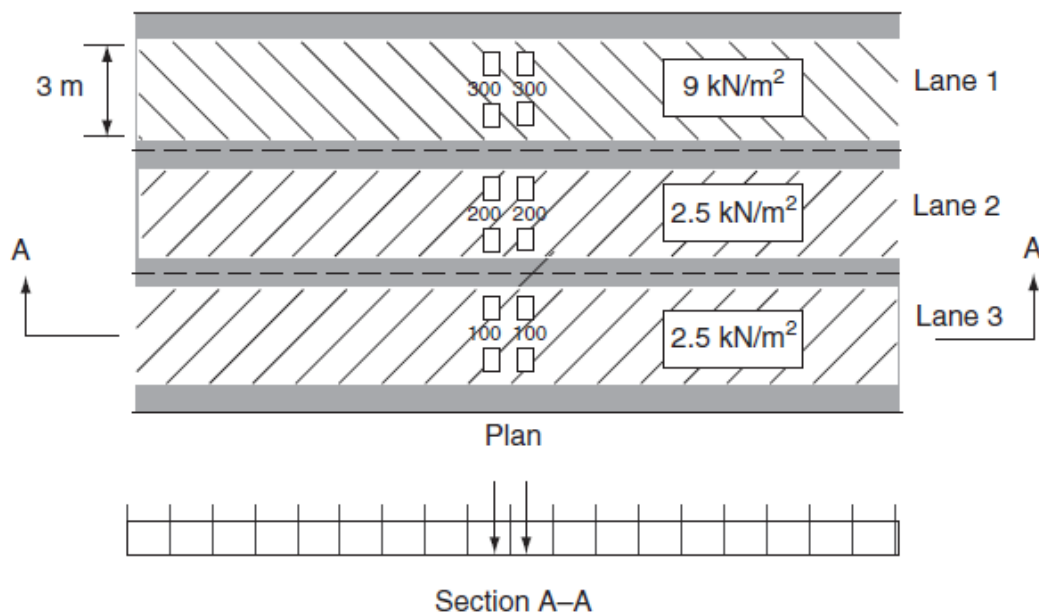


Figure 4.5: Application of LM1 [B09, p29]

Example of application of LM1 for $w=3\text{m}$ is summarized [Table 4.7]. The concentrated loads are distributed by the vehicle wheels with $0.4*0.4\text{m}$ contact area. The adjustment factors for LM1 are given in [Table 4.8].

	<i>Tandem system [kN]</i>	<i>UDL q_{ik} [kN/m²] * α_{qi}</i>
Lane 1	300	10.35
Lane 2	200	3.5
Lane 3	100	3.5
Other lanes	0	2.5
Remaining area	0	2.5

Table 4.7: Application of LM1 [Figure 4.5]

	α_{Qi}	α_{qi}
Lane 1	1.0	1.15
Lane 2	1.0	1.4
Lane 3	1.0	1.4
Rest	0	1.0

Table 4.8: Adjustment factor LM1

The positions of the loads from the edges of the bridge taking the restraint system is in accordance with the Dutch ROK (Richtlijnen Ontwerpen Kunstwerken).

Load model 2

This model is applicable for calculations of local actions on the carriageway and therefore it is valid only for the superstructure of the bridge. The effect of single axle load $\beta_Q Q_{ak}$ with $Q_{ak} = 400 \text{ kN}$, includes dynamic amplification factor with $\beta_Q = \alpha_{Qi}$ according to the National Annex. [NEN-EN 1991-2 art. 4.3.3].

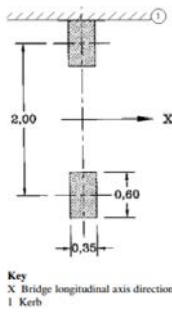


Table 4.9: LM2 The contact area of LM2 correspond is 0.35*0.6 m.

4.5.3 Secondary loads

4.5.3.1 Breaking loads

The horizontal forces in the longitudinal direction of the viaduct need to be taken by the bearings, abutments and piers of the substructure. In a case of intermediate support point the cross-beam will resist horizontal displacement. In [NEN-EN 1991-2 art.4.4.1] the calculation method for breaking and accelerating forces are given.

$$Q_{lk} = 0.6\alpha_{qI}(2Q_{lk}) + 0.1\alpha_{qI}q_{lk}w_lL \leq 900 \text{ (kN)}$$

Where L is the length of the deck or the part under consideration. The breaking force will be applied on the centreline of the governing lane.

4.5.3.2 Centrifugal and other transversal loads

According to [NEN-EN 1991-2 art 4.4.2] the centrifugal force (Q_{lk}) should be taken as a transverse force acting at the finished carriageway level and radially to the axis of the carriageway.

The centrifugal force TS: $Q_{lk} = 40Q_v/r$ (kN)

The centrifugal force UDL : $q_{lk} = 40Q_v/r$ (kN/m)

Where r is the horizontal radius of the carriageway centreline and Q_v is the total maximum vertical force of the TS or UDL.

4.5.3.3 Accidental

The load applied on the bridge by impact of vehicles on the edge of the road deck. The indicative static design load for highways roads is 2000 kN will have to be transmitted by the uniform diaphragm actions to the substructure [NEN-EN 1991-1-7 art. 4.3] [ROK].

There is also possibility for impact load of vehicles on the substructure of the bridge. This loads can be acting on the abutments or the piers of the bridge is 2000 kN in the direction of the traffic and 1000 kN perpendicular to the direction of the traffic. The force is applied 1.2 m above the road level

4.5.4 Wind

The wind load can is dominant load for a moveable bridge. But will be taken into account in static bridges up to length of 200 m. The wind can blow from every direction and it's fluctuate with time. Wind pressure acts on the areas of the surface resulting in force normal to the surface of the bridge. The Eurocode suggest simplified set of pressures or forces whose effects are similar to the extreme effects of the turbulent wind. [NEN-EN 1991-1-4 art 4.2 and art.4.3] [ROK art.5.4].

Basic values

The geometry of the structure and its location are known. The fundamental value to determined is the basic wind velocity (v_b), the mean velocity (v_m), the turbulence intensity (I_v) and the peak velocity pressure (q_p). The complete derivation of these parameters which is explained in the Eurocode [NEN 1991-4 art.4.2 – 4.5].

The wind on a bridge deck will be calculated with simplified method which depends on a range of parameters. The dynamics effects are not considered in this section. The following expressions for the longitudinal, transversal and vertical wind actions are given:

Longitudinal direction

Refers for wind loads parallel to the deck width. The following expression is valid for this load:

$$F_{w,y} = q_{p,y} * A_{ref,y} = \frac{1}{2} \rho v_b^2 C_y A_{ref,y}$$

Where:

$v_b = 28.1 \text{ m/s}$	basic wind speed NEN-EN art.4.2 form.4.1
$v_b^* = 23 \text{ m/s}$	Upper bound value for road bridge EN1990 - Annex A2.2.1
$\rho = 1.25 \text{ kg/m}^3$	air density NB art.4.5(1)
$C = c_e * c_f$	exposure factor as a function of the construction height NEN-EN 1991-1 art.4.5
c_e	wind load factor
c_f	force coefficient without free-end-flow NEN-EN 1991-1 fig.8.3
A_{ref}	reference area NEN-EN 1991-1 art.8.3

Transversal direction

The wind load in the width of the bridge deck is calculated similarly to the the previous one.

$$F_{w,x} = q_{p,x} * A_{ref,x} = \frac{1}{2} \rho v_b^2 C_x A_{ref,x}$$

The reference area for wind profile in the transverse direction consider the shape of the superstructure and applied for all elements higher than 2.0 m above the carriageway on the most unfavorable length. For example the solid parapet, noise barrier.

Vertical direction

Both upwards and downwards should be used to calculate vertical vibrations of the bridge deck. However, this force will have a significant effects in concrete bridges only if the upwards lifting wind forces is of the same order as the dead load. In this case the deck could flutter, causing unwanted vibrations and noise hindrance. The force coefficient

($c_{f,z}$) which influences the value of the vertical wind load factor (C_z) will take into account the influence of a possible transversal slope of the deck, slope of the terrain and the angle of the wind direction with the deck due to turbulences. This is explained in the Eurocode [NEN-EN 1991-1-4 fig.8.6]. As already given, the expression of the wind force component perpendicular to the deck will be:

$$F_{w,z} = q_{p,z} * A_{ref,z} = \frac{1}{2} \rho v_b^2 C_z A_{ref,z}$$

In this research possible light weight superstructure will be designed. In this case the lifting load caused by the wind is important.

4.5.5 Snow

The snow actions on concrete bridges is small compared to the roofs due to the serviceability demands. The snow would probably remove from the carriageway to allow disturbance free traffic flow.

4.5.6 Fatigue

Traffic actions on bridges produces stress spectrum which may cause fatigue. This stress spectrum is depended on the location and magnitude of the axial loads introduced by the wheels of the vehicles. Calculating the fatigue actions on bridge according to the Eurocode is based on five load models. LM1 and LM2 are intended to check the fatigue life of the structure whereas LM3 – LM5 are intended to be used for fatigue life assessment by reference to fatigue strength curves. [NEN-EN 1990-2 art.4.6].

The fatigue actions are important for the structural analysis of the bridge where the reinforcement and the concrete will be checked.

4.5.7 Thermal

This part describes the changes in the temperature of structural elements caused by the climatic seasonal changes. The most important cause for temperature problems are:

- Development of hydration heat in hardening concrete
- Climate influence

- Solar radiation
- Daily and seasonal cycles
- Rain, hail and snow
- Fire

These thermal actions effect the temperature distribution within the individual structural element. This section will focus on thermal actions regarding the climant influence. In case of free deformation of a structural element (static determined system) there are three thermal actions :

Temperature difference (ΔT_b): linear temperature distribution

Eigen temperature (ΔT_e): non-linear temperature result in Eigen stresses,

Mean temperature (ΔT_m): Integral of the thermal load along the width of section

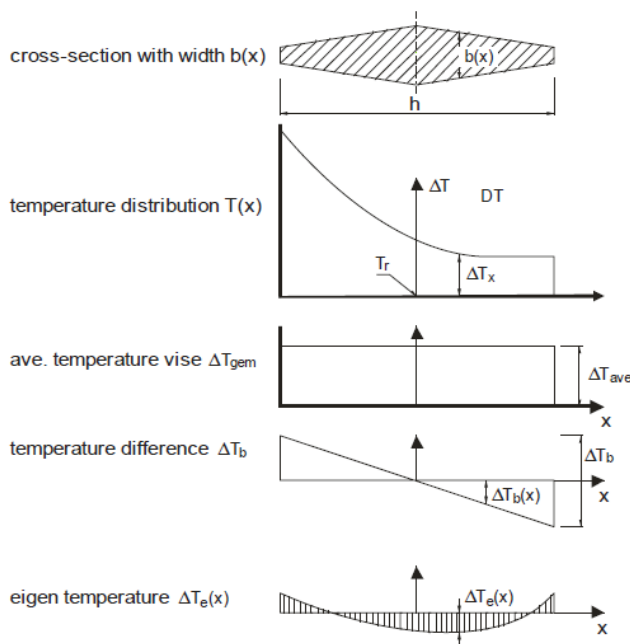


Figure 4.6: Subdivision of an arbitrary temperature load in components [B02, p18]

Since the coefficient of thermal expansion (α_e) is not zero, temperature variation will give rise to strains and corresponding deformations of structural elements or structures. When these strains and deformation are restrained, temperature stresses occur as well as corresponding structural forces. [NEN-EN 1991-1-5]

The Eurocode defines the action on concrete bridges as result of temperature load. Temperature variations give rise to expansion and shrinkage which may result in cracking and buckling of the element. In the case of object KW160 this action will introduce stresses to the concrete deck since the strains are restrained by the walls. In the other hand, object KW110 is defined as static determined structure. No additional stresses regarding temperature change in this case.

Uniform temperature component

The differences in temperature cause uniform elongation or shortening of the bridge deck and beams which influences the bearing and expansion joints. The characteristic uniform temperature range according to art. 6.1.3.3:

$$\begin{aligned}\Delta T_{N,con} &= T_0 - T_{min} && \text{maximum contraction} \\ \Delta T_{N,exp} &= T_{e,max} - T_{e,min} && \text{maximum expansion}\end{aligned}$$

Cross - sectional Temperature difference

The temperature of a bridge deck varies throughout its mass. The variation is related to the position of the sun and its intensity, thermal conductivity of the concrete, wind and the cross-section. For example temperatures near the top of the surface are controlled by incident solar radiation and temperature near the bottom are controlled by shade temperatures.

According to the National annex the recommended value for a linear temperature difference is 15 °C

Temperature difference components

The heating and cooling of the bridge deck's upper surface within time period will result in a temperature variation between the top and the bottom fiber of the cross-section. The NEN-EN 1991-1-5 art.6.1.4.1 (Approach 1) consider a non-linear temperature difference component for composite bridges.

Vertical linear component:

Determining the top temperature ($\Delta T_{M,heat}$) and bottom temperature ($\Delta T_{M,cool}$) values are found at Table 6.1. The values will be multiply by the factor (k_{sur}) according to Table 6.2 for thickness larger than 50 mm.

Vertical components for non-linear effects:

The non-linear effects take different cross-section with different materials into consideration. With input as thickness, cross-sectional area and moment of inertia the non-linear characteristic points of the non-linear temperature distribution can be determined. (NEN-EN 1991-1-5 Fig 6.2a, 6.2b, 6.2c)

4.5.8 Time depended loads

The shrinkage and creep characteristic of concrete induce internal stresses and deformation in superstructures. These are critical at the serviceability limit state and affects besides the main structure also the bearing and the expansions joints.

Creep

Defined as the increase of deformation in time relative to the direct elastic deformation at loading. The long-term effect of creep is discussed in section D.1.4 introduce the creep reduction factor (ϕ_c) which decreases the E-modulus.

$$\varepsilon_c(t, \tau) = [1 + \varphi(t, \tau)] * \varepsilon_{c0}$$

Where:

ε_c Total concrete strain at t
 ε_{c0} Elastic concrete strain at $t = \tau$

$$E'_c = \frac{E_c}{1 + \phi_c}$$

Where:

E'_c Long-term modulus of concrete

Please note, creep is influenced by the age of the concrete but also depends on the type of concrete and temperature. In this thesis this will have to be taken into consideration.

Shrinkage

Shrinkage stresses are induced in all concrete bridges. Generally the stresses are low and considered insignificant in most cases. However for composite bridge with layers of different material shrinkage can be significant. For example shrinkage produces compression in the top region of the precast concrete beam, when the concrete deck slab is poured it flows freely over the beam and additional stresses are induced due to the wet concrete, moreover when the top layer is hardened the bond between the two restraints the shrinkage of the poured in situ layer. Consequently tensile stresses are induced in the in situ slab and compression at the top region of the beam.

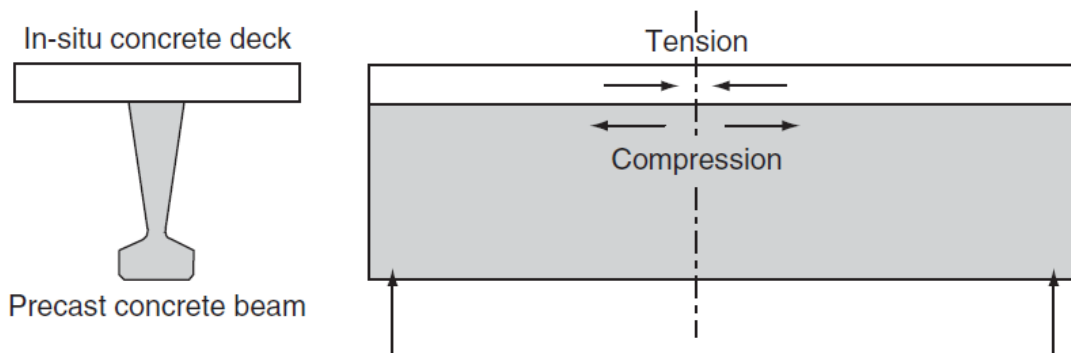


Figure 4.7: Effect of deck slab shrinkage on composite section [B09, p32]

Part III

Design study

5. Parametric analysis girder

The design process of innovative composite bridge can be divided into the familiar engineering design process. It begins with a research on the new type of concrete where the material characteristics are derived from experiments and literature [2]. In the second phase the feasibility study is carried out to evaluate the potential of the new type of concrete. The conventional design approach of the design process will begin starting with Conceptual design (CO) follows by the Preliminary design (PD) and finished with Detailed design (DD).

1. Literature study
2. Material study
3. Conceptual design
4. Preliminary design
5. Detailed design

This chapter represent the second and third stages of a engineering design process where an attempt will be made to clarify one explicit problem and study it at greater depth, i.e. to investigate the application of ACM in girders of bridges. Based on the literature study [2] the parametric study for all ACM types will initiated, This will followed by searching of alternatives for the typical prefabricated beams. The boundary conditions [4.4] and loads [4.5] are accounted for.

The design philosophy of the new girder should embraced the effective usage of ACM [D] and minimized the use of expensive material where it is not required. In this study several types of girders will be composed by looking at the interaction between the requirements and the material specifications, the so-called Design – Requirements interaction. Requirements in the context of beam composition are given in Table 5.1

<i>Functional requirements</i>	<i>Technical requirements</i>	<i>Material requirements</i>
Span	Strength	Concrete
Width	Stiffness	Reinforcement steel
Height	Stability	Prestressed steel
Load cases	Safety factors	Polymer
	Unity checks	Steel fibers

Table 5.1: Summary design – requirement hybrid bridge deck

5.1 Parametric study

The aim of this section is to obtain experience with the behavior of hybrid ACM girder. Hybrid girder means girder composed from different types of materials while utilizing the material capacities. The problem is heavily simplified in terms of loading- and boundary conditions, such that simple hand calculations can be used to investigate the effects of certain design parameters on the behaviour of the structure. The aim is to determine the technical feasibility of the ACM materials, and get a feeling for the dimensioning of the structure. Each material will be used to design static determined beam in accordance with the corresponded norm. The mechanics equations will be used for the Euler-Bernoulli beam to derive the state of stresses. The boundary conditions and limitations will be according to [4].

5.1.1 Actions

The beam will be subjected to typical traffic-load according to the Eurocode [NEN-EN 1992-2]. Accidental actions and local horizontal actions will for now be neglected. A more elaborate description of the loads and the accompanying values are given in the appendix

F.1] . The following actions which are calculated in spreadsheet, governing for span of 30 m and constant cross-sectional area of 0.9 m².

	q_{eq} SLS [kN/m]	q_{eq} ULS [kN/m]
Live load	20.6	30.6
Dead Load	Self-weight + Asphalt	(Self-weight + Asphalt)*1.2

Table 5.2: Characteristic and design load on the bridge deck with girders of h=1.6 m b=0.6 m

5.1.2 Prestressing

Prestressing is very common application for heavy traffic concrete bridges. Prestressed beams can resist very high bending moment compared to reinforced beam which is governing design parameter for high span/depth ration. And so designing the AMS-beam may include prestressing strands.

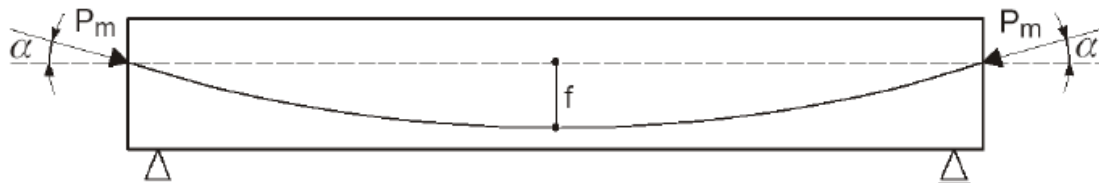


Figure 5.1: Prestressed statically determinate beam using a draped tendon anchored in the centroidal axis

The most important characteristic values of prestressing steel according to the EN 1992-1-1 is given in Table 5.3.

steel type	type	tensile strength		fracture strain	0,1% proof-stress	maximum tensile stress			slope discontinuity in the σ - ϵ diagram (ULS)	modulus of elasticity
						during pre-stressing	during pre-stressing with accurate jack	initial stress		
		f_{pk} MPa	f_{pk}/γ_s MPa	ϵ_{pu} ‰	$f_{p0.1k}$ MPa	$\sigma_{p,max}$ MPa	$\sigma_{p,max}$ MPa	σ_{pm0} MPa	f_{pd} MPa	E_p GPa
Y1030H	bar	1030	936	35	927	773	773	773	843	205 or 170
Y1670C	wire	1670	1518	35	1503	1336	1428	1253	1366	205
Y1770C	wire	1770	1609	35	1593	1416	1513	1328	1448	205
Y1860S7	strand	1860	1691	35	1674	1488	1590	1395	1522	195

Table 5.3: Important characteristics values of prestressing steel [C10]

The prestressing design of the concrete beam is followed by the simplified method given in Appendix F.5.2. The strands are curvature is parabolic resulting in upwards uniform distributed load (q_p).

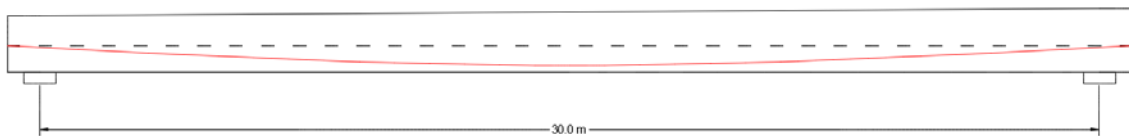


Figure 5.2: prestressing design

The drape of the strands at midspan is:

$$f = \frac{1}{2} * h - c$$

$$c = 200mm \quad \text{concrete cover}$$

The strands are located at the centre of gravity of the fictitious cross-sections at the edges of the beam.

5.1.3 Influence of geometry of the cross-section

A homogenous symmetrical cross-section will be accounted for the calculation of the stresses, which means that the cross-sectional properties become very simple because of the constant Young's modulus.

$$EI_y = E(I_y + A \cdot z^2)$$

$$ES_y = E \cdot A \cdot z$$

In [B10,p61] J.C. Walraven and C.R. Braam studied the influence of the cross-sectional area on the bending moment resistance of a statically determinate beam. Under the assumption that cross-sectional area (A_c) remain constant, the live load (M_q) is variable and the prestressing force $P_m = 1/2 A_c \sigma_{cp}$. The results are given in [Figure 5.3].

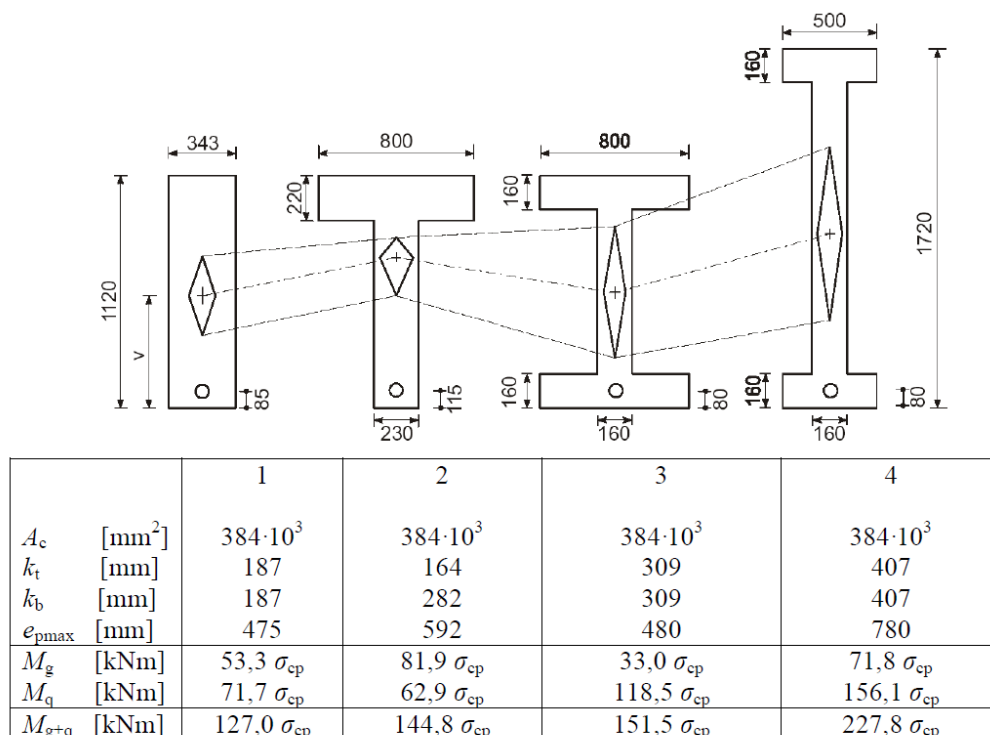


Figure 5.3 Several of cross-section to be accounted for [B10]

The main conclusions of this research is that symmetrical cross-sections are well suited for resistance low dead loads combined with high live loads. On the other hand, cross-

section with one compression flange with high dead load (e.g. selfweight) can sustain only relatively small live loads. Moreover it can be concluded that the greater the height of the kern area in the cross-section, the greater the moment capacity for live loads [B10].

From this it can be said that only substantial reduction of the dead-weight of cross-section with one compressive flange will be favourable optimisation. Symmetrical cross-sections are favourable for smaller spans (<35m) where the live load is dominant.

5.1.4 Constructional aspects

A simple analysis of rectangular beam with $h=1.8$ m and $b=0.5$ m is accounted for the calculation of the different capacities of the ACM beams. In each analysis the governing cross-section is considered. The constants [Table 5.4] will allow to compare only the concrete behavior disregarding the amount of steel.

<i>Constants</i>	<i>Unit</i>	<i>Value</i>
Concrete area (A_c)	m^2	variable
Steel percentage (ρ_s)	%	constant
Young's modulus prestressing steel (E_p)	N/mm^2	190,000
Young's modulus reinforcement steel (E_p)	N/mm^2	210,000
Young's modulus concrete steel (E_c)	N/mm^2	34000 - 58000

Table 5.4: Beam constants



Figure 5.4: The AMS rectangular massive beam. L , h , b are variables

Applying fiber reinforced concrete to a beam in environment of high load levels is impossible without the aid of prestressing steel or reinforcement bars. Compared to conventional beam the fibers will behave as an additional tensile reinforcement increasing the bending strength, but primary will reduce the crack width in the tensile zone. So adding micro-fibers would affect the pre-cracking behavior (UHPC) which increase the cracking moment capacity while and the post-cracking behavior (FRHSC or NSFRC) which increase ductility and reduce maximum crack width. The performance are investigated based on influence parameters:

- Maximum crack width (w_{max})
- Span (L)
- Structural height (slenderness) (d/L)
- Cementitious material (f_{ck} , f_{ctk} , E_c , ρ_s , ρ_{fb})
- Deflection (U_z)

The correlation between the influence parameter and the flexural performance is critical step in determining the application range of the advanced concrete in bridge structures.

Slenderness & Efficiency

The correlation between the bending moment and the curvature (M-k) describes the behavior of simple supported reinforced beam ($\rho_{s,long} = 1.0\%$) under bending load. The reinforcement takes the tensile forces when the concrete begins to cracks. Once the yielding strength of the reinforcement is reached, the deflection will increase without further increasing of the bending moment. The cracks in the beam will progress from the tensile zone into the compression zone, the compressive zone will get smaller and smaller until the beam will fail. The diagram bellow [Figure 5.5] explains this beahvoir for conventional concrete. The M-K curves under pure bending load will initially response elastically, followed by elasto-plastic behavior caused by yielding of steel, and finally fully plastic behavior with infinite curvature.

Structural height is strongly related to the maximum bending moment. The resistance moment depends on height squared. However functional requirements as clearance-height

under the bridge and abutment heights of the substructure often governing parameters for the construction height.

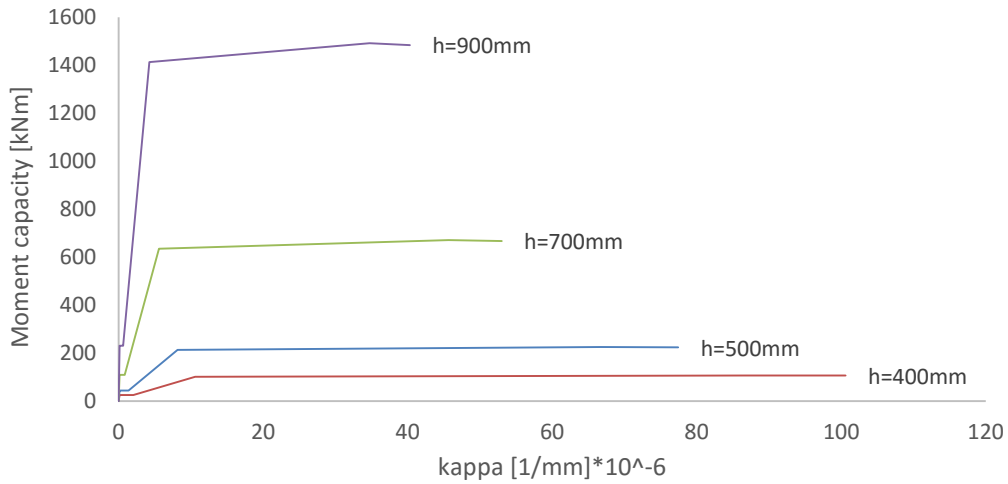


Figure 5.5: M-K diagram as function of girder height

The M-K diagrams for other types of concrete than conventional concrete valid for slender members only is presented [Figure 5.6]. It can be used for quantitative understanding the effect of fibers. It can be said that hybrid variant, thus combination of fibers and traditional reinforcement will characterise with favourable post-cracking behavior. Means adding bending resistance to the member once rebar yield. It is hence favourable for limiting the amount of longitudinal reinforcement and shear stirrups.

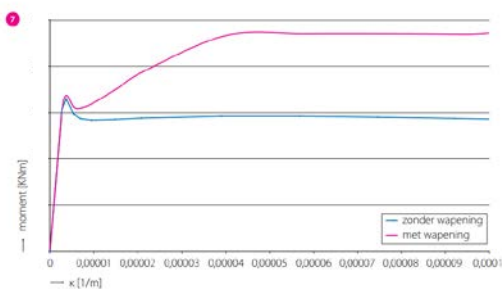


Figure 5.6: M-K diagram FRC¹ with/without conventional reinforcement [Cement 2010/6]

¹ FRNSC = Fibre reinforced normal strength concrete

In [Figure 5.7] cross-sectional analysis based on experiments results of FRC girder is presented. By greater heights is the permissible tensile strain decreases, this is due to the pull-out effect of fibers. Concluding that member's height should be limited when applying FRNSC subjected to bending where no traditional reinforcement are added.

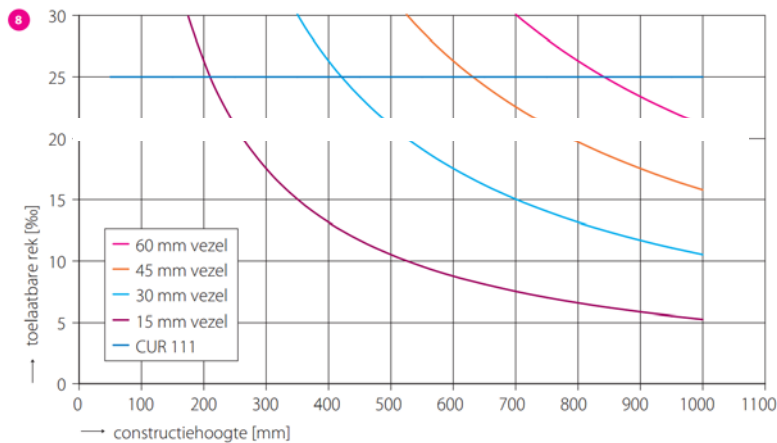


Figure 5.7: Permissible strain as function of member height

One more aspect of the girders cross-section is related to the application of prestressing together with advanced concrete. In [Figure 5.8] four concrete girders under pure external tensile load of $N_t=1000\text{kN}$, the amount of prestressing applied A_p is constant. The only two variables are the maximum allowable compressive stresses by prestressing ($\sigma_{max} = 0.6f_{ck}$) and the cross-sectional area of the concrete A_c . The steel ratio will change proportionally to the concrete area. The upperbound curve in [Figure 5.8] is based on the maximum compression stress while the lower bound curve is based on the requirement of no tensile stresses may occur.

It can be conclude that when applying high performance materials it is possible to utilize its strength capacities by reducing the cross-sectional dimensions. Means increasing the slenderness of the member, high efficiency, and reduced crack size. The slenderness of the members will be however limited by other requirements as sufficient concrete cover prestressing (durability), and space for anchorage. It may increase the member dimensions and reducing its efficiency.

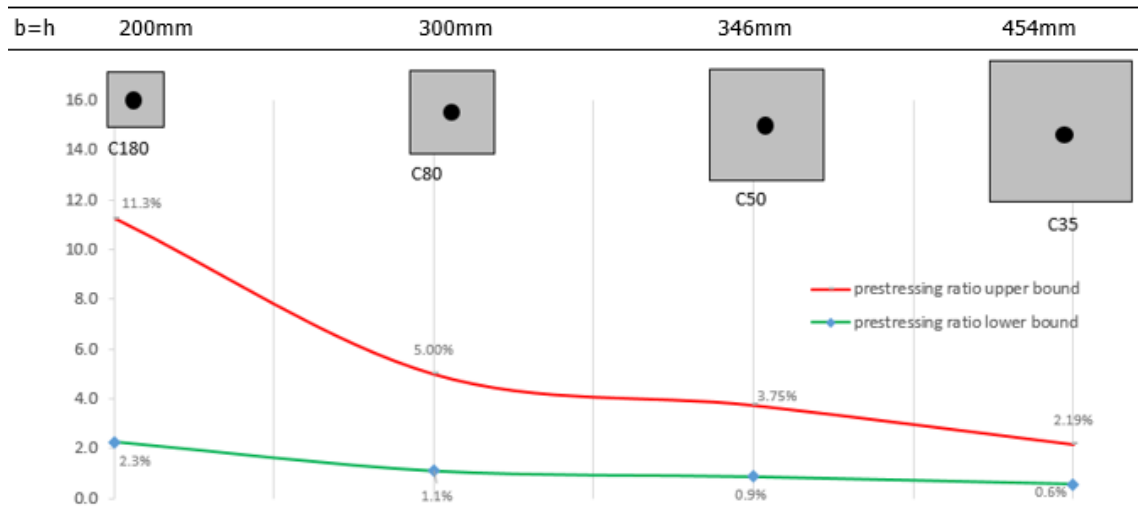


Figure 5.8: Cross-sectional efficiency for different concrete classes

Crack width

Crack control in girders which are fully prestressed (no tensile in concrete allowed) makes no sense. However it is practically impossible to guarantee that prestressed concrete remains uncracked. On the basis of this important conclusion, a new way of prestressing was developed, the so-called partial prestressing, which allows controlled crack formation.

Serviceability limit state cracks in precast concrete are not harmful from durability point of view when the cracks width is controlled. It possible to combine passive (reinforcement) and active prestressing allowing small tensile stresses at the bottom flange. This results in economically prestressing design. Please note, this may be applied only to the main load bearing direction, while in the transverse direction only reinforcement are applied.

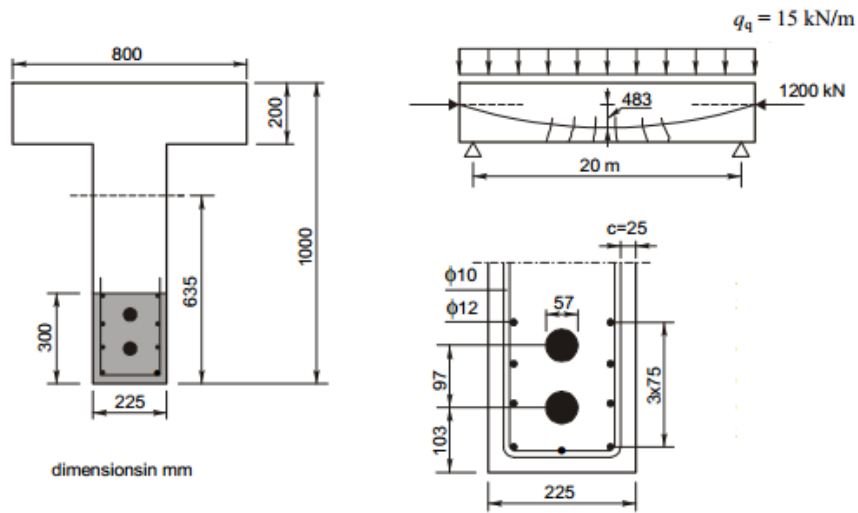


Figure 5.9: Crack control with prestressed beam [CIE4160]

Furthermore, the loads to which the structure is exposed during the life time cannot be exactly determine, means potential cracking of the concrete. For smaller cross-sectional dimensions of the concrete member creep and shrinkage will develop faster causing redistribution of stresses and unexpected cracking. In example [Figure 5.9] combining prestressing steel and reinforcement steel is limiting crack width.

The effect of altering the concrete class on the crack width is investigated. In [Figure 5.9] the girder is partially prestressed, 50% of the fully prestressed initial force (P_{m0}) is applied. The cracking width is calculated according to [EN-NEN 1992-1-1]

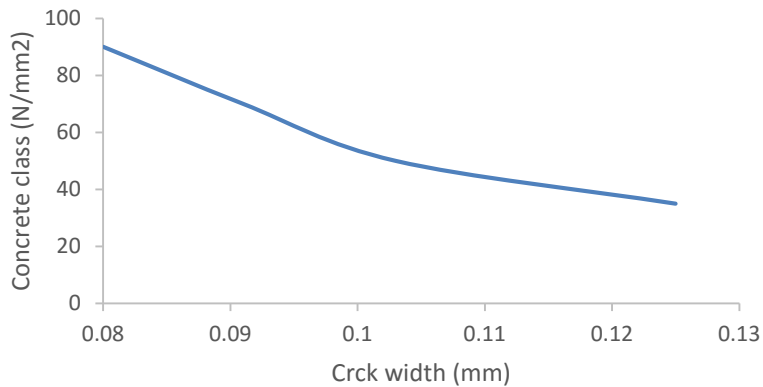


Figure 5.10: Crack width

Crack width UHPC

Alter the cross-section and span to: $L=40$ m, $h_f=170$ mm, $h=1500$ mm, $b_w=225$ mm, $b_f=1200$ mm. Use UHPC serviceability performance calculation [Setra] and derive the relation between crack width and amount of prestressing.

The derivation of the crack width for UHPC is according to [B14, p445] [C10] [SETRA] with the following equation:

$$w_{max} = 2 \cdot S_{r,max} \cdot (\sigma_s - 0.5\sigma_{sr}) \cdot (1/E_s)$$

According to [Cement - Rekenmodel VVUHSB] the value of $S_{r,max}$ is difficult to determine. This parameter represent the distance between the cracks in the tensile zone. It is not clear yet how the bond, effective area, fibers orientation influencing the magnitude of $S_{r,max}$. In [SETRA] it is defined as $(2/3) \cdot h$ while in [CUR-111] it is defined as $h-h_z$ [Figure 5.11].

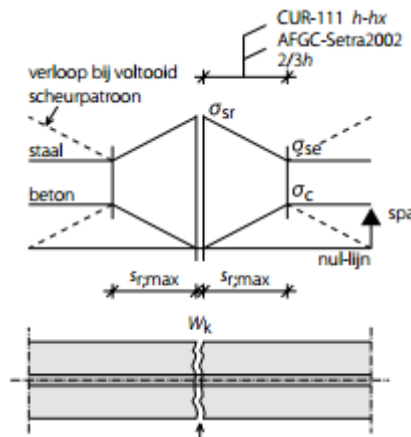


Figure 5.11: Characteristic length [Cement Rekenmodel VVUHSB]

In [B14, p445] the influence of the fibers on the crack width control is investigated for structural members with combined reinforcement and fibers. The fibers shape, slenderness, bond, pre-peak strength, post-peak strength are taken into account in this investigation. The value of $S_{r,max}$ is determined according to:

$$S_{r,max} = \frac{(f_{ctfm} - \sigma_{cf}) \cdot d_s}{2 \cdot \tau_{sm} \cdot \rho_{eff}}$$

Where d_s is the diameter of the reinforcement bars (12mm), and the bond stress is assumed to be constant $\tau_{sm} = 3.3 \cdot f_{ctm}$ ($f_R = 0.072$, $w_k = 0.10\text{mm}$). According to some researches the bond stresses UHPC can be up to UHPC bond $\tau_{sm} = 5 \cdot f_{ctm}$ [B01 p151], where f_{ctm} is the mean value of the elastic tensile strength of concrete in the un-cracked stage, this is equals to 10.27 N/mm^2 [SETRA – mean direct tensile strength]. The σ_{cf} is the tensile stress transferred by the fibers in the crack (pull-out strength) [Error! Reference source not found.], the contribution of the fibers in tension can be determined depending on the actual crack width. Simplification for SLS in $w > w_0$ stage is the characteristic value (maximum value) corresponding with w_0 .

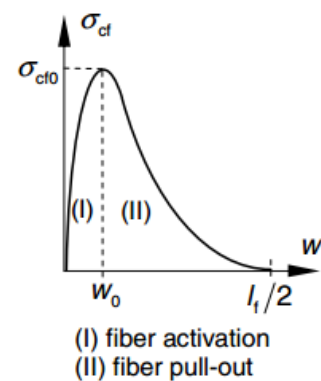


Figure 5.12 stress-crack opening relationship of UHPC

$$w_0 = \frac{\tau_{sm} \cdot l_f^2}{E_f \cdot d_f} = \frac{3.3 \cdot 10.27 \cdot 25.4^2}{210000 \cdot 0.4} = 0.26 \text{ mm}$$

$$\sigma_{cf}(w_0) = 0.484 \cdot \sqrt{f_{ck}} = 0.484 \cdot \sqrt{170} = 6.22 \text{ N/mm}^2$$

The results are presented in [Figure 5.13] shows reduction of the crack width by applying UHPC compared to conventional prestressed concrete. Moreover the maximum magnitude of the prestressing force is limited by conventional concrete due to low compressive strength.

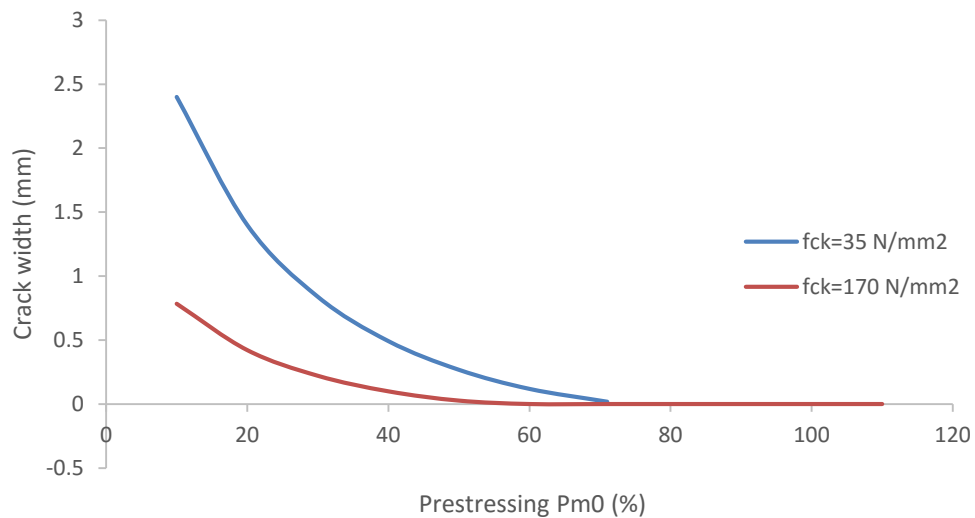


Figure 5.13: Crack width as function of the applied prestressing

5.2 Structural concepts

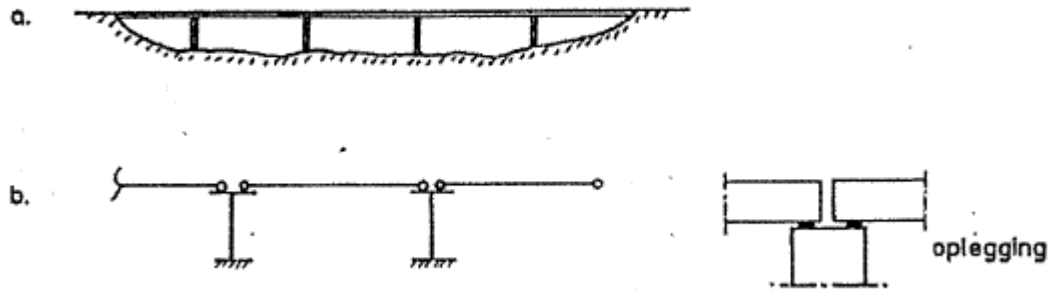


Figure 5.14: Structural concept

The conceptual study starting point is a static determined beam. The technical requirements, design requirements and functional requirements [Table 5.1] are governing for the design of the hybrid beam. The material properties [2] the stress-strain behavior [], the durability [3] the actions [4.5] and the results obtain earlier in this chapter are aspects which will be accountable for the hybrid design of the beam.

Initially, the topological shape of the beam is limited to a rectangular shape with discrete height and width and thickness. This volume will be define as the design domain where the critical region regarding the stiffness and strength will be identified. In the beam level, based on known material properties the best suitable material will be assigned to each region.

Later on the shape, size and material topology will be optimized by looking at standard parameters such as: Compressive/tensile/shear strength, modulus of elasticity and density. These parameters will be distributed within the design domain.

5.2.1 Simple beam

By means of thumb rules and common girder dimensions the girder concept can be sketched. The fundamental structural aspect discussed in [4.6.4] are used in this section. The depth/span ratio should be as high as possible resulting in slender design. A statically determined beam [Figure 5.15] is loaded with uniform load.

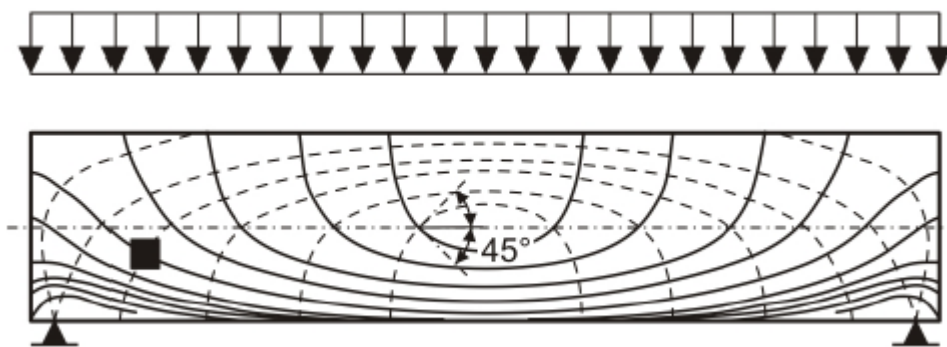


Figure 5.15: Principle stresses trajectories in uncracked simple supported beam [B03]

The stress solution of the beam [Figure 5.15] under the stated load is associated with the principle trajectories, this forms the principle stress values for which each small element only compression (dashed line) and tension (line) are activated. Places where the trajectories lying close by each-other exhibit greater normal forces. For instants at midspan outer fibers. With the constitutive, equilibrium and kinematic relationship the unknown displacements, stresses and the strains can be found.

The trajectories can be transformed into bending moments, shear forces and normal forces. These are discussed in the following sections

5.2.2 Flexural capacity

Consider a statically determinate simply supported beam of homogenous, linear-elastic material [Figure 5.16].

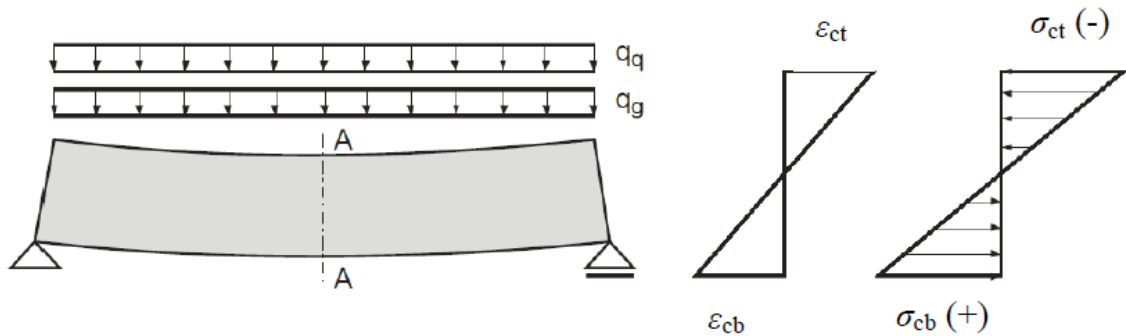


Figure 5.16: Stress as a result of uniform dead and live loads in a linear elastic beam [B10]

When the concrete cracks, a new equilibrium system is formed. The reinforced beam will be in equilibrium by the two force components, the compression strength and the tensile steel reinforcement. This conventional (hybrid) beam with steel and concrete is designed for optimal material usage following simple design principles. When the concrete is cracked the compressive forces follow the compression arch to the supporting points [Figure 5.17].

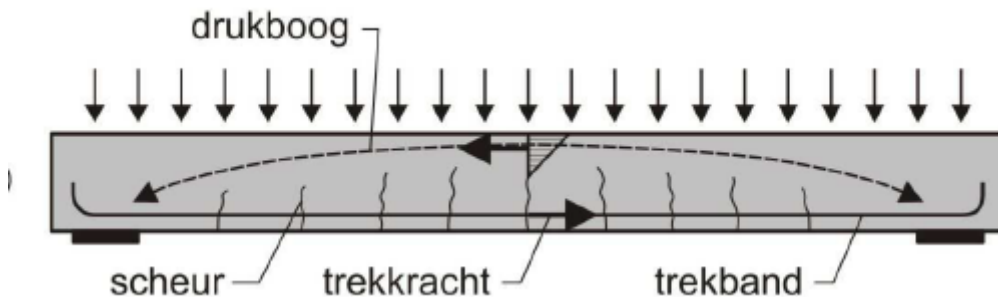


Figure 5.17: Force flow in cracked concrete

As the ductile behavior of the steel reinforcement is major advantage reinforced beams are very common. The plastic deformation capacity of steel is large which means the beam will crack and deflect before failure. The longitudinal reinforcement percentage in typical beam is between 0.6 – 1.2%.

When the span of the beam is small the concrete compressive force will follow a diagonal line between the supporting point and the applied force while the tensile force will be acquired by the steel tensile bars [Figure 5.18]

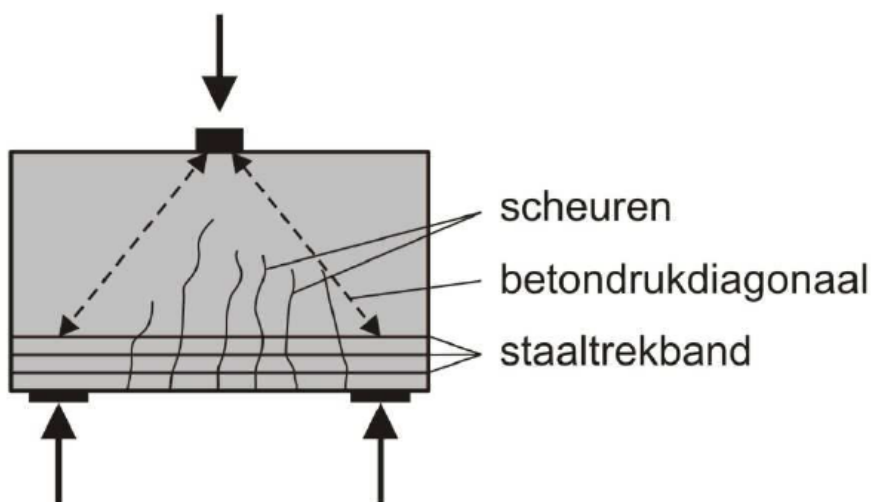


Figure 5.18: Compressions lines

It is important to remember this fundamental principles during the design of the girder

5.2.3 Shear capacity

This is the more complicated force component. Generally combination of the bending and shear forces result in oblique tensile forces in the web of the beam. As result the cracks will form perpendicular to the tensile forces in the oblique directed to the supporting points. Without shear reinforcement the concrete will have to contain this forces. Conventional concrete in heavy traffic bridges cannot deal with the high shear forces caused by the traffic load without shear reinforcement.

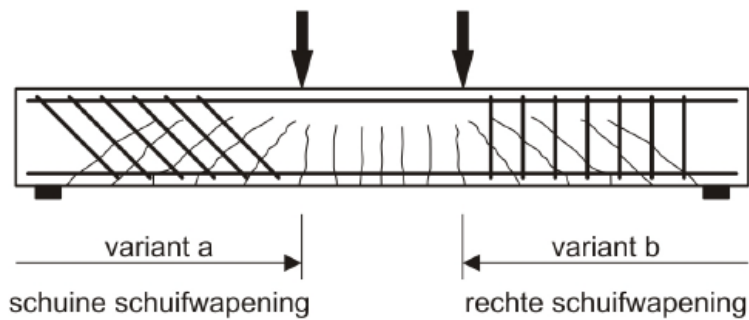


Figure 5.19: Shear behavior of simply supported beam

In this research the shear behavior of the beam will be a critical design parameter. In the scope of this research an attempt to reduce or to eliminate the percentage shear reinforcement by applying concrete with higher shear strength, adding fibers or by mitigating the oblique tensile forces through changing the orientation of the material.

In the zone where bending moment is dominant, and the shear forces are negligible, quasi vertical flexural cracks will develop. In the zones where high shear forces observed, inclined cracks develop. There are two types of inclined cracks: Flexural shear cracks and tensile shear failure

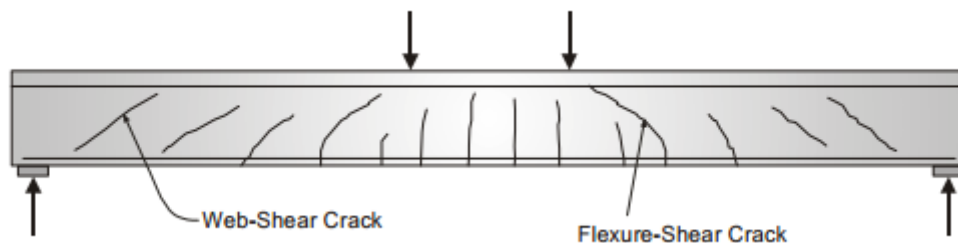


Figure 5.20: Cracked concrete beam

The flexural shear cracks are result of vertical flexural cracks which initiate from the bottom fiber and gradually bended with the height of the beam developed into a shear crack. This type of primary cracks will develop with secondary cracks at the longitudinal reinforcement. The shear failures in this case are shear tension failure (when cracks develop nearby the supports), and shear compression failure (when concrete is shattered at the top of the crack).

a) Diagonal tension failure, (b) bursting concrete upper zone crack, compression zone, (c) shear tensile failure, and (d) shear compression failure

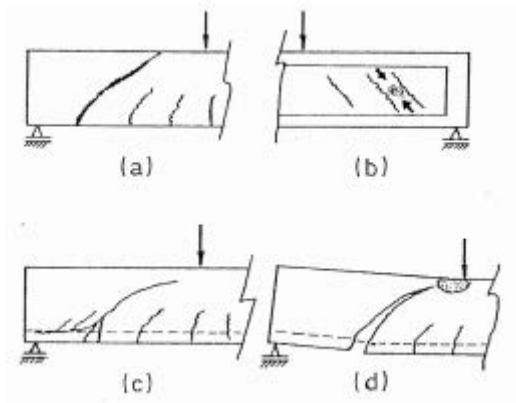


Figure 5.21: Shear failure modes

Explanation:

- (2) Aggregate interlock decreases with the crack opening and with the roughness of the crack surface (stiffness aggregate and matrix, diameter aggregate)
- (3) Dowel action longitudinal reinforcement cause tensile stresses in the concrete around the rebars. This can cause splitting cracks. The contribution for the shear resistance is limited.
- (4) Occur only when the a/d ratio is smaller than the critical value. The beam/plate will fail in shear-compression

Conventional methods to increase shear resistance:

- Increase the longitudinal reinforcement bar ratio, than the height of the concrete compression zone will increase, the crack width will decrease. This will follow by increasing of aggregate interlock and of the dowel action of the longitudinal reinforcement
- Decrease the ratio of the height of the beam/plate and the maximal aggregate diameter (h/d_g) .
- Increase compressive strength concrete to increase the concrete tensile strength result in longer uncracked phase and cracks which are less developed. This will increasing shear strength of the compressive zone and the dowel action.

- Apply stirrups to increase shear strength and to prevent the occurrence of brittle failure caused by inclined cracks. Applying stirrups will allow to increase the load without risking brittle failure

5.2.3.1 Brittle failure

Typical heavy-traffic bridge beam may not fail due to brittle shearing. Without shear reinforcement (steel stirrups) shear crack developed in the compression zone will continue to develop vertically and then horizontally owing to parallel shifting of the cracking planes caused by the beam deformation.

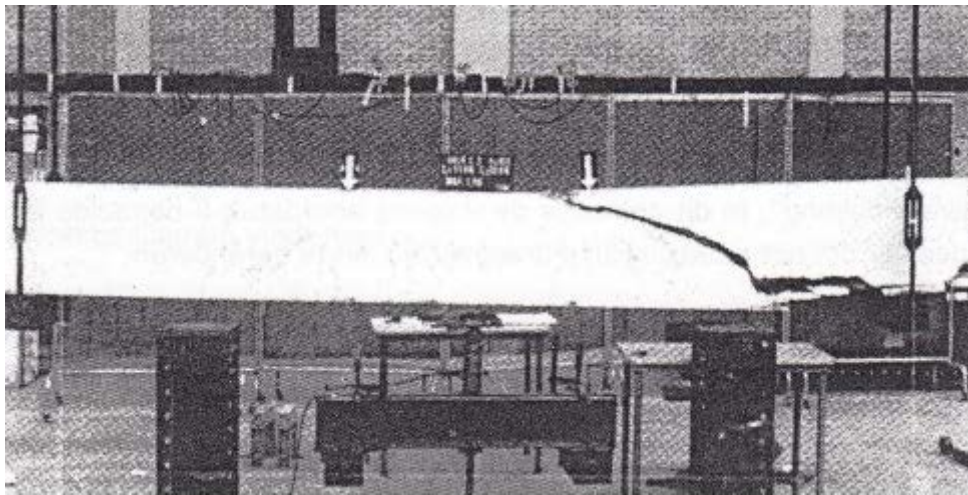


Figure 5.22: Brittle flexural shearing of beam without shear reinforcement

The beam [Figure 5.20] shows the crack pattern for displacement control ultimate limit state load. First vertical shear cracks appears at the compression zone, the shear cracks jumps to flexural cracks, the cross-section tries to find equilibrium unsuccessfully so the crack begins to propagate horizontally in the direction of the support. Eventually the beam fails in shear cause while the bending bars are not yet yielded. This has to do with the span-to-depth ratio $a/d \leq 2.5$.

5.2.3.2 FEM shear model

Due to the complexity of the shear failure mechanism universities around the globe conducted studies trying to comprehend and predict the shear failure. One research conducted at the TUDelft [Laurens Bouvy, 2010] models the shear failure mechanism for I-profile UHPC beam in DIANA [Figure 5.21]

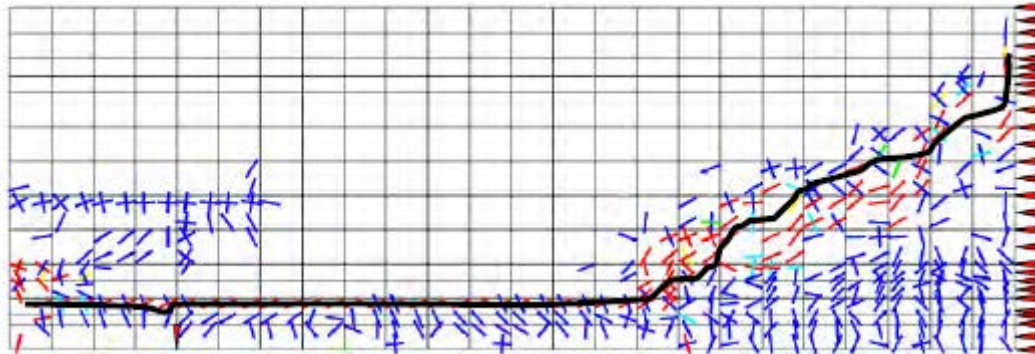


Figure 5.23: Crack pattern at ultimate failure

The FEM of UHPC without stirrups or fibers fails seems to correspond with the lower boundary value according to the Dutch VBC code:

$$V_{max} = \tau_1 * h * b$$

$$\tau_1 = 0.2 * f_{ctm}$$

One interesting conclusion of this research is that the shear capacity of the beam without stirrups but with 2 vol% steel fibers will dramatically increase due to longer tensile – softening behavior: higher tensile strength, higher fracture energy [Hordyk model].

5.2.3.3 Behavior nearby support

Beam subjected to uniform load [Figure 5.22] exhibits the largest shear forces nearby the supports. However the uniform load at that region (region I) is transferred by compression of the concrete to the bearings. This direct bearing of the load is favorable but is limited by the large ratio of $L/d < 2.5$

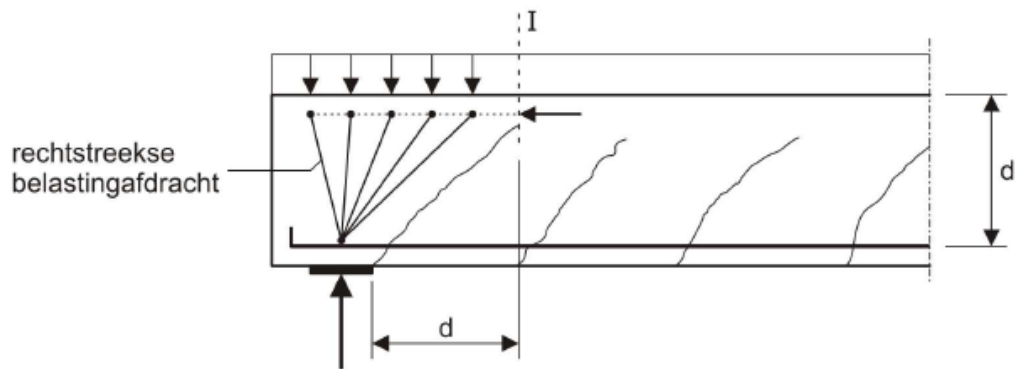


Figure 5.24: Behavior nearby support

Engineers adding usually massive anchorage block to the edges of the beam in order to increase the shear capacity which is larger than the increase of the shear force due to the extra weight. This anchorage blocks are also important for the transfer of prestressing forces nearby the support. Though this won't be the governing design criteria's for the beam.

5.2.4 Bending stiffness

The bending stiffness of a beam consist of the E-modulus (material) and the moment of inertia (geometry).

5.2.4.1 Modulus of elasticity

The modulus of elasticity for CC (up to C90/105) can be calculated by the empirical expressions given by the Eurocode and can be approximated according to the CUR-97 (CUR aanbeveling Hoge sterkte beton commissie)

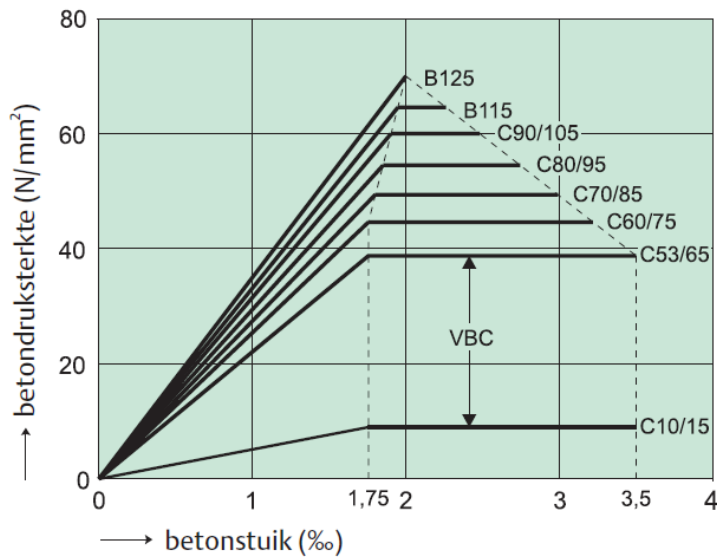


Figure 5.25: Stress-strain diagram according the CUR-recommendation

However the CUR cannot supply any recommendation concerning the calculations rules of concrete with higher class then C90/105. Hence the expressions valid for concrete up to C90/105 class is found reliable lower-limit values. For example the mean elasticity (E_{cm}) of C170/200 in accordance with the CUR-97 is 52,000 N/mm² while in practice the mean elasticity scatters between 50,000 – 70,000 N/mm². Creep and shrinkage effects are not taken into account.

5.2.4.2 Moment of inertia

As mentioned also the moment of inertia affects the bending stiffness:

$$M_z = E * I_{zz} * K_z$$

$$\varepsilon(z) = z * K_z$$

$$\sigma_x(z) = E * \varepsilon(z)$$

Which can be re-written into:

$$\sigma_x(z) = E * z * K_z = \frac{M_z * z}{I_{zz}}$$

$$M_z = \frac{\sigma_x(z) * I_{zz}}{z} = \frac{f_{ck} * I_{zz}}{z}$$

For non-symmetrical inhomogeneous beams the uncoupled expression are used:

$$M_z = \frac{f_{ck} *}{z * \sum(EI_{zz})_i}$$

We see that geometrical factor, the moment of inertia (I_{zz}) contribute to the bending stiffness of the beam. Maximizing this value will maximize the efficiency of the cross-section, material with high elasticity should be located as far as possible on the z-axis correspond with high bending stiffness. High I_{zz}/z ratio is therefore governing for the bending capacity of the cross-section under bending loads.

5.2.4.3 Optimal cross-section

Regarding the normal stresses in a cross-section the material with the lowest strength is governing (either compressive or tensile). Hence the cross-section with material put at the outer fibers would be more efficient. Thus shapes like T-profile and I-profile are having effective material usage. The theoretical optimum of a cross-section is reached by two zones loaded to full capacity: Tension and compression zones.

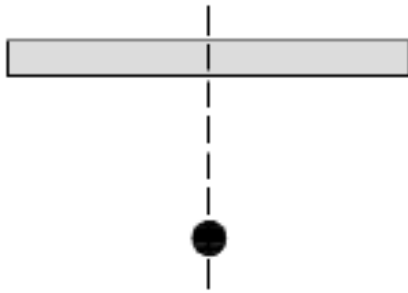


Figure 5.26: Optimal bending moment cross-section

5.3 Fibers Reliability

5.3.1 Shear

It is important to distinguish between two different types of fiber concretes. On the one hand conventional fiber reinforced concretes, with coarse aggregates particles and large steel fibers. This is the first type of composite concrete. And on the other hand the modern types of high performance fiber concrete, with small aggregate particles and fillers, reinforced by fine, short fibers. A third option is a combination of both types of composites.

The hybrid action of concrete and fibers is different for FRC and HPFRC and therefore the role of the fibers in the structure. In conventional reinforced fiber concrete the large fibers will be activated when major cracks in the concrete will occur, just like traditional reinforcement. In HPFRC the fibers are much smaller, they are activated when micro-cracks occur from the moment that the structure is loaded, just like composite material. As mentioned combining different types of fibers may optimize the mechanical properties provided that the design rules can cope with such challenge.

Valid for concrete class up to C50/60. Brite Euraam project suggest design method for plates and beams with traditional longitudinal reinforcement. With the proposed expression the fiber contribution to the shear carrying capacity can be computed [Figure 5.27]

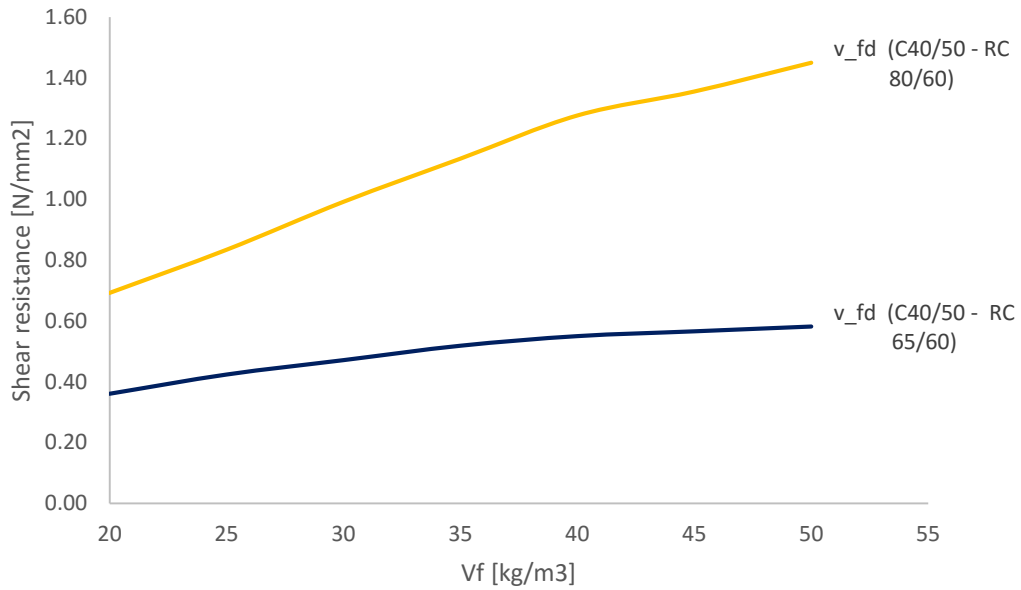


Figure 5.27: Shear contribution fibers (RILEM)

	<i>Length</i>	<i>Slenderness</i>
RC 80/60 BP	$L_f = 60mm$	$\frac{L_f}{D_f} = 80$
RC 65/60 BN	$L_f = 60mm$	$\frac{L_f}{D_f} = 60$

Table G.5

R= Hooked edges,

C= fibers are glued together in plate form

B= bight (without cover layer)

P= High carbon content, high tensile strength $f_y > 200,000 MPa$

N= Low carbon content, normal tensile strength $f_y = 200,000 MPa$

Designing bridge with steel fibers as replacement for the traditional stirrups introduce unknown degree of uncertainty. The disadvantages of this ACM are primary related to the material properties dispersion during production and execution. The uncertainty lies on the discontinuous material properties supported by large scatter of the bending tensile tests compared to the traditional reinforced concrete. Not only has the nature of the production of the FRC affected the limit state design, but also the execution phase. Mistakes can be made by the contractor during the execution phase leading to bad quality. It is essential that actors in the infrastructure sector would be capable of guaranteeing excellent FRC quality.

Applying of FRC will be probably be applied as replacement minimum reinforcement for element with large dimensions. For massively reinforced concrete elements traditional reinforcement will stay the ultimate solution. Combining of both types of reinforcement would probably be the best option. The quality of the FRC is highly related to the several of factors which are part of the basis governing failure mechanics of FRC, the fiber pull-out:

- Orientation of the fibers
- statistical distribution in the mixture
- Efficiency of the fibers in the mixture
- Bond levels between fiber and concrete: Mechanical, friction, adhesion, interlock
- Reliability in limitation size of grain to increase random fibre orientation and distribution
- Packing density

5.5 Design alternatives

Now with the aid of the parametric study [5] and the structural concepts [5.2] a few concepts for girder design will be discussed.

5.5.1 Variant 1. Arch²

Although bridge designer will tend to work with straight lines rationalizing execution the application of arch-like construction in the bridges industry may be very attractive or designers regarding its stresses distribution. The perfect form of the compression arch (pressure line) subjected to uniform load can be obtained by mirror position of simple curved chain (Antoni Gaudi, 1852-1926).

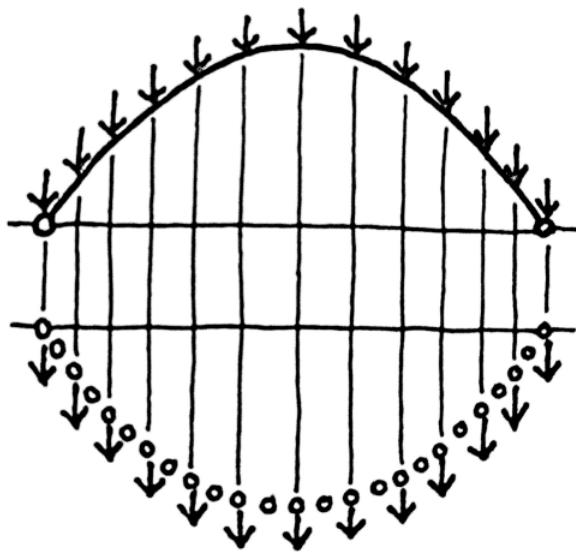


Figure 5.28: Mechanical schematization of chain and arch [B14]

The arch forces transfer is based on mainly compression forces. The arch axial stiffness is the dominant parameter besides the bending stiffness.

Applying the arch theory into the Euler - Bernoulli beam bending theory with the live-load distributed to the supports along the pressure lines. In this way the arch element is

² . Arch [John R. Hilman, HC bridge company]

subjected to mainly compression forces which associate with reduction of the required material.

5.5.1.1 Idea and concept

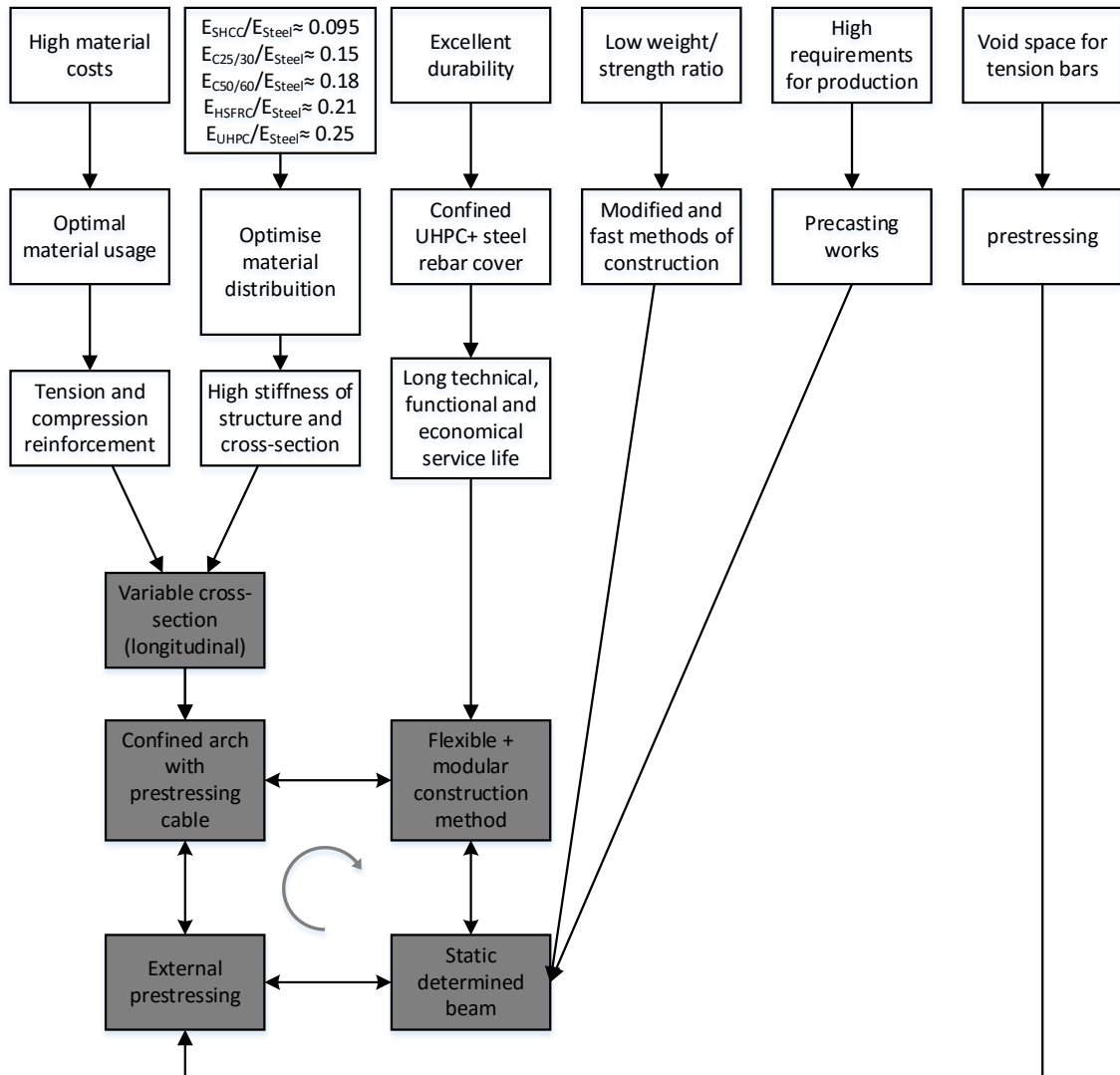


Figure 5.29: construction principles

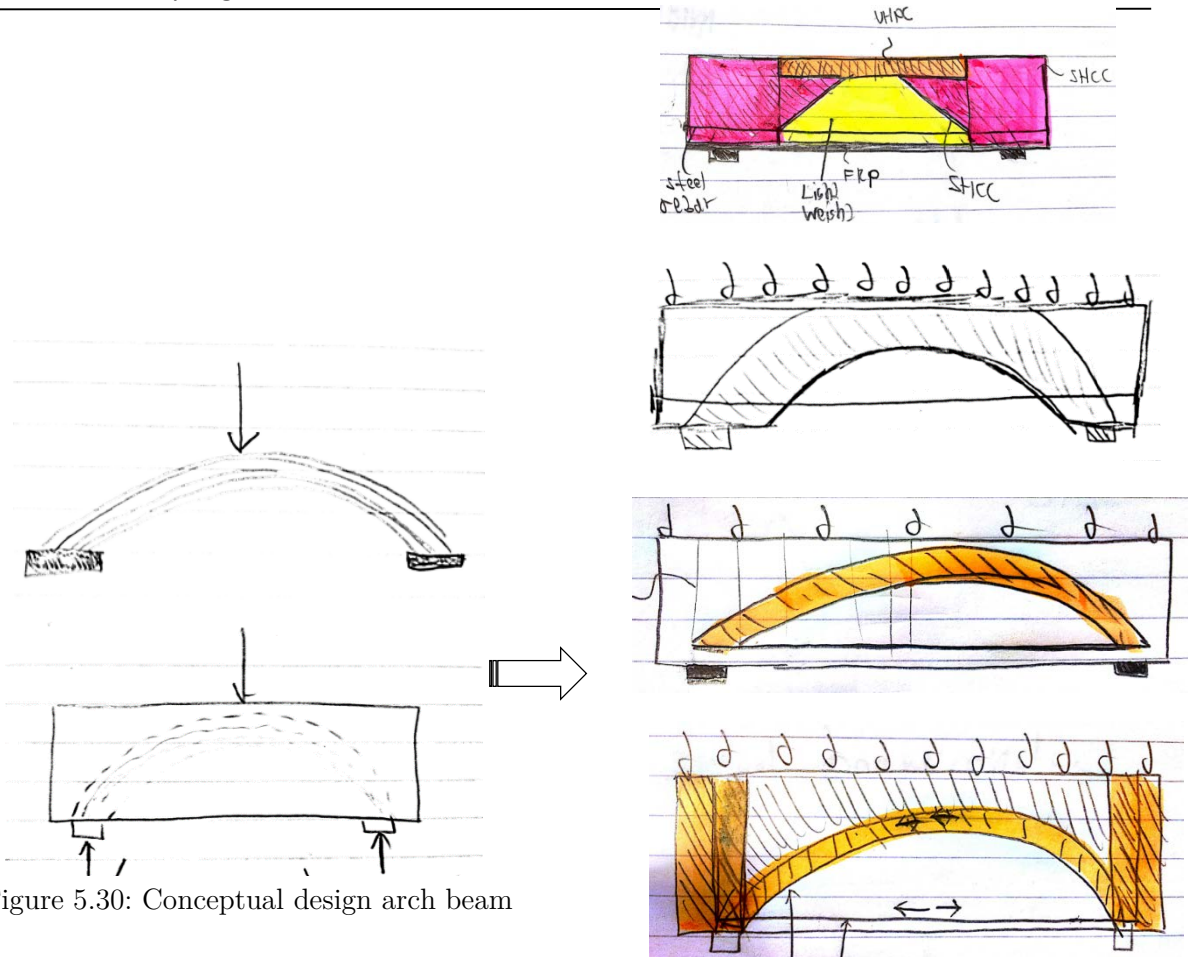


Figure 5.30: Conceptual design arch beam

The concept of this beam is very simple, a high strength concrete arch spans between the supports with rise limited by the beam height. This element is purely the compression reinforcement. The arch may be confined by FRP-shell in order to increase its compression capability and to resist buckling, shear and bending moments. At the edges massive anchorage block takes the horizontal force component from the arch, increasing shear capacity at the edges and practical solution to the anchoring of the prestressing cables which function as the tensile reinforcement.

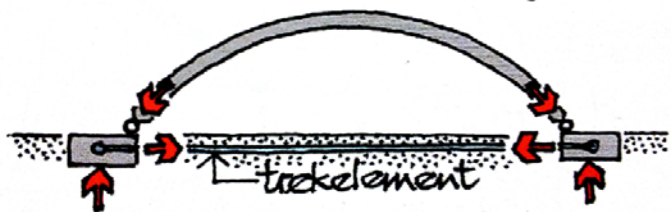


Figure 5.31: The main idea of the load transferring system [B14]

Now when first draft of the load transferring elements is accounted for, the other technical requirements [Table 5.1] can be handled. As mentioned in [4.7.3], the shear resistance is one of the governing design aspects. Adding massive concrete block at the edge of the beam is beneficial to the shear resistance where the maximum shear load is present. The white area in Figure 5.29 represent the unused design space. Correlating the shear force distribution arch beam result in

In the increasing of the material requirement nearby the supports and possibility to save material about the midspan.

The light grey colour of the arch beam [Figure 5.30] can be considered as the web and therefore AMS with high shear capacity as SHCC or HSFRC will be applied.

The voyage under the arch can stay open or filled with ultra-light weight foamed concrete to increase the durability.

The durability of the rebars can be increased by thin cover of SHCC concrete or other concrete with large tightness.

The shape of the design is optimised to bear the near-uniform forces arising from the dead-loads, which is the dominant load. The critical load is found by plotting the influence lines. For uniform load, this is often loading a half-span.



Figure 5.32: The arch beam, first considering compression forces and then adding tensile element

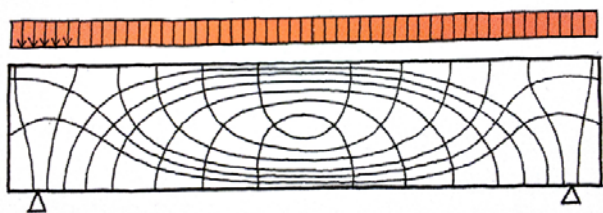


Figure 5.33: Shear distribution embedded in the design, steel bars covered with SHCC

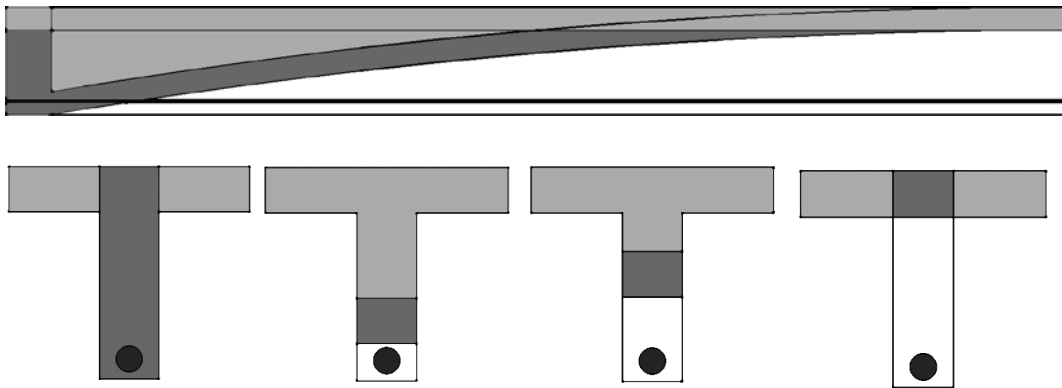


Figure 5.34: Cross-sections for different longitudinal locations

5.5.1.2 Continuity

Lines or surfaces can be connected with different levels of continuity. There are four levels of continuity:

- C0 – lines/surfaces just connected $\frac{dy_1}{dx}(x_0) \neq \frac{dy_2}{dx}(x_0) \rightarrow \varphi_1(x_0) \neq \varphi_2(x_0)$
- C01 – tangents of the two surfaces lines/surfaces are the same at the connection line $\frac{dy_1}{dx} = \frac{dy_2}{dx} \rightarrow \varphi_1(x_0) = \varphi_2(x_0)$
- C02- The curvature of two surfaces are the same at the connection line $\frac{d^2y_1}{dx^2} = \frac{d^2y_2}{dx^2} \rightarrow \kappa_1(x_0) = \kappa_2(x_0)$
- C03 – The third derivative of the surface shape in the direction perpendicular to the connection line at the connection line $\frac{d^3y_1}{dx^3} = \frac{d^3y_2}{dx^3} \rightarrow V_1 = V_2$

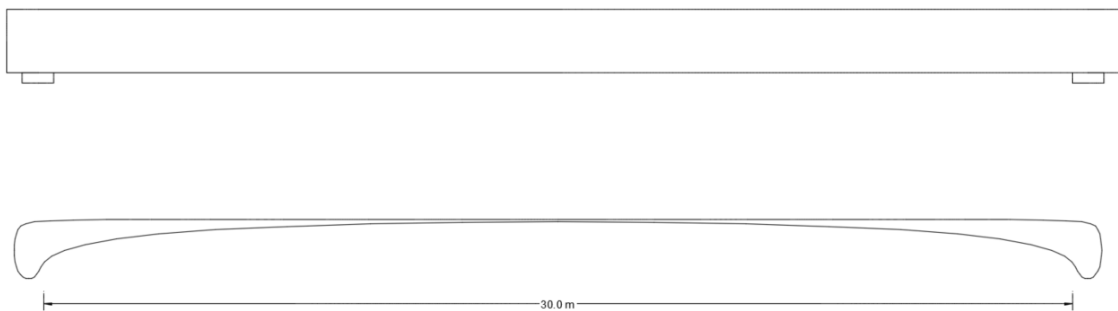


Figure 5.35: Using splines to draw the arch within the design domain (C02 continuity)

5.5.1.3 Optimal cross-section

From previous research of research of T.J.P.M de Goede, 2011 [T06] it has been found that the efficiently and effectiveness regarding the shear stress line of the cross-section are the best for rectangular cross-section. However for bending moments I-profiles would perform better. Hence, it may be prove to be effective to use both cross-sections in different locations on the bridge with considerable material saving by application of voids. By doing so the load M_{Ed} is decreased. It can be concluded that combining different cross-sections into one bridge girder design is probably advantageous since the governing cross-sectional checks aren't located at the same positions.

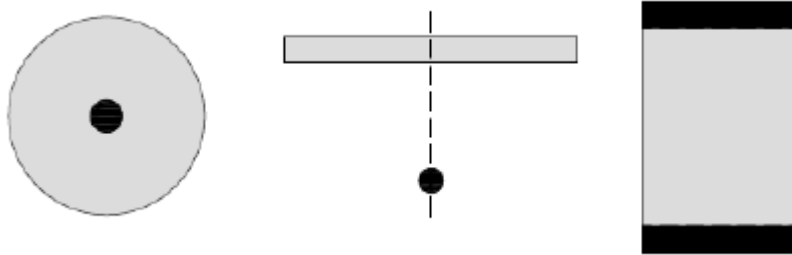


Figure 5.36: Optimal shapes for normal force, bending moment and shear force [T06, p45]

Looking at the cross-section located at the beam edge [Figure 5.31] ignoring the flanges resulting in slender rectangular cross-section. When the shear force line decreases (linearly) and the bending moment line increasing (quadratic) web will get smaller and smaller. Further optimisation of the structural performance may be sought in massive rectangular cross-section at the edges of the beam instead of T-beam. This conceptual design may include design alternatives such as circular compressive arch instead of rectangular which is preferred due to stability issues. The thickness of the upper flange can be further optimise by allocating high capacity material to the top fiber whilst the rest of the flange consist of normal capacity material (economically). Furthermore, adding fibre reinforced polymer sheets confining the beam is suggested for increasing shear capacity.

5.5.2 Variant 2. Topological optimization

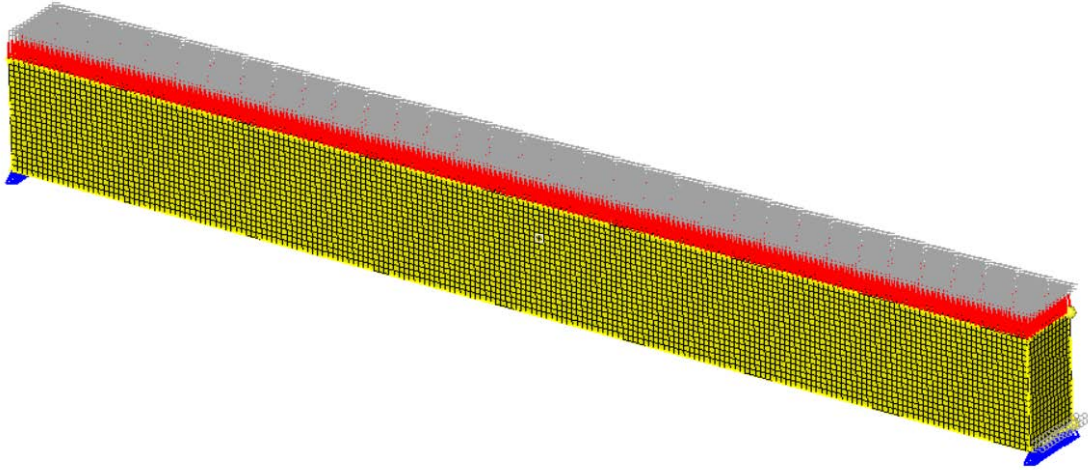


Figure 5.37: Static determined beam with design region $L=20\text{m}$, $h=2.0\text{m}$ and $b=1.2\text{m}$

This variant will be introduced without extensively description of the theory of topological optimization. Further information is available in various of literatures. The topological optimisation of the geometry and topology of structure lay-out has great impact on the performance of structures. With mathematical approach the design space of the beam [Figure 5.34] will be optimise for a certain loads and boundary conditions.

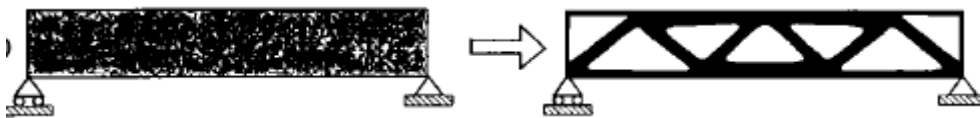
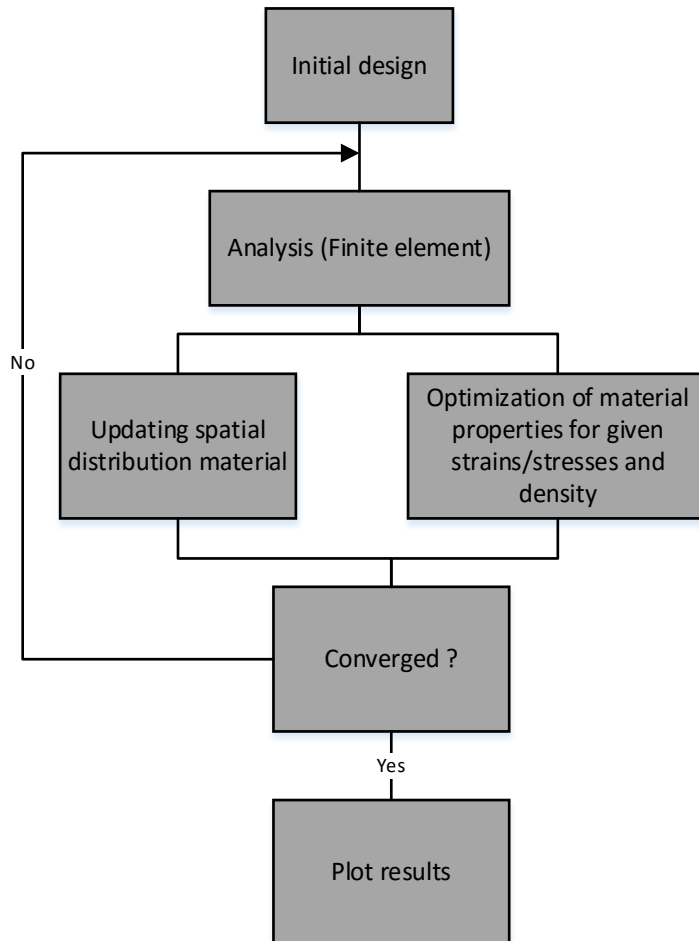


Figure 5.38: The initial problem on the left hand side and the optimal solutions are shown on the right

5.5.2.1 Idea and concept



5.5.2.2 Design procedure

Initially the design space, boundaries, material properties and loads are determined and entered into the FEM software. In the second step the topological optimisation response, objectives and constraints are determined. Based on the stresses distribution, displacements and stiffness of the entered start structure the finite element algorithm will eliminate parts of the structure which have the least contribution. In the following iteration these parts are no longer considered in the design space. The process will repeat until the design has been reached to the in advanced defined constrains.

The final optimal structure can be further analysed by export the model to other finite element package such as ANSYS or DIANA where it can be meshed and analysed.

Design input Hypermesh:

The model beam is meshed with 3D quadratic elements with the following properties:

Total DOF's	64,554
E-modulus	26000 N/mm ²
G-modulus	8000 N/mm ²
Poisson's	0.15
Load	27 kN/m ²

Optimization defines with the following input:

Optimization responses

Weighted compliance (strain energy): Response from load case

Volume fraction: New volume/original volume

Vertical displacement

Constraints

Volume fraction = 0.25

Upper bound displacement -> $L/300=70\text{mm}$

Objectives

Minimizing Weighted compliance* -> Increasing stiffness

*Compliance design and stress design are equivalent if the stress criterion is consistent with the elastic energy measure. The classical stress-constrained used in this analysis will find the minimum weight structure that satisfies the stress constraint and which is in elastic equilibrium with the external forces.

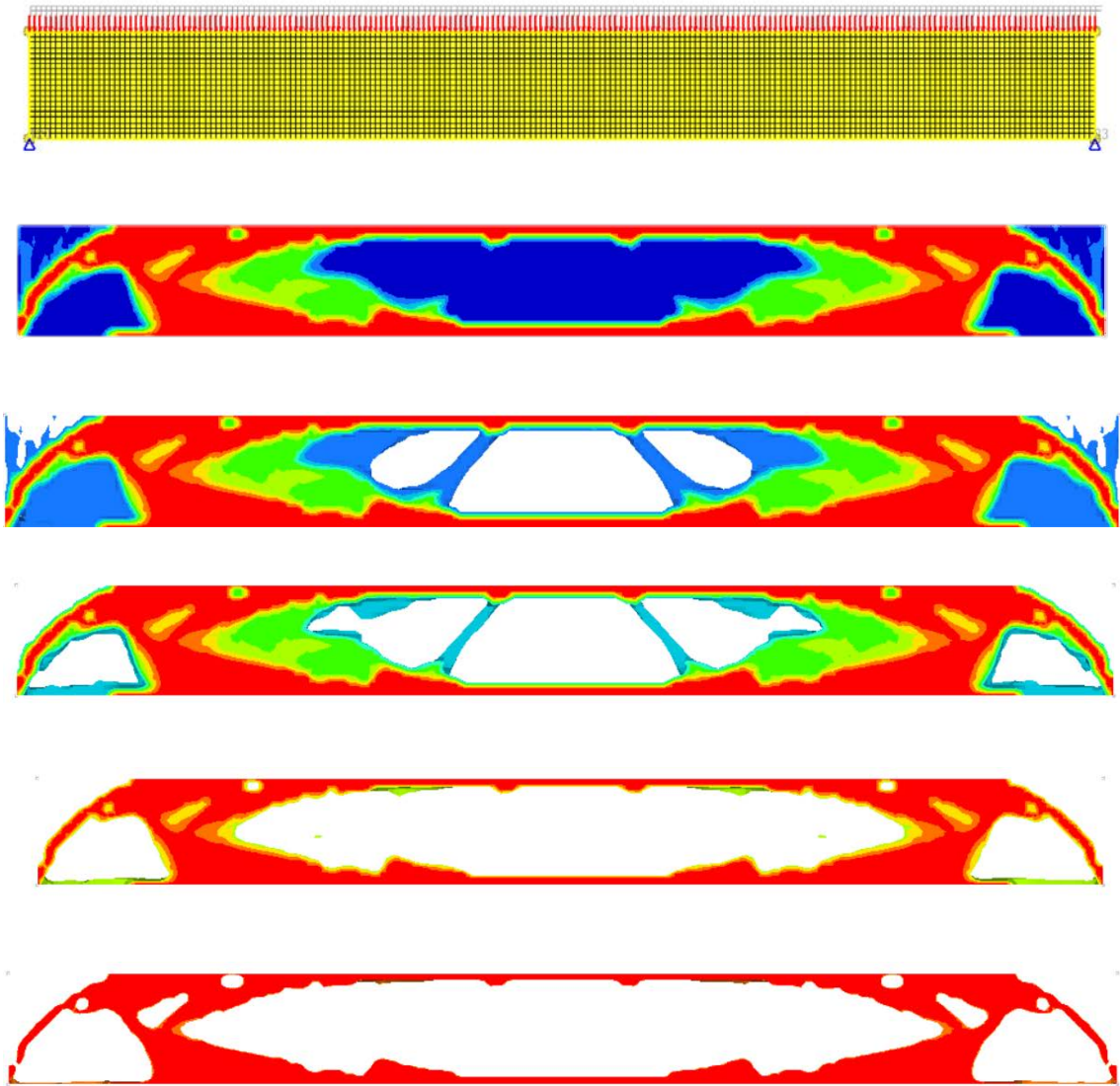


Figure 5.39: Topological optimization 3DBeam with target density 80% weight reduction

Limitations:

The topological optimizations described above is valid for homogenous isotropic material whereby one material can be applied for each predefined design space. The theory for the optimization of composite structures involves besides choice of material, also choice of orientation and the layup of the laminates. The essence of an algorithm which can optimize certain design space for given set of materials can be beneficial.

5.5.2.3 Multi-material topological optimization

Finding the optimal distribution of several materials in a fixed working domain introduced by a new algorithm based on the splitting of a multiphase topology optimization problem into a series of binary phase topology optimization sub-problems which result in straightforward procedure.. The desired phased (P) are the number of to apply material. The materials distribution is determined by pre-defined spatial domain. The end volume-fraction of each material is constraints by the

user. The representation of the multimaterials properties are by a tensor with the local volume fractions and physical properties. In this problem the material properties is represented by the elasticity tensor as function of local volume fraction. The phase algorithm is proposed by R. Tavakoli and S.M Mohseni and rewritten to simulate uniform loaded 2Dbeam with $L=20\text{m}$ and $h=1.5\text{ m}$. The following assumption are made while writing the Phase Algorithm:

- **Assumption 1.** *The solutions are globally convergent*
- **Assumption 2.** *Iterations will be strictly feasible with respect to all constraint.*
- **Assumption 3.** *The objective functional decrease monotonically as iterations of the algorithm proceed.*

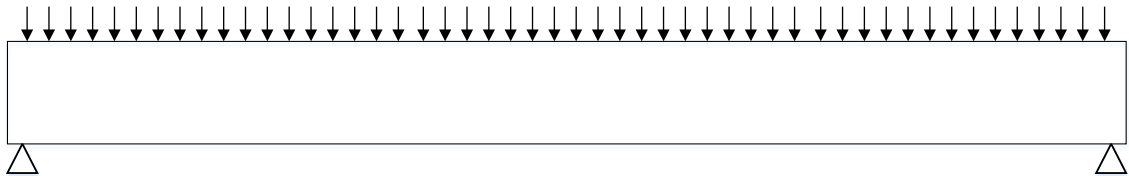
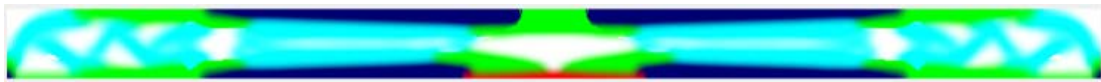


Figure 5.40: Mechanical constraints and loads

<i>Legend</i>	<i>Elasticity</i>	<i>Volume fraction</i>
White: void	E=0	20%
Red: steel	E=210000	1.4%
Cyan: NSC C25/30	E=31000	38.6%
Green: C90/105	E=44000	20%
Blue: UHPC	E=50400	20%



White: void	E=0	30%
Red: steel	E=210000	1.4%
Cyan: NSC C25/30	E=31000	28.6%
Green: C90/105	E=44000	20%
Blue: UHPC	E=50400	20%



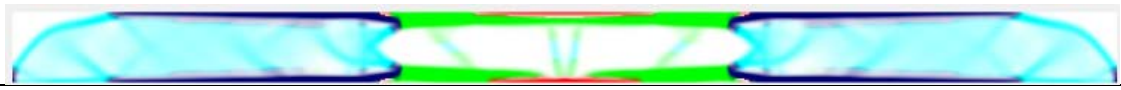
White: void	E=0	40%
Red: steel	E=210000	1.4%
Cyan: NSC C25/30	E=31000	18.6%
Green: C90/105	E=44000	20%
Blue: UHPC	E=50400	20%



White: void	E=0	50%
Red: steel	E=210000	1.4%
Cyan: NSC C25/30	E=31000	28.6%
Green: C90/105	E=44000	10%
Blue: UHPC	E=50400	10%



White: void	E=0	60%
Red: steel	E=210000	1.4%
Cyan: NSC C25/30	E=31000	28.6%
Green: C90/105	E=44000	10%
Blue: UHPC	E=50400	10%



White: void	E=0	10%
Red: steel	E=210000	1.4%
Cyan: NSC C25/30	E=31000	58.6%
Green: C90/105	E=44000	10%
Blue: UHPC	E=50400	10%

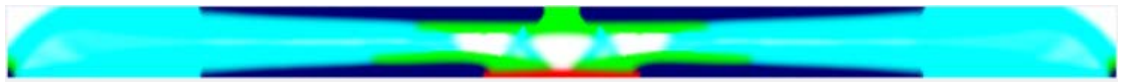


Table 5.6: Results of multimaterial optimization after 200 iterations

5.5.3 Variant 3. Truss

Truss is a structure composed of a number of bars, each of which is pin-connected at its ends to other bars, will normally form a stable framework called a truss. The joints can be welded, pinned or bolted which result in zero moment. The centroidal axis of each member, assumed to be straight coincides with the line connecting the centers of joints.

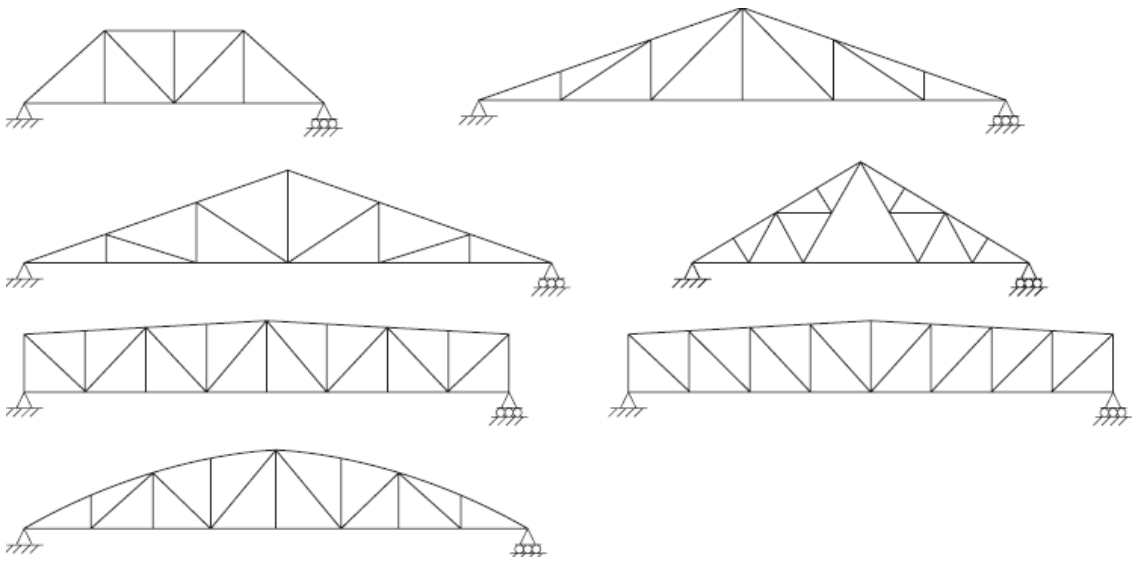


Figure 5.41: Typical truss structures

Reinforced concrete truss structure have built in the past, but they are not often used in the modern practice because the building costs are high due to the complexity of formwork and reinforcement. The challenge is to sustain high slenderness, which means that the angled members is smaller than 45° . This leads to smaller effective height and less applied angled members. A flatter angels will therefore result in less complex design. However, maintaining the resistance levels of this new design will require stronger materials. Modelling the force transfer of concrete truss is simply possible with the common used truss analogy. The motivation to re-design the concrete truss bridge is due to the weight reduction, potential for ACM, relevant experience with other closed cross-sections

5.5.3.1 Segmental truss

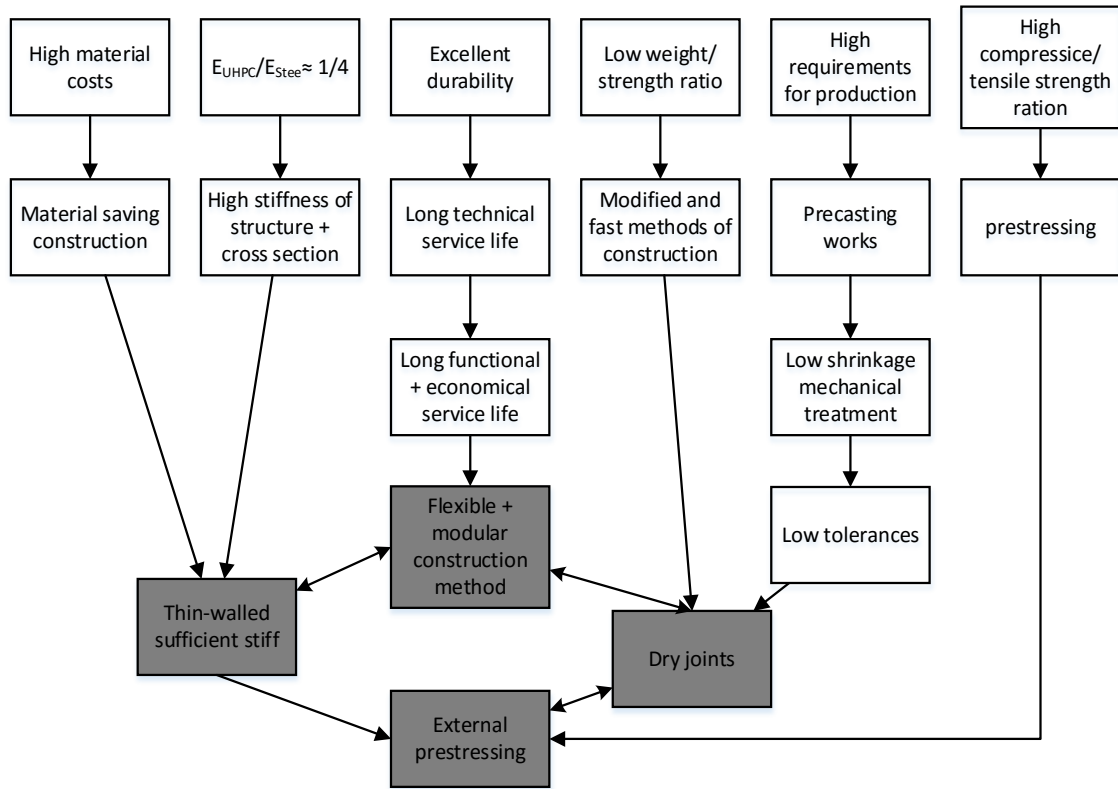


Figure 5.42: Construction principles UHPC prestressed segmental truss bridge [B01, p210]

New applications of UHPFRC (ultra-high performance fiber reinforced concrete) utilizing the high compressive strength and other excellent properties of UHPFRC in precast bridge element. The idea [Figure 5.40] was to design durable light weight segmental truss cross-section for railway traffic. The structural concept behind the design is based on utilizing the compressive strength of the concrete and avoiding tensile stresses by high prestressing levels.

By such a structure all of the details must be adequate for the durability and long-life time. .

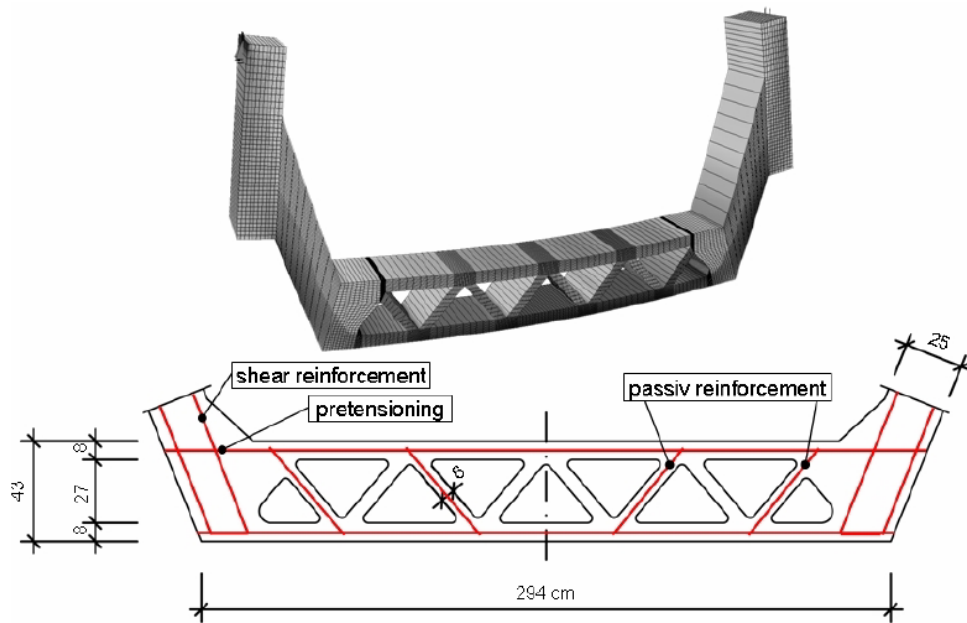


Figure 5.43: Cross-section of standard segment [B01, p290]

5.5.3.2 Truss girder

Typically trusses built and designed only of steel or wood. The disadvantages of these materials are that they are not resistant to fire, have a very high cost of maintenance, and are less durable, in comparison with the Concrete Truss. The concrete truss beam of Javier Mentado-Duran [Figure 5.41] is truss with reinforced steel, including pre-and post-stressing, with high performance concrete offers high resistance to forces with an high level of structural integrity. The members are secured together by monolithic means, welded in a triangular web like configuration

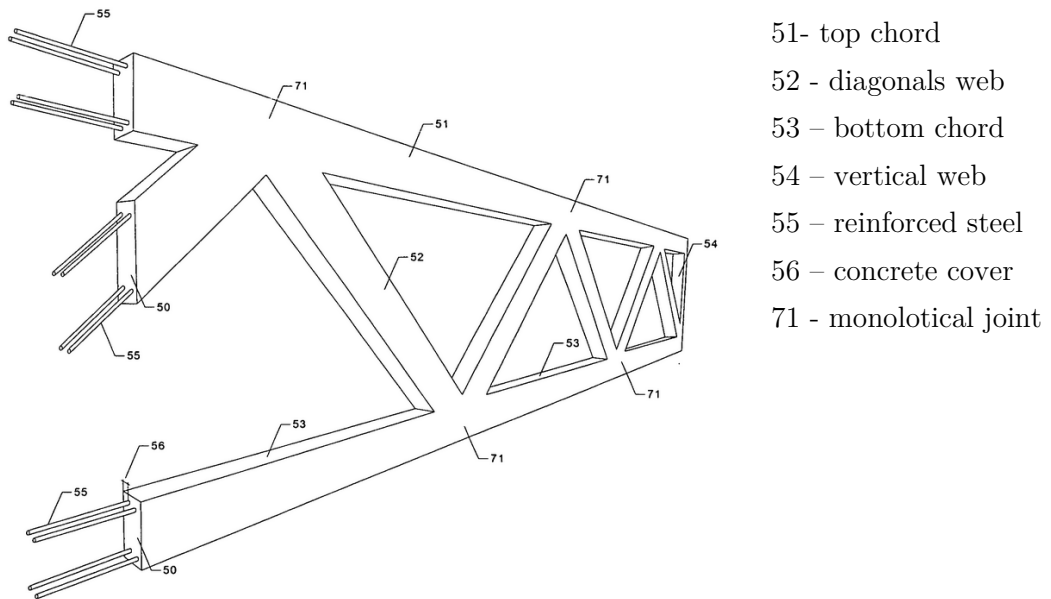


Figure 5.44: Concrete truss beam [Javier Mentado-Duran]

5.5.3.3 State-of-the-art truss girder

The idea is to further optimize the current UHPC truss into truss where materials are more effectively added where their strength capacity and high durability can be utilize to make this design cheaper and as simple as possible. From practical point of view the concrete members will have rectangular shapes limited by the framework. However concrete is a flowable material which can flow and shaped in any form. Using textile framework make curved shapes possible. This method release the designer from the conventional designs.



Figure 5.45: Concrete beam casted into textile formwork designed with topological optimization in ANSYS [C.A.S.T. Manitoba University ,Canada]

Finding structural shape:

The model [Figure 5.42] is the result of study conducted by Huang et al (2006).

Where the BESO algorithm remove the least stressed elements in iterative. The BESO algorithm is implemented in ANSYS with the intention of carrying out fully finite element analysis on the optimized form.

Where on the left side is the best optimized structure and on the right side arch structure was forced in a second optimization run where they removed initial domain material at midspan. This is similar to the Arch beam variant discussed in section 4.8.1

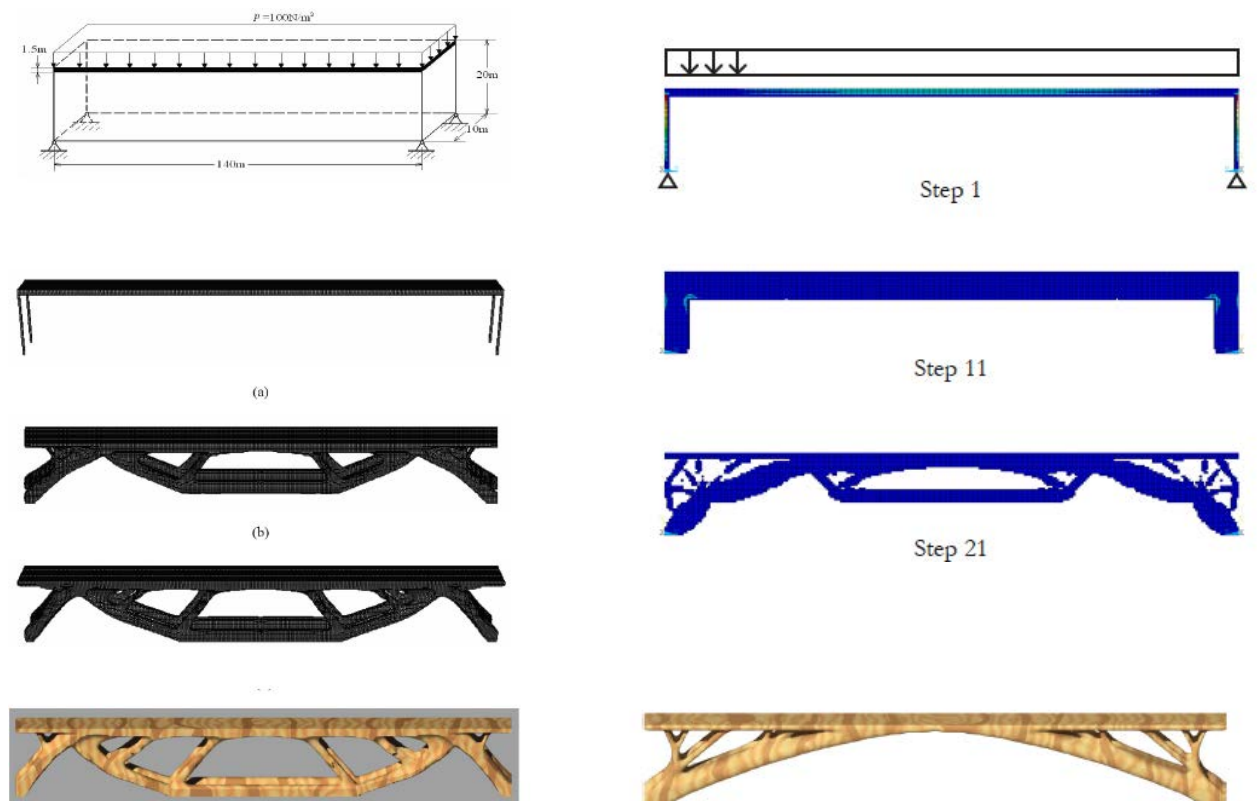


Figure 5.46: Evolutionary structural optimization in ANSYS using BESO algorithm (Huang , 2006)

The use of strong fabric mold for casting a concrete is existing practical concept. It is flexible formwork allow very different shapes of molds than those resulting from

conventional concrete. It includes several of curved shapes, however manufacturing is not yet economically competitive to the simple casting methods for complex shapes. The fabric types used are cottons or polymers. This material is orthotropic and highly non-linear as it will stiffen under increasing tension until some ultimate strength is reached. Which means that the Young's modulus is not constant. Several of researches comparing the convention rectangular beam with fabric-formed beam mentioned in Figure 5.42 reveals that the first by far less stiff using the same amount of volume and fails earlier than fabric-formed beam. So it is superior in both serviceability limit state (deflection) and the ultimate limit state (failure).

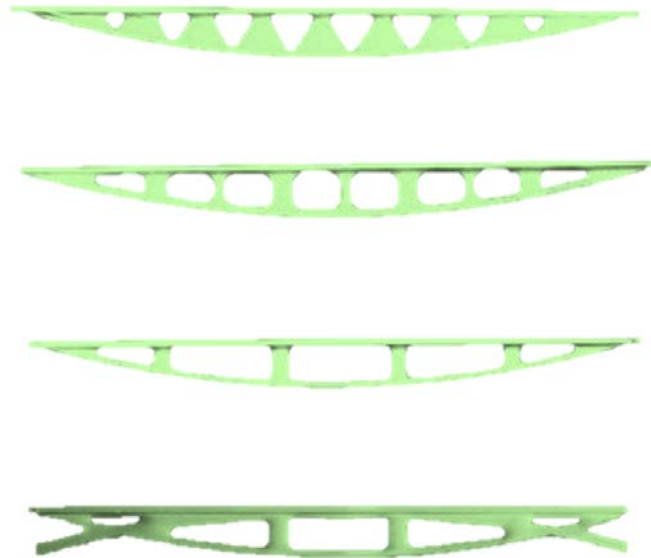


Figure 5.47: Variety of truss design with fabric formwork

Multi-material model

After this short introduction with three inspired design methods of concrete trusses it is the time to refocus on design with more than one material, as already agreed have lot of potential to reduce costs and increase the efficiency of the structure. Based on the experience obtained in this research a conceptual models are proposed [Figure 5.45] [Figure 5.46].

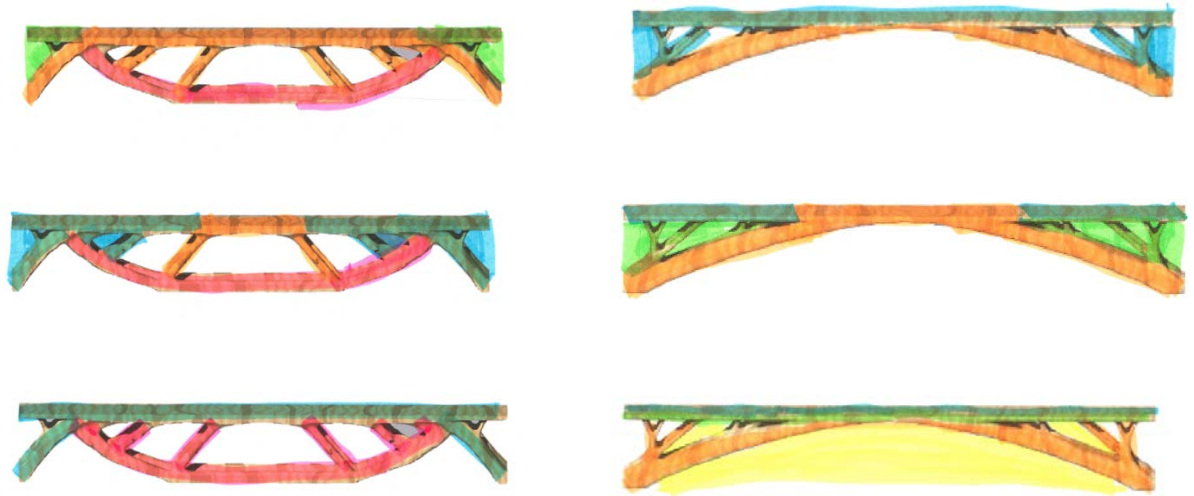


Figure 5.48: Tension element (red), high performance concrete (orange), Strain hardening concrete (green), conventional concrete (blue), fibre reinforced concrete (dark green), and foamed concrete (yellow)

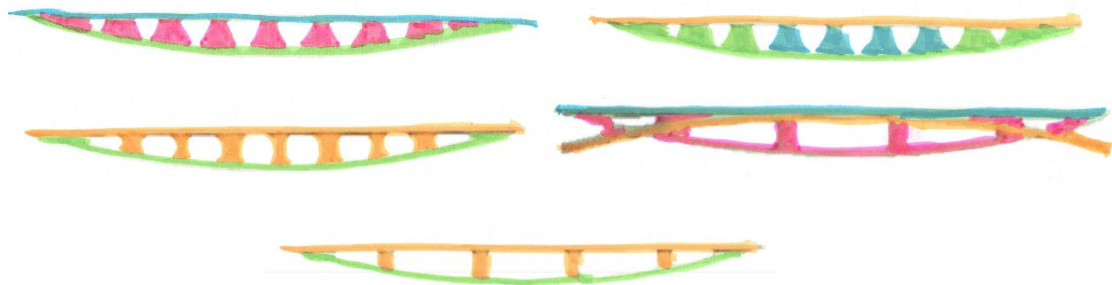


Figure 5.49: Multi material Fiber-formed truss with high performance concrete (orange), strain-hardening concrete (green), fiber reinforced concrete (blue) and self-compacting concrete (pink)

Using the Matlab algorithm introduced in [4.8.2.3] result in topographic plot of the material distribution.

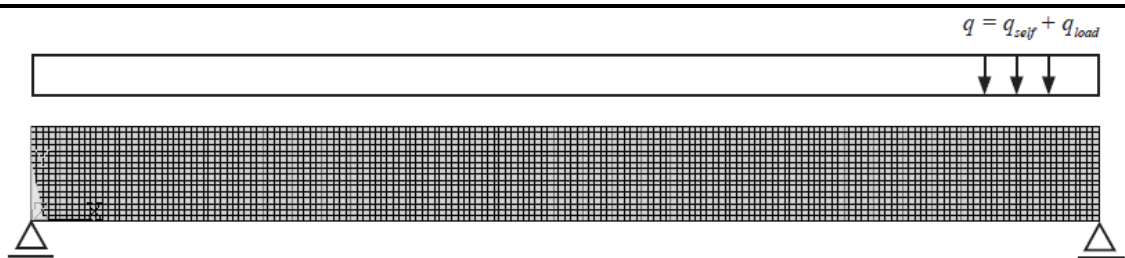


Figure 5.50: General load case. Support conditions and initial design domain for BESO algorithm in ANSYS [Diederik Veenendaal, 2008]

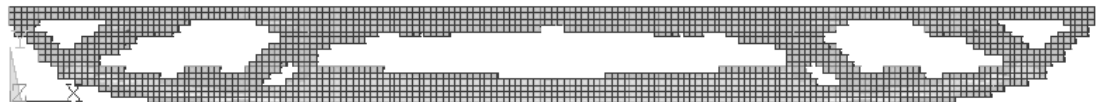


Figure 5.51: Result after 13 iterations for BESO run with $E=28.485 \text{ N/mm}^2$, $f_{ck}=28.2 \text{ N/mm}^2$, $f_{ct}=2.98 \text{ N/mm}^2$ including longitudinal reinforcement

White:	void	$E=0$	30%
Red:	steel	$E=210000$	1.4%
Cyan:	NSC C25/30	$E=31000$	28.6%
Green:	C90/105	$E=44000$	20%
Blue:	UHPC	$E=50400$	20%

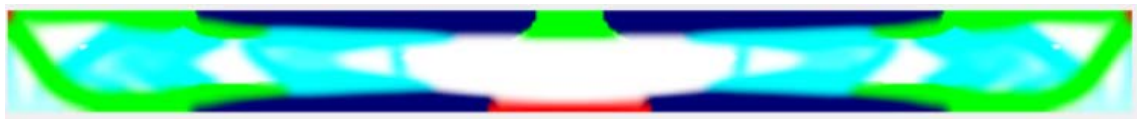


Figure 5.52: Result after 200 iterations with run of Matlab algorithm with equivalent beam geometry and boundaries

Construction principles concrete truss:

The major functional, technical and material requirements [Table 5.1] are processed into design choices [Figure 5.50]. These will be the guidelines while developing the preliminary design.

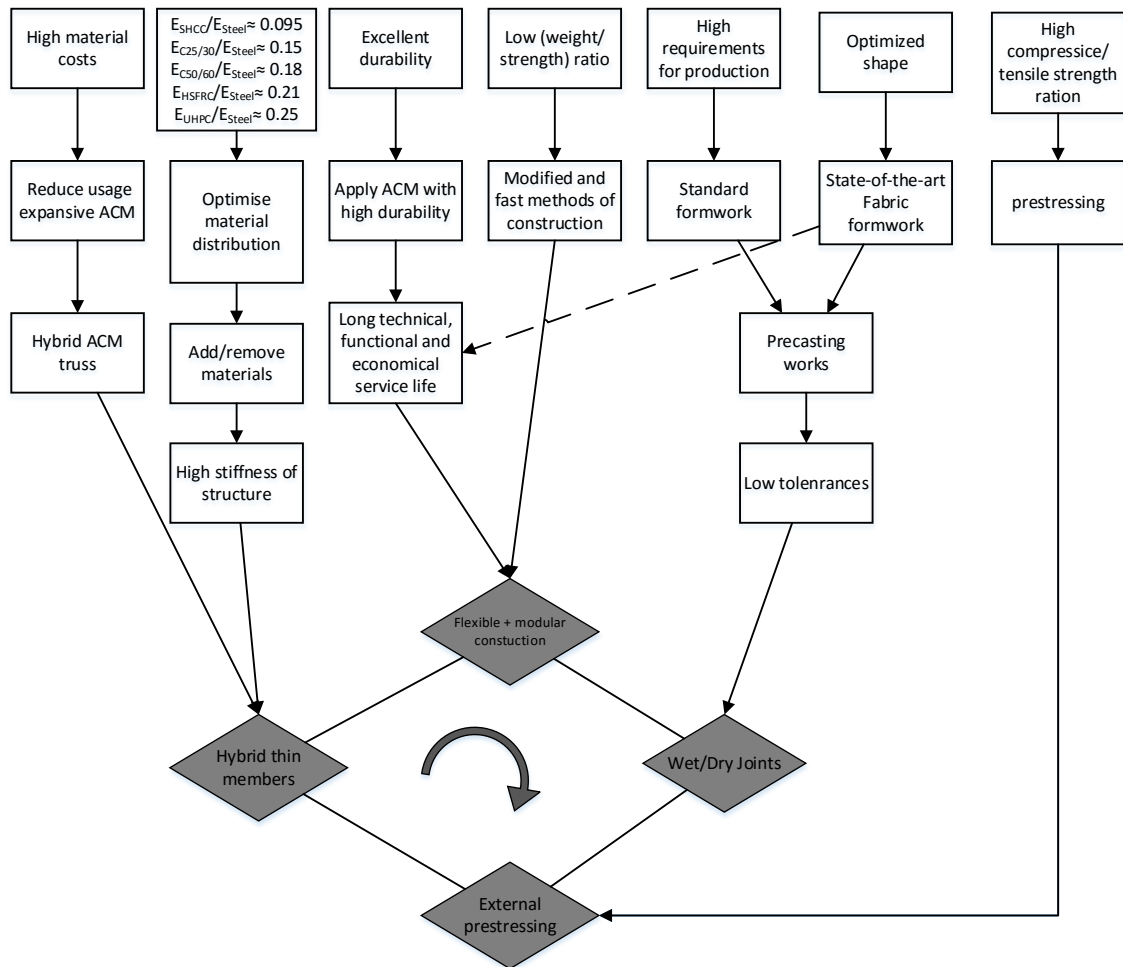


Figure 5.53: Modified construction principles hybrid truss

5.5.4 Variant 4. State-of-the-art beam

Throughout evaluating possible design alternatives for bridge beams, the research is encounter with relative two new technologies: The Fabric-Formwork and the 3D Concrete Printer. These new technologies are up until now not applied in the infrastructure sector. However, in China 3D printer with high strength concrete of 2-stores houses is already a reality. Also in the Nederland the project “3D printing Canal House” under the collaboration of The Municipality of Amsterdam and leading architects, constructors in the Netherland is developing technics to deal with 3D concrete printer. In this project 3D wall is printed with shafts, which will be casted with concrete, and will so create the structural framework of the house. Think about printing of framework with curved lines or shafts for multiple materials

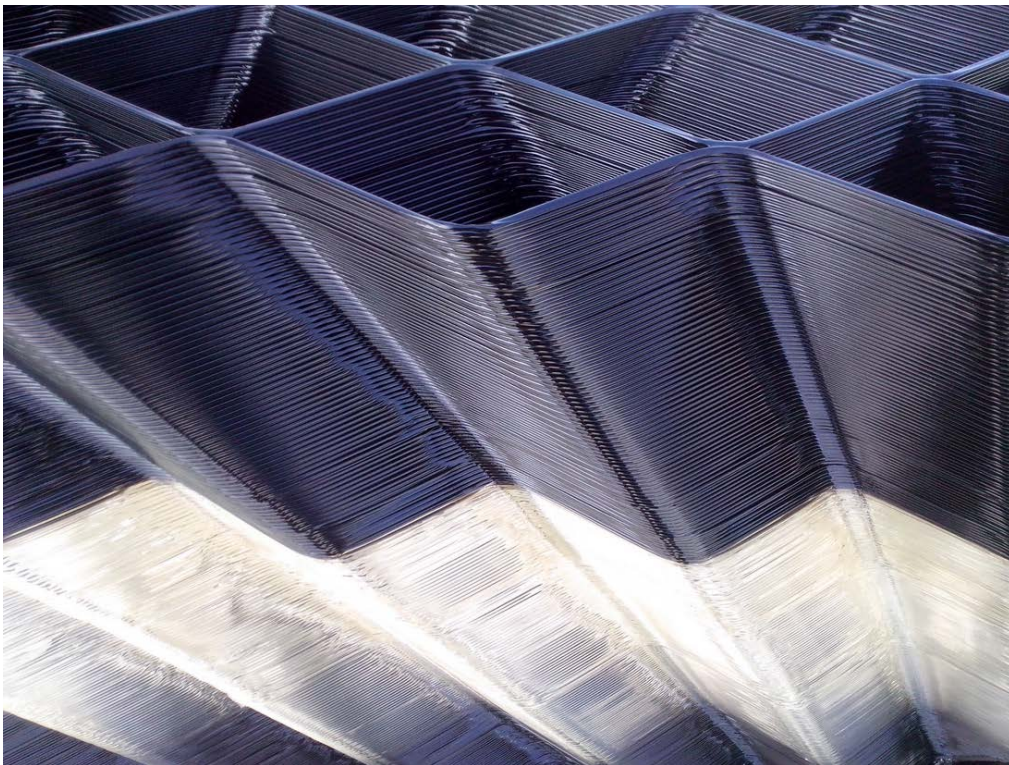


Figure 5.54: The oriented shaft [www.3dprintcanalhouse.com]

As discussed in [4.8.3.3], the Fabric-Formwork for reinforced concrete construction is extraordinary light and inexpensive formwork which use 100 times less material than conventional formwork, and providing zero-waste system. Beams can be simply casted by hanging flat fabric sheet horizontally as a long open trough. The reinforced concrete beam with varying depth in proportion to its own bending moment [Figure 5.52] doesn't behave as rectangular prismatic beam. For example the shear stresses are considered in rectangular beam with installation of stirrups to resist the tension stresses in the web. A beam shaped to follow its own bending moment curve has no such a tension stresses because the forces are naturally channeled along the curved edges of its tension zone.



Figure 5.55: Volume of fabric-cast compared to conventional rectangular beam

5.5.4.1 Evaluation

The mentioned technics are of course still vision for the future and not practical solution which will be implemented in the coming years. Nevertheless it is just a matter of time before this technologies will replace the conventional counterparts. Consequently short evaluation in the form of advantages – disadvantages is presented in this section:

3D printing:

- Advantages
 - Elimination of construction waste
 - Saving transport costs
 - Standardization of elements
 - High level of details (esthetics)
 - Design customized to fit construction needs
 - Adding details will not affect the labor intensive and costs
 - Additive manufacturing technics, raw material => final product
 - Production can be worldwide implement
- Disadvantages
 - Complying with regulations
 - Insulations
 - Fireproofing
 - Wind loads
 - Foundations
 - Bridge sub-structure
 - Stability during printing

Fabric Form-work:

- Advantages
 - Esthetics
 - Efficient, more material is strained more equally
 - Reduction concrete volume
 - Reduction dead weight
 - Compared to an equivalent orthogonal section 35% concrete material saving
 - Longer spans are possible
 - Beam shape follows the forces path = no shear stresses for UDL
 - Curved shapes economically possible
 - Simple and fast execution with reduction reinforcing steel
 - Sustainable material saving design
 - Reducing the need of stirrups, shape follows principle directions
 - Higher durability= carbonation, chloride ingress
- Disadvantages
 - Complexity reinforcement for variable section member
 - Reinforcement bars need to be fully anchored at the edges
 - Transverse reinforcement due to point load
 - Inclined longitudinal reinforcement
 - Eurocode empirical relations might not be valid
 - Fireproofing
 - Bond reinforcement - concrete

Example:

The University of Bath has conducted an extensive research about the application of Fabric Form-Work. In this research T-beams are designed for house slab with span of 8.0 m. Four beams with different longitudinal and transversal reinforcement arrangement are tested. The concrete strength is between 33 – 44 N/mm². Concrete cover of 20 mm is applied.

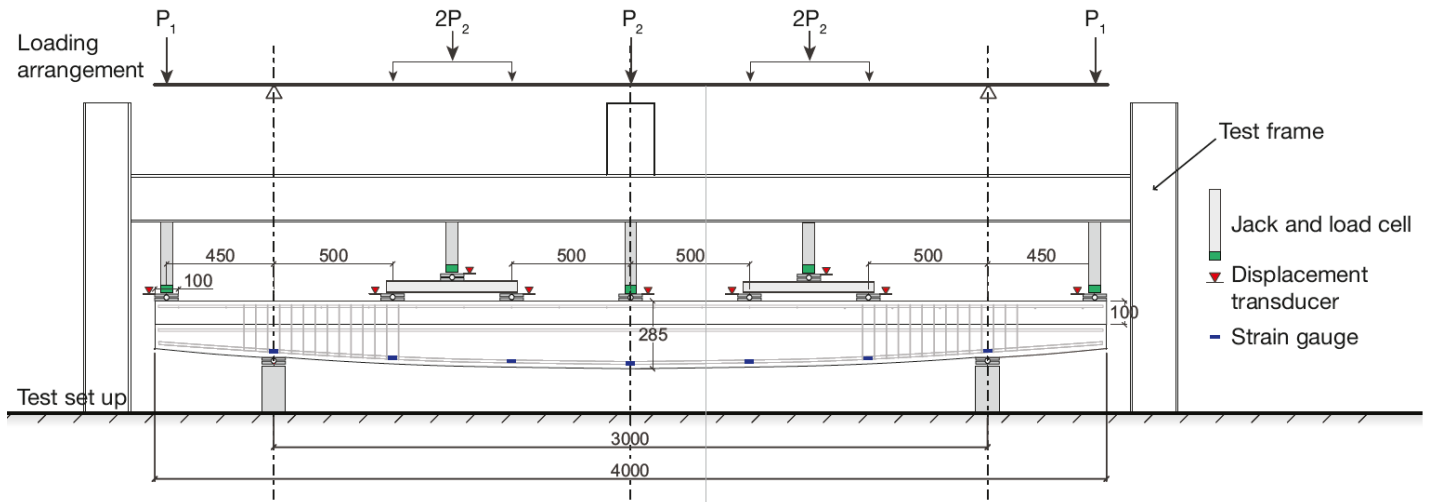


Figure 5.56: Tests set up [University of Bath]

All beams displayed ductile response, with yielding of the longitudinal steel ($\rho_s = 0.2\%$) leading to compression failure in the top slab [Figure 5.54]. No shear failure was recorded and cracking was well distributed in the tension zone.

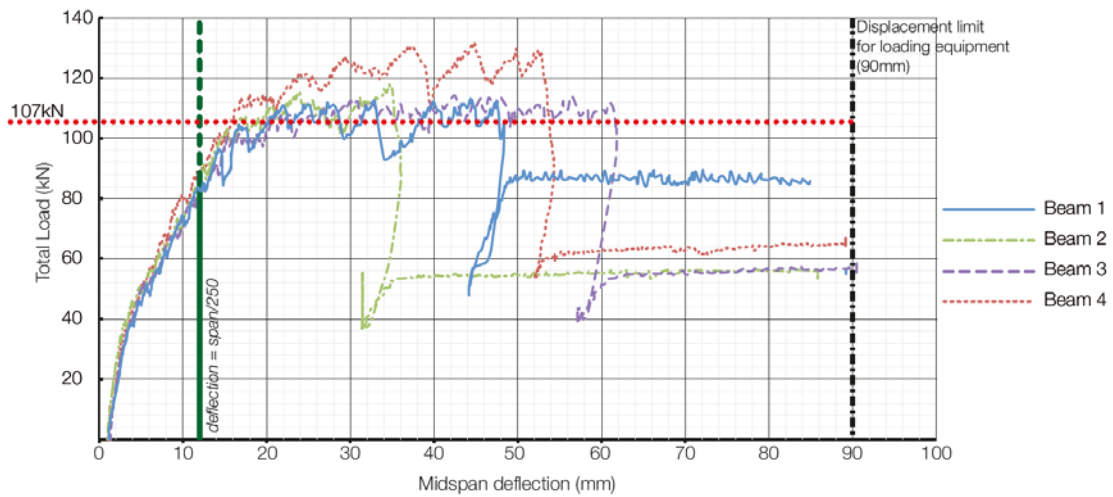


Figure 5.57: Tests results [University of Bath]

Due to its higher flexibility the serviceability limit state may be become concern, Applying the deflection limit of $L/250$ reduces the permissible load capacity by around 30% as highlighted [Figure 5.54]. Therefore the usage of prestressed reinforcement together with application of different ACM will provide an ideal solution.

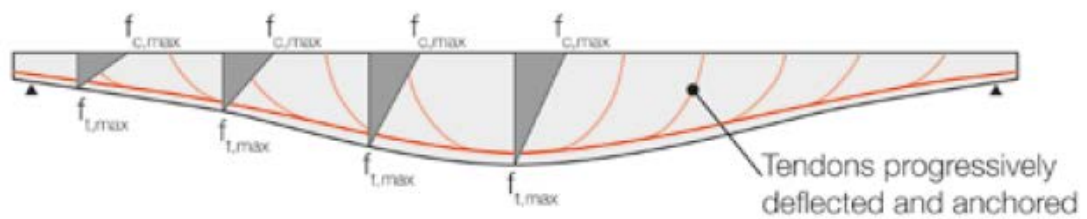


Figure 5.58 Uniform strength prestressing beam [Guyon]

5.5.5 Variant 5. Local Strengthening

Slender beam will be defined as a beam with span/length ratio larger than 25. Such a slenderness rates are favorable for large spans where self-weight represents 60% of the total load while stiff connections (static undetermined) are responsible for the other 40% of the total loads.

5.5.5.1 Idea and concept

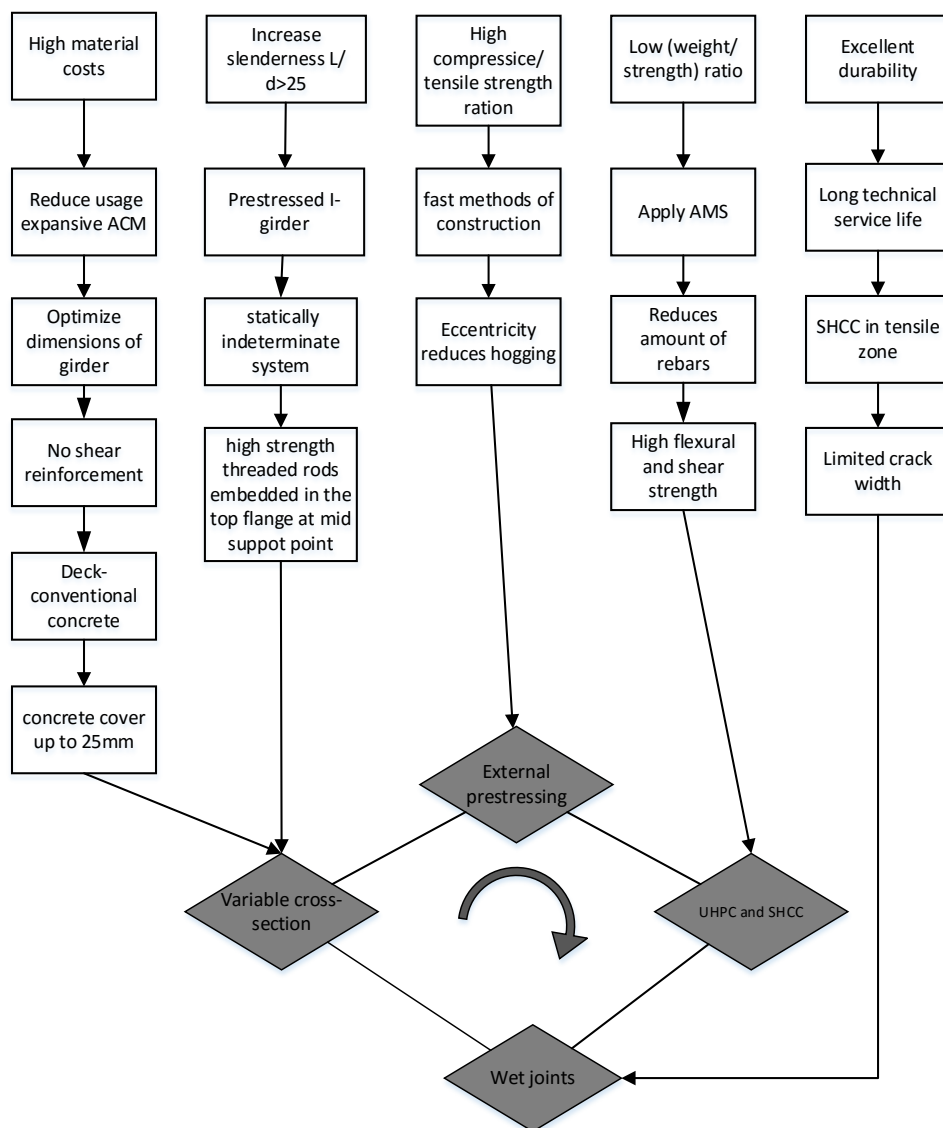


Figure 5.59: Local strengthening of the girder

5.5.5.2 Composite I-girder

Slab-on-Stringer system.

In bridge structures undergo traffic loads, prestressing is currently the most effective method to reduce the structure height. Slender beams will be more sensitive to shear deformation, dynamic loads and vibrations. The problem with slender bridge beams or decks is the high amount of prestressing steel, reinforcing bars and shear reinforcement needed to resist the actions. Consequently reducing the dead weight of the bridge carriageway will translated into reduction of the required prestressing steel.

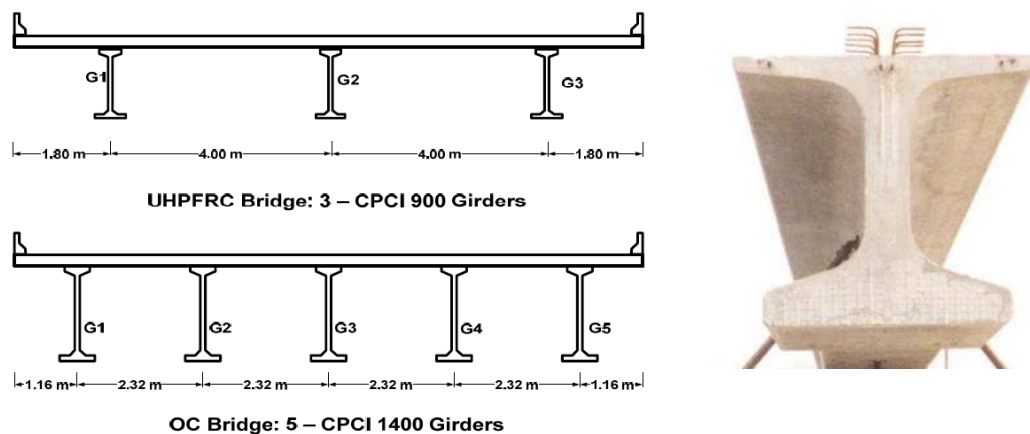


Figure 5.60: Comparison of UHPFRC an ordinary concrete precast prestressed girder bridges, NU I-girder [B01, p333]

Such a construction [Figure 5.57] is called slab-on-stringer system is pretty much straightforward. The prefabricated UHPFRC bridge girders are assembled on site which follows by adding cast in situ or prefabricated concrete deck elements. The composite connection between the deck panels and the supporting girder must be capable of carrying significant shear and tensile forces. This can be fulfilled by adding rebars or studs that extend from the girder into the deck .

Cross-sectional level.

The prestressed ultra-high performance I-girder can be very slender. High slenderness ratio is an important design criteria in the Netherland due to the flat geography. By using AMS the massive rectangular cross-section optimized in the favor of reduction in dead weight. This will be translated into reduction of the prestressing steel. Assuming girder is fully prestressed utilizing the high compressive capacity ($f_{ck}=170 \text{ N/mm}^2$) and considering the critical zones in bridge girders:

- Transversal hogging bending in the top flange centerline
- Shearing force in the webs
- Transversal bending in the bottom flange

Looking at the web, bottom and top flanges as individual elements make it possible to suggest few improvements in the design:

1. Top flange
 - 1.1 Top flange connects to the concrete deck with conventional shear bars => increase stiffness
2. Web
 - 2.1 If bonded prestressing is chosen web thickness is related to the concrete cover.
 - 2.2 Apply deflected and straight strands with ratio 0.8-1.0 Variable web thickness => reducing dead weight => complex execution
 - 2.3 Alternatively increasing shear capacity => add SHCC to the web at the girder edges
 - 2.4 SHCC connects to the flanges with wet joints
 - 2.5 SHCC with glass rods => increase tensile capacity
 - 2.6 Minimum SHCC layer thickness 30mm
 - 2.7 Prestressing force eccentricity => limiting hogging

3. Bottom flange

- 3.1 Encase prestressing tendons and resist sagging bending moments
=> add SHCC permanent framework
- 3.2 Protecting the steel from corrosion
- 3.3 Smaller concrete cover is possible up to 25mm between tendons and from tendons to outer fiber
- 3.4 narrow crack widths => increase durability
- 3.5 Shallower bottom flange

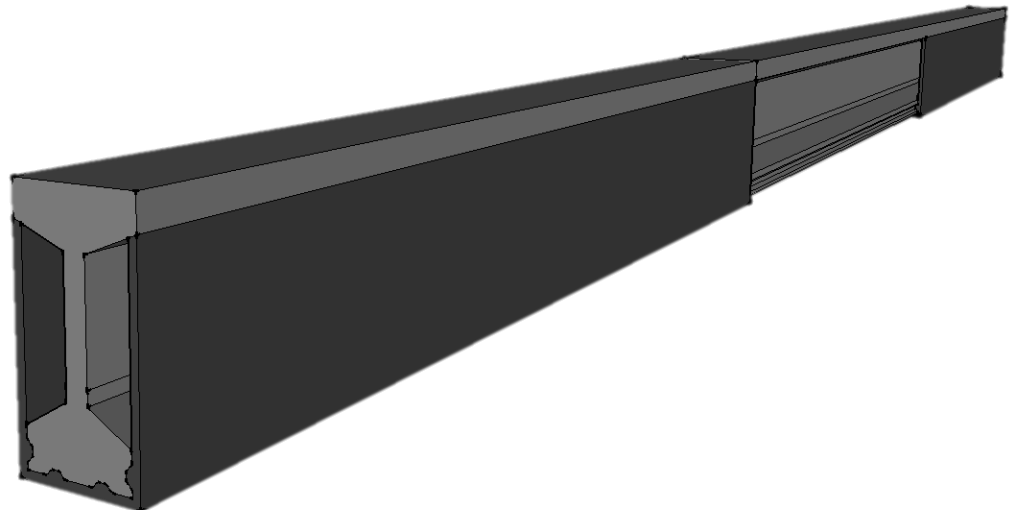
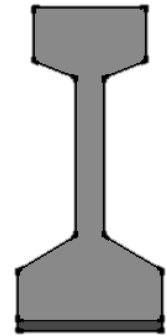


Figure 5.61: 3D sketch of the proposed girder

Mechanical system level.

The aim of this variant is to find a way to increase the slenderness in a straightforward means because as mentioned this affect the efficiently of the girder. After optimizing the cross-section above, we'll zoom out to investigate the mechanical system of the superstructure. The following will be considered: girder spacing, full/partial prestressing, statically indeterminacy, joints and deck-girder interface.

Considering statically undetermined system will increase the slenderness of the bridge due to reduction of the field moment on the account of hogging moment in the joint

between the precast segments over the pier. This will reduced girder size or reduce girder spacing, consequently reducing costs.

5.5.6 Conclusion & Remarks

Optimization of existing girders such as prestressed ZIP, SKK girders is difficult task. These girder are cheap, cost-efficient, and supplied by local prefabrication factory with set of design tools which is easy to use for any structural engineer. In the contrary, ACM bridges are more expansive, with deficient design tools and require specialist's structural engineers and martial knowledge.

Hence the introduction of Multimaterial Hybrid girder design with large span and with 50% material reduction will be the leading motives in the next chapter [6]. The following design principles will be accounted for:

1. Compressive strut
2. Local strengthening
3. Topological optimization
4. 100% Modular
5. Hybrid (Multimaterial)
6. Large span
7. Limited construction height

Compressive strut

The compressive strut in the shape of an arch transfer is based on mainly compression forces. Apply high strength concrete arch spans between the supports with rise limited by the beam height. This element is purely the compression reinforcement. At the edges massive anchorage block takes the horizontal force component from the arch, increasing shear capacity at the edges and practical solution to the anchoring of the prestressing cables which function as the tensile reinforcement.

Local Strengthening

No constant cross-section, the arch strength and stiffness will be increased by local application of elements, for example linear elements under and above the arch.

However increasing the stiffness of the girder opposing the desirable reduction of approximately 50% of the material. Therefore only local strengthening of a girder is chosen based on topological optimization with predefined boundaries such as overall stiffness and maximum displacement.

Topological Optimization

By finding the optimal distribution of several materials in a fixed working domain. With mathematical approach in Matlab software, the design space of the girder (span, height, width) will be optimise for a certain loads and boundary conditions. The result will be indicative for application of materials maximizing the bending stiffness while minimizing the material usage.

100% Modular

Large spectrum of the ACM materials (UHPC, SHCC, FRC) is completely prefabricated. The goal is to prefabricate the girder for later transport to the building site where it will be assembled. Secondly 100% modularity means high flexibility regarding the girders dimensions that can theoretically be change upon demand. This is new innovative approach for constructing bridge superstructure compared with traditional ZIP or box-girders. The level of prefabrication and modularity is in this stage of the research unknown. Yet issue's like creep, shrinkage, transport limitations, construction stages will determine the level of modularity and prefabrication.

Hybrid & Multimaterial

Girders for heavy traffic bridges sustain very high loads. Therefore an optimized combination of concrete properties is very interesting in terms of application. For instance ultra-high performance materials reinforced with steel fibers have favourable strength, ductility, stiffness and durability compared to conventional concrete. On the other hand they are more expansive and suffer from shortage in design codes and existing design codes which are not compatible with the existing Eurocode. Therefore J.C. Walraven [HPFRC July 2007] suggested in his study to develop hybrid structure based on combination of traditional reinforcement, prestressing steel and fiber. This also

favourable in elimination of the unreliable shear strength and tensile strength of the fiber reinforced concrete. The second principle is to use multimaterial approach in parallel to the fourth principle (100% modular) to reduce costs. Or in other words apply ultra-high performance materials only where it's needed.

Large Span

Large span, light and elegant structure is possible due to use of advanced cementitious materials. It allows slender design with secondary effect of reduction of the number of intermediate supports includes bearing, expansion joints, columns, piers, foundations, joints.

Construction height

Slender superstructure are not only more elegant. Increasing the construction depth has major cost implications such as the need to raise the embankments. It is however unlikely to be economic to use the minimum depth. The optimum construction depth is the most economical depth.

5.6 Iterative analysis

<i>Principle</i>	<i>Feature</i>
1	Compressive strut
2	Local strengthening
3	Topological optimization
4	100% Modular
5	Hybrid (Multimaterial)
6	Large span
7	Limited construction height

Table 5.7: Deign principles

The design strategic will follow the Cyclic Engineering Process [Figure 5.59]. During which choices are made guided by the design principles [Table 5.6] until final concept is stabilized. It is important that the green line [Figure 5.59] will be followed, which can be accomplished by fixing certain parameters in a certain time point. In this way the design will optimized in each iteration approaching the final stable state.

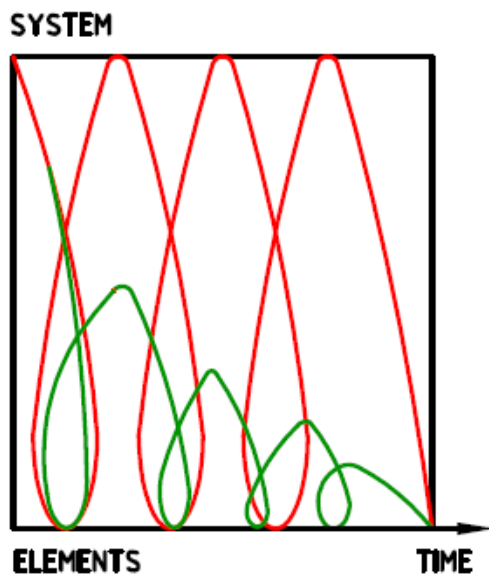


Figure 5.62: The cyclic design process where the design progresses to the end-product (green) or the design stays in endless cycles (red).

For the design the girder each design cycle have to meet the various requirements given in [Table 4.4] [Table 4.5] [Table 4.6] and summarized in [Table 5.1], Discrepancy with these requirements will lead to extra cycles for the optimization of the design.

5.6.1 Global concept

The global outlines of the bridge deck was initially a rectangular. The truss-like girder [Figure 5.60] follows the principle forces distribution is the result of topological optimization analysis. The cross-section of the structure is not constant over the full span of the bridge just as the non-constant stress distribution of the different load models. The variability girders shape [Figure 5.60] result in lightweight cost-effective structure. Symmetry and repetition of the girder decreases when variability in the longitudinal axis increase. This will result in complex details and specifications, time consuming calculations, and construction errors. Nevertheless, increase in variability is the key for increasing efficiently of the girder. Apply pre-stressing, post-stressing and reinforcement bars where the concrete tensile strength is exceeded.



Figure 5.63: Global concept [A. Rietsema]

The idea behind this concept is a system of force couplers with non-constant internal lever arm $Z(x)$ which is large at $x=0.5L$ and goes to zero for $x=0$ and $x=L$. The compressive strut and the tensile tie concept, local strengthening principle, and material saving principles are observed in this global design.

5.6.2 Iteration I – Span & minimizing materials use

Follows from the parametric study, the span will be increased up to a level for which the ACM girder will be feasible concept.

When the span of a bridge increase, it is cheaper to support the slab by beams, rather than to thicken the slab. So talking about saving will refer only to the beam.

When the span increases, the bending moment caused by constant dead-load increases proportional to $\frac{1}{8}q_G l^2$. The ratio between the dead load and the live load becomes more and more unfavourable.

The first case [Figure 5.61] analysed is of massive rectangular prefab girder with height very between 0.4 to 2.0m with compression layer of 200mm ($h=1/10 - 1/15 L$). The width of the beam is $b=(1/3) h$. The girder is loaded with uniform variable load of $q_{var}=20$ kN/m. The intersection point of both curves is the point where the influence of the variable load equals to the influence of the self-weight. Further from this point increasing the span result in more dominant self-weight which is inefficient state.

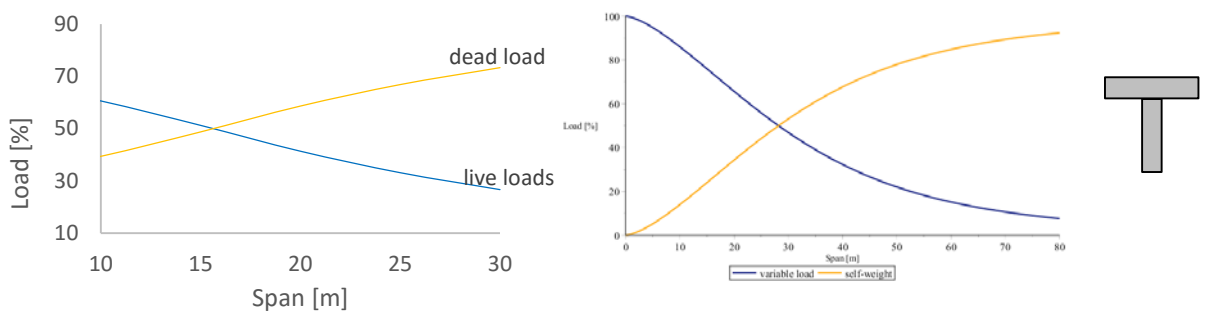


Figure 5.64: Massive rectangular girder with compression top layer (bridge deck),

In [Figure 5.61 left] the intersection point is at $L=16.0$ m. This is valid only for strength requirements (Ultimate limit state). In [Figure 5.61 right] the result of SLS analysis (bending stiffness) is plotted with maximum displacement of $u_{max}=L/400$. The intersection point is much larger $L=28.0$ m. Hence, the dimensions meet the strength and stiffness requirements when the strength requirements is met.

The influence of the variable load and the self-weight can be also plotted for prestressed ZIP-girder [Figure 5.62] with compression layer of 200mm for ZIP1000-1700 and 200mm for ZIP1800-2400. Concrete class ZIP C60/75 and C28/35 for the cast in situ compression

layer. The intersection point moved forward compared to [Figure 5.61] as expected due to increase of cross-sectional efficiency.

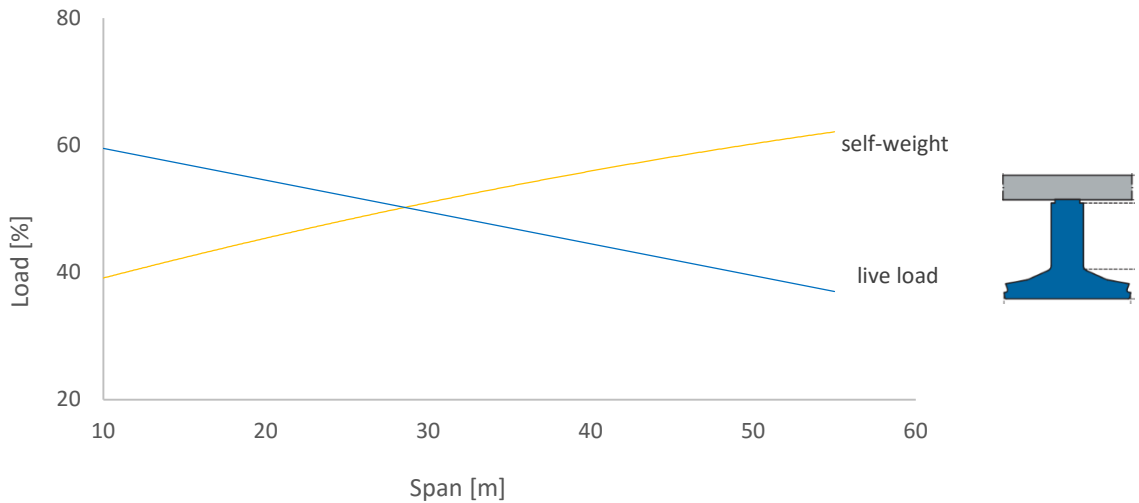
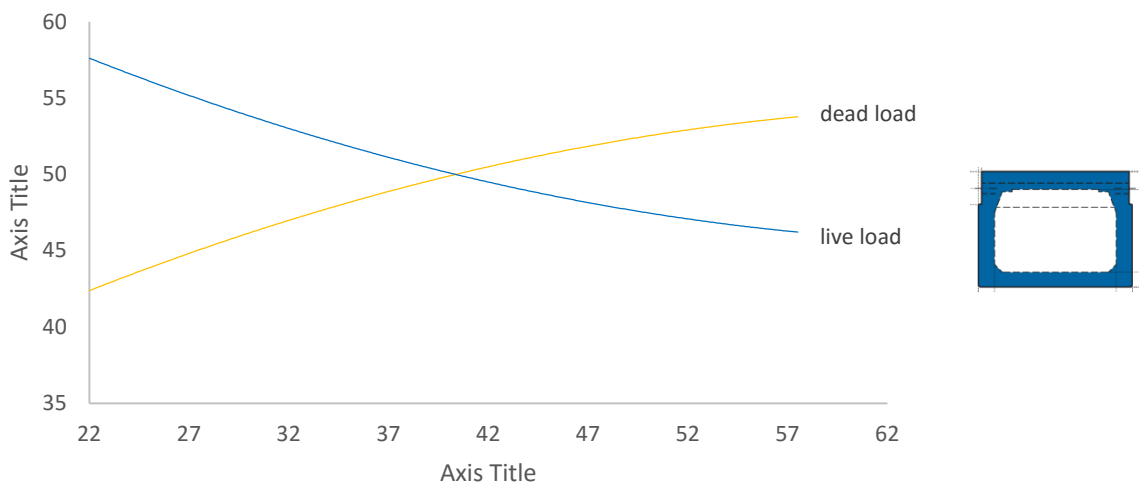


Figure 5.65: Zip girder with top compression layer of 200mm [Spanbeton]



The same analysis is carried out for statically determined simply supported beam of a SKK girder [Spanbeton]. The point of intersection in this case is about $L=40m$. This is

because box-girders do not require a compression layer. The girders are prestressed in the transverse direction which gives the bridge its torsion stiffness and transversal stiffness. To conclude the dead load remains dominant at very large spans. Hence, reduction of dead-load in large span bridge girders has potential for economic and structural benefits.

5.6.3 Iteration II – Compressive strut

The compressive strut is the leading concept of the new girder. The first global dimension of this arch can be determined with boundaries according to [4.3] and [4.9.2]. The Arch spans 50.0 m with maximum height comparable to SKK-1800, $h=1.80\text{m}$) [Spanbeton] including compression layer of 170mm. The cross-sectional dimensions of the arch relate to the moment of inertia, buckling, and strength. Assume the Arch is casted completely from UHPC with $f_{ck}=180\text{ N/mm}^2$, $E_{cm}=58000\text{ N/mm}^2$ and $f_{ct}=8\text{ N/mm}^2$

5.6.3.1 Arch shape

The optimal Arch shape can be described with a parabolic function. A parabolic arch with a uniform load carries load via normal force only. In reality moments and shear forces will be present in the arch due to point loads (tendon load), deformation due to axial loading, shrinkage & creep of concrete, and temperature load. For now only uniform load is accounted for. The parabolic function of the arch $z(x)$ is given below:

$$z(x) = \frac{4fx(L-x)}{l^2}$$

$z(x)$ =arch function, f =sagitta, l =span

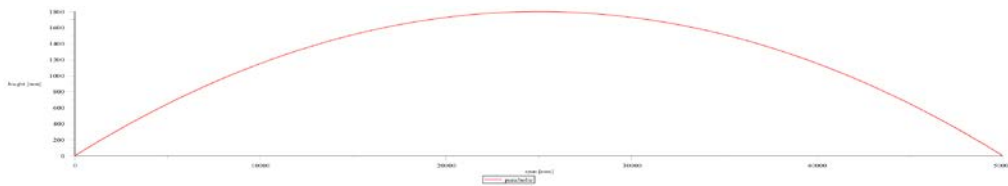


Figure 5.66: Plot of the arch center line for L=50.0m and f=1.8m

5.6.3.2 Thickness

The thickness of the arch increases on the one hand the self-weight resulting in larger normal stresses: $N = \frac{\Delta l}{l} * E * b * t$. But on the other hand it contribute exponentially to the bending moment resistance $W = \frac{1}{6} b t^2$ (assumption: rectangular cross-section) and normal force. Now consider an arch loaded by uniform traffic load and concentrated loads according to LM1 [NEN-EN 1991-2]. The normal forces will be the largest at the supports [Figure 5.64].

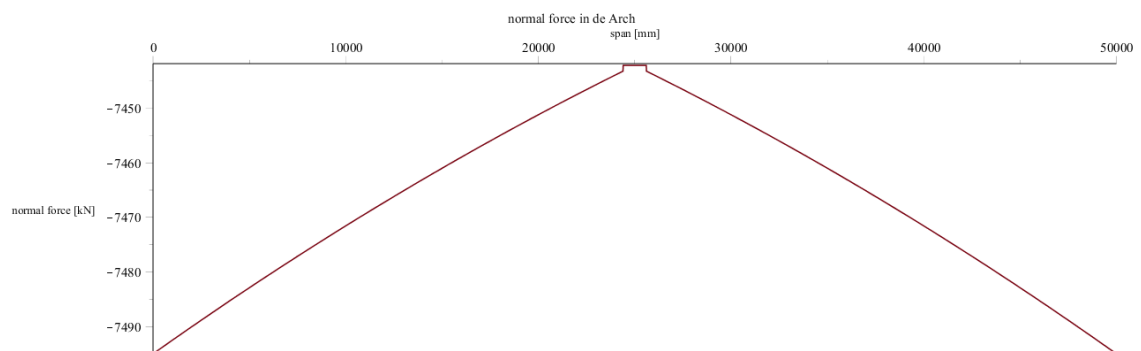


Figure 5.67: Normal forces (vertical axis) in arch on Figure 5.63 loaded according to LM1 with only uniform load and self-weight.

It proves that constant thickness is inefficient, determining the thickness of the arch according to the governing normal forces at the edges will result in unnecessary material usage. However thickness will assume to be constant. This principal of variable thickness is important design criterion especially when arch exhibits large shear and bending moments.

5.6.3.3 Elastic Stability

Now the structural stability is checked for the arch with the initial shape according to [4.3]. Important phenomenon lies in the abrupt alter in the initial form of equilibrium which may lead to collapse. Initially only the in-plane buckling is of parabolic arch with constant thickness and uniform load is observed. The critical load may be calculated by the formula:

$$q_{cr} = K \frac{EI}{l^3}$$

With parameter K obtained by numerical differential equations analysis of assuming linear elastic behavior (Hook's law), center line arch is incompressible, and loads are conservative.

Parabolic Arch:

f/l	0.1	0.2	0.3	0.4	0.5	0.6	0.7	1.0
Hingeless	60.7	101.0	115.0	111.0	97.4	83.8	59.1	43.7
Two-hinged	28.5	45.4	46.5	43.9	38.4	30.5	20.0	14.7

Table 5.1: Parameter K for parabolic uniform arch

Shallow sinusoidal Arch:

The proposed compressive arch shape in the previous section have very low sagitta/span ration, $f/l=(1/34)=0.036$. This shallow arch ($f/l<0.3$) leads to new form of instability regarding the change in length of the arch axis due to axial strain. In this arch snap-through buckling mode [Figure 5.1] which is likely to be governing for in-plane stability. Buckling shapes with three or more half sine waves lead to a lower buckling length compared to snap-through modes and thus a higher buckling load.

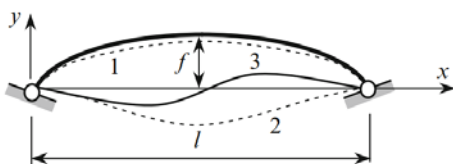


Figure 5.1: Shallow arch exhibits snap through buckling mode (1) (2) symmetrical and (3) anitsymmetrical

Timoshenko [Theory of Elastic Stability, Art 7.8] derived the K values for very flat sinusoidal arch. It can be used as approximation of the critical uniform load.

The initial centre line of the flat arch:

$$y = a \sin\left(\frac{\pi x}{L}\right)$$

The complete derivation of the buckling equations according to Timoshenko is available in the literature. In this article the representative equations will be given:

The centre line after loading of hinged flat arch (deflection function) is derived from the differential equations according to the beam-theory:

$$EI \frac{d^4 y}{dx^4} + P \frac{d^2 y}{dx^2} = q$$

The general solution of the DV for sinusoidal hinged arch with uniform load is:

$$y_2(x) = \frac{a(1-u)}{1-\alpha} * \sin\left(\frac{\pi x}{L}\right)$$

With:

$$u = \frac{5}{384} \frac{ql^4}{EIa}$$

$$\alpha = \frac{Hl^2}{\pi^2 EI}$$

a =sagittal

The solution is depended on the thrust (H). The equation for calculating the thrust is obtained by equating the change in length of the span due to deflection to the compression of the bar due to thrust:

$$\frac{HL}{AE} = \frac{1}{2} \int_0^l \left(\frac{dy}{dx}\right)^2 dx - \frac{1}{2} \int_0^l \left(\frac{dy_2}{dx}\right)^2 dx -$$

After integrating:

$$(1-u)^2 = (1-m\alpha)(1-\alpha)^2$$

For $m < 1$ the nonlinear function above have a stable equilibrium for:

$$u < 1 - \sqrt{\frac{4}{27} \frac{(1-m)^3}{m^2}} \quad \text{convex equilibrium}$$

$$u > 1 + \sqrt{\frac{4}{27} \frac{(1-m)^3}{m^2}} \quad \text{concave equilibrium}$$

f/l	0.01	0.02	0.03	0.04	0.05	0.06	0.07	0.08	0.09
Two-hinged	1.09	2.18	3.28	4.37	5.46	6.55	7.65	8.47	9.83

Table 5.2: Parameter K for parabolic uniform arch with symmetrical snap through buckling mode

Concluding, for shallow arch with $L=50.0\text{m}$, $f=1.8\text{m}$, $E=58000 \text{ N/m}^2$, $b=600 \text{ mm}$, and constant thickness $t=300\text{mm}$ the critical uniform load is $q_{cr}=111 \text{ kN/m}$ which including the self-weight and the uniform distributed traffic load (LM1).

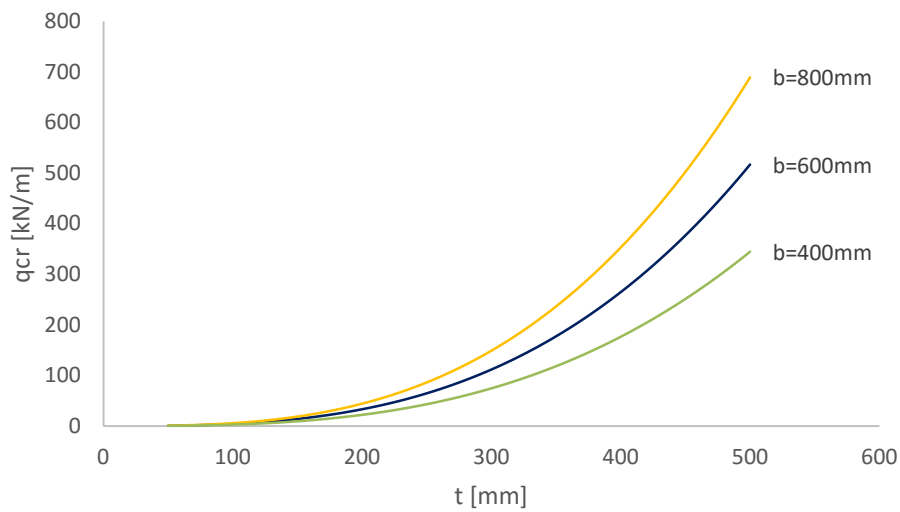


Figure 5.68: Critical load as function of the constant arch thickness

Parabolic Arch with Tie:

Let us consider two hinged symmetric parabolic uniform arch with tie at the level of support. We define the thrust without the tie (H) and the thrust with tie (H_{tie}).

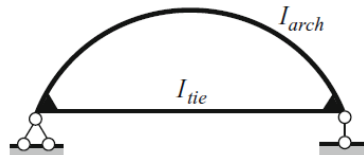


Figure 5.69: for two hinged arch with tie

H/H_{tie}	1.0	0.9	0.8
K	45.4	50.5	57

Table 5.8: Critical parameters K for two hinged arch with tie for $f/l=0.2$

One should pay attention to the unusual fact, decreasing of the stiffness (EA) of the tie at the fixed stiffness of the arch (EI) leads to decreasing of the axial force which arise in the tie. This concept is presented in Table 5.7 where the ratio H/H_{tie} is decreasing for increasing coefficient K. So decreasing the axial load in the tie (H_{tie}) leads to decreasing of the compressed force in the arch.

Deformations:

There are two deformation modes of the arch under traffic actions [Figure 5.67]. The first mode is the Extensional deformation (left) whereby the surface is stretching due to the loading so the loading is carried mostly by normal forces and a little bending moments, this mode is quite stiff.

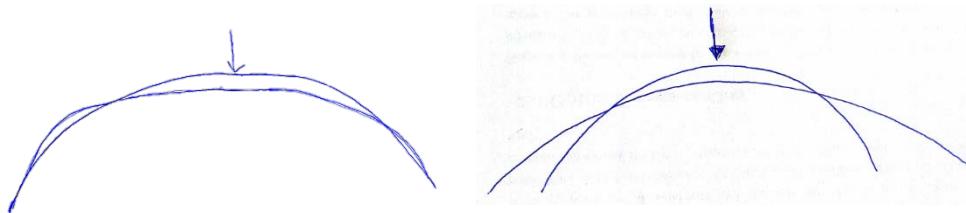


Figure 5.70: Extensional deformation (left) and In-extensional deformation (right)

The second mode is the In-extensional deformation (right) of an arch free of its supports. This deformation doesn't involve stretching of the center line, the loading is carried mostly by bending and only a little by normal forces. This mode is not stiff at all. In the first mode the secondary effects such as buckling under compression will be important. In the second mode the tensile capacity of the tensile cable will be important.

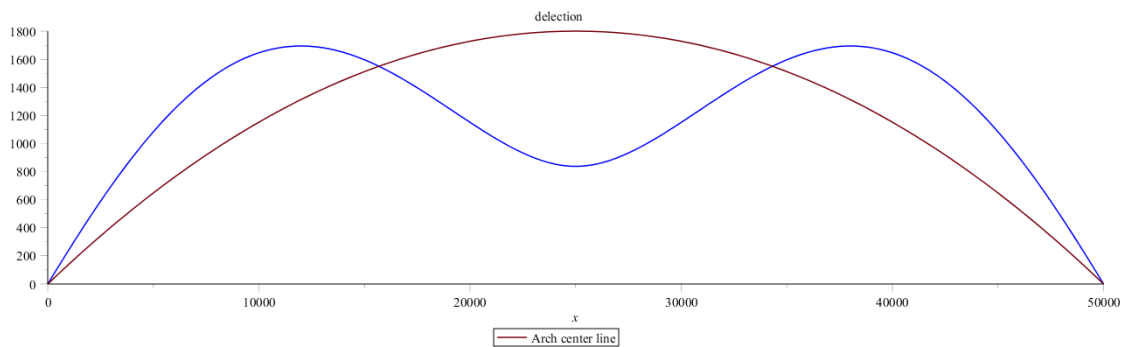


Figure 5.71: Deflection of two-hinged arch loaded with uniform and tendon load with $E=58000 \text{ N/mm}^2$

The stiffness (EI) of the arch is insufficient for SLS design: $U_{\max}=L/400=125\text{mm}$. The stiffness of the arch needs to increase without increasing the significantly the cross-section. In [4.9.7] this principal will be extensively elaborated.

5.6.3.4 Strength analysis

Any load (temperature, imposed deformation, live load) on the structure leads to its deformation. It means that the structure will change its shape. Both shortening due to compressive strain and the flexible horizontal support conditions lead smaller thrust force (H) when stiffness (k_{supp}) decrease [Figure 5.69]. The relations between those two can be found with the classic equation of the thrust for two-hinged arch:

$$H = - \frac{\int \frac{M^a z}{EI} dx}{\int \frac{z^2}{EI} dx + \frac{l}{EA} + \frac{1}{k_{supp}}}$$

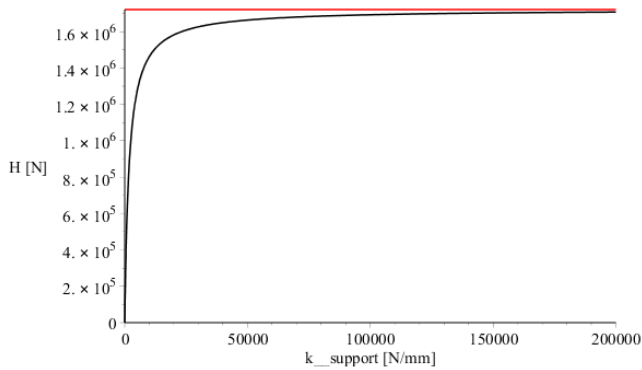


Figure 5.72: Influence support stiffness on horizontal thrust

Now assuming the arch is hinged at both of the supports. We apply dead loads and live loads according to [Table 5.8].

	Value
Dead load (self-weight)	4.93 kN/m
Live load: uniform load (LM1)	9*1.15*2 kN/m
Live load: tendon load	2*300 kN

Table 5.9: Applied actions

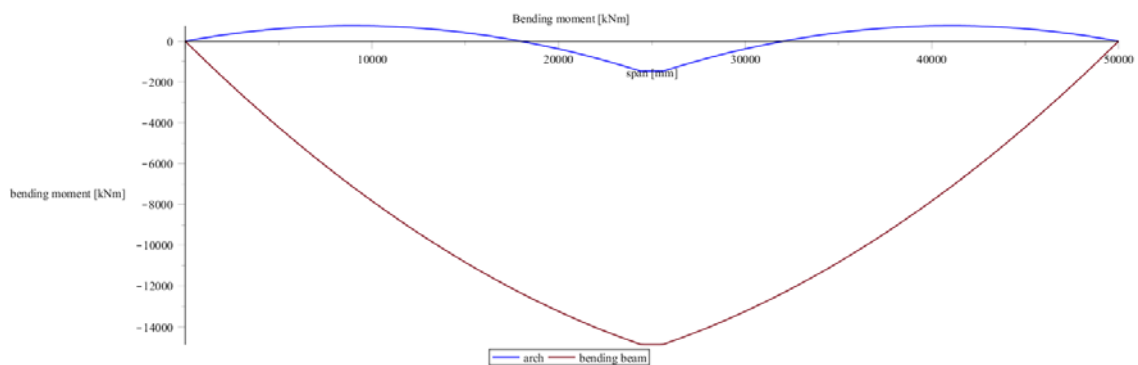


Figure 5.73: Bending moments in statically determined beam (red) and in the parabolic arch

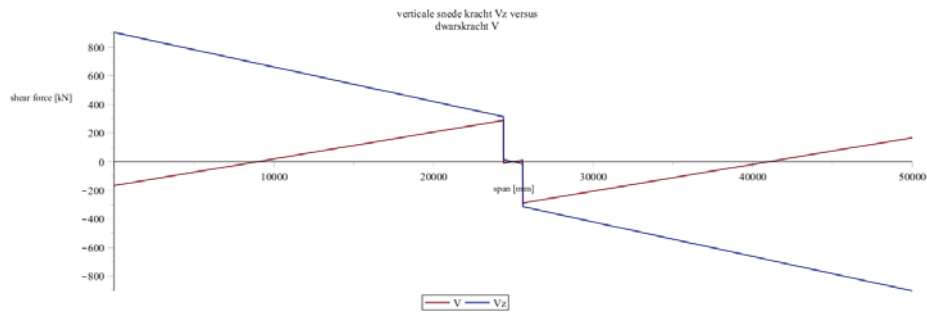


Figure 5.74: Shear forces in a statically determined beam (red) and in the parabolic arch (blue)

Since this is elastic-linear analysis the stresses in the arch as result of this forces in SLS are plotted. The maximum compression and tensile stresses are found around the midspan: -300 N/mm^2 and $+200 \text{ N/mm}^2$.

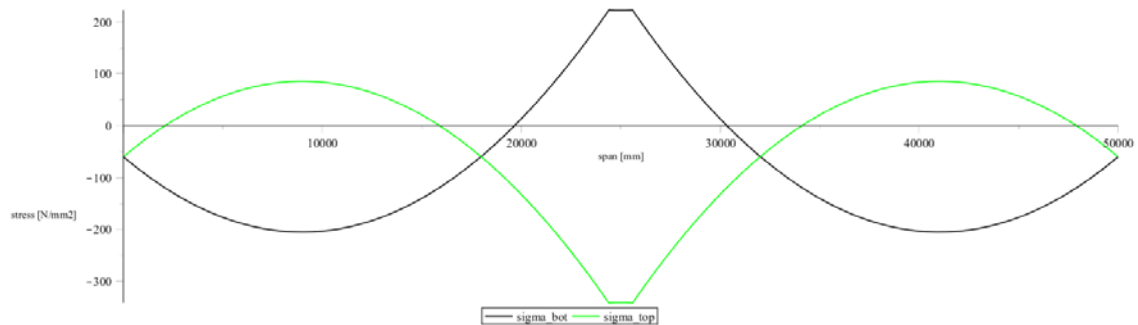


Figure 5.75: Normal stresses parabolic arch

Largest shear stresses as expected near by the supports especially if the point load is shifted in the direction of the support. The arch cross-section will be increased proportional to the shear stresses.

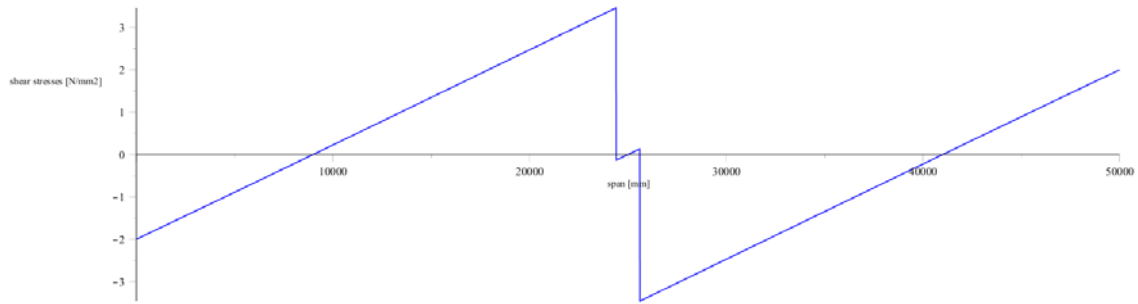


Figure 5.76: Maximum shear stresses parabolic arch

The highest shear stress of 3.5 N/mm^2 is observed about the midspan. Concluding the strength analysis of the arch by choosing the appropriate material fundamental design step. Obviously that the observed stress value are strictly related to the arch dimensions and therefore changing these dimensions may influence the material choice. Moreover, the compression arch needs to be more massive. Ultra-high Performance Concrete is recommended as the most suitable material

5.6.4 Iteration III – Functional requirements

Typical Traffic Bridge is subjected to very high loads. These tends to increase throughout the years. Engineers following the European norm will have to cope with increasing of the bridge dimension in order to sustain the live loads or wishing to increase the bridge spans. As result the self-weight of the bridge will become the dominant load. Reducing it will require state-of-the-art solutions. Considering the functional requirements [4.4] will result in rectangular shape with compressive arch [Figure 5.74].



Figure 5.77: Rectangular beam with compressive arch.

The rectangular frame plotted as lines around the arch will need to sustain the loads. For instance the upper straight line of the rectangular stands for the top compressive flange. The bottom straight line of the rectangular stands for the tensile tie spans from arch supports. Furthermore the arch stiffness should be increased, the vertical lines on both sides are members which increase the stiffness.

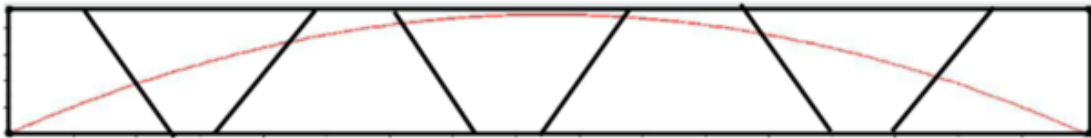


Figure 5.78: Increasing stiffness with truss members

5.6.5 Iteration IV – Technical requirements

Recalling the technical requirements of the structure [4.4], the design will be further optimized. The most important requirements are given in [Table 5.9].

<i>Technical requirements</i>
Strength
Stiffness
Stability
Safety factors
Unity checks

Table 5.10: Technical requirements

In the previous section [4.9.3.4] the linear-elastic stresses for the arch are derived. The cross section of the beam at this cycle [Figure 5.76] simulate the perfect cross-section: Tie at the bottom and compressive concrete element with variable lever-arm.

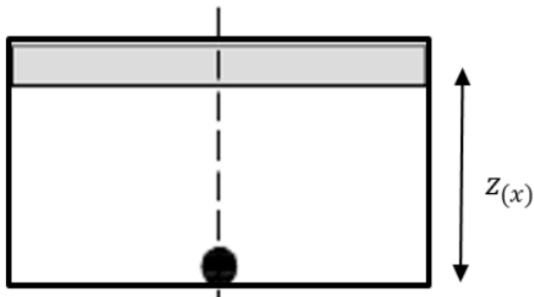


Figure 5.79: Proposed cross-section at $x=0.5L$

The current arch beam cannot fulfil any of the technical requirements. The rectangular frame which is accounted for the beam shape will have to be thick sustaining the high load-levels. The design will have to bear additional shear forces and tensile stresses as result of non-uniform loads. So a concrete web is added to the beam [Figure 5.82] and upper flange which connects to the web. Prestressing will be applied to prevent tensile stresses.

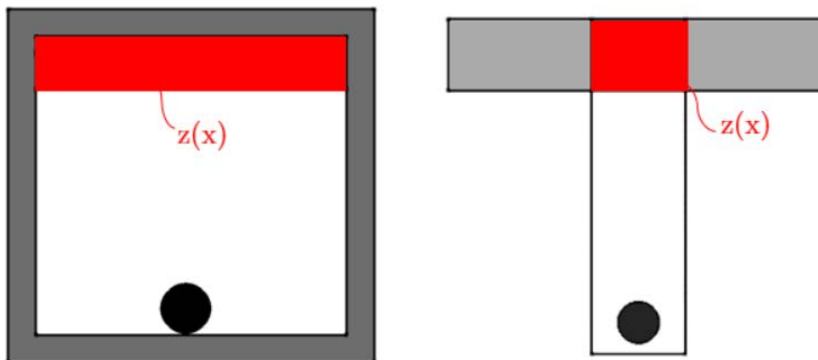


Figure 5.80: Possible realistic cross-sections at $x=0.5L$, with variable compressive arch (red) height $z(x)$

Yet the beam will require excessive amount of material to meet the strength limit state. In the longitudinal direction the thickness of the compressive arch will vary corresponding to the magnitude of the compressive forces [Figure 5.78]



Figure 5.81: Side-view arch beam

5.6.5.1 Shear capacity

The shear capacity (tensile capacity) is primary a function of the steel fibers in the concrete and shear reinforcement. In the case of UHPC fibers will increase shear capacity dramatically however variability in properties result in hybrid design is accounted. Assume that the arch will not buckle and that the compressive stresses are lower than the compressive capacity. Additionally assume that the tensile tie is yielding. The nett shear force taken by the web (V_{nett}) is equal to the subtraction of shear force taken by the compressive arch (V_c) from the total vertical shear force (V) .

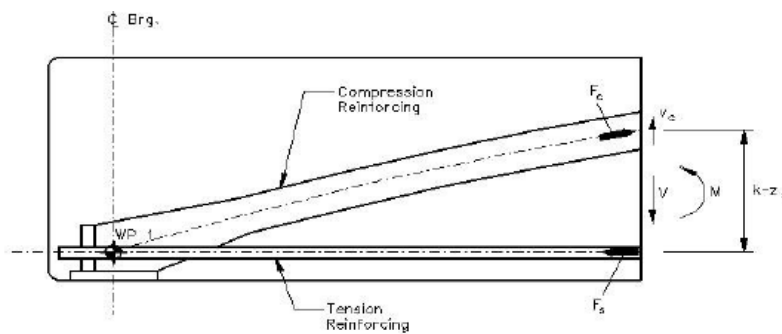


Figure 5.82

$$V_{nett}(x) = V - V_c = V - M \frac{k'}{k - z_s}$$

With

M bending moment at $x=x_0$

k' slope of the arch profile at $x=x_0$

$k-z_s$ moment arm

The advantage of load sharing effects resulting from the arching action of the compressive reinforcing, the residual stresses in the web can be reduced substantially. The nett shear stresses are calculated to be 53% smaller than the total shear for the critical sections at the end of the beam.

In the last assumption only the arch and the tie is considered. Now the web of the beam [Figure 5.77] is accounted for. The web can be subjected to in-plane stresses both horizontally and vertically as well as shear stresses and out of plane bending stresses resulting from bending at the interface with the flanges. These components are working in hybrid-composite beam with anisotropic material.

5.6.5.2 Deflection

Arch beam with tie at the supports will suffer from relatively large deflection which is the governing design criteria. It will require to design a beam with reserve ULS strength capacity in order to meet this criteria. The serviceability limit state (SLS) of the arch beam has to meet maximum vertical deflection of $L/250 = 68$ mm.

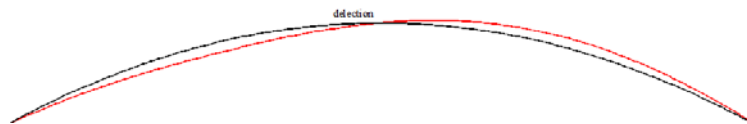


Figure 5.83: max deflection when $F_{TD} \Rightarrow x=0.2*L$

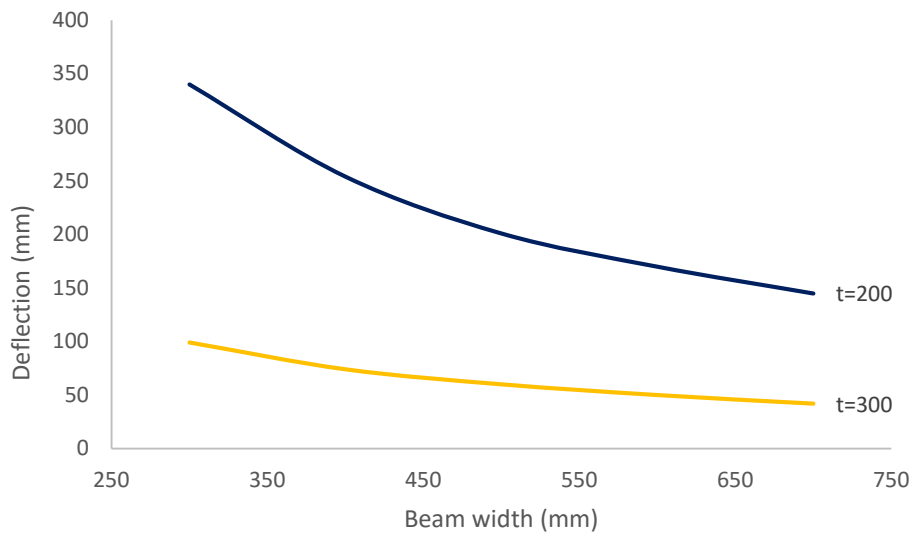


Figure 5.84: Deflection as function of the arch for tendon load at $0.2 \cdot L$

The arch thickness should larger than 300mm with a width larger than 500mm. However considering the present of a concrete web will dramatically increase the stiffness of the beam. It is important to know that in many conventional bridge structures the cross-section of the girders is prismatic, or constant over the length of the beam. For simply supported beam, this simplify deflection calculations. Variety in rigidity (EI) over the length and different material (hybrid) results in more complex (Non-linear) calculations.

5.6.6 Iteration V – Topological optimization

5.6.6.1 Mechanical interpretation

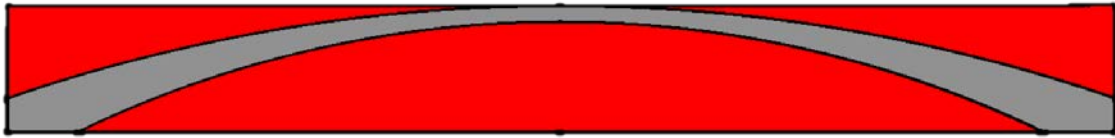


Figure 5.85: Massive arch beam with concrete web (red)

The 2D arch beam [Figure 5.82] will probably be simple to execute and more cost/effective if the red area will be massive, casted from single material other than the high performance concrete used for the arch. This massive arch beam will have an improved stiffness in the longitudinal and the transversal direction. However, this will not fulfil some of the research goals, namely: increasing the efficiency by optimized material usage, or in other words, apply AMC where its strength and stiffness characteristics can be fully utilize. Topological optimization [4.8.2] is initiated for the design domain coloured in red result in system of working couples [Figure 5.83] with internal lever-arm as function of x-axis (longitudinal axis).

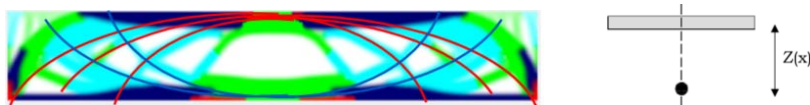


Figure 5.86: Multi-linear optimised beam

Without getting into the mathematical theory behind the topological optimization, 2D optimization problem will be considered in order to save calculation time. First some practical solutions will be discussed with the aim of understanding the optimization process. In the first example [Figure 5.84] typical massive rectangular concrete bridge

beam is subjected to stationary loads. The 2D model indicates very clearly where the present of material is vital and where material can be removed. Unsurprisingly the material is effective where the force couple is the largest, thus where the largest tensile and compressive forces are expected. Furthermore it is observed that the force couples between the compressed and tensioned bars occur under inclined bars. The massive beam is transformed to a system of force couples with four compressive bars and four tensile bars.



Figure 5.87: Coupling of compressive and tensile arch in a beam

In the second example the working of the force couples is illustrated. In this case there is one compressive bar (red), three inclined tensile bars, and two probably compressive diagonals (blue). In this example the guardrail is used as constructive element resulting in a very slender deck with less prestressing cables. The problem with this design is the higher probability of failure for any damage to the guardrail.



Figure 5.88

5.6.6.2 Target density

The target density will define the objective of the optimization. The massive arch beam will be transformed into a light weight efficient arch beam.



Figure 5.89: TD=30%

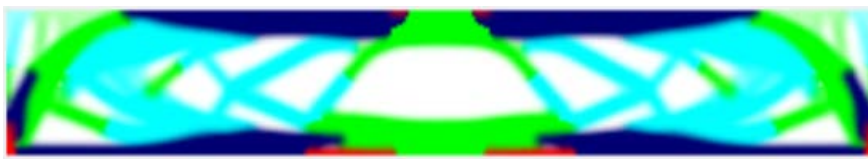


Figure 5.90: TD=60%

5.6.7 Iteration VI – Linear analysis

Verification of two design principles is the purpose of this iteration. Span , and topological optimization models. In [Figure 5.88] [Figure 5.89] topological optimization analysis conducted for simple supported bridge beam.



Figure 5.91: Topological optimizations, the colours are indication of the stress levels in each element.

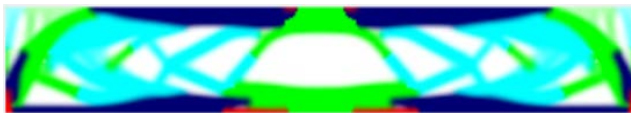


Figure 5.92: Multi-material Matlab analysis. Blue=UHPC, light blue=NSC, green=SHCC, red=steel

In the last 5 iterations steps knowledge is obtained on the girder design. The level of specification built-up gradually with each iteration. Now the first full scale analysis is carried on. Linear elastic 1D FEM analysis is carried out where the girders shape is plotted only with line elements. This analysis is carried out for girder with short span of 17m and height of 600mm. The results of this analysis should suggest that the taken dimensions are unrealistic, supporting the results of the study in iteration I [4.9.2].

Few models are drawn in AutoCad within the design domain, the rectangular frame, functioning as the geometrical limitation. Line elements are added according to the topological output. These lines are drawn with splines which are smooth curves with continuity level C2. This continuity level assure a design with low stress concentrations, usually only at the connection line, this happens because the curvature of the two surface are the same at the connection line.

The models presented in the next page can be divided into four groups:








<p>Model 1</p>  <p>Description: Compressive arch full spans between edges, two compressive diagonals at 45° at midspan, and three tensile arches (upside-down)</p>
<p>Model 2</p>  <p>Description: Compressive arch full spans between edges, two compressive diagonals at 45° at midspan, and three tensile arches (upside-down) connected to the same node.</p>
<p>Model 3</p>  <p>Description: Compressive arch full spans between edges, compressive arch span half of beam length, two compressive diagonals at 45° at midspan, and three tensile arches (upside-down)</p>
<p>Model 4</p>  <p>Description: Compressive arch full spans between edges, smaller compressive arch at midspan, and two tensile arches connected to the same nodes.</p>
<p>Model 5</p>  <p>Description: Compressive arch full spans between edges, and three tensile arches (upside-down) connected to the same node at midspan.</p>
<p>Model 6</p>  <p>Description: Compressive arch full spans between edges, one small compressive arch at midspan, three tensile arches connected to the same node, and two compressive diagonals at the edges of the beam</p>
<p>Model 7</p>  <p>Description: Compressive arch full spans between edges, two compressive diagonals at 45° at midspan, two compressive diagonals at 45° at the edges of the beam connected to one of the tensile arches.</p>

Figure 5.93: Overview one dimensional models

5.6.7.1 Topology versus location of concentrated force

On the girder acting besides the Dead loads also Live loads. The governing Live loads for this analysis are the uniform distributed load and the concentrated tendon loads. Because this model is based on the topological optimization based on the location of the loads, it is important to understand the effect of load locations on the models.

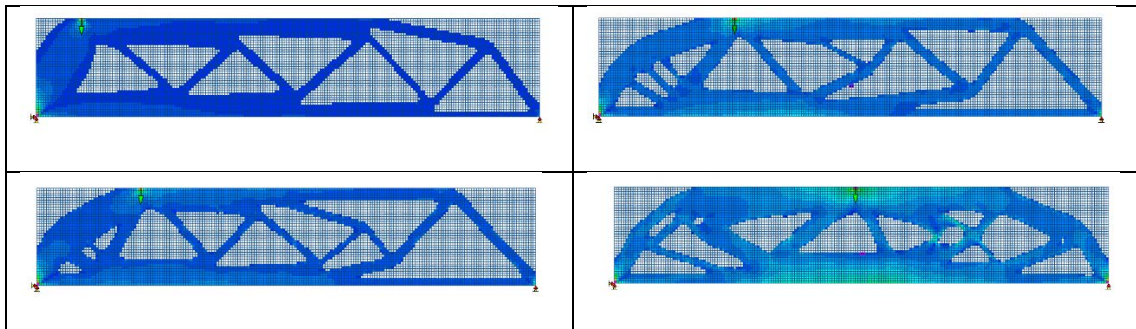


Figure 5.94: location concentrated load

The shape of the arch and the curved members are as expected change their location and shape according to the stresses in the XY plane. It assumed that the governing load act at midspan (Largest bending moment).

5.6.7.2 Connections



Figure 5.95:

The bottom and upper lines of the models delimit the height of the girder. Although these outer lines of the model look the same, in reality they're fulfilling different role. The upper line is carrying the traffic load, and the dead weight of the asphalt. It is subjected to uniform, and tendon loads according to the EC2. On the other hand the bottom line modelled a tensile tie anchored to the edges of the compressive strut. In order to increase the stiffness, curved elements and straight elements will follow the path according to the

topological optimization analysis [Figure 5.89]. The compressive arch, the upper span, and the tensile tie linked by curved elements following the principle directions in the XZ plane.

Recalling the requirement of 100% modularity, the connections between the elements is critical design criteria. Investigating the effects of connection type on the structure forces distribution is considered. First elements are hinged (reduced shear forces and moment) follows by rigid connection (stiffer structure, shear forces and bending moments). The stiffness range of the connection with the lower bound and upper bound is given bellow. In practice the stiffness of the connection will be somewhere in between.



Figure 5.96

The curved tensile member will be clamped to the arch with prestressed steel cable or bar. The bearings will accommodate the movements (rotations, thermal expansion), and transfer the forces from the member to the arch.

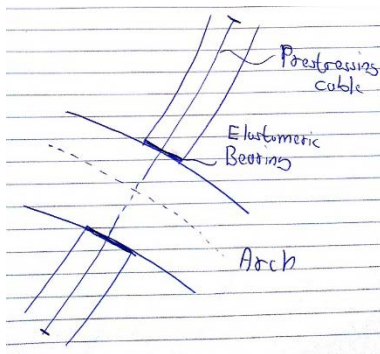


Figure 5.97: Connections

Analysing both models bellow allows to compare the effect of connection type on the force distribution.

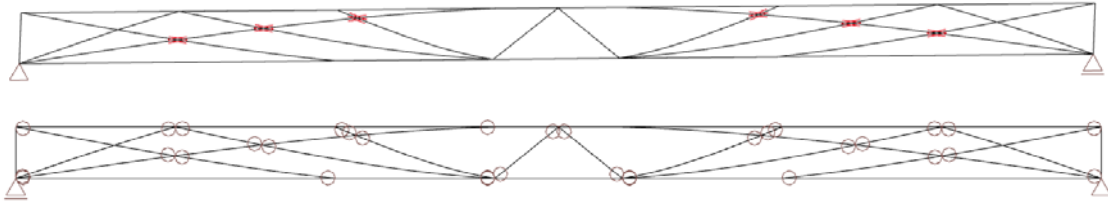


Figure 5.98: Rigid connection and hinged connections SCIA model

Results presented [Table 5.10] are the internal forces of 1D model [Figure 5.95] subjected to traffic loads according to [4.5.2].

	<i>Rigid N</i>	<i>Hinged N</i>	<i>Rigid My</i>	<i>Hinged My</i>
Compressive arch	-19.17	-19.5	-0.6, 1.49	1.5, -0.92
Curved members	-16.67, 12.14	-13.69/11.97	2.11, -0.6	-0.7/2.10
Diagonal	-2.00	-3.0	0.93	0
Frame	-40.66	-41.61	-0.72, 1.12	-0.68, 1.29
Tensile cable	42.27	43.27	1.58	1.69

Table 5.11: Envelope values 1D model. Negative moment = tension upper fiber, Negative normal force = compression force. Units [KN] [kNm]

Analysing the results indicates that the upper/lower bounds of the connections type do have effect on the forces distributing in the hybrid girder. However 1D analysis is used to dimensioning the members and not to test the ultimate limit state of the girder.

Therefore the influence of the connection type will be neglected assuming relative small deviations of the rigid model from the hinged one.

5.6.7.3 Dimensioning members

Model number 1 [Figure 5.90] is further analyzed. The dimensions of the members is based on quasi-elastic load stage when the concrete response is linear-elastic. The load combinations is the envelope of uniform load + tandem load located in six different location in the length of the beam.

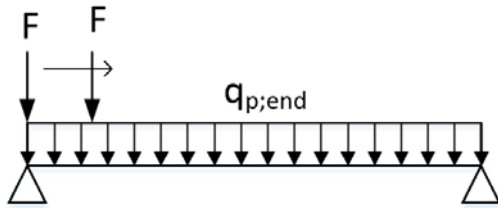


Figure 5.99: Illustration of loaded the girder with LM1

Uniform distributed load	kN/m	10.35
Tendon load	kN	300

Table 5.12: Load Model 1

Governing internal forces

In total 5 load combination were considered, the envelope internal forces draws the highest values for each combination. In

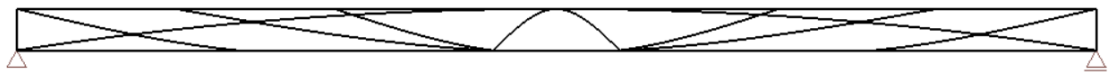


Figure 5.100: 1D FEM model

	<i>Negative moment</i>	<i>Positive moment</i>	<i>Compression</i>	<i>Tension</i>	<i>Shear</i>
	kNm	kNm	kN	kN	kN
1 Curved members	115	255	668	1266.9	290
2 Arch	170.7	326	1735	0	265
3 Upper frame	270	228	1821	0	396
4 Lower frame	0	145	0	3766	33
5 Small Arch	0	177	-1255.5	301.45	205

Table 5.13: Internal forces 1D model

Members

The results of [4.9.7.3] are plotted in Figure 5.98. The compressive stresses are summation of the bending and normal stresses. Recalling the maximum height of the beam ($h=600\text{mm}$) the members would have to be larger than expected.

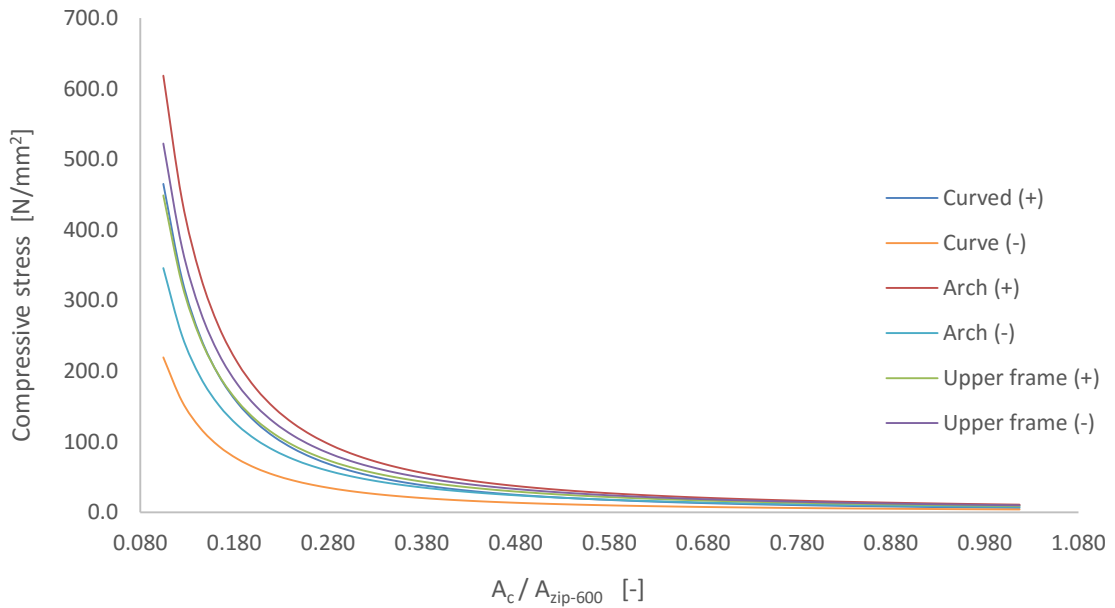


Figure 5.101: Compressive stresses as function of ratio between member area and reference member.

Ignoring the tensile stresses and shear stresses in the curved members and in the frame, the cross-section can be computed based on the internal stresses and the concrete compressive strength. The compressive arch would have to be prefabricated with concrete class of 140 MPa and with arch area of 0.079 m^2 ($b \cdot h = 400 \cdot 200\text{mm}$). The curved members and the frame members would have to be so thick that the girder become massive

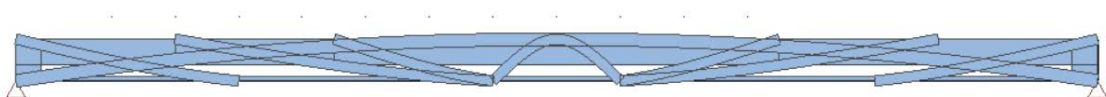


Figure 5.102: 2D FEM

The primary function of the members up until now was to bear the internal compressive forces disregarding the size of the elements. With this design cycle 1D truss girder is transformed into 2D truss girder. Comparing the hybrid girder with reference girder with constant cross-section Zip-600 [4.3] reduction of 37% material is achieved. Based on the last five design iterations it can be said that this proposed girder layout would be more suitable for larger spans with greater height.

Prestressing members

Members need to restrain the tensile stresses, bending tensile stresses and shear forces. The compressive stresses are however favourable.

Assuming the following simple calculation according to the EN 1992-1-1:

<i>Prestressing</i>		
Characteristic diameter	mm	45.2
Cross-section steel	mm ²	140
Design value of failure load ($A_p f_{pk} / y_k$)	kN	235
Maximum prestressing force after tensioning ($\sigma_{pm0} = 0.75 f_{pk} = 0.75 * 1860 = 1395$)	kN	194

Table 5.14

The total amount of prestressing force required will be:

$P_{m0} = \frac{M}{W} * A_c + N_t$ The prestressing load are applied at $t=0$ before tensile stresses will be present at the member. Therefore it is important to verify that the concrete compressive strength haven't exceeded.

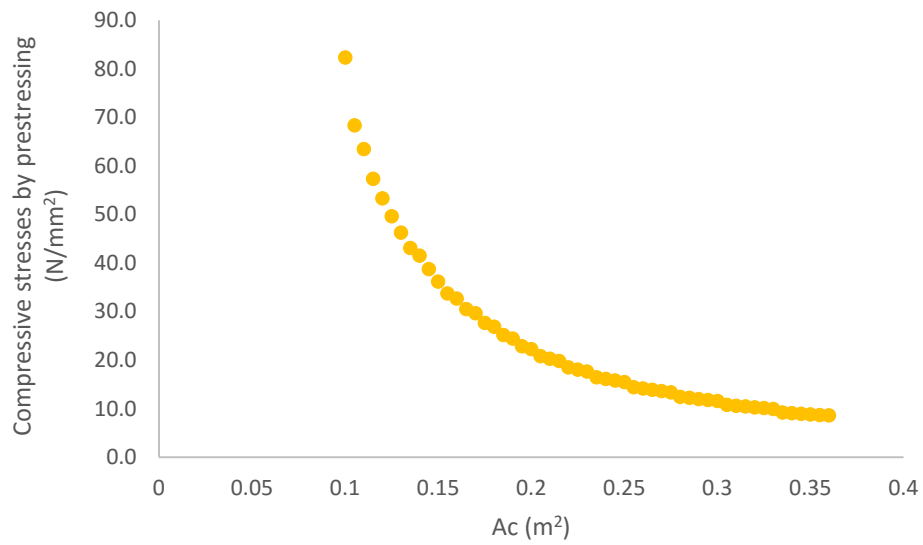


Figure 5.103

The diagram [Figure 5.100] shows the relation between the required prestressed force to overcome the tensile bending force and the normal tensile force, and the cross-sectional area of the concrete member.

5.7 Recommendation

The truss-style layout with compressive strut and tensile tie is explored with the aid of topological optimization and linear finite element analysis. The knowledge collected during the research on advanced cementitious materials [2.3] and the design principals such as 100% modularity [4.8.3], local stiffening [4.8.5], and compressive reinforcement arch [4.8.1] was significant as the parametric analysis [4.6]. The Sharebrooke footbridge resembles the usage of these principals for a pedestrian bridge.



Figure 5.104: Sharebrook footbridge

Engineering the girder of the future to be a practical alternative for traditional one is a great challenge. Concluding this chapter with recommendation for Part III of the research the design study concerns the following:

- Design criteria
- Design principles
- Complication

5.7.1 Design criteria

These are partly discussed during the parametric study [4.6] and partly defined at the requirement & conditions new design [4.4]. The criteria used in the next chapter are used iteratively, means that the girder dimensions, shape, prestressing, reinforcement, and applied material are fine-tuned until they converge into workable preliminary concept.

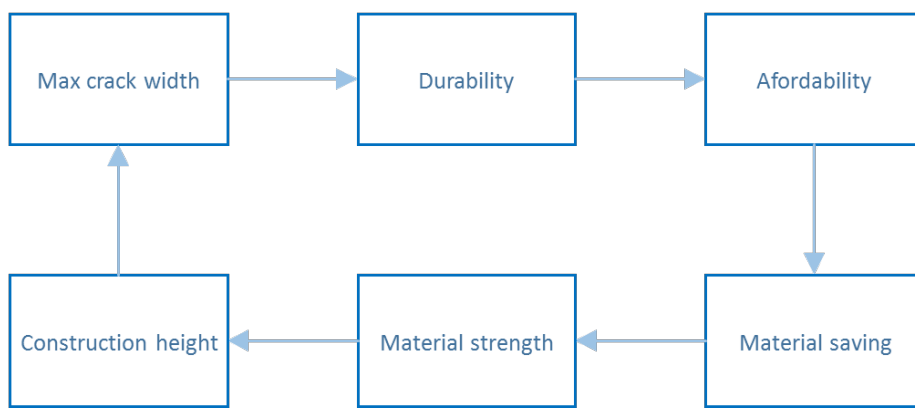


Figure 5.105: Design criteria cycle

5.7.2 Design Principles

As discussed in [4.8.6] the 7 leading principles would guideline of the girders final design. The conducted structural analysis in this chapter is the proof and initial evaluation of the structural feasibility of the proposed bridge design. However, the level of details is still low, a more details analysis will be conducted op to a level of safe and functional Preliminary design.

5.7.3 Complications

Tensile stresses

Concrete members need to restrain the tensile stresses caused by bending and normal tensile forces. Throughout multimaterial topological optimization based on stiffness [4.9.6], parametric study, and 1D FEM linear analysis the cross-sectional dimensions of the member and the applied material determined. Failure will occur if shear stresses, flexural stresses and normal stresses exceeds the corresponding ultimate strength parameter. Possibly applying prestressing together with steel reinforcement is the solution. This will be discussed in the next chapter.

Shear

As stated earlier in [4.9.5.1] shear strength are function of the steel fibers in the concrete. Shear strength of concrete members without shear reinforcement with steel fibers is one of the most interesting field of application of advanced cementitious materials. It has been proven that with the right amount of fibers and fiber type, sufficient shear capacity is possible. Throughout designing in the principal directions and hybrid approach and stirrups shear stresses are controlled.

The tendency to adopt the steel fiber as replacement for traditional reinforcement introduce unknown degree of uncertainty. The reliability of steel fibers (microfibers and macrofibers) is still insufficient, especially slender members have high probability of local downgrade in properties cause by variability fibers orientation.

Connections

Prefabricated elements are post-tensioned with strands that anchored to steel end-plate. The end-plate is connected by welding or bolting to a connection plate which form the joint. This is only one possible solution to the connection of the concrete truss elements.

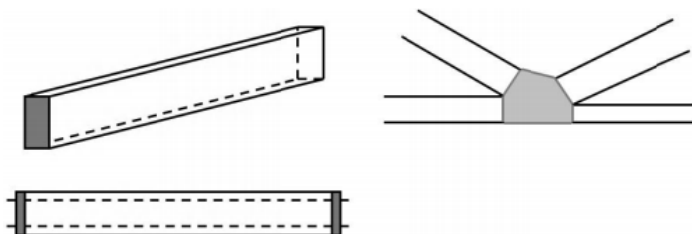


Figure 5.106: Connections of truss elements with POT strads. [B04, p623]

The connections between the truss members are the weakest link with high tensile and shear forces from multiple directions. It is important to find a simple elegant solution for connections concrete members. It is recommended that the concept can be worked out with details and calculations.

Stability

Local instability such as buckling due to high compressive force and high slenderness, lateral instability, or second order effect is accounted for. The Eurocode approach based mainly on coefficients (engineering approach) is used in this study when necessary. Instability caused by buckling should be solved without increasing the dimensions of the structure but by increasing the stiffness and the structure shape. Transversal stability of the bridge structure should be taken into account.

Dynamic load

Dynamic analysis is required. The natural frequency of the girder should not exceed the calculated values. Increasing stiffness may be necessary.

Reliability

In material level adding fibers reinforcement contribute to the maximum crack width in the post-cracking stage while adding micro fibers control pre-cracking stage. From structure point of view a reliable structural limit state design. However the uncertainty lies on the discontinuous material properties supported by large scatter of the bending tensile tests compared to the traditional reinforced concrete affected the limit state design.

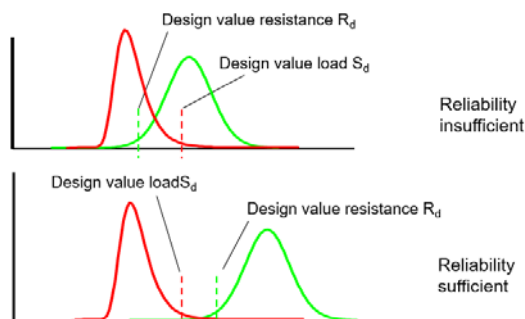


Figure 5.107

Moreover it remains difficult to gain a rational description of the fibers contribution due to its heavily non-linear behavior. The ultimate strain capacity requires calibration taking into account material knowledge at specimen level and the structural response influenced by fibre orientation and size of member.

Affordability

The aim of design according to [4.8.2] is to minimizing material use within 50%. This is possible throughout out-of-the box design and the usage of expansive ACM. In this case concrete costs superstructure will increase despite the reduction of materials. However, the reduction of the superstructure dead-loads means lighter superstructure. As result the substructure (abutments, piers, columns, embankments, and foundation) can be lighter as well which again can be translated to material costs. Increasing the slenderness ($L/h > 25$) of the superstructure will further reduce the substructure costs due to reduction of soil-bodies dimensions.

In [Figure 5.105] the effect of concrete quality of superstructure in terms of price is plotted. The total costs of substructure will be reduced when high concrete class is applied.

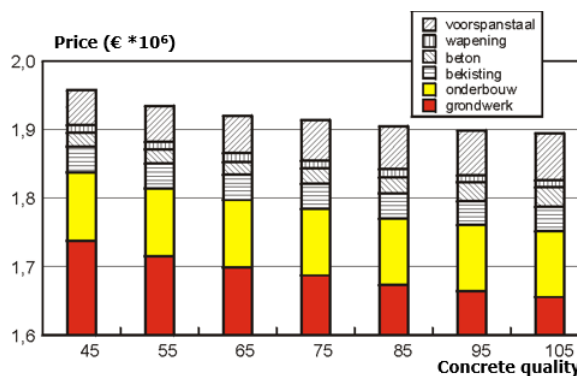


Figure 5.108: Reader Dimensioneren van Betonnen Bruggen C. van der Veen, CIE4160

6. Preliminary design

This chapter will focus on the preliminary design of the ACM girder. The design is therefore not final, and further optimization will be required to finalize this new concept of concrete girder.

6.1 T-girder

In [4.6.3] the influence of cross-section type on the dead- and live load capacity is described. It states that unsymmetrical cross-sections (T-girder) with high dead-load can sustain only relative small live loads. So for large span T-girder where the dead load is predominant limited capacity is left for the variable load. Henceforth, it is recommended to reduce the dead-loads substantially in order to be able to use T-girders for large spans. Symmetrical cross-section on the other hand are well suited for small dead loads combined with high live loads therefore suitable for smaller spans where the live loads are more predominant.

6.2 3D – dimensioning



Figure 6.1: Multimaterial topological optimization, $L=50\text{m}$ $h=1.80\text{m}$. 200 iterations, 50% material reduction.

Based on the design principals in [4.9.6] the 1D optimized girder will be translated to 3D design. The initial materials topology is further based on [Figure 6.1]:

- Flanges= UHPC
- Truss elements=NSC
- Tensile element= UHPC or SHCC,
- Web=SHCC or HSC

Furthermore because the geometry is optimised for a uniform loads, loading the entire span based on influence lines theory is critical. In this way the most critical case can be addressed.

In [Figure 6.2] [Table 6.1] impression is drawn of the girder in 3D environment. The yellow area will be designed based on [Figure 6.1] in SCIA 3D environment with accent on global stiffness, material saving and Construction phases. Once the structure has gone outside the elastic range there is no guarantee that it will recover from deflection or crack opening caused by transient load, hence design within the linear–elastic range.

t_1	thickness deck	to be determined
B_1	width deck	to be determined
B_2	width compressive strut (web)	to be determined
L	span	determined
h	total height	follows from slenderness requirement $L/d > 25$
Yellow area	Web zone	to be determined

Table 6.1: Dimensions of the individual girder

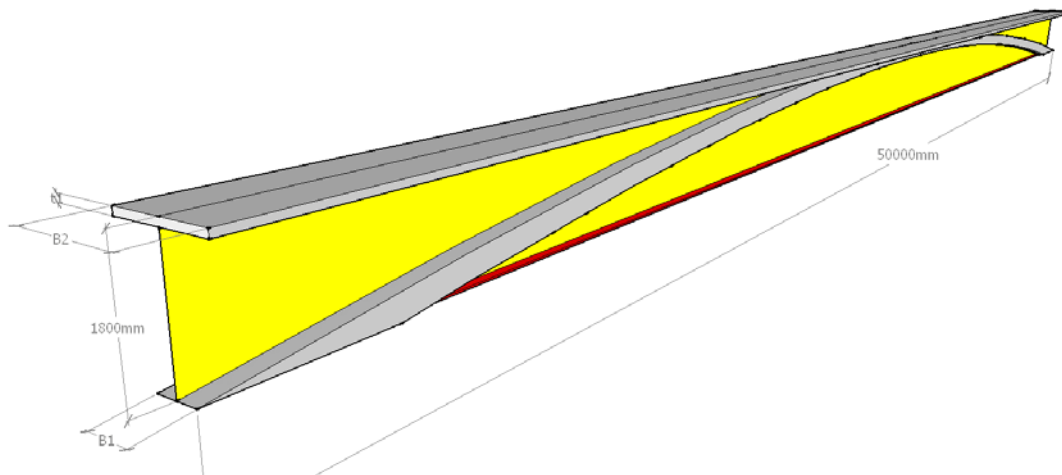


Figure 6.2: 3D impression, concept version of the girder, the height and span correlate with that of SKK girder [Spanbeton].

The yellow area in [Figure 6.2] should be attain a structural concept supporting the compressive arch and the flanges. It is known that truss members will be the most effective. There are further two options:

- **3D truss** – The truss members are forming a triangular shape connected at the bottom to one tensile member and at the top nearby the edge of the flange. This forms a stiff shape also in the transversal direction and is already an existing concept. [Figure 5.101].
- **2D truss** – Truss members are replacing the web of the T-girder (yellow area). The truss members are connected to the tensile tie at the bottom and to the compressive strut at the top. This shape is however unstable at transversal direction and required a compression layer.

6.3 Finite element analysis

6.3.1 Reference girder

Dead load: 117.5 ton

Maximum vertical displacement: 1000mm

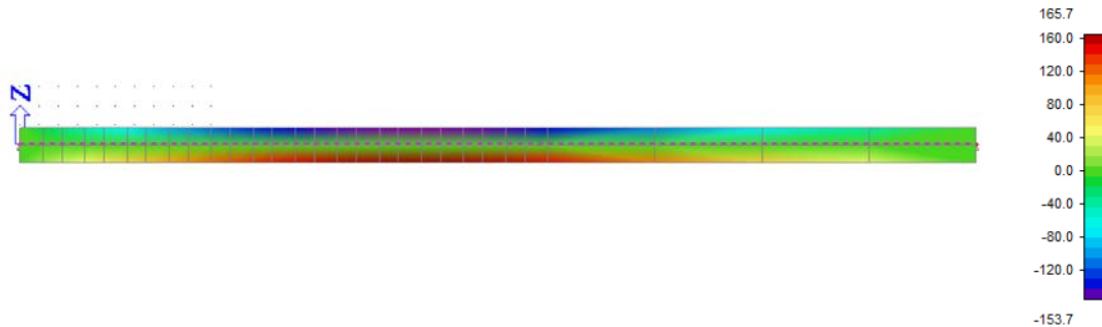


Figure 6.3: SLS envelope normal stresses. SKK-1800 girder, L=50.0m

The reference girder is simple supported 1D beam with span of 50m. The loads on the beam are identical to the loads on the other models and represent traffic loads [NEN-EN 1991-2]. The maximum normal compression stresses of 160 MPa occur as expected at midspan top fiber.

6.3.2 Ultra-light girder

Dead-load: 96.92 ton

SKK1800: 117.5 ton

Maximum vertical displacement: 405mm

This model represent minimum weight reduction of 17.50% compared to typical SKK1800 girder of similar span. The normal compressive stresses in SLS are varying per element. The main convex arch is under average normal compressive stress of 55 MPa with local peaks at the connections around 120MPa. The beams plotted in red are in tension, these will be prestressed (Figure 6.4). The concave arch at midspan is under

normal compressive stress of 120 MPa at the top fiber and under tensile at the bottom fiber, prestressing is required.

The top flange is under average normal compressive stress of 55 MPa with local peaks of 160 MPa caused by the tandem load. These can be neglected if the load dispersion accounted for by applying additional compression layer.

This model is unrealistic because the prestressing cables of the main convex arch requires end-blocks to anchor the tensile cable and because shear behavior is not accounted for.

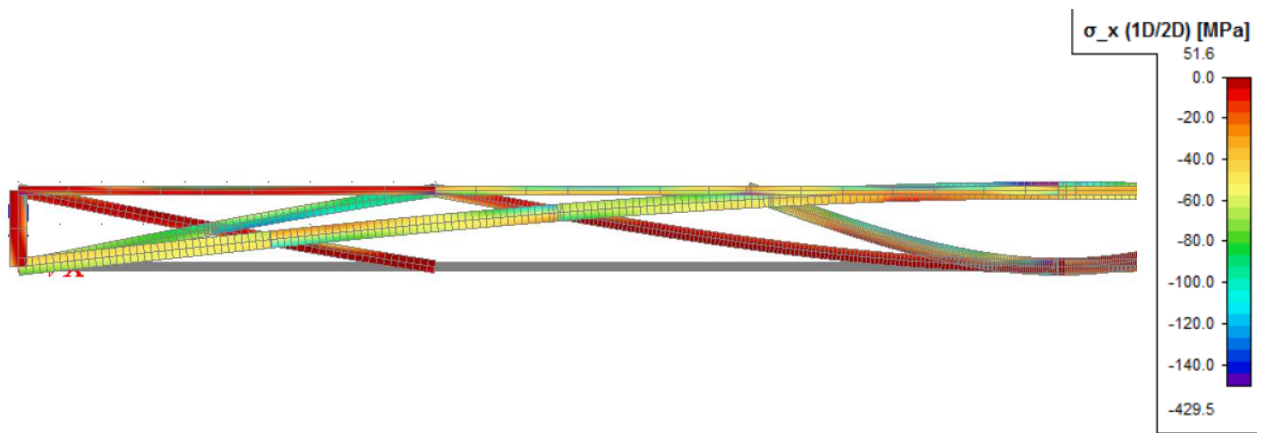


Figure 6.4: SLS envelope normal stresses 1D FEM analysis

	b	h	<i>Material</i>
Convex arch	500	400	HSC
beams	400	300	UHPC
Concave arch	400	400	UHPC
Flange	1400	150	UHPC
Weight reduction		17.5%	

Table 6.2: dimensions

6.3.3 T-girder with curved truss elements

Dead-load: 87 ton

SKK1800: 117.5 ton

With minimum weight reduction of 26.0% and massive web in the direct shear transfer zone ($a/d < 2.5$) this model represent the progress in design from theoretical model to fully operational girder. This is 2D in-plane model shows high shear stresses (12 MPa) in the web nearby supports and high compressive stresses of the deck (-120 MPa). A solution will be to increase the deck thickness from 277mm to 350mm. The shear stresses are reduced by prestressing and by increasing thickness of the web.

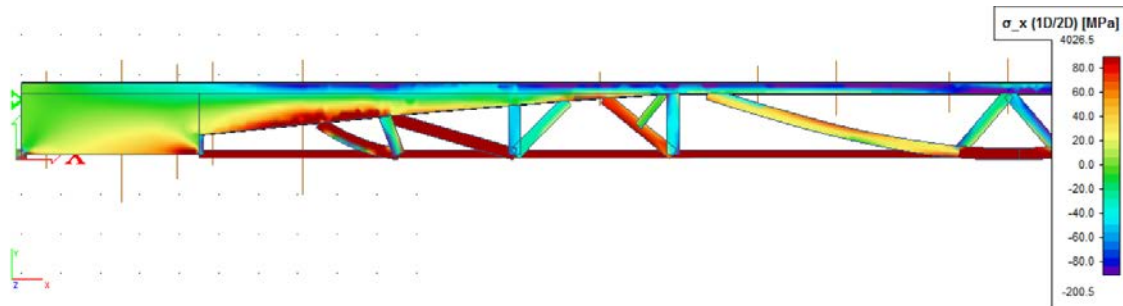


Figure 6.5: SLS envelope normal stresses, 2D in plane FEM analysis

	t	b	h	<i>Material</i>
deck	x	1400	277	UHPC
2D arch	400	400	300	SHCC
2D endblock	400	4500	1500	SHCC
Curved 1D arch	x	400	300	UHPC
1D beam low	x	200	200	HSC
1D beam high	x	300	300	UHPC
Weight reduction			26%	

Table 6.3

The development of tensile cracks in the different elements is postpone by prestressing in the tensile zone. The shear capacity of the prestressed beam will increase provided that

prestressing will compensate the flexural tensile stresses at area b [Figure 6.6]. Flexural cracks will occur where the tensile strength is exceeded.

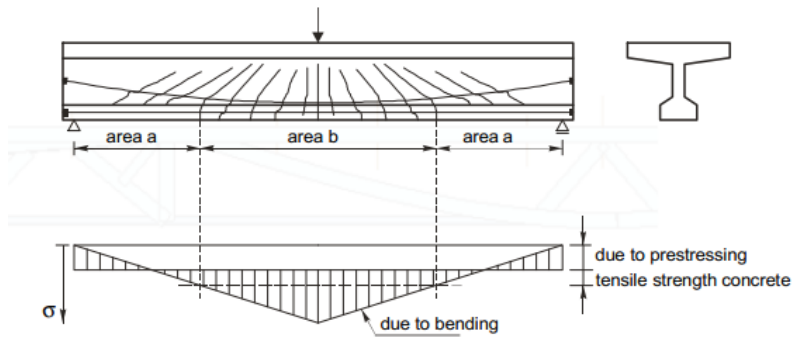


Figure 6.6

In area a [Figure 6.6] where the cracks would start at the web, where the principal tensile stress in concrete reach s the tensile strength of concrete. In this case inclined crack occur and the girder will fail, it called tensile splitting shear failure [EN 1992-1-1].

$$V_{Rd,c} = \frac{I b_w}{S} \sqrt{f_{ctd}^2 + \sigma_x f_{ctd}} = 0.5059 * 10^6 * \sqrt{2.3^2 + \sigma_x * 2.3} = 24289kN$$

$$I = 3.1217e - 01 m^4$$

$$S = 0.2468 m^3$$

$$f_{ctd} = 2.3 \frac{N}{mm^2} \quad C90/105$$

$$\alpha_1 = 1.0$$

$$\sigma_{cp} = \frac{N_{Ed}}{hb_w} = 0$$

$$v_{Rd,c} = \frac{V_{Rd,c}}{db_w}$$

Shear capacity without prestressing: $1.93 N/mm^2$ prestressing required.

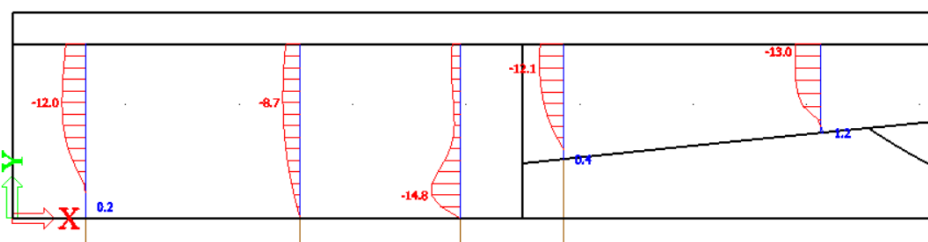


Figure 6.7: Shear stresses distribution

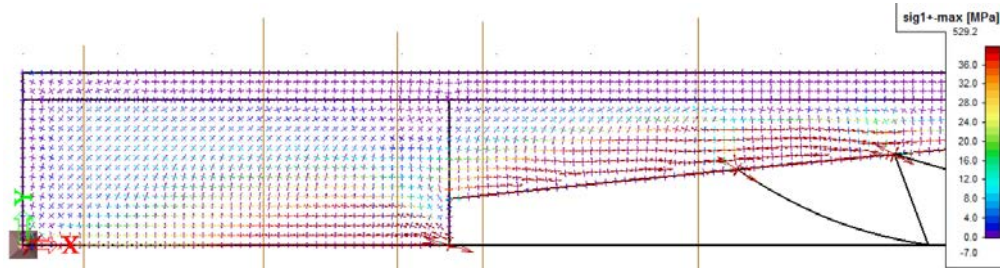


Figure 6.8: Principal tensile stresses trajectories

This model is further optimized. Curved truss elements are as expected introduce eccentricity which result in larger bending moments.

6.3.4 Warren T-girder

The girder is further optimized, although the algorithm [4.8.2] reduces the total mass of the structure and produce an idea for optimized shape and optimized material distribution, the design can be interpreted to a more realistic shape. The truss layout of Warren is preferred It has minimal number of joints which reduce the costs, and from aesthetic point of view it is simple triangle system with the best appearance when the bridge is viewed from skew angles.

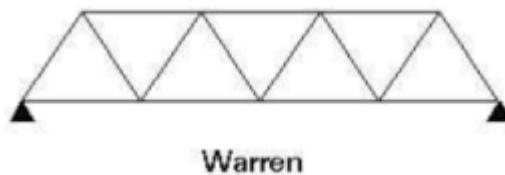


Figure 6.9: Warren truss layout

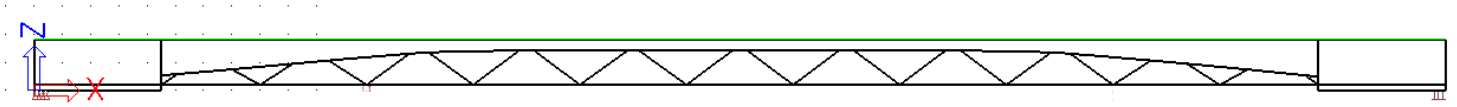


Figure 6.10: The Warren T-girder

The dimensions of the Warren truss elements and the tensile element are presented in Table 6.4].

	B [mm]	H [mm]	Material
Truss	200	200	UHPC
Flange	1400	170	UHPC+NSC
Web	250	Variable	UHPC

Table 6.4: Dimensions

A complete bridge deck is model in 3D environment with 1D and 2D elements. The concentrated traffic loads, and the uniform distributed loads will disperse on more than one beam. The degree of load dispersion is influenced by the bending stiffness in both span directions. Based on the governing girder (third from left), the dimensions of each element will be refined, further the type of material is determined.

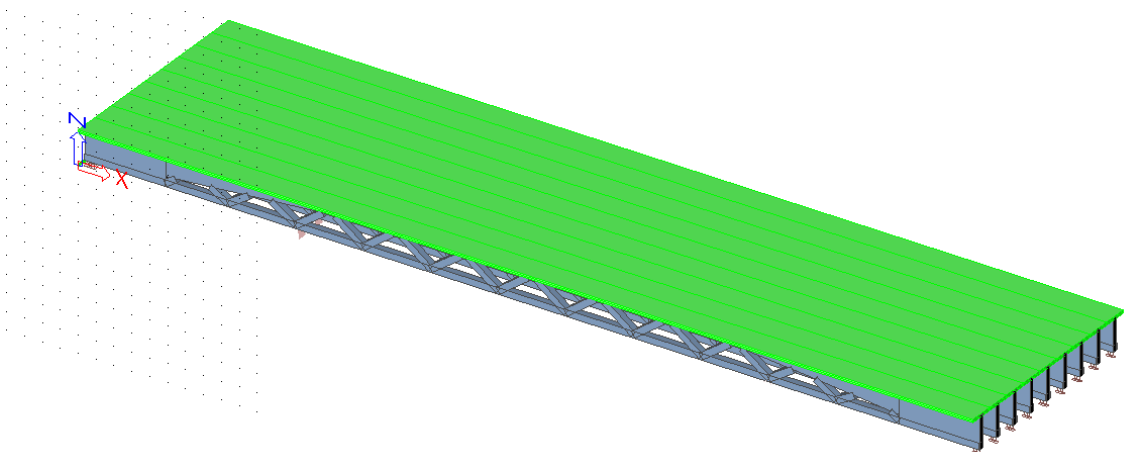


Figure 6.11: Complete bridge deck with width of 11.2m and 50m span. In green the cast in situ top flanges.

With a total weight of approximately 761.5 ton the weight reduction compared to SKK1800 is 35.00%. The cross-sections of each structural elements are based on this FEM analysis. Nevertheless there are more relevant issues to discuss which will affect the sizes of each member, the most important are: Displacement, post-tensioning, pre-tensioning, connections truss members, transversal stiffness, stability and strength during construction (construction phases).

6.3.4.1 Point of concern

Tensile member the tensile tie at the bottom of the girder. The member have a large eccentricity result in hogging moment and tensile stresses at the top-flange. This should be limited and controlled by analyzing the stresses during prestressing. The tensile tie will be mounted between the end-blocks of the compression tie by applying continuous post-tensioning with coupler at the connections in order to provide connection under pure compression stresses in ULS. The type and amount of strands, the concrete cover, and ULS stresses are governing for the final dimensions of the member.

Precast deck plate the precast deck plates with prefabricated prestressed 40mm thick UHPC plates spans between the girders (span=1.40m) and top layer of 130mm cast in situ normal strength concrete furnished with rebars in longitudinal and transverse direction in order to ensure the required torsion stiffness.

Concrete truss members all of the members will be made of the same material with identical dimensions to avoid execution errors, to increase modularity, and to increase repetition. The members will be also post-tensioned without pre-tensioned strands due to its short length of 1.50m.

Construction phases The stresses during mounting of members should not exceed the ULS design.

6.4 The Warren T-Girder

Construction phases, connections, stability, and prestressing design are considered in this section. In [Figure 6.12] the concept of the Warren T-girder is presented. The compression layer (top flange) is consist of thin precast UHPC plate of 40mm with on top in-situ casted layer.

While the top flange have constant dimensions, the web height will decrease from $h=1630\text{mm}$ at the edges to $h=210\text{mm}$ at midspan. This compression strut ($4.5 < x < 13.3\text{m}$ and $36.7 < x < 45.5\text{m}$) with two massive end blocks will be prefabricated.

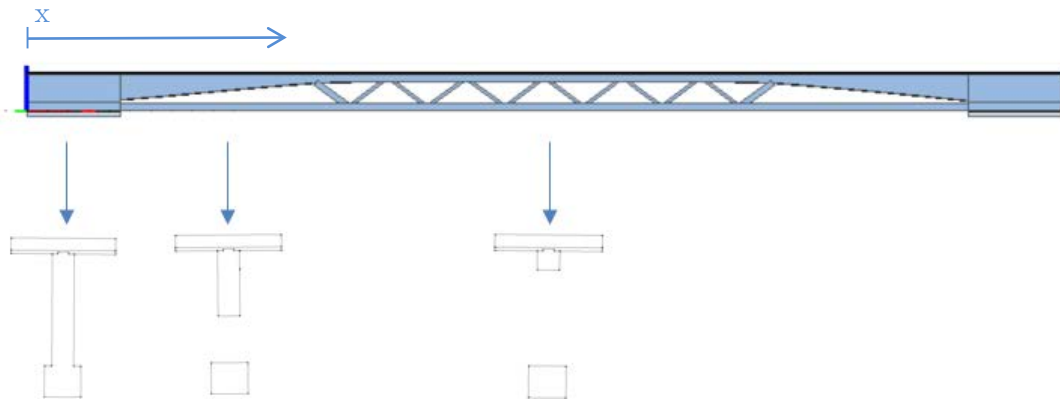


Figure 6.12: The Warren T-girder

Between the massive cross-sections ($4.5 < x < 45.5\text{m}$) the precast tensile tie will be prestressed at the bottom flange. Concrete truss members are added to take shear and the increase stiffness ($13.3 < x < 36.7\text{m}$).

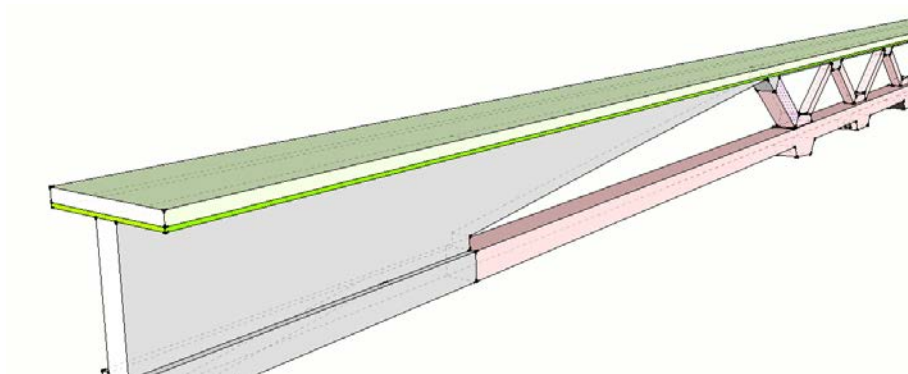


Figure 6.13: 3D sketch of the girder

Overview girder's elements:

$0 < x < 4.5\text{m}$, $45.5 < x < 50\text{m}$	massive ends
$4.5 < x < 45.5\text{m}$	compression strut
$13.3 < x < 36.7\text{m}$	truss members
$0 < x < 50\text{m}$	top flange

6.4.1 Construction stages

Creep & Shrinkage

Designing structural elements with different dimensions and from different materials (stiffness, strength) need special attention. Loads due to permanent imposed deformations such as differential settlements induced by differential shrinkage and creep can cause problems in continuous structures. For example casting the compressive strut, tensile tie, and truss members [Figure 6.12] as one unit introduce restrained deformation result in tensile stresses and cracks. The easiest way to solve this problems is found in the modularity principle. The girder will not be casted as one unit but will prefabricated with 4 elements: The compressive strut, tensile tie, and truss members. In this way the elements are stored at the fabric until creep & shrinkage effect is minimized. Later they will be mounted to each other. This proves the importance of the 100% modularity principle.

Strength & Stability

The stability and strength during all construction stages should be guaranteed. Assembling the girder will be divided into 4 stages considering lifting, prestressing, mounting and turning the individual members and the complete girder [Figure 6.14].

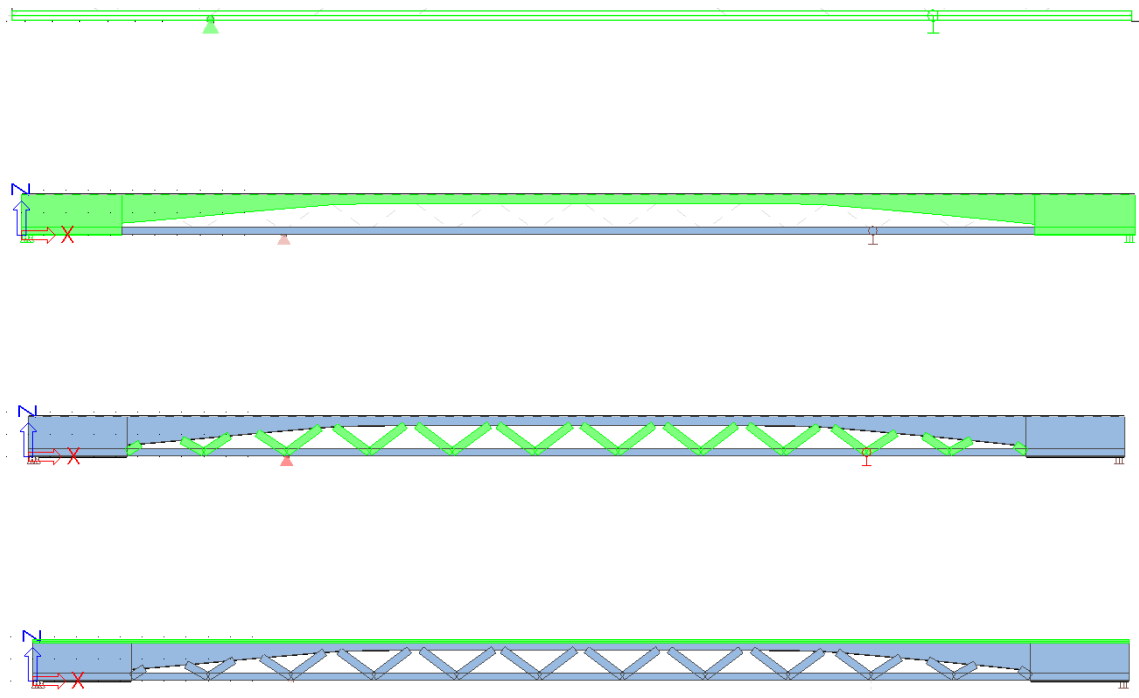


Figure 6.14: Four construction phases are modelled

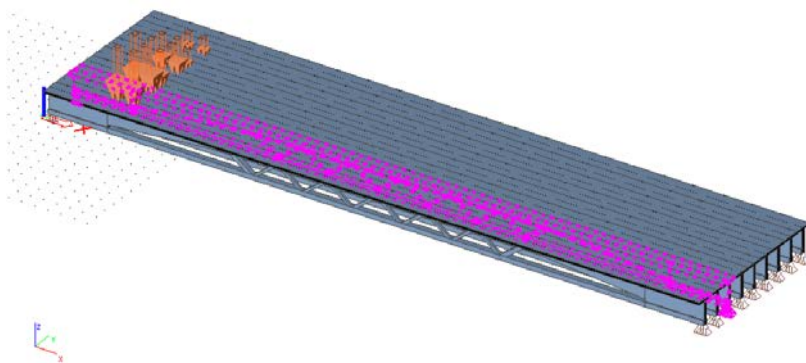


Figure 6.15: Governing girder no.3 from left have the largest internal forces

6.4.1.1 Stage 1.

Rectangular tensile member is delivered with pre-tensioned strands. 2 ducts for post-tensioned strands which will be used during mounting the member to the girder, and joints for truss members. At both ends of the tensile tie the post-tensioned strands are anchored with couplers to the girder. The POT strands will be prestressed at the girders ends. The tie-member is provided with 20 12.9mm PRT strands, 2 POT ducts with 15.7mm strands and stirrups (8mm)

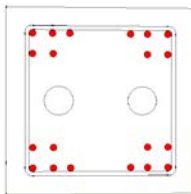


Figure 6.16: PRT strands in red.

The member is prefabricated and lifted towards the prefabricated girder to which it will be connected. During lifting the member deformations and stresses are checked. The location of the lifting points are chosen for minimal displacement.

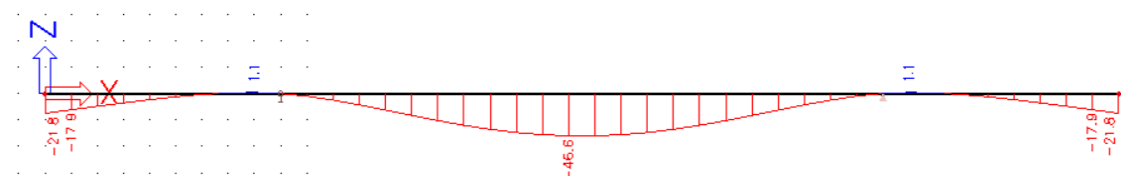


Figure 6.17: Deflections due to self-weight of the member

$$\text{Deflection of the main span: } 46.6\text{mm} < \frac{(41 - 9 * 2)}{350} = 65.7\text{mm}$$

$$\text{Deflection of the cantilever part: } 21.8\text{mm} < \frac{9}{350} = 25.7\text{mm}$$

The stresses during lifting may not exceed the maximum allowable tensile stresses. In [Figure 6.18] unity check includes all working forces indicate that there is no tensile

stresses during lifting, with substantial high rest capacity. Only 34% of the PRT prestressing force is required during lifting [Figure 6.19].

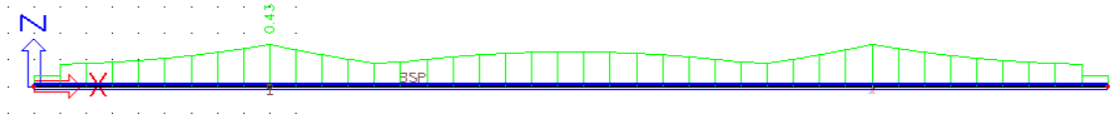


Figure 6.18: Unity check tie member during lifting

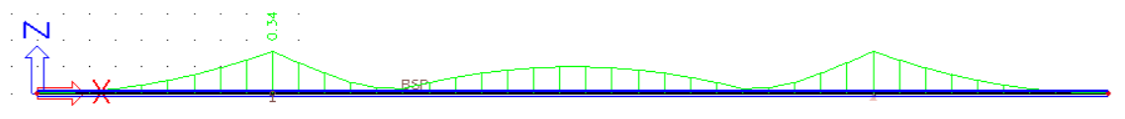


Figure 6.19: Capacity PRT strands check

The tie member is lifted to its final position, and connected to the girder with compression joint by prestressing the tie member with POT strands. Please note, the tie member will be prefabricated including the joints for the truss members. The complete joint design is extensively described in [4.5.4]. Also the shear capacity is controlled ignoring the fibers contribution

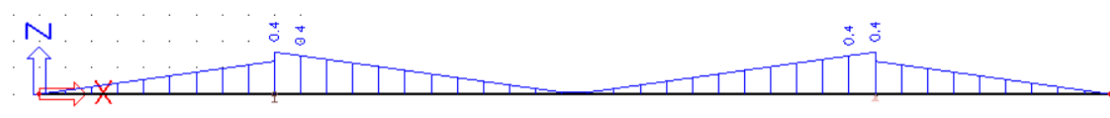


Figure 6.20: Acting shear stresses during lifting

$$v_{Rd,c} = 0.12k(100\rho_l f_{ck})^{1/3} + k_1 \sigma_{cb}$$

$$k = 1 + \sqrt{200/355} = 1.75$$

$$\rho_l = (10 \cdot 0.25 \cdot \pi \cdot 12.9^2) / (355 \cdot 420) = 0.00876$$

$$k_1 = 0.15$$

$$\sigma_{cb} = (A_{p,PRT} \cdot \sigma_{p,\infty}) / A_c = (2614 \cdot 1100) / (420 \cdot 355) = -19.3 \text{ N/mm}^2$$

$$v_{Rd,c} = 1.11 + 2.895 = 4 > 0.4 \text{ N/mm}^2$$

6.4.1.2 Stage 2.

The girder is prefabricated in controlled environment with the included required ducts, stirrups, and duels. Connecting the tensile tie to girder with post-tensioning strands is the trickiest moment. The tie member will be connected to the girder throughout using 2 POT cables prestressed from girder ends connected to tie member throughout coupler.

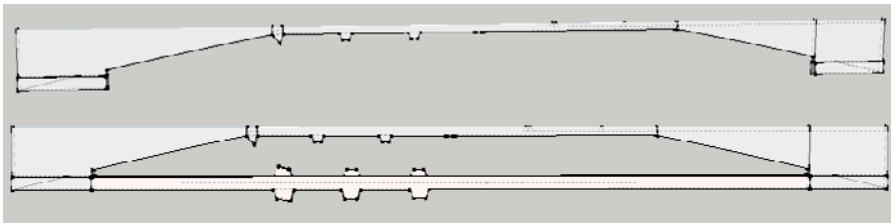


Figure 6.21: Stage 2. Connecting tie member to girder. Stages 2.1 and 2.2

The girder is casted while resting on its side which is simpler with less mixing problems. Furthermore the side position is preferred due to instability of the compressive strut without tie member.

Once the fresh concrete of the girder obtain sufficient strength, the tie member can be mounted. Similar to stage 1 [4.4.1.1] it is important to control the stresses when the tie member is prestressed by POT strands to the girder since this is the only force acting on the girder.

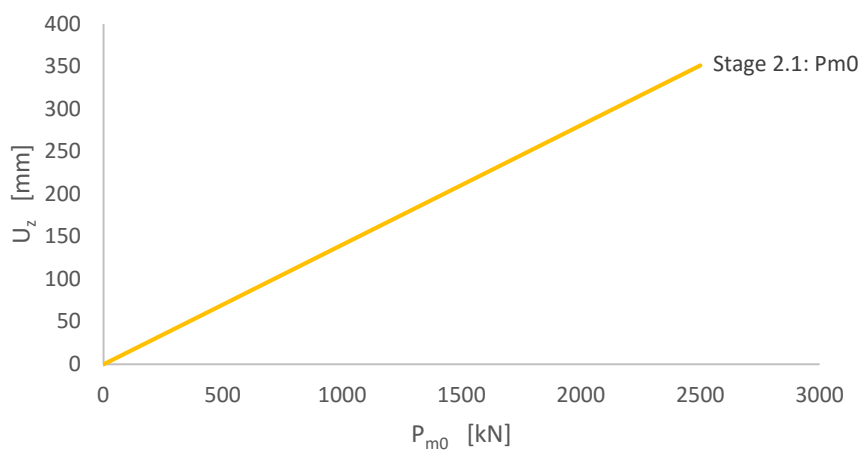


Figure 6.22: Linear FEM analysis of stage 2 maximum deflection as function of applied prestressing

First (stage 2.1) the girder is on its side face when self-weight is inactive the tie member is prestressed to the compressive strut. The maximum allowable prestressing force should be limited [Figure 6.22] to restrain the vertical displacement.

<i>Prestressing</i>	<i>Stage 2 n_x [kN/m]</i>
500kN	pure compression
1000kN	pure compression
1600kN	pure compression

Table 6.5: Stresses top fiber midspan compressive strut stage 2.1

In stage 2.1 apply $P_{m0}=1000$ kN. The midspan upwards displacement 25.2mm is negligible, no tensile forces are present at this stage. No additional reinforcement is required at this moment.

Secondly (stage 2.2) at least two midspan truss members are added previous to the overturning of the girder to standing position. This is important to avoid midspan displacement of the compression strut cause by its own weight, and avoiding high midspan displacement of tensile tie and easy installation position of the truss members.

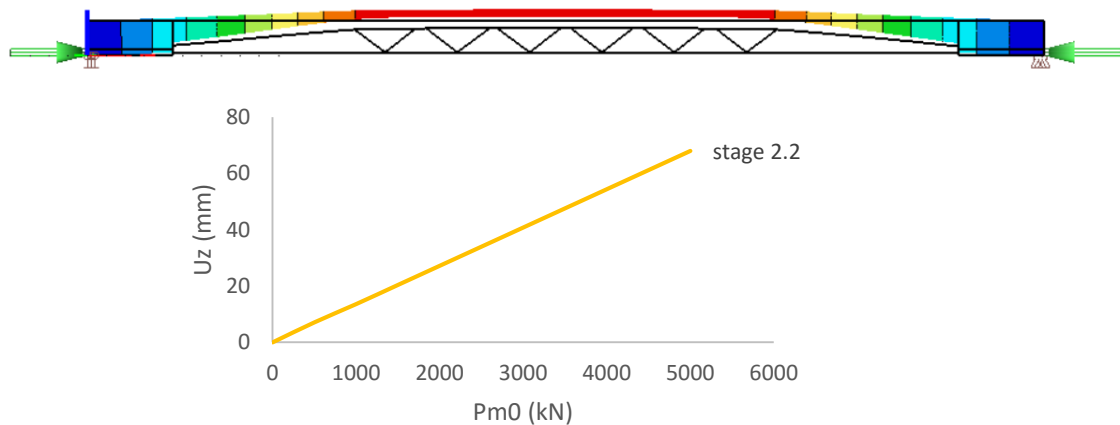


Figure 6.23: Stage 2.2 prestressing the tie member up to full prestressing load

The stresses at midspan the bottom fiber of the compression strut are controlled for this stage as well. It is observed that for prestressing force of 1000kN applied in stage 2.1 no additional reinforcement is required at the midspan of the compressive strut. Though minimum reinforcement is applied Apply 2 ϕ 20mm which is equivalent to tensile force of $N_{Rd}=A_s f_{yd}=273 \text{ kN} = 1093 \text{ kN/m}$

In similar project with prefab concrete [Den-Bosch station over de Diezen] the constructive coupling between two bridge elements are formed by longitudinal compressive stresses, consist of prestressing cables between both ends of the massive part and the tensile member. The capacity of the joint is realized by compressive stresses only at the connection surfaces. This connection is completely under compression which means that it is not sensitive for fatigue. There is no reinforcement between the two prefabricated elements



Figure 6.24: Coupler [VSL]

6.4.1.3 Stage 3.

In stage no.1 the tie member is prestressed by 24 PRT straight strands with the resultant force in the CoG (pure compression). Later on in stage no.2.1 the tie member is prestressed to the girder with POT strands. Please note, only 62.5% of the prestressing force (P_{m0}) is applied in the end of stage no.2.2. This is related to the upwards deflection of the girder. In stage no.2.2 the 12 truss members that are connected are prestressed. The girder is in standing position.

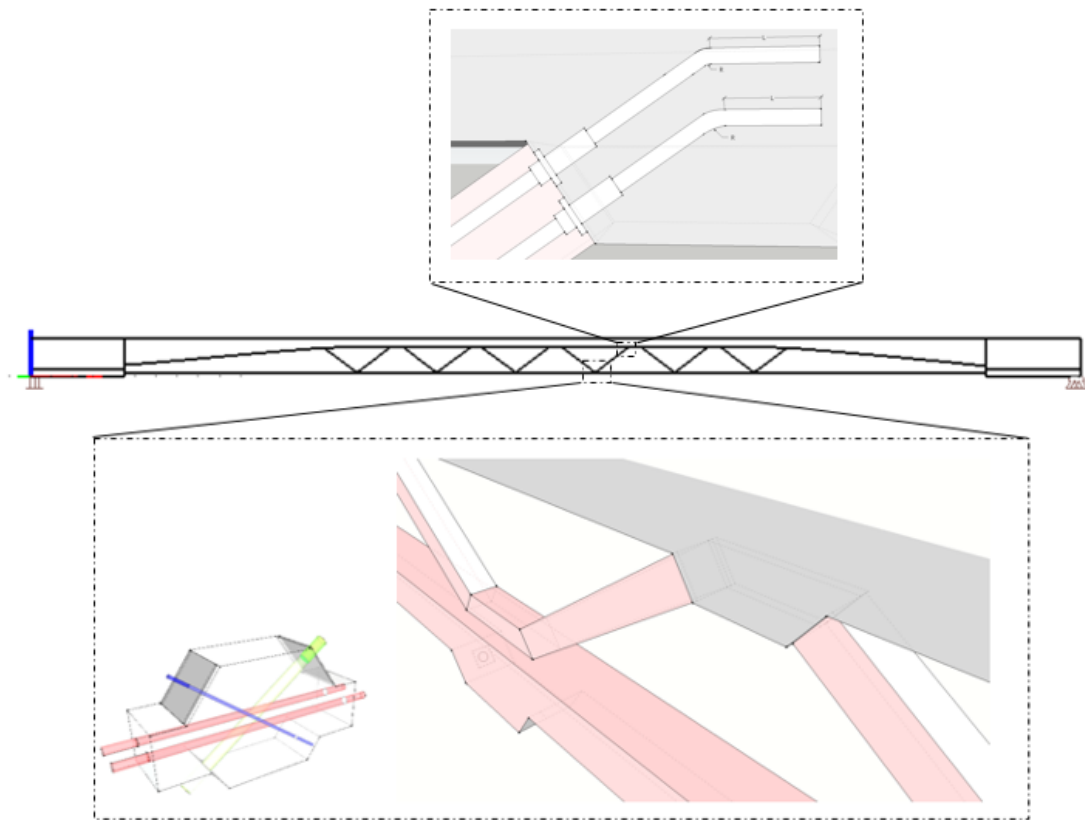


Figure 6.25: Connections tie – truss and top web - truss

In this stage the superiority of the UHPC as material with excellent durability, improved tensile strength capacity, and high compressive capacity are presented.

The truss members are 1.5m long each with identical cross-sectional dimensions (except of the first and the last member). During the designing of the prestressing of these members one should consider the following long term prestressing losses:

- Shrinkage,
- Creep
- Elastic deformation
- Friction

The short term losses during tensioning of the members are compensated during prestressing and therefore may be neglected. The long term losses are assumed to be 15% .

The POT tendons consist of bars (not strands) can be stressed to $\sigma_{pmax} = 773 \text{ N/mm}^2$ during stressing. The maximum prestressing steel stress is verified directly after grouting. In this stage the external tensile load ($N_{t,SLS}$, $M_{t,SLS}$) is activated while the prestressing losses are still zero. Therefore it might be not correct to prestress the bars up to the maximal allowable stress.

Furthermore, due to the nature of the passing traffic load, some members could be under favourable pure compression load. So one possible scenario will be working compression load, compression bending stresses and prestress compression load. In this state it is verified that at $t=0$ and $t=\infty$ the concrete compressive force smaller then $-0.6 \cdot f_{ck}$.

Accordingly when all of the possible load scenarios [Table 6.6] [Table 6.7] are checked one can continue to stage no.4. The third stage however is very important and relative complex, therefor it will be extensively described in [4.5.3].

Scenario 1	$t=0+\epsilon$	SLS load and prestressing without losses	Maximum prestressing stress $\sigma_{p0} = 773 \text{ N/mm}^2$
Scenario 2	$t=0$	self-weight and prestressing without losses	Tensile stress concrete $< -2 \text{ N/mm}^2$ Compressive stress $< -0.6f_{ck}$
Scenario 3	$t=\infty$	SLS load and prestressing with losses	Tensile fiber concrete $< -2 \text{ N/mm}^2$ Compressive stress $< -0.6f_{ck}$
Scenario 4	$t=\infty$	ULS load with prestressing with losses	Tensile fiber concrete $< -2 \text{ N/mm}^2$ Compressive stress $< -0.6f_{ck}$

Table 6.6: governing prestressing versus external load combinations

	<i>Compression</i>	<i>Tension</i>	<i>Bending tension</i>	<i>Bending compression</i>	<i>Prestressing</i>
Scenario 1	•			•	•
Scenario 2		•	•		•
Scenario 3		•	•		•
	•			•	•
Scenario 4	•			•	•
		•	•		•

Table 6.7: Stress component being controlled

6.4.1.4 Stage 4.

In this final stage the tie-member which is already prestressed with PRT strands and 62.5% of the POT strands is prestressed. Now the girder will be prestressed up to full capacity previous to transport to the building site and placement between the bearings. In [Figure 6.26] the girder without the top compression layer of 170mm thick is prestressed. The hogging moment and the self-weight deflection are within the acceptable range regarding the displacement and the stresses

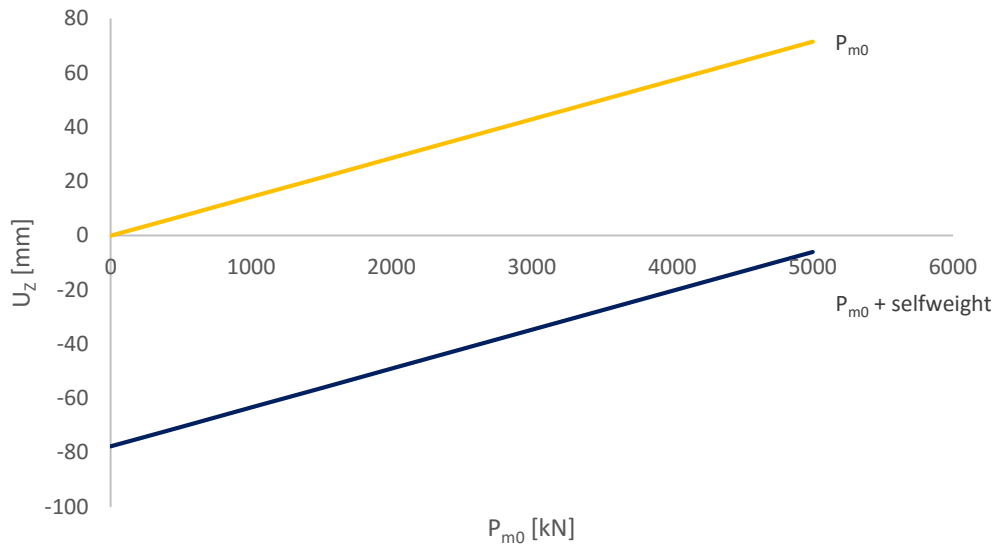


Figure 6.26: Linear FEM analysis of stage 4 deflection

Stage 4 can be divided again into two sub-stages, first the tie-member is prestressed up to its full capacity, and then the compression top layer is added. Further there are no tensile forces at the girders web, no need for additional reinforcement than in stage no.2 applied reinforcement.

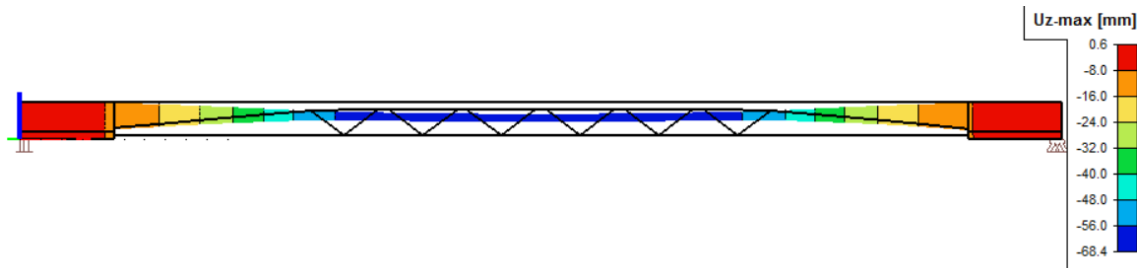


Figure 6.27: : Max deflection $U_z = 68.4\text{mm}$ for $P_{m0}=1600\text{ kN}$ and self-weight without deck

6.4.1.5 Stage 5.

Now when all of the members are fully prestressed the partially prefabricated slab can be constructed. First thin prefabricated UHPC plates of 40mm thick are mounted. This are used as permanent formwork (stay plates) for the 130mm thick cast in situ concrete. In this way costs and labor are reduced, superior durability, larger tensile strength capacity, reduction self-weight.

For the transfer of shear forces from the truss diagonals and web to the UHPC plates, prestressed bolted friction connections are used. For a thin plate elements the dominating fiber orientation can be observed to be parallel to the formwork.

The cast in situ top layer is casted in one day so the entire deck will be one monolithic diaphragm. The interaction between the deck and the web is by sufficient amount of shear connectors preventing slip between the layers. Assume ideal rigid interaction without relative displacement (slip) between the web and the deck.



Figure 6.28: Types of shear connectors [CIE4121]

The distribution of the longitudinal shear in the beam is not constant, so also the connectors close to the supports are subjected to higher loads. In [Figure 6.29] this is illustrated.

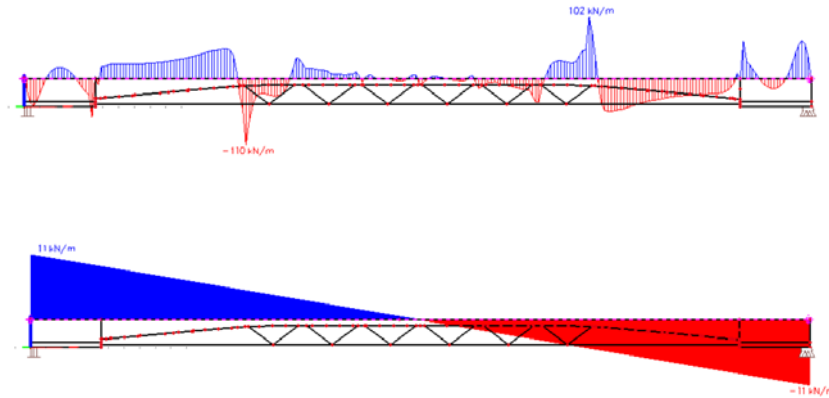


Figure 6.29: Shear force n_{xy} [kN/m] for uniform distributed traffic load

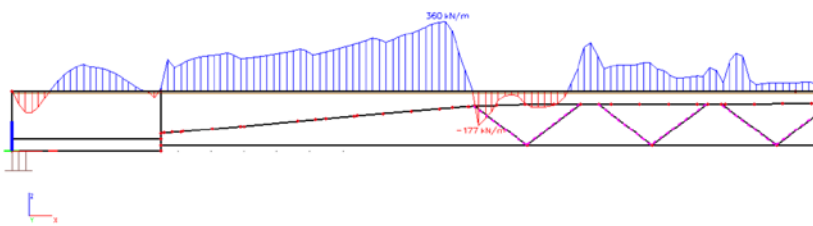


Figure 6.30: Shear force n_{xy} [kN/m] for ULS

6.4.2 Failure mechanism

The characteristic compressive strengths of the concrete vary from 35 MPa up to 170 MPa. The strands tensile strength is between 1700 MPa to 1900 MPa while the prestressing level is 1350 – 1450 MPa, the bars tensile strength is around 1030 MPa while the prestressing level is 773 MPa.

A good design is balanced failure design, all structural elements in bending must show extensive cracking with large deflection prior to the yielding of the strands/bars. All members under high axial loads should show extensive cracking prior to the yielding of the strands/bars [Figure 6.31]. Failure moment of the girder occur when ULS strength is exceeded.

Please note, applying ACM such as UHPC means non-linear post-cracking behavior. The girder may show hardening behavior after cracking increasing the ULS capacity. However in this chapter only the linear elastic design is considered.

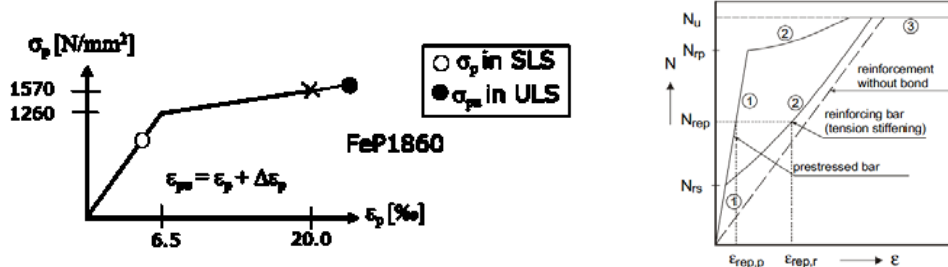


Figure 6.31: Left - Balanced design, strands/bars are yielding prior to crushing of concrete, Right – axial loaded truss is cracked before steel is yielding [CIE4160]

In this way ductility of the structure is guaranteed, and structure which warns before it fails. Other way to increase the ductility is to use other materials than conventional concrete [2]. Throughout the data assembled in this thesis about ACM, the final girder will be composed of the following different material:

Top flange Rectangular thin UHPC prefabricated slabs are laid between the girders and used as permanent form-work for an in-situ concrete topping. The flanges will be executed with reinforcement grid to reduce cracking as result of shrinkage, creep, tensile stresses during construction. Shear capacity is achieved by steel fibers and prestressing. The duels pins are responsible for the interaction between the cast in situ deck and the girder. The top layer is also responsible for the torsional stiffness.

Compression strut The compression strut (web) consist of the massive part with height of 1630mm and the slender part with height of 210mm [Figure 6.12]. The web follows an arch shape according to [4.8.1]. It transfers the compression loads to the support, increase bending stiffness, and together with the truss members accountable for shear capacity. The high shear stresses and its function as anchorage point for the tie demands limit state checks. Assume it will be prefabricated with FRHSC or conventional concrete class C50/60.

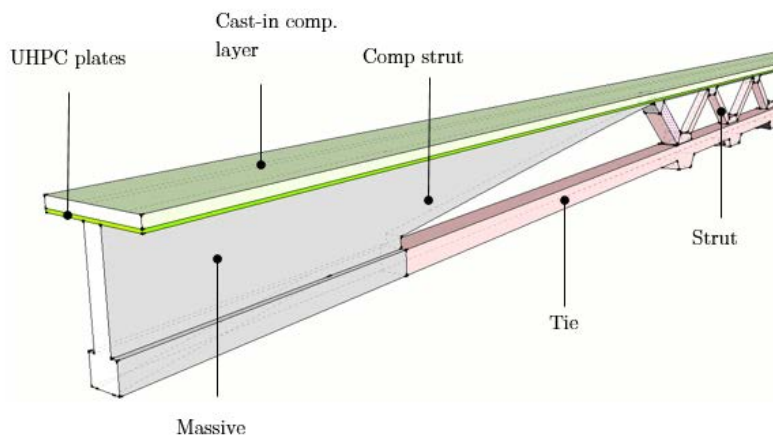


Figure 6.32: The girder

Truss members The UHPC truss members transfer shear forces, supports the compression strut, supports the bridge deck. The truss members supports the top layer with constant span of 3.5m between each connection point. This limits the bending moment of the top layer. Further the truss are with high slenderness and due to their short length of 1.5m will be prestressed with bars.

Using UHPC is necessary due to the requirement for weight reduction, and due to high compressive stresses with some tensile and shear stresses. This material characteristics will be fully utilized.

Tensile tie The tie runs between both sides of the massive parts [Figure 6.14]. It has to carry high tensile loads and some bending moments from truss-members. The tie member will be long (L=41m) rectangular beam prefabricated with POT and PRT strands, and with joints for truss members.

Because steel members are avoided in this thesis the only solution for the tie member is to apply prestressing strands to overcome the tensile forces considering the hogging moment affecting the top flange. This flange needs to be slender as well. Therefore UHPC will be used again.

6.4.3 Prestressing system

6.4.3.1 Live anchorage system

This VSL POT system [Figure 6.33] is for strands type 12.9mm and 15.7mm. The factory dimensions are given in [Table 6.8] [Table 6.9].

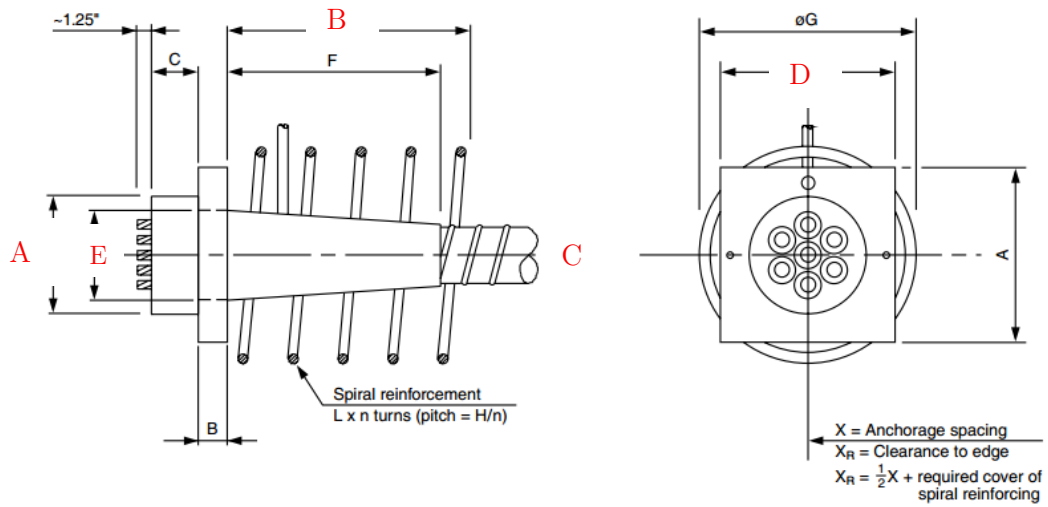


Figure 6.33: Prestressing tendon type E [VSL]

Max strands	A	B	C	D	E	Spacing anchorage	Clearance to edge	Spacing duct	Duct cover
1 strand	42	89	25	70	15	90	70	v40 h50	55
3 strand	90	150	55	115	50	154	102	v40 h50	55
4 strand	95	150	60	130	55	180	115	v60 h60	55
7 strand	101	200	70	175	74	235	142.5	v70 h70	55
12 strand	150	379	80	230	104	305	177.5	v80 h80	55

Table 6.8: POT system VSL ES 12.9mm. [mm]

Max strands	A	B	C	D	E	Spacing anchorage	Clearance to edge	Spacing duct	Duct cover
1 strand	53	90	25	75	18	105	100	40	55
3 strands	95	150	55	135	55	184	117	55	55
4 strands	110	200	60	160	84	210	130	60	55
6 strand	134	249	70	204	84	280	165	70	55

Table 6.9: POT system VSL E 15.7mm. [mm]

Eurocode and fabrication requirements

- Spacing anchorage from CoG of tendon X
- Spacing duct from CoG of tendon EN 1992-1-1 8.10.1.2 - $ver = \max(40\text{mm}, \Phi)$
 $hor = \max(50\text{mm}, \Phi)$
- Duct cover from edge of duct 1992-1-1 4.4.1.2 55mm
- Cover added to spiral $C_{min} = 25\text{mm}$
- Strand cover from edge of duct 1992-1-1 4.4.1.2 $\max(2.5\Phi, 80\text{mm})$
- Lower limit for the thickness of the web, because of the required minimum concrete cover on the web reinforcement (e.g. stirrups and longitudinal web reinforcement) and the required shear capacity (of the concrete struts loaded in compression).

6.4.3.2 Dead anchorage system

Dead end anchorage is applied when a cable is prestressed at one end. In [Figure 6.34 (a) (b)] two possibilities for the non-stressed ends are given. In the case of the truss members these will be connected to the girder web at the top side and prestressed from the bottom tie-member. Due to lack of space option (b) or (c) are the most suitable. Where type (c) is anchorage plate and nut in case of POT bars.

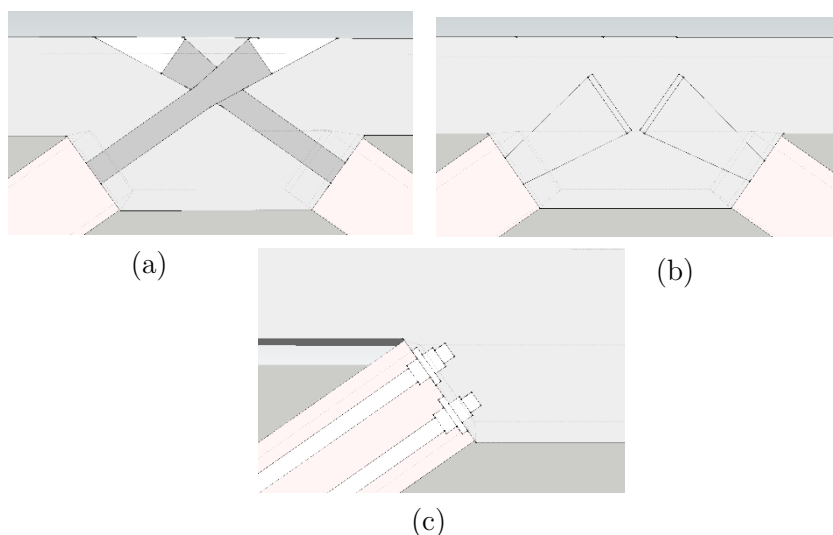


Figure 6.34: Dead end anchorage systems for top side of truss member

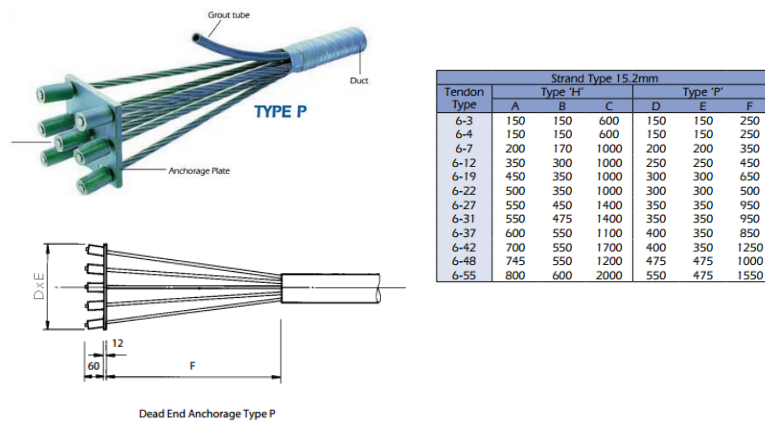


Figure 6.35: Dead end anchorage type P for POT strands of 15.9mm

6.4.3.3 Threaded bars system



Figure 6.36: Threaded bars

Available steel type for post-tensioning of bridges Y1030H. The bars made of hot rolled steel and are ribbed or plain steel. Ribbed bars have a better bond and can extend by coupling. The E-modulus is $E=205000 \text{ N/mm}^2$.

Prestressing with bars instead of with strands is favourable due to the absent of wedge set, ideal solution for short tendons and frame ties, economically, simple to use, simple connections, protection against corrosion is available.

Anchoring the threaded bars is possible with End-anchorage [Figure 6.37 – left] and with different coupling system. Bars can be bent and cut according to requirements.

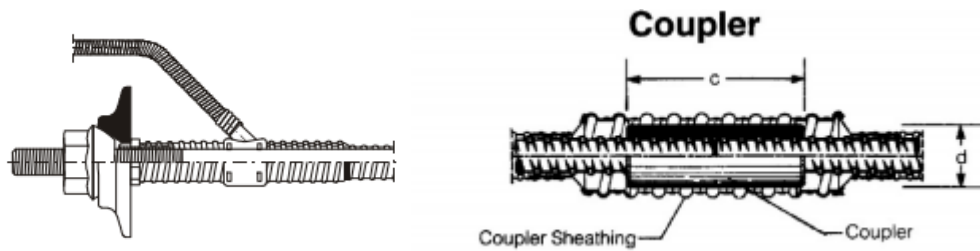


Figure 6.37: Anchorage and coupler of threaded bar

6.4.3.4 Evaluation prestressing

<i>Parameter</i>	<i>Strands (Y1860S7)</i>	<i>Bars (Y103H)</i>
Yielding strength	1860 N/mm ²	1030 N/mm ²
Max stress during prestressing	1488 N/mm ²	773 N/mm ²
Max initial stress	1395 N/mm ²	773 N/mm ²
Young's modulus	195 GPa	205 GPa
Anchorage	wedges	nut, wedges
Wedge set	yes	no
Long term losses	low	high
Shape	straight, curved	straight
Bond	good	good
Applicable in UHPC model	Yes	Yes
High bending moments	+++	+
Protection of anchorage against corrosion	+++	+++
Suitable for short tie members	+	+++
Simplicity	-/+	+++
Space required anchorage (slenderness design)	+	+++
Economically	+++	+

Table 6.10: Evaluation

POR bars placed in ducts are more suitable for short tie members with low bending moment. Anchoring the bar by means of spherical nuts that bears against rectangular bearing plate cast into the concrete is significantly simpler than dealing with POT strands system.

The tendons can be grouted for multiply levels of protection [Figure 6.37]. In this case the bars are anchored at the tie-member side and prestressed (live anchorage) while at the web side the bars will be connected to a coupler which is further embedded in the web to transfer the tensile forces.

6.4.4 FEM main model

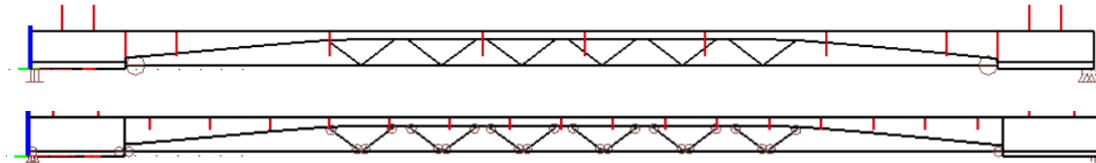


Figure 6.38: FEM main model

In [Figure 6.38] one girder is presented, the tensile tie and the truss members are modeled with hinged connection and with fixed connection. In reality the stiffness of the connection will be somewhere in between. The effect of the joint stiffness (rigid, flexible) is observed in the working bending moments in the truss members. With flexible connections the bending moments is significantly reduced. Altering the type of connection will further not change the stresses, displacement of the girder.

Second change made in the FEM 3D model is the number of truss members, this is reduced from 20 to 12 members only per girder, which means less expansive connections and more efficient forces distribution. At the location where truss members are eliminated the compression strut will have to take the shear forces or in other words, stresses peaks should be verified. Further the overall stiffens of the girder and the deformation is hardly changed.

The truss members are initially identical, rectangular members of 200*200mm with 1.50m long each. The internal forces in the members are though different. Some members are loaded only with compression, the other with tension/compression, and some members are loaded with substantial higher forces then the others. The most optimal scenario will be identical members prestressed up to a level for which no tensile load occur. Adding material to some truss members is unwanted, because this will increase its volume (self-weight) and stiffness causing a different deformation and stress concentrations in other segments of the girder.

6.5 Global design

6.5.1 Global design tensile tie member

6.5.1.1 Midspan = maximal forces

The following alternatives are possible:

- Massive rectangular member with PRT and POT
- Hollow rectangular or circular UHPC cross-section with external prestressing
- Steel tube filled with UHPC and prestressed with PRT

The dimensions of the truss members are rather small, only 1.5m long with diameter of 250-350mm. So hollow concrete members with external is unlikely to be realistic. Steel tube filled with UHPC with prestressing, and massive rectangular member are a good options for the tie member and the truss members. The first option is already applied in Bourge Les Valence in France. Massive rectangular tie member will be design as it within the scope of this thesis.

Conform the FEM of the bridge the tensile tie member undergoes large normal force and small bending moments which are maximal at midspan cross-section where the eccentricity is the largest. The governing forces in the governing girder [Table 6.11]:

<i>Midspan $x=25.0m$</i>	<i>Normal force N_t</i>	<i>Bending moment M_y</i>
$t = \infty$ (ULS)	4099	88
$t = \infty$ (SLS)	2772	62
$t = 0$	1836	51

Table 6.11: Forces in KN from FEM analysis of the bridge

- Prestressing

Strands FeP1860, diameter of 12.9mm or 15.7mm are applied

$$f_{pu} = 1860 \text{ N/mm}^2$$

$$f_{pd} = 0.9 * \frac{1860}{1.1} = 1520 \text{ N/mm}^2$$

$$f_{pi} = 1395 \text{ N/mm}^2$$

$$f_{p\infty} = 0.85 * f_{pi} = 1186 \text{ N/mm}^2$$

- Global design

The prestressing force is calculated with 15% prestressing losses. The allowed (initial compressive strength) is $\sigma_c = 0.6 * f_{ck} = 0.6 * 150 = 90 \text{ MPa}$ [EN 1992-1-1 cl. 5.10.2.2 (5)].

To make sure that the member remains uncracked (high stiffness to limit deformations), a compressive stress of $-2,0 \text{ N/mm}^2$ is required when the member is subjected to the maximum loading according to SLS. The equation consist of two parts, normal forces and moments. Apply PRT strands to take the bending moments and normal force.

Full SLS load no tension $t=\infty$

$$\sigma_c = -\frac{0.85P_{m0}}{A_c} + \frac{N}{A_c} + \frac{M}{W_c} \leq -2 \text{ N/mm}^2$$

Not too high compressive stresses directly after anchoring the tendons. Only self-weight $t=0$

$$\sigma_c = -\frac{P_{m0}}{A_c} + \frac{N}{A_c} + \frac{M}{W_c} > -0.6f_{ck} \text{ N/mm}^2$$

$$\sigma_c = -\frac{P_{m0}}{A_c} - \frac{M}{W_c} > -0.6f_{ck} \text{ N/mm}^2$$

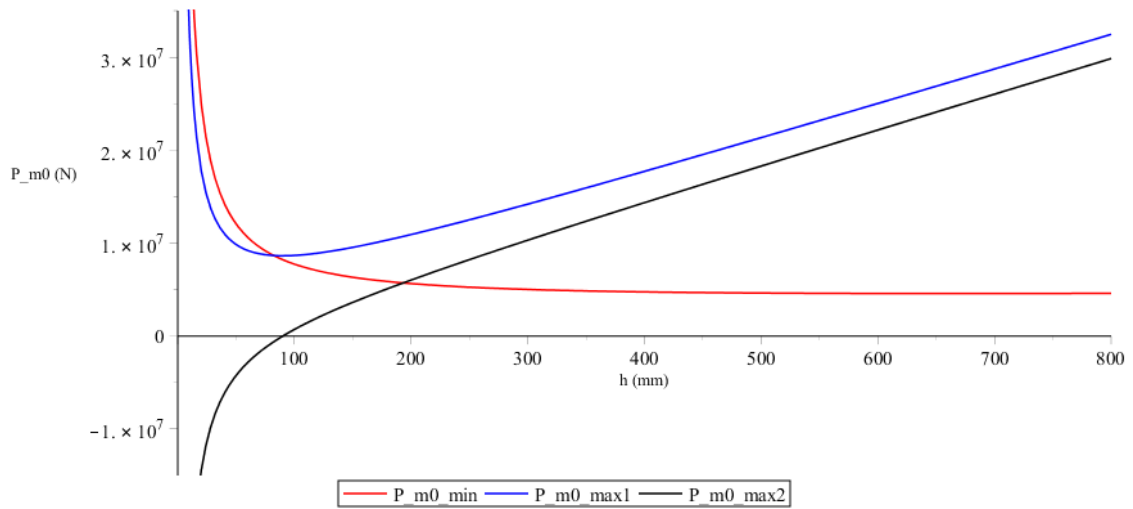


Figure 6.39: For $b=420\text{mm}$, Area confined between the black and the red lines is the design space.

Final result is member with cross-sectional dimensions of $b=420\text{mm}$, $h=355\text{mm}$ with $P_{m0}=4844\text{ kN}$ and $A_{p,\min}=3472\text{mm}^2$.

Further it should be checked whether the member has sufficient reserve against ULS failure.

$$A_p f_{pd} \geq N + \frac{M}{W_c} * A_c = 3670\text{ mm}^2 \text{ (conservative approximation)}$$

	P_{m0}	A_p
Normal tensile force	3535 kN	2693 mm ²
Bending moment	1583 kN	1135 mm ²

Table 6.12

Apply PRT strands of 12.9mm ($A_p=100\text{mm}^2$) and POT strands of 15.7mm ($A_p=150\text{mm}^2$) in order to keep the member slender and to avoid large hogging moment during prestressing. The number of POT strands are limited by lower-bound: the connection stresses between tie - girder, and by upperbound: hogging stresses at the top flange. For

the simplicity the bending stresses will be seen as if the maximum stresses at the outer fibers acting along the entire cross-section.

To summarize, PRT strands are applied with resultant in CoG of the tie member. Then on-site post-tensioning applied with two ducts of 4 - 15.7mm each. The POT strands provide the required compression at the connection joint between tie – massive part [Figure 6.14]. The required concrete cover is according to [NEN-EN 1992-1-1. Table 4.5N].

- Detailed calculation

The stress in the prestressing steel (N_p) in SLS when live load is activated directly after stressing and grouting. The remaining part of the tensile force is carried by the concrete (N_c) and result in reduction of compressive stresses from prestressing.

$$\Delta N_p = \alpha_p \left(F_q + \frac{M}{W_c} \right) \quad \Delta N_c = (1 - \alpha_p) \left(F_q + \frac{M}{W_c} \right)$$

$$\alpha_p = \frac{\alpha_e \rho_p}{1 + \alpha_e \rho_p} \quad \alpha_e = \frac{E_p}{E_c} \quad \rho_p = \frac{A_p}{A_{c,net}}$$

The maximum value of the initial prestressing should not exceed $1395 - 81.94 = 1313$ N/mm² from which the maximum prestressing force follows $P_{m0} = 4819$ kN.

- Control

Bending moments and normal forces

$$t = 0 \rightarrow \sigma_b > -0.6f_{ck} \quad \sigma_t > -0.6f_{ck}$$

$$t = \infty \rightarrow \sigma_b \leq -2 \quad \sigma_t \leq -2$$

Stress in prestressing steel

$$t = 0 \rightarrow \sigma_{pm0} \leq f_{pi}$$

$$t = \infty \rightarrow \sigma_{pm\infty} \leq f_{pd}$$

Shear

$$\tau_d \leq \tau_1$$

$$\tau_1 = v_{fb} + v_c + v_s$$

$$\tau_d = 0.23 \text{ N/mm}^2$$

The total shear resistance is the summation of contributions of plane concrete, stirrups, and fibers.

Concrete contribution:

The mean axial stress in the cross-section due to loading or/and prestressing

$$\sigma_{cp\infty} = \frac{N_{Ed}}{A_c} = \frac{P_{m\infty, M} + P_{m\infty, N} - N_p}{A_c} = \frac{1583 * 10^3}{A_c} = 10.61 \text{ N/mm}^2$$

$$k = 1 + 3 \frac{\sigma_{cp\infty}}{f_{ck}} = 1.187$$

$$v_c = \frac{0.24}{\gamma_E \gamma_{fb}} k f_{ck}^{1/2} = 0.13 * 1.187 * 170^{1/2} = 2.0 \text{ N/mm}^2 \text{ [SETRA]}$$

Reinforcement:

$$v_s = \frac{A_{sw}}{S} z f_{ywd} \cot(\theta) = 0.54 \text{ N/mm}^2$$

$$A_{sw} = 2 * (0.25\pi 8^2) = 100.5 \text{ mm}^2$$

$$S = 300 \text{ mm}$$

$$z = 0.9 * 306 = 275 \text{ mm}$$

$$\theta = 30 \text{ [recommended value according to SETRA]}$$

Fibers contribution:

$$v_f = \frac{\sigma_p}{\gamma_{bf} \tan(\beta_u)} = \frac{8}{1.3 * \tan(45)} = 6.15 \text{ N/mm}^2$$

σ_p the residual tensile strength, K orientation factor, $w_{lim} \max(w_u, 0.3 \text{ mm})$, $\sigma(w)$ experimental characteristic post-cracking stress

$$\sigma_p = \frac{1}{K} \frac{1}{w_{lim}} \int_0^{w_{lim}} \sigma(w) dw$$

Total design value shear strength [AFGC/SETRA 2002, fiber 1.6%vol] is:

$$v_c = 2.0 + 0.54 + 6.15 = 8.70 \text{ N/mm}^2$$

This value of 8.70 N/mm² is a typical shear value one can find in the literature, about 8 to 11 MPa in direct tension and 25 to 40 MPa in bending. So in this case If shear stresses are typically below 5 MPa, they are carried by the fibers so shear reinforcement is not needed.

6.5.1.2 Connection point tie – girder

The tensile force at the connection is replaced with compression from POT strands. The forces at the joint at SLS $t=\infty$ (full load), $t=0$ (only self-weight) and ULS are verified similar to the analysis executed for midspan cross-section. The result is prestressing force $P_{m0}=1726\text{kN}$ with $A_p=1237.3\text{mm}^2$.

Apply 2 ducts of $5-15.7 = 1500\text{mm}^2$. The PRT strands will be then $A_p=3671-1500=2171\text{mm}^2$ equal to 22-12.9mm. Apply 24-12.9mm PRT strands to form symmetry.

<i>Connection $x=4.5m$</i>	<i>Normal force N_t</i>	<i>Bending moment M_y</i>
$t = \infty$ (ULS)	2438	0
$t = \infty$ (SLS)	1726	0
$t = 0$	1200	0

Table 6.13: Working forces at tie – girder connection

6.5.1.3 Minimum reinforcement

According to [NEN-EN 1992-1-1 art. 9.2.1.1] minimum reinforcement shouldn't be smaller than:

$$A_{s,min} = 0.26 \frac{f_{ctm}}{f_{yk}} b_t d = 225.64 \rightarrow 2\phi 12$$

Where:

$$b_t = 355\text{mm}$$

$$d = 355 - 60 - 8 - 0.5 * 12 = 281\text{mm}$$

$$f_{ctm} = 4.35 \text{ N/mm}^2 \text{ (UHPC)}$$

$$f_{yk} = 500 \text{ N/mm}^2$$

However applying the PRT strands and using UHPC with steel fibers can be assumed to be more than sufficient for the ductility behavior of the tensile tie and for the cracking behavior. The cracking behavior of the tie will not be part of this section.

6.5.1.4 Bending moment capacity

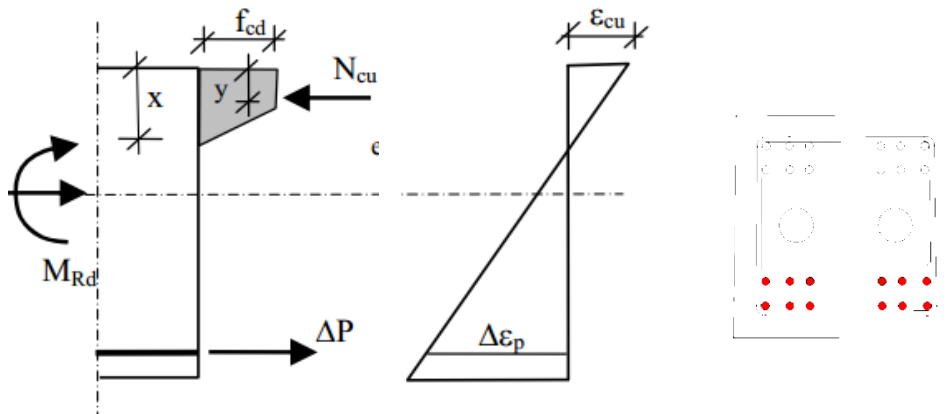


Figure 6.40: Forces distribution in the cross-section, fiber contribution is neglected [CIE4160]

Fibers contribution to the ULS capacity will not be considered because of the reliability aspects related to the fibers orientation. The fibers are taken into account in the SLS

design. Only the sagging bending moment is accounted for, therefore the resistance part of the strands in the top fiber and the strands in the CoG will be neglected [Figure 6.40]

The following parameters of the tie are known:

$$d_{p2} = 355 - 49 - 12.9 * 2 - 0.5 * 12.9 = 273.75mm$$

$$d_{p1} = 355 - 49 = 306mm$$

$$d_p = \frac{A_{p1} * d_{p1} + A_{p2} * d_{p2}}{A_{p1} + A_{p2}} = 293.1mm$$

$$A_s = 0$$

$$A_p = 12 - 12.9mm = 100 * 12 = 1200mm^2$$

$$\sigma_{pu} = 0.95 * f_{pk} / \gamma_s \text{ (Assumption)}$$

$$P_{m\infty} = 4942.5kN$$

$$\alpha = 0.56 \text{ (UHPC)}$$

Horizontal forces equilibrium, The stress in the prestressing steel is assumed to be $0.95 \frac{1860}{1.1} = 1606 N/mm^2$:

$$X_u = \frac{A_s * f_{yd} + A_p * 0.95 * f_{pk} / 1.1}{\alpha * b * f_{cd}}$$

$$\varepsilon_s = \frac{d_s - X_u}{X_u} \varepsilon_{cu3}$$

$$\Delta\varepsilon_{p1} = \frac{d_p - X_u}{X_u} \varepsilon_{cu3} =$$

$$\varepsilon_p = \varepsilon_{pm\infty} + \Delta\varepsilon_p =$$

$$\sigma_p = 1522 + \frac{\varepsilon_p - 7.81}{35 - 7.81} (1691 - 1522) = 1473 N/mm^2$$

Apparently the total strain is too small. Recalculation of X_u again for $\sigma_p = 1473 N/mm^2$ will result in $\sigma_p = 1473 N/mm^2$.

The bending moment resistance:

$$M_{Rd} = P_{m\infty}(e_0 - y) + N_s(d_s - y) + \Delta N_p(d_p - y)$$

$$y = \beta * X_u = 0.337 * 72.24 = 24.40mm$$

$$N_s = A_s * f_{yd}$$

$$\Delta N_p = A_p(\sigma_p - \sigma_{pm\infty})$$

$$M_{Rd} = 224 \text{ kNm}$$

$$M_{Ed} = 90 \text{ kNm}$$

$$M_{cr} = f_{ctm,fl} * W_c = (6.22 * 1.245) * \frac{1}{6} * 420 * 355^2 = 68.30 \text{ kNm}$$

6.5.1.5 Elastic shortening

- Prestressing with PRT strands

The maximum steel stress in SLS is $\sigma_{pm0} = 1395 \text{ N/mm}^2$. During prestressing it is allowed to use $\sigma_{pm\infty} = 1488 \text{ N/mm}^2$.

$$\Delta P_{elastic} = \frac{\alpha_e \rho_p}{1 + \alpha_e \rho_p} = \alpha_p P_{max}$$

$$\rho_p = \frac{A_{p,PRT}}{A_c} \quad \alpha_e = \frac{E_p}{E_c}$$

$$\Delta P_{elastic} = 0.057 P_{max}$$

The maximum initial stress is:

$$\sigma_{p,max} = \frac{1}{1 - 0.053} * 1395 = 1473 \text{ N/mm}^2$$

So, it is not possible to make full use of the stress increase to 1488 N/mm^2 since this will cause a too high maximum initial stress ($\sigma_{pm0} = 1395 \text{ N/mm}^2$)

The initial prestressing force and the losses due to elastic shortening are:

$$P_{max} = A_p \sigma_{p,max} = 2400 * 1473 = 3535 \text{ kN}$$

$$\Delta P_{el} = 0.053 * 3233 = 187.3 \text{ kN}$$

$$\Delta \sigma_{el} = 0.053 * 1465 = 78.0 \text{ N/mm}^2$$

The force transferred to the concrete:

$$P_{max} - \Delta P_{el} = \frac{1}{1 + \alpha_e \rho_p} P_{max} = 0.944 * 3535 = 3337 \text{ kN}$$

The maximum compressive stress in the pre compressed tie will be:

$$\sigma_{ct} = -\frac{3337 * 10^3}{355 * 420} = -22.4 \text{ N/mm}^2$$

This value, valid for all cross-section along the 41m long member meet unity check for Stage 1 [4.4.1.1].

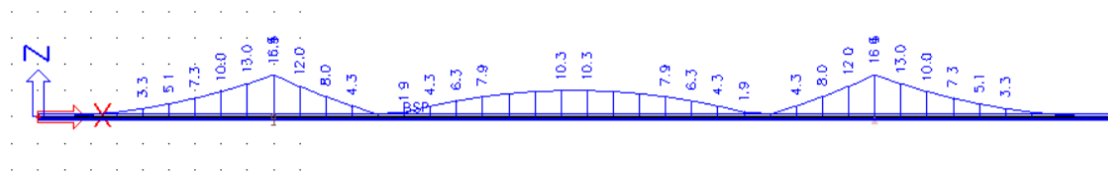


Figure 6.41: Tensile normal bending stresses in the tie member as result of self-weight only

- Prestressing with POT strands

The elongation of the prestressing steel and the shortening of the concrete at the level of the tendon is called relative displacement: $\Delta L_{p,rel} = \Delta L_p - \Delta L_c$

If the elongation of the prestressing steel is not checked, flexural cracks may occur in the tie member by the selfweight. Prestressing of the straight tendons (2 tendons of 5 – 15.7mm). The maximum stress allowed 1488 N/mm². So the maximum prestressing force $P_{max} = A_{p,pot} * 1488 = 10 * 150 * 1488 = 2232 \text{ kN}$. Maximum prestressing per tendon 1116 kN.

The mean loss in each tendon is:

$$\Delta P_{el} = A_p E_p \sum \frac{j * \Delta \sigma_c(t)}{E_{cm}(t)}$$

$$j = 0.25$$

$$\Delta \sigma_c(t) = \frac{P_{m0}}{A_c} = \frac{1116}{h * b} = -7.5 \text{ N/mm}^2$$

$$\Delta P_{el,mean} = 5 * 150 * 195000 * 2 * \frac{0.25 * 7.5}{58000} = -9.45 \text{ kN}$$

$$\Delta\sigma_{el} = -2.8 \text{ N/mm}^2$$

$$\Delta P_{el,tendon} = 5 * 150 * 195000 \frac{7.72}{58000} = -19.0 \text{ kN}$$

These losses can be compensated by overstressing of the tendons (up to 5% is allowed)

- Wedge set

Wedge set losses cases by wedge set $w_{set}=6\text{mm}$, $k=0.01$, $\mu=0.22$. The friction losses of bonded straight tendons is linear. The maximum allowable stress during prestressing is 1488 N/mm^2 .

$$\Delta\sigma_{\mu} = 1488 * (1 - \exp(-\mu(0 + k * x))) = -128.3$$

$$\frac{\Delta\sigma_{\mu}}{\Delta x} = \frac{-128.3}{41000} = -0.003129 \text{ N/mm}^2/\text{mm}$$

$$L_w = \sqrt{\frac{w_{set} E_p}{\Delta\sigma_{p\mu,m}/\Delta x}} = 17.6 \text{ m}$$

Stress losses at anchorage:

$$\Delta\sigma_{\mu} = 2 * L_w * \frac{\Delta\sigma_{\mu}}{\Delta x} = -109 \text{ N/mm}^2$$

Stress loss at distance L_w

$$\Delta\sigma_{p\mu m}^{lw} = L_w * \frac{\Delta\sigma_{\mu}}{\Delta x} = 54.5 \text{ N/mm}^2$$

Check whether the steel stress directly after anchoring is not too high:

$1488-54.5=1433 \text{ N/mm}^2$. This value is more than permitted (1395 N/mm^2). Use lower stress during prestressing $1488-38=1450 \text{ N/mm}^2$

$$\Delta\sigma_{\mu} = 1450 * (1 - \exp(-\mu(0 + k * x))) = -125 \text{ N/mm}^2$$

In [Figure 6.42] the wedge set losses of the 41m long tie member are plotted. It seems that the maximum initial stress of 1395 N/mm² is exceeded. Reduce the stress during prestressing to 1450 N/mm².

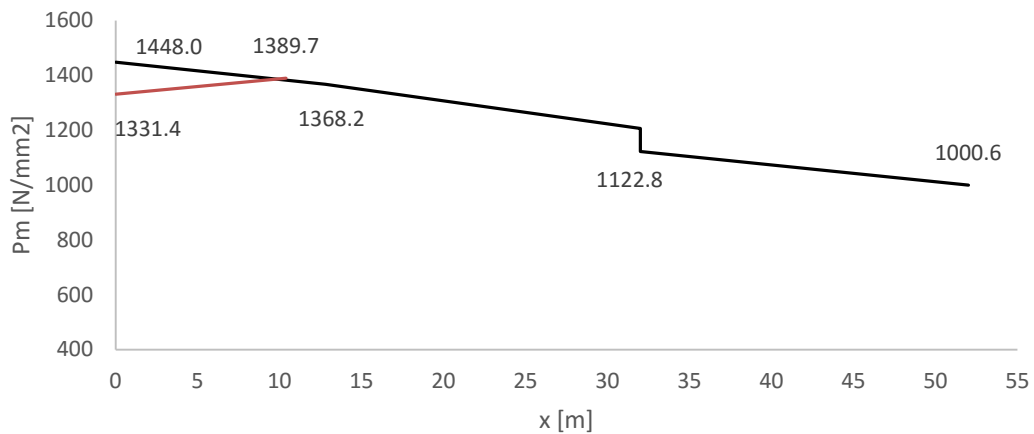


Figure 6.42: Wedge set losses, anchorage prestressed from left side only

- Shrinkage losses

The shrinkage of UHPC is mainly autogenous. The long-term drying and autogenous shrinkage according to SETRA is $\epsilon=525 \cdot 10^{-6}$ result in $\Delta\sigma_s=-102$ N/mm².

- Elastic deformation (long term)

The losses due to the shortening of the concrete during service time

$$\Delta\sigma_{el} = -70.0 \text{ N/mm}^2$$

$$\sigma_{c;b/t} = -\frac{P_{m0}}{A_c} + \frac{N_{SLS}}{A_c} \pm \frac{M_{SLS}}{W_c}$$

$$\epsilon_c = \sigma_{c;b/t} / E_c$$

$$\Delta\sigma_{el} = \epsilon_c * E_p$$

- Creep

According to SETRA and to other sources a conservative value for the creep coefficient for UHPC without thermal treatment is 0.8. $\Delta\sigma_{el} = -0.8 * 70.0 = -56 \text{ N/mm}^2$

- Relaxation

$$\Delta\sigma_{pr} = 0.8 * 0.0487 * 1395 = -54.35 \text{ N/mm}^2$$

- Total working prestressing force at $t=\infty$

The working prestressing force taking the time-dependent losses into account (shrinkage, creep, relaxation) and losses as result of friction are less than the assumed 15%.

$P_{m0}=5120 \text{ kN}$ assumed prestressing losses of 15% (768 kN). The calculated losses are 7% (337kN)

6.5.2 Global design connections

The surfaces roughness between the tensile member and the girder is high to increase the friction. No tensile forces are allowed in ULS design. This is verified with the load combination including the self-weight and traffic loads. The coupler used to connect two prestressing ducts so the anchorage force is applied at the end of the girder. Additional reinforcement are not required as long as the joint is in pure compression. [Figure 6.43]

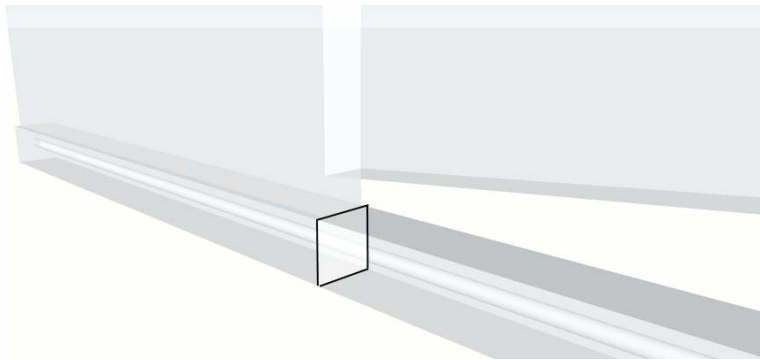


Figure 6.43: Joint

The connection of the truss members is possible in two methods: Only the members are prestressed with POT, steel reinforcement bars added to the joint transferring the tensile forces. The second option is to apply POT to prestress the truss member between the joints [Figure 6.44].

- Prestressed member with POT strands, anchored at end-member reinforced concrete joint
- Prestressed member with POT strands, anchoring at joint
- Steel Joints

6.5.2.1 Conventional reinforced joint

One possibility is to execute the joint with conventional steel reinforcement. Members which are loaded with compression forces require small amount of steel reinforcement. The other members under substantial high tensile forces will require prestressing with strands anchored at the member ends. This joint will be complex with substantial amount of reinforcement at the connection joint of the member. Cracking behavior is in this case very important. Another disadvantage of this solution is that inspection of the anchorage points at the member's ends will be impossible once girder is completed.

[Figure 6.44]

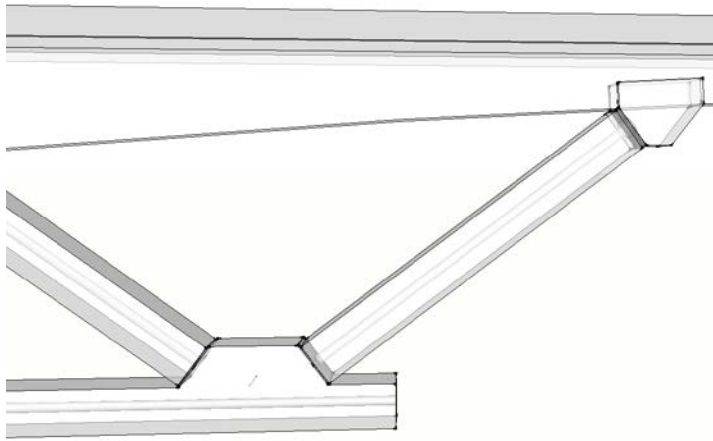


Figure 6.44: Connection truss members with girder and tensile member

The reinforcement bars [Figure 6.45] will be installed during prefabrication of the tie member and compression strut, the members will be casted with sleeves for the bars, when the member is levelled between both connections the bars will be grouted.

The reinforcement will be anchored to the joint with U-shaped hairpins with sufficient capacity to take the tensile forces in the truss members.

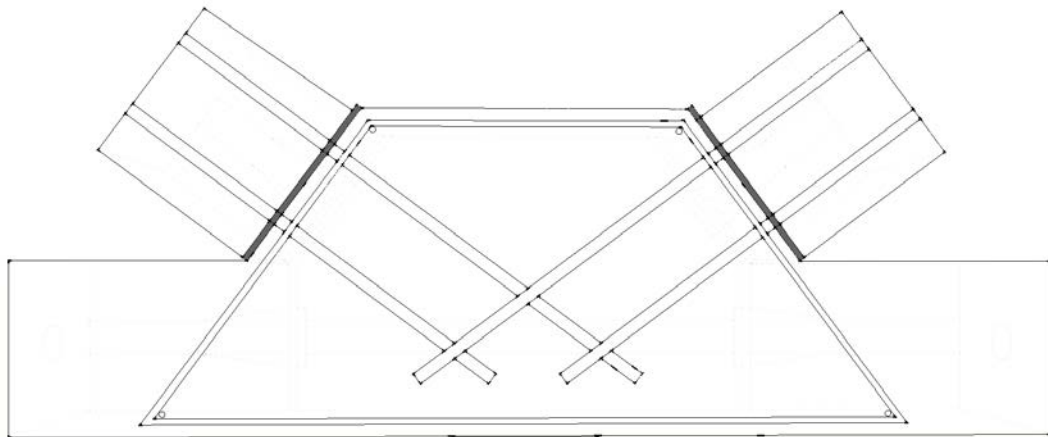


Figure 6.45: Conventional reinforced joint, the bars will be anchored with U-shaped hairpins

6.5.2.2 Multiple cables prestressing with straight strands or bars

The truss members are rectangular massive beams of 355*355mm UHPC with different lengths from 1m up to 2m. The members are connected to the girder by prestressing the POT tendon to the joint. One method to design the joint is proposed by C.K Cheung [TU Delft 2002]. The POT strands of the member continue through the joint and will be anchored on the other side of the joint [Figure 6.46].

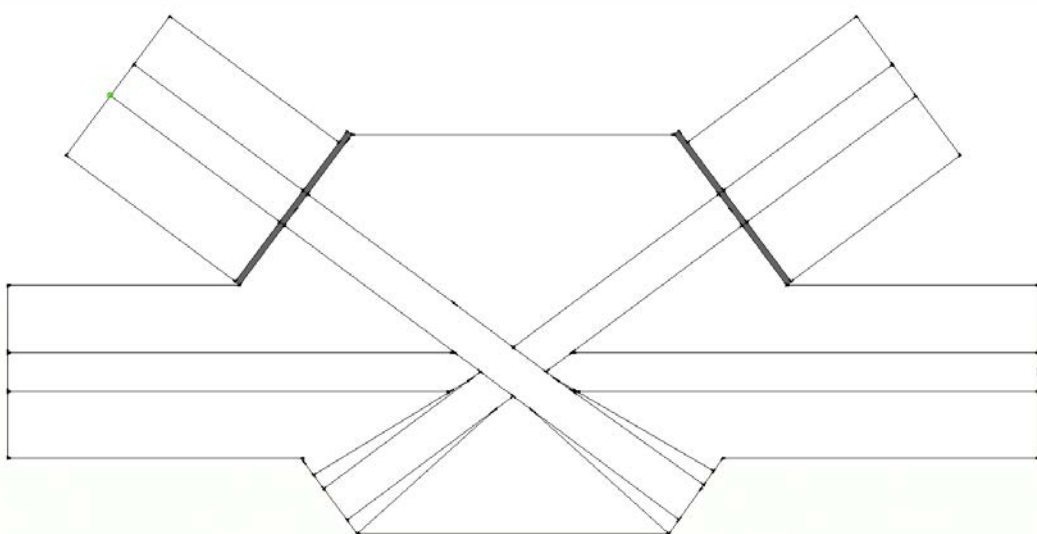


Figure 6.46: Multiple cables

The POT strands are compressed and anchored to the other side of the joint. So the ducts anchored at the other side of the joint belongs to different members will cross each other. The crossing of the strands can be solved in several of methods: Eccentricity and dividing of the cable into two small cables. Eccentricity will result in additional bending moment in the joint, this will require lager dimensions of the joint. Splitting the cables into two small cables which can cross each other at the joint is favorable, keeping the self-weight low and avoiding additional loads in the joint.

The POT strands of the tensile members can cross-each in the space between the POT strands of the tensile tie [Figure 6.47].

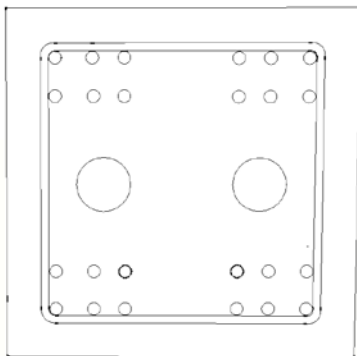


Figure 6.47: Cross-section tensile tie space between POT strands will be used for crossing of POT members strands.

6.5.2.3 Steel joint

This alternative uses precast steel connection to which members and tie members are connected. The 41m long tie member will be divided in this case to 7 smaller tie segments with in between prefabricated steel joints. Later the truss members can be connected to the steel joints.

This alternative reduces the weight of the joint, the design will be more elegant with flat underside. However the welding details will require additional costs. Durability due to corrosion, and fatigue will be important.

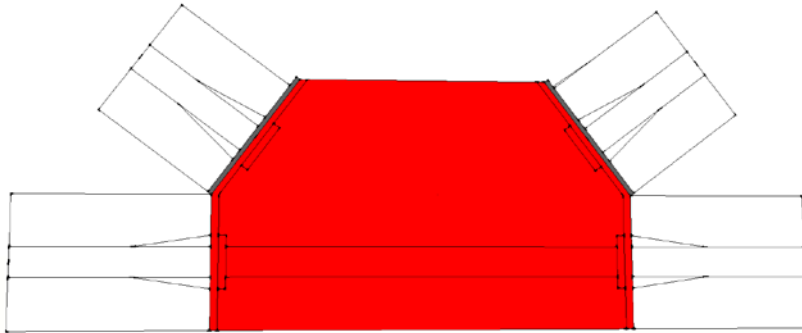


Figure 6.48: Seven identical tie – truss steel joint are required

6.5.2.4 Evaluation

Steel joints [4.5.2.34.5.2.2] and concrete joint with POT anchored at the joint [6.8.5.2] are the best alternatives. The durability of UHPC is larger than the steel thanks for its high density. Choosing for steel joints means the tensile tie will be divided into 7 tie members, 5 with identical lengths of 3.50m and 2 more of 11.75m length each.

Going for the concrete joint alternative means higher durability, less segments, better fatigue resistance, and a avoiding joints with higher stiffness (young's modules) but also more complex design.

Keeping track with the scope of the thesis the concrete joint will be further analyzed.

The prestressed joint looks a more simple option to carry out and to avoid tensile stresses in the joint and/or truss members.

6.5.3 Global Design truss members

The dimensions of the truss members are rather small, only 1-2m long with approximated of 250-350mm. So hollow concrete members with external prestressing is unlikely to be realistic. Steel tube filled with UHPC with prestressing and massive rectangular member are a good options. The steel tube filled with UHPC is already applied in Bourge Les Valence in France

Assuming rectangular truss member [4.4.1.3] with $h=b$ and identical lengths. Within a substantial number of iteration the following aspects are optimized: internal forces, size of prestressing bars/strands, concrete cover, prestressing levels, anchorage space, simplicity design, stiffness change, type of connection, and ductility.

The most suitable dimension of the truss members are 200*200mm ($h*b$). Further as discussed in [4.4.1.3], using POT strands means that a wedge set losses are accounted for, reducing the prestressing stress during prestressing to 1377 N/mm^2 [Figure 6.49] means that the Initial prestressing at $t=0$ is reduced to 1377 N/mm^2 .

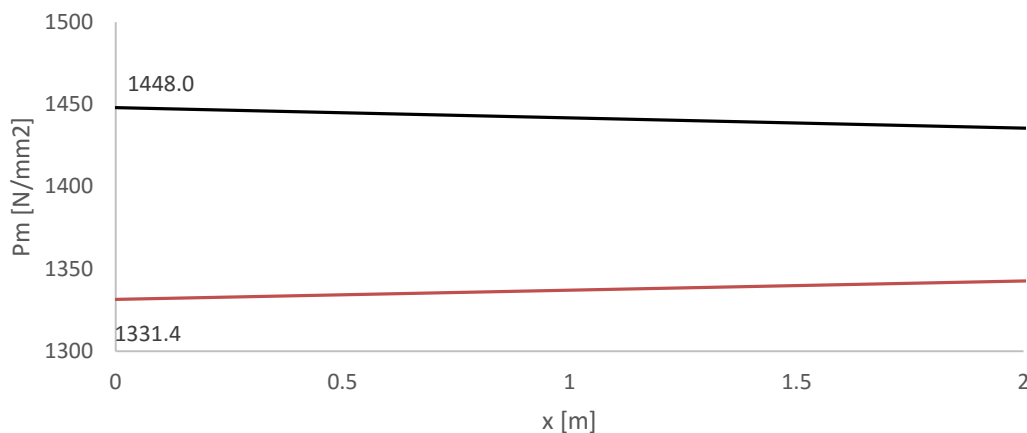


Figure 6.49: Wedge set losses truss member

As an alternative use prestressed bars to avoid wedge set losses. The low tensile strength capacity of the bars is proved to be sufficient for this application.

Finally by means of FEM analysis including the real-time working forces, the final prestressed truss members can be designed.

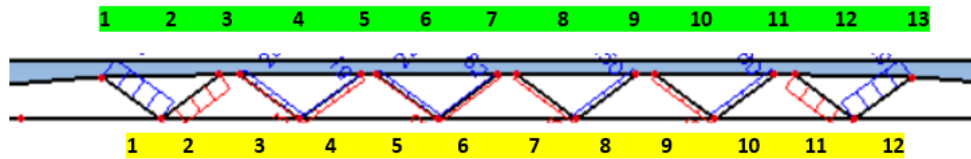


Figure 6.50: The truss members in x-z plane

There are also small moments around the x-axis and z-axis. These are rather small, verify the stresses are smaller than the concrete tensile bending strength.

X-axis: between 0-2 kNm $\rightarrow \sigma = (2 \cdot 10^6) / (1/6 \cdot 200 \cdot 200^2) = 1.5 \text{ MPa}$

Z-axis: between 0-2 kNm $\rightarrow \sigma_c = (2 \cdot 10^6) / (1/6 \cdot 200 \cdot 200^2) = 1.5 \text{ Mpa}$

UHPC can take this bending tensile forces without using any reinforcement or prestressing. Additionally UHPC concrete might be used containing micro fibers which increase the tensile bending strength or HSFRC which increase the ductility of the cracked concrete. It is assumed that under this countermeasures this small moments can be ignored.

6.5.3.1 Classification

Similar to the analysis performed in [4.5.1] the truss members prestressing will be design considering two options: Y1030H bars or Y1860S7 strands.

First truss members are classified, compression and tensile members are distinguished.

For each member the prestressing force is determined, this should fulfill the ULS design.

The number of bars/strands can be determined and the prestressing losses due to shrinkage, creep, relaxation, friction and wedge set (only for Y1860S7).

<i>Member 3</i>	<i>Strands Y1860S7</i>	<i>Bars Y1030H</i>
Strands/Bars	3 -15.7mm	2 -26mm
Time depended losses	7%	17%
Wedge set	$\sigma_{m0} = 1377 \text{ N/mm}^2$	$\sigma_{m0} = 773 \text{ N/mm}^2$
Connection	complex	simple

Table 6.14: comparison prestressing system

6.5.3.2 Result

<i>member</i>	$A_{p,min}$ [mm^2]	<i>Bars Y1030H</i>
1	2312	2 – 38mm
2	94	2 – 26mm
3	861	2 – 26mm
4	594	2 – 26mm
5	814	2 – 26mm
6	677	2 – 26mm
7	655	2 – 26mm
8	302	2 – 26mm
9	555	2 – 26mm
10	893	2 – 26mm
11	94	2 – 26mm
12	2337	2 – 38mm

Table 6.15: Summary applied Y1030H bars for each truss member.

The calculation of the applied prestressed bars in this section is defined iteratively with maple script. This is not added to the appendix but can be supplied upon request.

6.5.4 Joint

6.5.4.1 Tie - truss

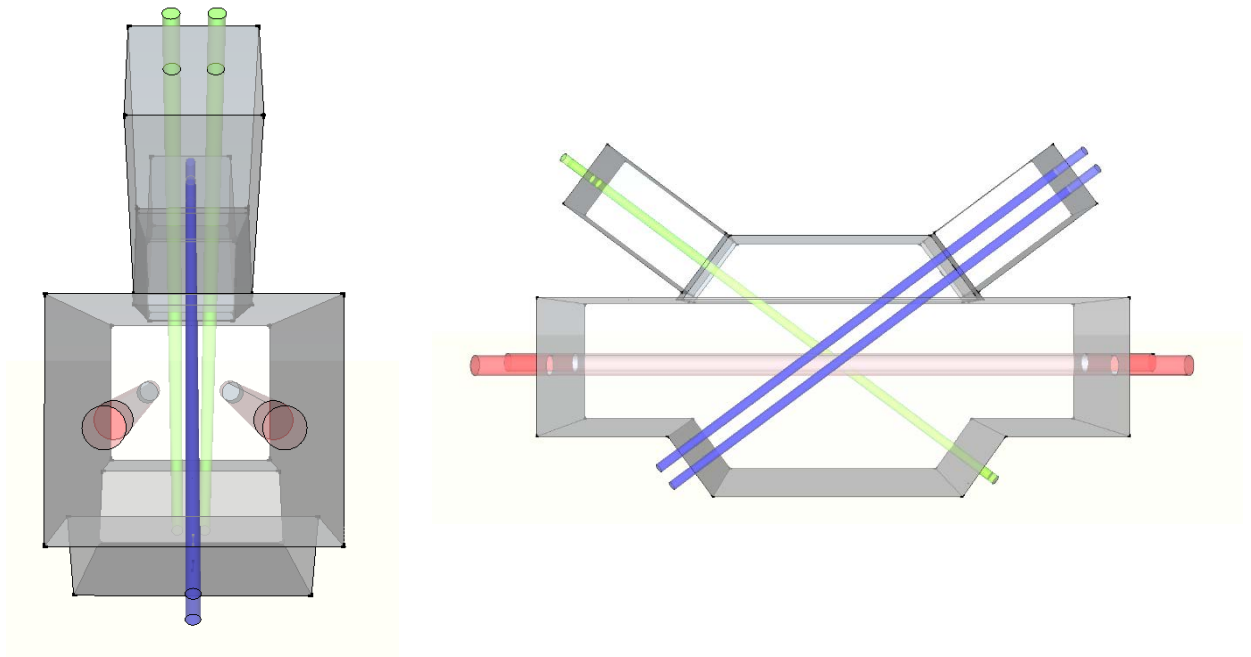


Figure 6.51: Tie – truss joint

Joint number 4 [Figure 6.51] is almost identical to all other truss – tie joints. In this connection both members are prestressed with 2–26mm bars. The member bars are crossing through the joint and anchored. The dimensions of the joint are adjusted for the dimensions of the maximum applied bars. So the joints dimensions are identical (high repetition).

All members including the tie member are loaded with tensile and compressive forces. Eliminating the tensile forces from the truss members is with prestressed bars while the tie members includes POT and PRT strands. The truss members will be brought under compression by the bars by anchoring them to the joint on one side and tensioning the bars on the other side of the joint. This is valid for the bottom side of the member where joint is designed [Figure 6.52].

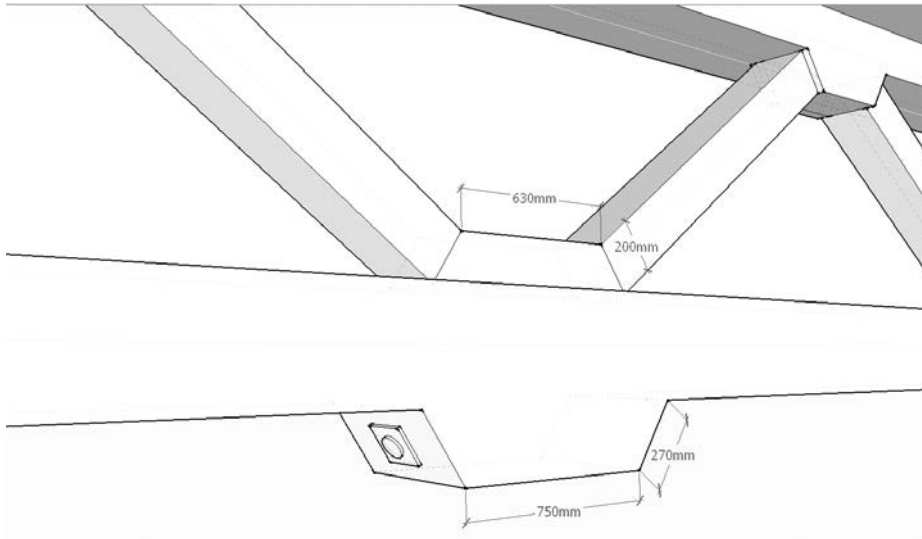


Figure 6.52: Outer dimensions tie – truss joint

6.5.4.2 Strut - truss

The compressive strut – truss joint on the other hand is anchored with coupler with locks nut system. The $\Phi 26\text{mm}$ bars are connected bar embedded in the concrete. This embedded bar will be anchored according to [NEN-1992-1-1 art. 8.4]. The required anchorage length for bent bar is calculated.

Bent bars

First option is bars bent and embedded in the concrete. This will reduce the required anchorage length compared to straight bars.

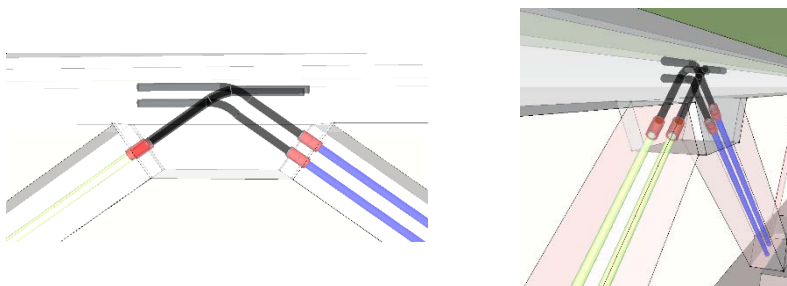


Figure 6.53: Bars connected to coupler (red) connected to anchorage bar with total length $L_{b,reqd}$ [NEN-1992-1-1 art. 8.4].

$$l_{b,rqd} = (\Phi/4)(\sigma_{sd}/f_{bd})$$

$$f_{bd} = 2.25 \eta_1 \eta_2 f_{ctd}$$

$$l_{bd} = \alpha_1 \alpha_2 \alpha_3 \alpha_4 \alpha_5 l_{b,rqd} \geq l_{b,min}$$

Where:

$$f_{ctd} = f_{ctk,005}/\gamma_s = 4.35/1.15 = 2.9 \text{ N/mm}^2$$

$$\eta_1 = 1.0$$

$$\eta_2 = 1.0$$

$$\alpha_1 = \alpha_2 = \alpha_3 = \alpha_5 = 1$$

$$\alpha_4 = 0.7$$

$$l_{bd} = 624\text{mm}$$

Loop anchorage

The minimum mandrel diameter required to avoid damage to the reinforcement is to large. For bars with diameter of 26mm the mandrel diameter is $7\Phi=191\text{mm}$ which not met the concrete cover requirement. One can reduce the diameter of the bars but this can create error during execution and insufficient anchorage strength.

End anchorage at compressive strut

A more elegant possibility is to use straight bars embedded in the concrete. Because the required anchorage length ($l_{bd}=892\text{mm}$) cannot be achieved, the bars are anchored with End-anchorage at the top side of the compressive strut [Figure 6.54]

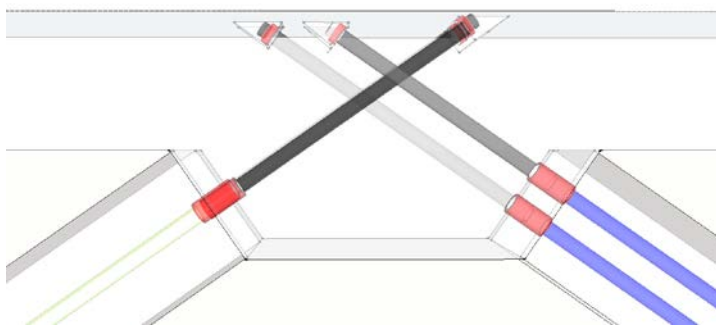


Figure 6.54: compressive strut-truss connection with straight anchorage bars

Conclusion

The bars can be anchored with bent bars or with straight bars with end-anchorage at the top side of the compressive strut. The post-tensioned bar in the truss member will be connected to the anchorage bar with standard coupler with lock nuts [VSL].

The bent bars solution do not required special shuttering and the bars are completely embedded in the concrete with a minimal concrete cover. Hence an exposure of the bars to corrosive environment is limited compared to straight bars.

6.5.4.3 Strength

Only by means of FEM sub-model with volume elements (ANSYS) of the joint it is possible to determine the forces distribution. The model should include the steel anchore plate to which the strands are anchored, the geometry of the joint, hollow area in the joint of the ducts which is a local weakening, and finally the model should include the truss elements which transfer the load into the joint. The FEM model should be non-linear one which can simulate the post-cracking behavior.

In this analysis it should be verified that nowhere in the joint the tensile strength of 8 N/mm² is exceeded and that the compressive stresses are smaller than 150 N/mm². Thid can occur by several of reasons for instance imposed deformation of truss members, creep, shrinkage.

In the research of [C.K. Cheung] for similar connection with UHPC it has been found that the UHPC joints prestressing strands anchored meet the strength requirements. Although local high peak stresses will occur nearby the anchor plate and the connection of the truss members to the joint. This high peak stresses are according to [[C.K. Cheung] due to assumption made in the FEM model: linear behavior concrete, anchorage is not in the model, fixed connection of the truss members instead of hinged connection, hollow area in the joint is modelled incorrectly.

It is recommended that full FEM non-linear model should be performed to further investigate the stresses distribution in the UHPC joint.

6.5.4.4 Compressive nodes without tensile bars [1992-1-1 art. 6.5.4.]

The rule for nodes [NEN 1992-1-1 art. 6.5.4.] is applied to the joint, where concentrated forces are transferred. In this joint concentrated nodes may develop where the point loads are applied.

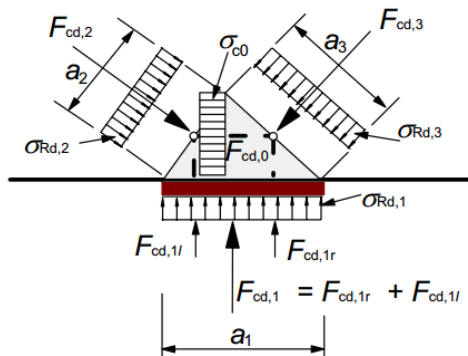


Figure 6.55: Compression node without ties [NEN 1992-1-1 art 6.5.4]

Compression nodes are checked according to [NEN 1992-1-1 art 6.5.4] the maximum compressive force at the node is $F_{max} = A_{strut} * f_{cd} = (250 * 250) * 150 = 9375 \text{ kN}$ ok.

Considering the transverse tension, the maximum applied force is

$$F_{max} = A_{st} * v' * f_{cd} = (250 * 250) * (1 - 180/250) * (180/1.5) = 2100 \text{ kN} \text{ ok}$$

6.5.5 Anchorage

The anchorage of the POT ducts is at the ends of the girder. The anchorage plates require sufficient clearance from the edge and sufficient spacing. This requirement is not only for the hydraulic jacks but also to dissipate the large concrete compressive stresses in the anchorage. The cross-section at the anchorage is adjusted to fulfil the requirements according to the fabricator [VSL] [Figure 6.56]. Shortly after installing the anchorages, the open space between the tendons and the ducts is injected with a special grout to protect the very corrosion sensitive prestressing steel. Finally, for corrosion protection, the anchorages are covered with concrete.

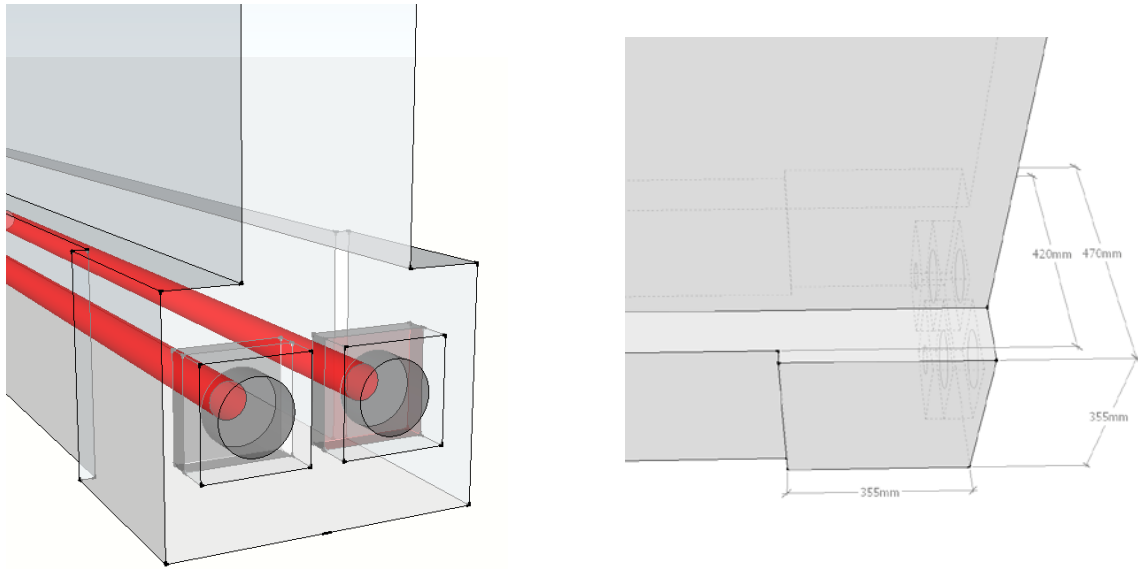


Figure 6.56: Anchorage of 5-15.7mm duct

6.5.7 Bridge Deck

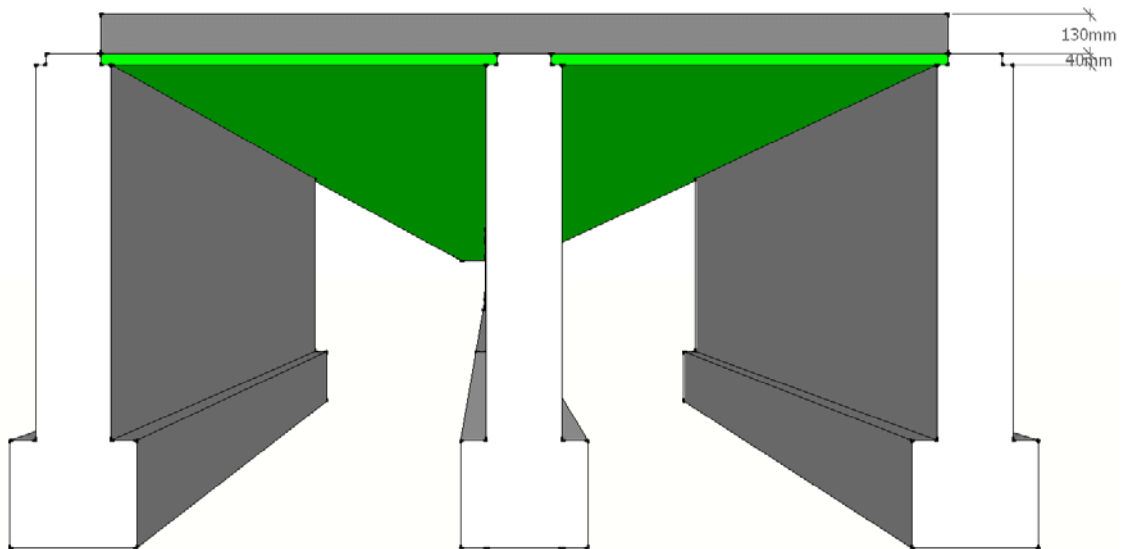


Figure 6.57: Concrete deck $h_{\text{deck}}=170\text{mm}$

The concrete deck consists of UHPC thin permanent plates with a top layer of cast-in-situ conventional concrete. The girders are produced with shear reinforcement protruding upwards to be used as a shear connection between the cast-in-situ layer and the prefabricated layer. The compressive layer will be reinforced with a steel grid according to [NEN-EN 1992-1-1 Art. 9.2.1.1] to prevent cracks due to creep and shrinkage. This is very important since the top flange is very slender where shrinkage and creep will develop faster. This compressive layer is also responsible for the torsional stiffness of the bridge.

6.5.7.1 Longitudinal reinforcement

The deck between $14 < x < 36$ is very slender with low thickness of 400mm including the web and 170mm thickness without the web. The governing bending moments are given in [Table 6.16]. Using rule of thumb to calculate the required reinforcement based on bi-linear stress yields the following reinforcement:

Moment	rebar	M_{Ed}	d	b	z	$M_{Ed}/(z f_y)$	$A_s/ (b d)$	Long. rebar
$m_x D-$	y-direction	60	140	1000	127	1086	0.77%	$\emptyset 20 - 250mm$
$m_x D+$	y-direction	13	140	1000	127	235	0.16%	$\emptyset 20 - 500mm$
$m_y D-$	x-direction	50	140	1000	127	905	0.64%	$\emptyset 20 - 250mm$
$m_y D+$	x-direction	13	140	1000	127	235	0.16%	$\emptyset 20 - 500mm$

Table 6.16

The minimum reinforcement according to the Eurocode is $240mm A_{s,min}=0.26f_{ctm}b_t d/f_{yk}$. The contribution of the UHPC thin plates to the bending moment resistance is neglected in ULS design but are very effective in SLS design. Further is the favourable effect of the prestressing force (hogging bending moment) is neglected in this calculation.

6.5.7.2 Hogging moment caused by eccentricity

During prestressing of the tensile tie into the girder there are no truss members and no external loads. In [4.4.1] the importance of partial prestressing is used to control the tensile stresses caused by the hogging moment. Prestressing the girder up to the full prestressing load [4.5.1] is controlled and verified so nowhere in the deck the tensile strength is exceeded.

6.5.8 Shear

$0 < x < 4.5\text{m}$

The web of the girder is not constant along the x-axis. For $0 < x < 4.5$ where $a/d < 2.5$ the shear forces will be transferred directly into the supporting point. In [4.3.3] this is already explained. The capacity is calculated for cross-section [Figure 6.64], The value of V_{cd} for uncracked parts $0 < x < 4.5\text{m}$ ($a/d < 7$) of tensile splitting failure is derived with the following formula:

$$V_{Rd,c} = \frac{I b_w}{S} \sqrt{f_{ctd}^2 + \sigma_x f_{ctd}} = 151 * f_{ctd} = 800\text{kN}$$

$$I = 2.4600e - 01 \text{ m}^4$$

$$S = 0.40738 \text{ m}^3$$

$$b_w = 0.25\text{m}$$

$$f_{ctd} = 5.3 \frac{\text{N}}{\text{mm}^2}$$

$$\alpha_1 = 1.0$$

$$\sigma_{cp} = \frac{N_{Ed}}{hb_w} = 0$$

This lower bound value is not taking into account any normal forces.

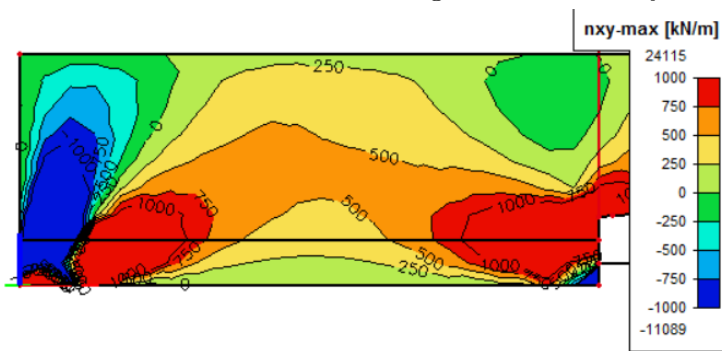


Figure 6.58: nxy-max, ULS load class

Required shear reinforcement:

$$A_{stir} = \frac{V_{Ed}}{z * f_{ywd} * \cot\theta} = \frac{800 \text{ kN/m} \cdot 0.25 \cdot 10^3}{1420 * 435 * \cot(21.8)} = 0.129 \text{ mm}^2/\text{mm}$$

For $A_{sw} = 226 \text{ mm}^2$ (2 legs) and $S_{max} = 0.75d < 600\text{mm}$, recommended $S_{max} = 300\text{mm}$ [NEN 1992-1-1 art. 9.2.2 (8)]

Apply $\emptyset - 300\text{mm}$ in the zone $0 < x < 4.5\text{m}$.

4.5 < x < 25m

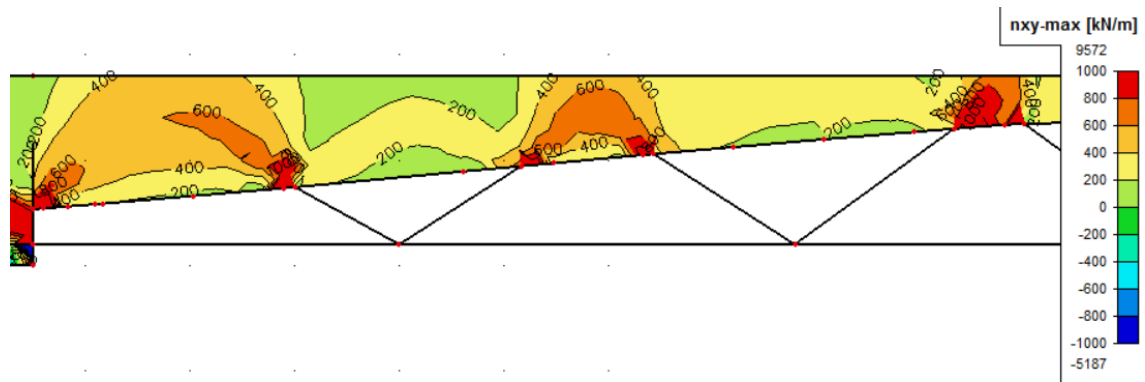


Figure 6.59: shear forces in the compressive strut

Required shear reinforcement is based on the following relation with shear force (V_{Ed}) and lever-arm (Z) as function of x-axis (longitudinal axis).

$$A_{stir} = \frac{V_{Ed}}{z * f_{ywd} * \cot\theta} = \frac{V_{Ed}(x)}{z(x) * 435 * \cot(21.8)} = mm^2/mm$$



Figure 6.60: Example duels protruding from web

The shear force in ULS in kN/m vary along the girders length at the connection point web-deck [Figure 6.61].

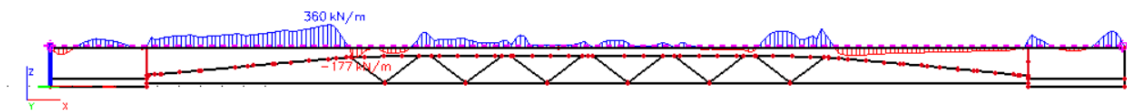


Figure 6.61: ULS web-deck connection shear force in kN/m

In regions where the shear force is smaller than the concrete shear capacity theoretically no shear reinforcement are required.

$$v_{cd} = 0.12k(100\sigma_l f_{ck})^{\frac{1}{3}}$$

Where:

$$k = 1 + \sqrt{200/d} \leq 2$$

$$\sigma_l = \frac{A_{sl}}{b d}$$

Analysing the shear in the compressive strut result in shear reinforcement as follows:

Coordinate	Stirrups calculated	Stirrups Applied
$4.5 < x < 6.7\text{m}$	$\Phi 8 - 600\text{mm}$, 2 legs	$\Phi 8 - 300\text{mm}$, 2 legs
$6.7 < x < 9.5\text{m}$	$\Phi 10 - 600\text{mm}$, 2 legs	$\Phi 8 - 300\text{mm}$, 2 legs
$9.5 < x < 13.2\text{m}$	$\Phi 10 - 250\text{mm}$, 3 legs	$\Phi 10 - 250\text{mm}$, 3 legs
$13.2 < x < 25\text{m}$	$\Phi 10 - 300\text{mm}$, 2 legs	$\Phi 10 - 300\text{mm}$, 2 legs
Above the comp. strut – truss members joints	$\Phi 10 - 80\text{mm}$, 3 legs	$\Phi 10 - 80\text{mm}$, 3 legs

Table 6.17: Applied shear reinforcement

6.5.9 Detailing spalling and splitting reinforcement

Lack of understanding of the flow of forces can lead to irreversible damage to the structure. The strut and tie model can be used to trace the flow of forces. In case of POT steel the concentrated forces in the anchorage are gradually spread in the member. The length required to have a uniform distribution (S) [St-Venant] is the length where splitting reinforcement is required (hairpins) closed stirrups. Because only one or two tendon is used (higher slenderness) the splitting tensile force will be significant.

Furthermore, in the stage of prestressing, splitting forces along the free end may occur. Their magnitude and location depends on the sequence of prestressing. Also when the prestressing force is introduced eccentrically, the position of the splitting tensile force and its magnitude can be determined with a strut and tie model.

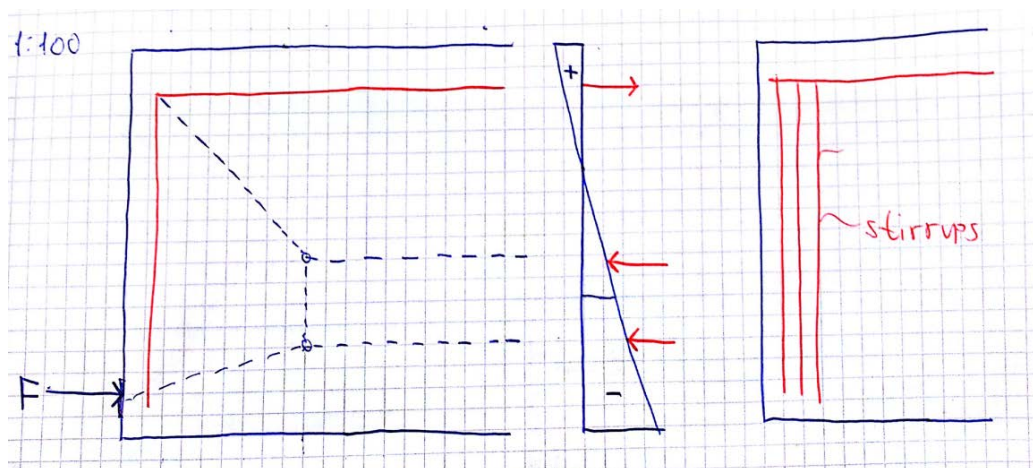


Figure 6.62: Location of splitting reinforcement individual member (side view)

In [Figure 6.62] two point loads must be distributed. The disturbance length is, therefore, $h / 2$ where h is the beam height. The struts and ties that deflect the forces are in the first half of the disturbance area.

The beam have only top-flange, the resulting force have eccentricity

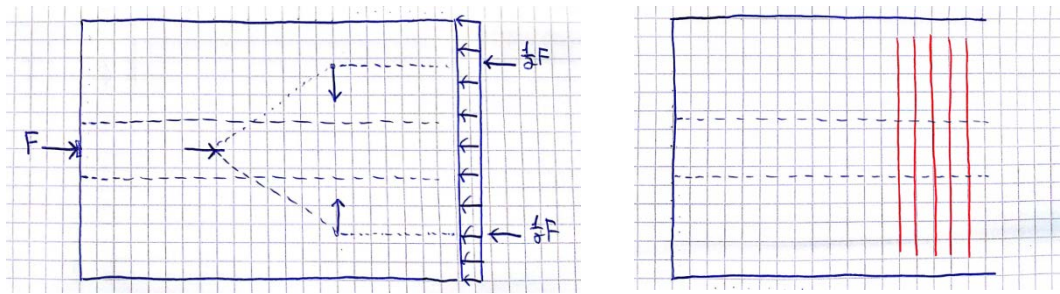


Figure 6.63: Top-view

Exact calculation:

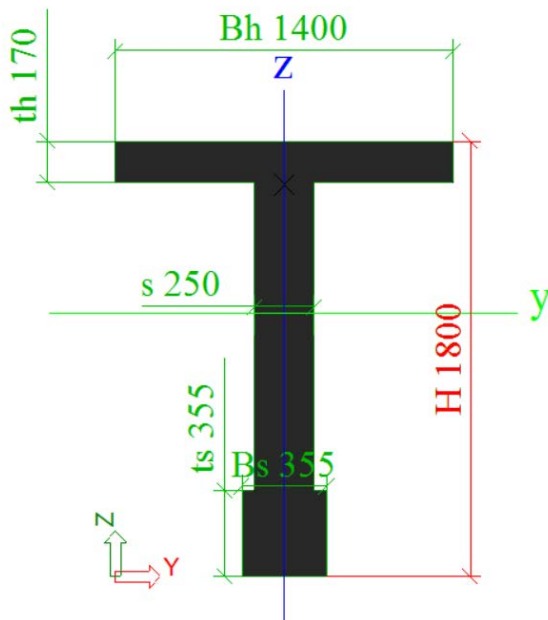


Figure 6.64: Cross-section girder $0 < x < 4.5\text{m}$ and $46.5 < x < 50\text{m}$

The non-symmetrical cross-section with top flange and bottom flange is eccentric loaded with POT force $F=1000\text{kN}$ (only for calculation $F=1000\text{kN}$). The normal force and the bending moment can be derived to plot the complete stress distribution. The stress diagram is split into three parts such that the tensile force (αF) is compensated for by a compressive force (βF). The resulting major compressive force is noted by (δF). Please note, the width is variable along the height and is taken into account.

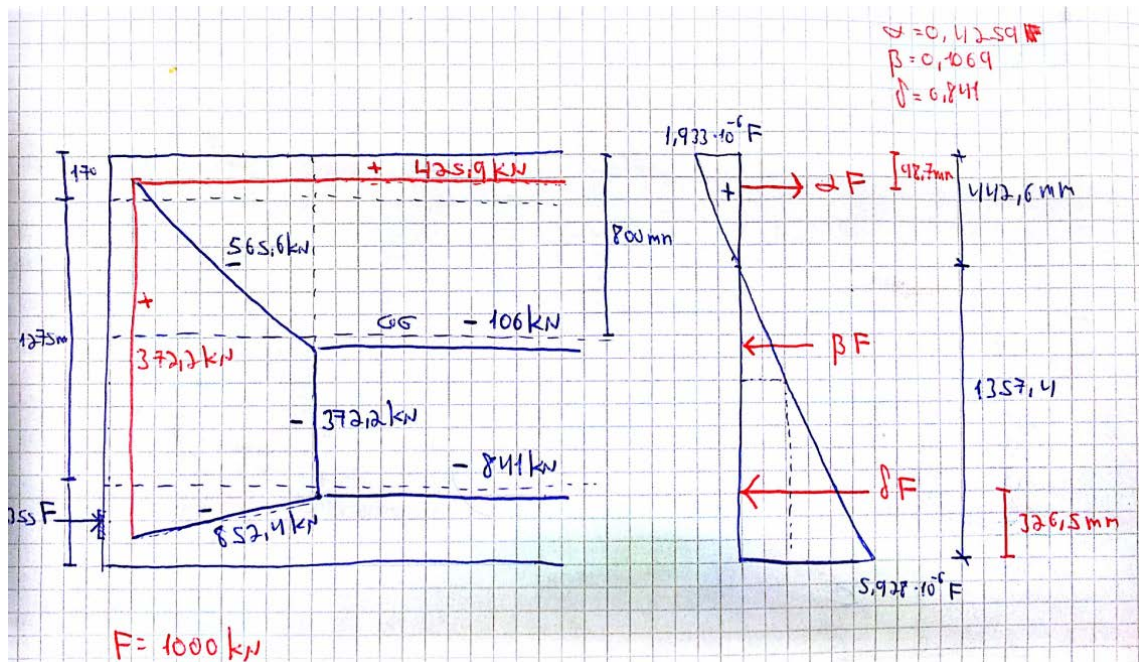


Figure 6.65: Strut-Tie model

Splitting reinforcement (stirrups) are required close by the anchorage and will confine the cross-section. Longitudinal rebar at the top flange is necessary as well.

$$N_{spl} = (1595/1000) \cdot 372.2 = 593.65 \text{ kN}$$

The cross-sectional area follows from

$$\text{Hairpins: } A_{spl} = N_{spl} / \sigma_s = (593.65 \cdot 10^3 / 200) = 2968.25 \text{ mm}^2$$

Which equals to $\varnothing 14 - 150 \text{ mm}$, 2 legs

Where:

$\sigma_s = 280 \text{ N/mm}^2$ correspond with $\varnothing 12 - 150 \text{ mm}$ [NEN-EN 1992-1-1, Table 7.2N Table 7.3N]

Horizontal bars: $A_{spl} = (425.9 \cdot 10^3 / 200) = 2129.5 \text{ mm}^2$ which equals to $5\varnothing 25 - 50 \text{ mm}$

Compression node are checked according to [NEN 1992-1-1 art 6.5.4] the maximum compressive force at the node is $F_{\max} = A_{\text{strut}} \cdot f_{cd} = (250 \cdot 250) \cdot 150 = 9375 \text{ kN}$ ok.

Considering the transverse tension, the maximum applied force is

$$F_{\max} = A_{st} \cdot v' \cdot f_{cd} = (250 \cdot 250) \cdot (1 - 180/250) \cdot (180/1.5) = 2100 \text{ kN}$$
 ok

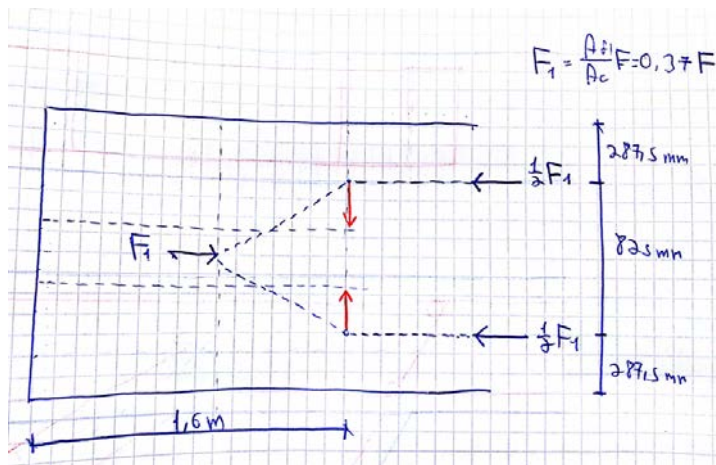


Figure 6.66: Top view

Supports:

When part of the supporting forces act outside the influencing area of the reinforcement damage will occur. This should be prevented [Figure 6.67]

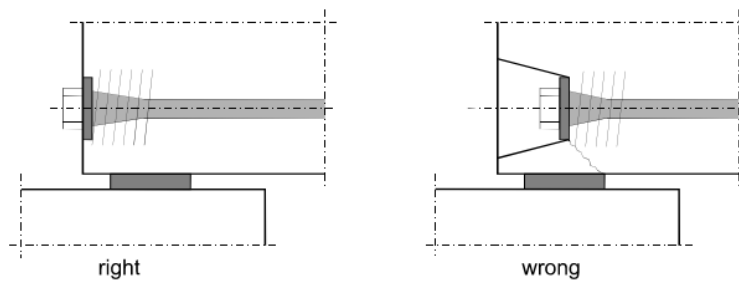


Figure 6.67: Girders supports

Fibers contribution

When UHPC or SHCC are applied the additional steel fibers will contribute significantly to the resistance against splitting of the concrete, the tensile capacity during the post- and pre cracking stage are favorable [2.3E] [F]. Theoretically it will be possible to reduce the amount of splitting reinforcement. Therefore UHPC is used for all truss members and bottom tensile member. As for the girder web NSC will be applied to reduce the costs.

Spalling stresses

Generated by the eccentric introduction of prestressing force. The POT strands have in the girder large eccentricity relative to the CoG. According to [NEN-EN 1992-1-1 cl. 8.10.3] the required transverse reinforcement is different for PRT and POT. The PRT strands are located at $4.5 < x < 45.5$ far enough from the supports and analyzed in the individual member level.

The POT strands however act with eccentricity of approximately $e_p = 1.6m$. The tensile forces need to be determined with strut and tie models

6.6 Overview design

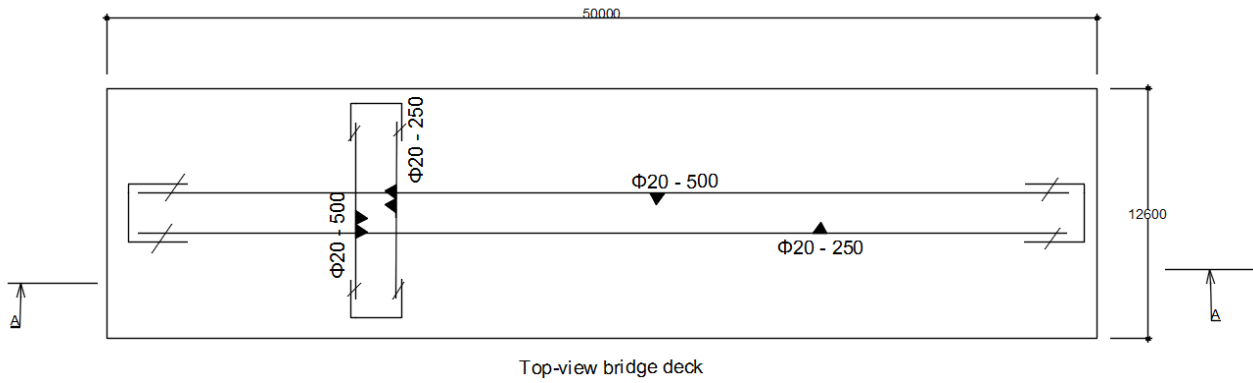


Figure 6.70: Top-view bridge deck longitudinal reinforcement

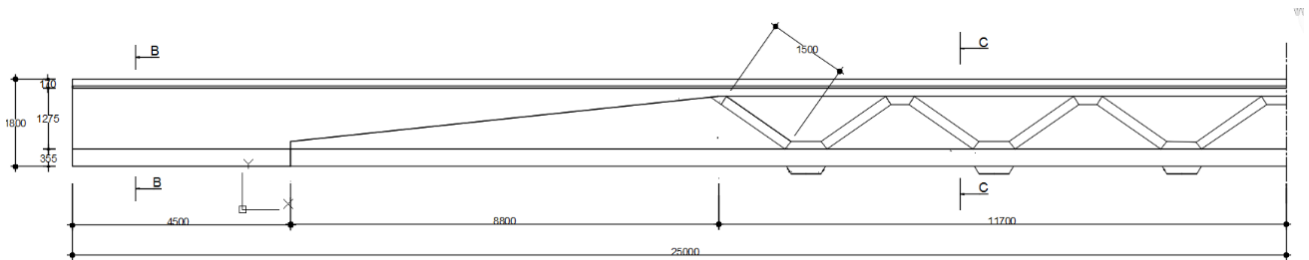


Figure 6.68: Cross-section A-A , reinforcement details

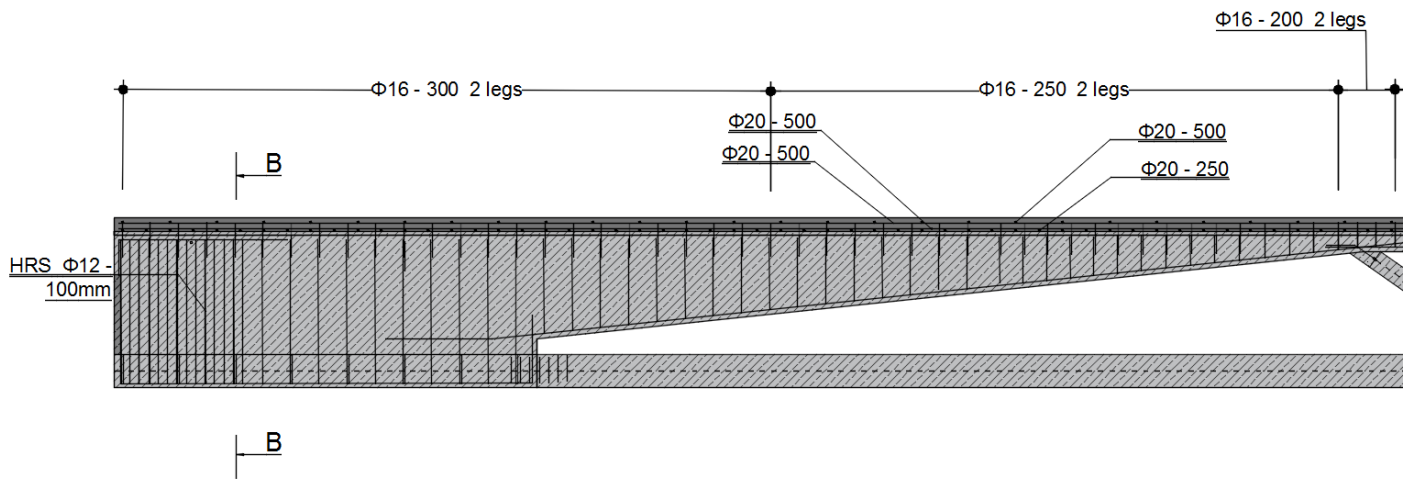


Figure 6.71: Cross-section A-A, reinforcement details

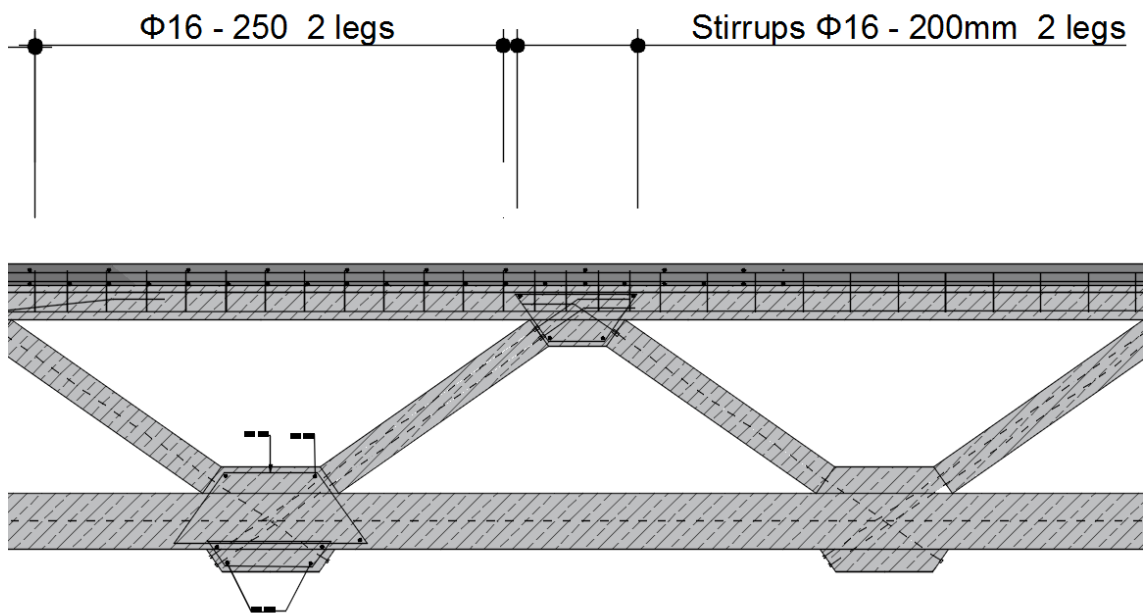


Figure 6.72: Cross-section A-A, reinforcement details

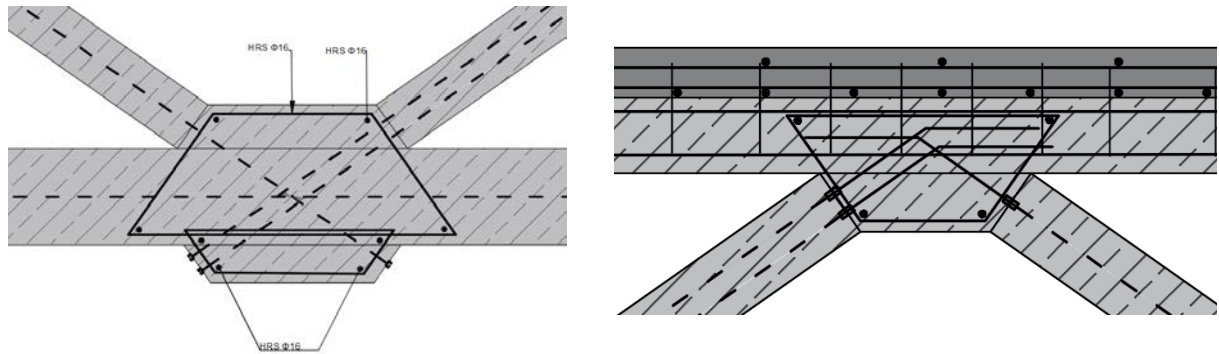
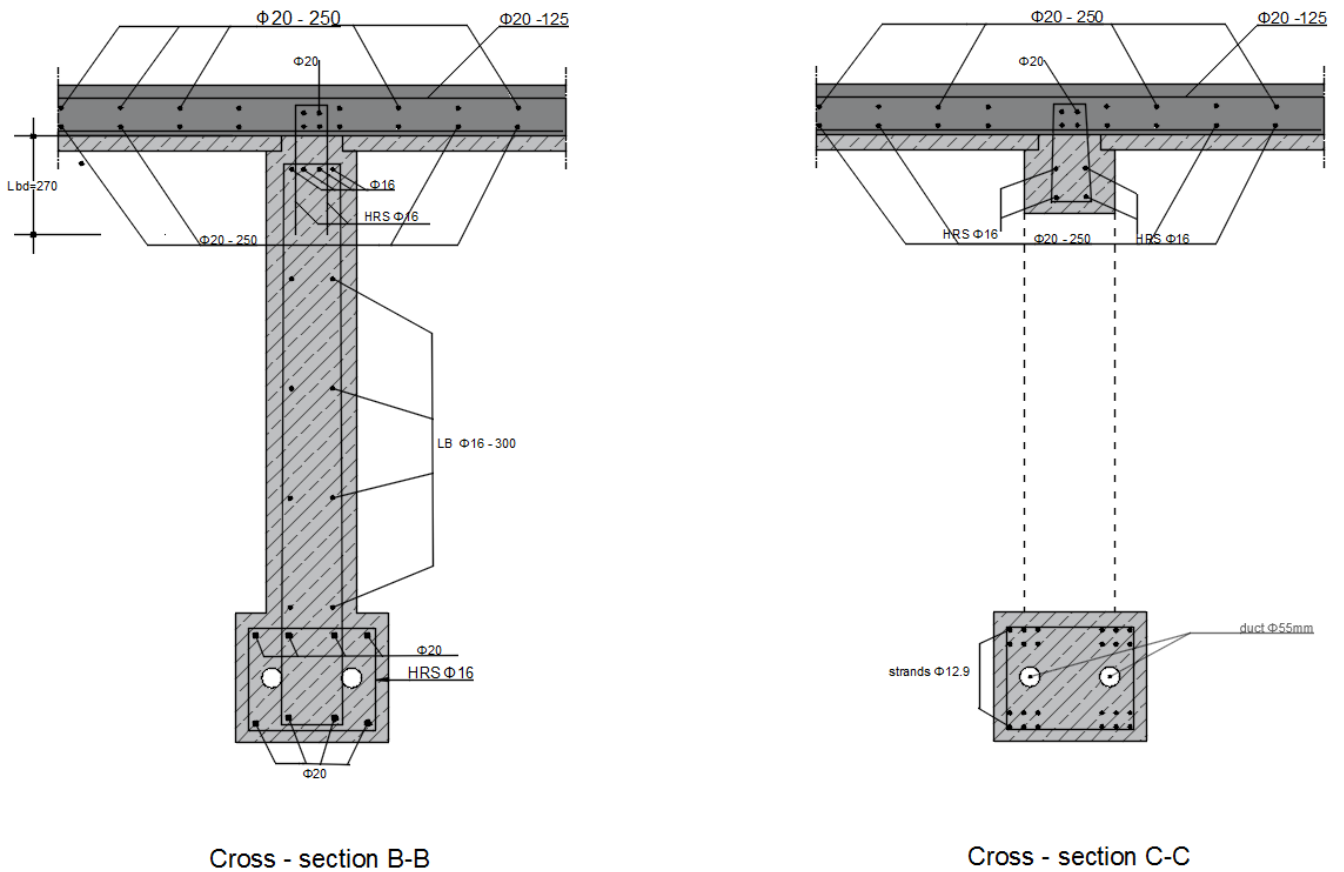


Figure 6.73: Reinforcement details truss-tie connection and truss-strut connection



Cross - section B-B

Cross - section C-C

Figure 6.74: Reinforcement details cross-sections B-B and C-C

6.7 Remarks & Suggestions

The girder design is initiated with parametric study follows by the preliminary design in this chapter. The outcome of these two chapters is a concept for application of advanced cementitious materials such as UHPC in heavy traffic bridge.

The development of new type of bridges with ACM , emphasizing high durability with market-oriented costs and with suitable design for replacement of existing bridges and reconstruction of existing bridges with possible large scale production (prefabrication) is the optimal solution for the future bridges industry. The solution offered in this thesis compared to similar box girder with identical span offers approximated of 35% self-weight reduction. The reduction in material costs could be largely offset by labor and production costs. Because the superstructure is lighter than conventional one, using high span is possible with smaller impact on the substructure.

High durability of the design is achieved by using materials with high density and low permeability (UHPC) where water are accumulated. Corrosion of the steel is reduced by reducing the overall maximum crack width and sufficient cover. So compared to steel bridge this structure have high durability with minimized maintenance costs and long service time. However this design have some flaws. For example accidental action (transversal point load) by moving truck under the bridge will cause failure due to the absent of transversal members. Therefore for this level of design no traffic flow is allowed under the bridge. Further this design requires larger assemble time. Time means increasing costs for space in the factory, for worker, and lower production rate. However due to high repetition and experience obtained during the production this part of the costs is expected to decrease over time.

Part IV

Conclusion & summary

7. Conclusions

The objective of this research was to find the potential of application of advanced cementitious materials in infrastructure and to apply the knowledge to design a new superstructure as replacement for the traditional heavy traffic bridge. In this chapter the conclusions of this research will be presented.

7.1 Part I – literature study

Plotting the characteristics of advanced cement based materials (ACM) together with the characteristics of traditional concretes enables to compare the fundamental differences of the materials. Some of them are stronger and more durable, the other are very ductile with significantly improved tensile-strain behavior while another type of ACM is brittle, expansive with low reliability index. In order to capitalise the full potential of the ACM a different design approach is required from conventional concrete approach. The knowledge described in the literature study tries to overcome the challenges of using advanced materials in infrastructure. In [Table 7.1] characteristic of the different ACM is given together with their potential of application in infrastructure.

7.1.1 Strength and stiffness

One example of Advanced Cementitious Material mixture composition is composition of high amount of silica fume, cement, quartz powder together with high quality steel fiber with high slenderness ($L=13\text{mm}$). This composition is known as Ultra High Performance Concrete. The compressive strength is significantly higher the compressive strength of traditional concrete. Under compression in linear-elastic stage (pre-cracking stage) behavior can be described by existing recommendations (EC2, CUR, SETRA, JAP). Increasing the stiffness refers to modern type of concrete compositions with small aggregates partials and fillers, reinforced by fine, short fibers. In the non-linear stage (post-cracking stage) high strength ($f_{ck}>150\text{ MPa}$) comes with price. The material tends to be very brittle results in safety issues. The two most common approaches are adding long steel fibers to the mixture ($L=80\text{mm}$) or use prestressing and steel bars. The short fibers increase the stiffness while the large fibers are activated when macrocracks occur under the influence of increasing external load. With sufficient fibers volume, UHPC composed structure elements are much slender, light and durable. It is also more sustainable to minimize the amount of material, less CO₂ emission during production and transport and long service life. Therefore, using high performance concrete will mainly result in minimizing the structure dimensions.

Under flexural tensile stresses and normal tensile stresses the role of steel fibers is extensively discussed in the literature study. On the one hand it has been proven to be highly effective when using long hooked fibers and short straight fibers, on the other hand relying only on fibers in infrastructure (high dead and live loads) is impossible due to the variability of properties (fibers orientation). Therefore it is highly recommended to develop a hybrid solution which combines traditional reinforcement, prestressing steel, and steel fibers when designing infrastructure with concrete compositions other than conventional composition. Hence, the hybrid configuration was chosen as a starting point for the design of the infrastructure.

7.1.2 Ductility

Ductility is about a structure that gives an adequate warnings prior to failure by means of plastic deformation. The manufacturer of high performance compositions solved this

problem by adding sufficient amount of fibers. One example is the Strain-Hardening Cementitious Composite. This very special material is favourable in terms of post-peak behavior allow large plastic strain to occur without failure. This material is suitable for elements under tensile stress. The recommendation is to address ductility issues in material level, not in structure level. When concrete cannot provide reliable ductility, steel bars and prestressing steel need to be accounted in the design. Combining both leads to a composite with very high strength and ductility with high reliability.

7.1.3 Multi-material topological optimization

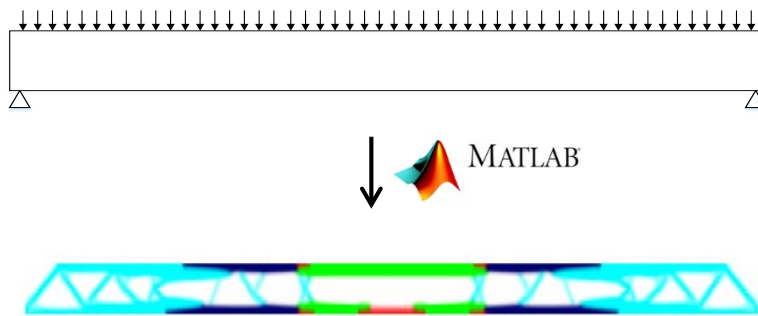


Figure 7.1: Topological optimization with Matlab script, 50% material reduction

A global bridge structure can be analysed by using software's as Matlab or ANSYS. The type of materials , space domain, material saving, and maximum deflection can be predefined. The output regarding superstructure with slenderness compared to conventional heavy-traffic bridge will probably not be realistic. In reality issue's like stability, cracking, connections, durability, prestressing design, and reinforcement design will result in a more massive superstructure then obtained in [Figure 7.1]. The final material reduction is 35% compared to box-girder SKK1800.

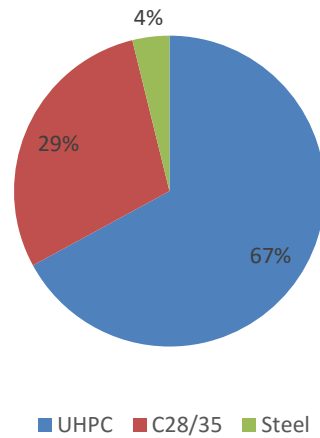


Figure 7.2: Distribution material in superstructure

7.1.4 Costs

Applying concrete types with improved properties as UHPC or SHCC is in general more expensive. This is caused by the material costs, production methods requiring more manual labour than traditional concrete, and the low market penetration. However, in the long-term ACM applied in infrastructures is estimated to have a very long life-cycle compared to conventional concrete, and steel alternative. Moreover, by creating a modular system, segments in the structure that suffer from severe degradation can be replaced with new segments which further extend the service life of the structure. Transportation costs can be saved by reducing the size of the segments for which no special transport is required.

Nevertheless, improving material efficiency has its own limits. Further reduction of the costs is possible by rethinking the traditional manufacturing methods. Possibly the use of automated fabrication of the structural segments will reduce costs drastically.

Advanced material	Replace conventional material	Less expansive	Longer life	Sustainable solution	Improved properties	Applied heavy-traffic infrastructure
Ultra-high performance	Yes	No	Yes	No	Yes	Yes
Strain-hardening cementitious composite	Yes	No	Yes	No	Yes	Yes
High strength concrete	Yes	No	No	No	Yes	Yes
Foamed concrete	No	Yes	No	No	Yes	No
Textiel reinforced	Yes	No	Yes	No	Yes	No
Geopolymer concrete	Yes	Yes	Yes	Yes	No	No
Reactive powder concrete	Yes	No	Yes	No	Yes	No
Self compacting concrete	Yes	Yes	No	No	No	Yes
Polymer modified concrete	Yes	No	Yes	No	Yes	No

Table 7.1: Overview potential application ACM

7.2 Part III – Design study

The design study includes chapter 5. Parametric study and chapter 6. Design study, includes the application of the ACM in superstructure of bridge with large span. The parametric study provided a good impression of the materials potential and influence on the structure design. Different constructional aspects as maximum crack size, strength, durability, slenderness, reliability and deflection are investigated. This followed by iterative optimisation of the structure shape in chapter 6 with strong emphasis on the seven design principles [4.8.6]. After the general framework is worked-out in chapter 5. the bridge superstructure is further elaborated by complete description throughout modelling, drawings, and all essential specifications up to preliminary design level. The design was subjected to a load-combinations, and boundary conditions according to chapter 4.

7.2.1 100% modular

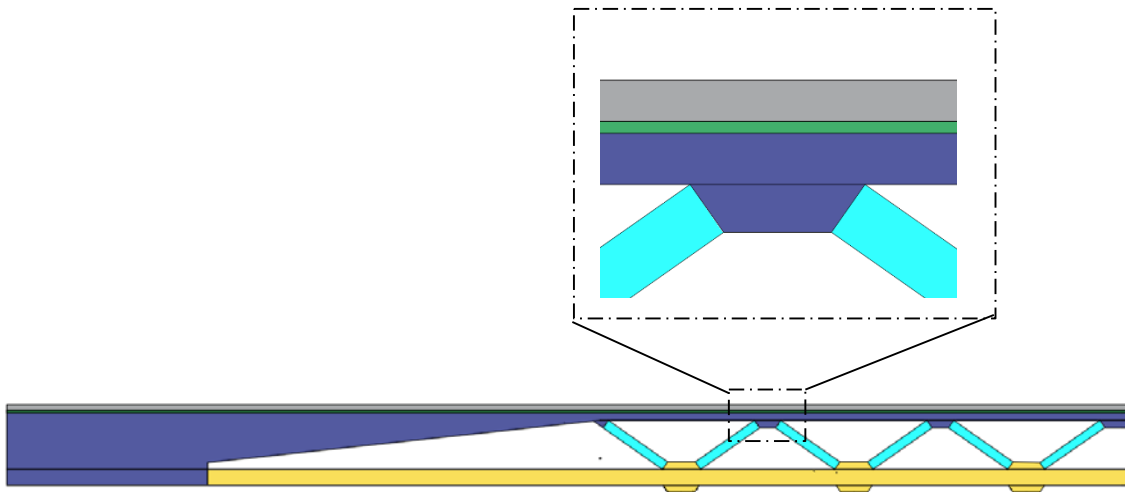


Figure 7.3: The modular girder with 5 structural elements: tensile tie (yellow), compressive strut (blue), truss members (light blue), UHPC thin plate (green), and cast in situ layer (gray)

The principal of modularity combined with extensive material research and Hybrid approach resulted with robust innovative superstructure composed from two concrete types, prestressing cables, and steel reinforcement. The concept of prestressed slender ultra-high performance concrete elements proved to be efficient application of this expansive material. By dividing the structure into groups of identical elements [Figure 7.3] imposed deformation caused by creep & shrinkage is avoided. Due to the different sized of the elements and different materials the differential deformation of the segments would cause unwanted tensile stresses leading to cracks and possibly failure.

7.2.2 Geometry

Using materials more efficient by applying ultra-high performance materials in accordance with the forces distribution resulted in a lightweight³ superstructure with no constant cross-section over the bridge span. The new structure slenderness is limited to $L/h < 25$ in order to equals it to slenderness of box-girder increase the attractiveness of this design. Introducing slender elements like the truss members and tensile tie would normally result in stability issues, however applying prestressing bars and strands means that elements can never buckles. Considering the transversal stability of the structure against perpendicular impact of vehicles on the edge of the superstructure (accidental) $F=2000\text{kN}$ will have to be transmitted by uniform diaphragm actions to the substructure [NEN-EN 1991-1-7 art. 4.3] [ROK]. In this case an additional transversal members between the girders are added in the same principle as the existing truss-members.

7.2.3 Conclusion research question

Can advanced cementitious materials be used to develop technically and economically feasible heavy-traffic bridge as a realistic alternatives for the existing conventional bridges? [1.5]

During this research the application of advanced cementitious materials in the field of heavy-traffic bridges has been demonstrated. The solution offered in the design study is a feasible alternative for the existing conventional bridge in terms of strength, durability, self-weight, and innovation. Some challenges concerning the amount of labour required to build the girder, the high materials costs, and fibers contribution are also explained in this study. Solution to all technically problems are developed and verified. However, it is most likely that the total costs of the designed superstructure will be higher than an equivalent conventional superstructure with the same span. Nevertheless the multimaterial approach, material reduction, and improved durability are the counterweight to the high costs of the superstructure. Hence superstructure composed of Advanced Cementitious Materials can be a technically- and economically alternative for traditional heavy-traffic superstructure.

³ compared to traditional concrete heavy-traffic superstructure

7.3 Future research

The structure can be further designed looking extensively into structural aspects as fatigue, structure dynamics, and 3D FEM models of connection. Due to limited scope of this thesis and lack of time some other interesting application of the design superstructure may be assessed. The recommendation for further investigation of the design are the following:

7.3.1 Modularity

In [4.8.6] the principle of modularity is introduced. An interesting area of further research will be designing the superstructure in such a way that it can be extended in the span direction by different requirements and boundaries. When the superstructure needed to be extended an additional plates, truss members, and tensile tie are added to the existing construction [Figure 7.5]. The cross-sectional dimensions of the different elements can be estimated with the aid of modelling the new force distribution in FEM software. In this way a dynamic design method is introduced where small segments are easily transported to the building site for assembly.



Figure 7.4: [www.Praxis.nl]

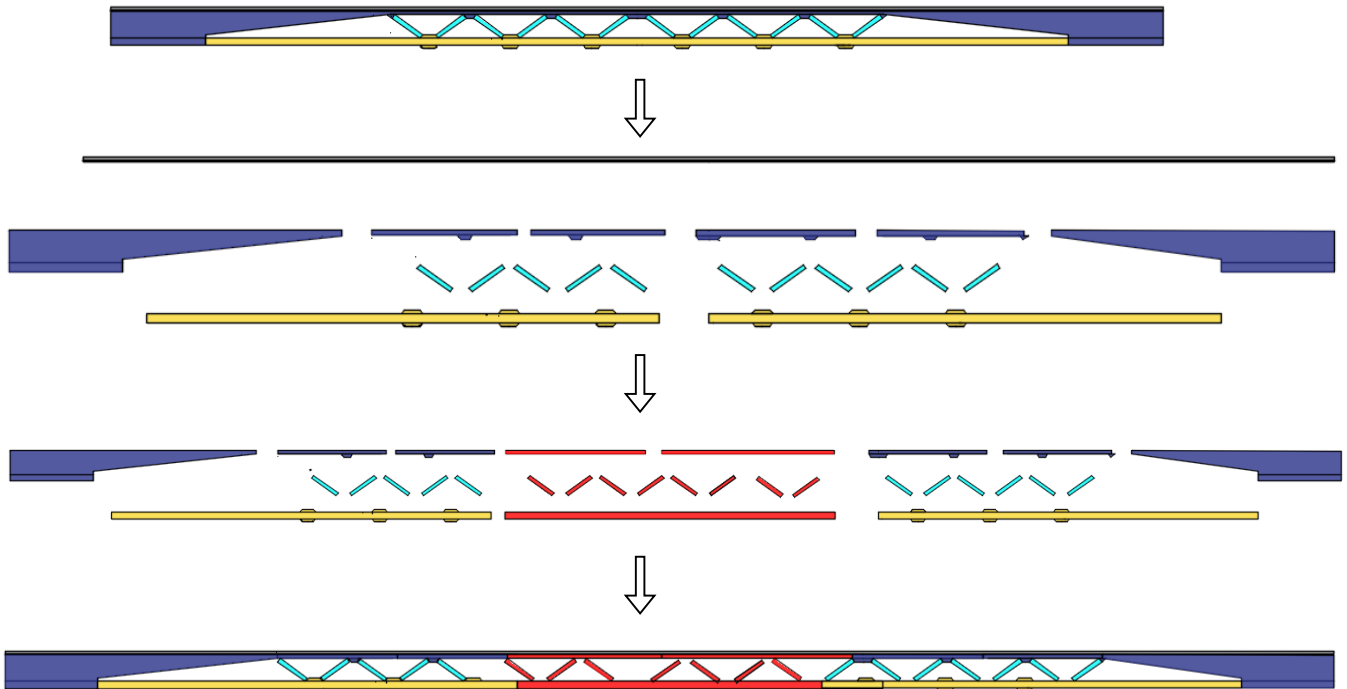


Figure 7.5: Further dividing the girder into segments with possibility to enlarge the span by adding segments to the midspan.

7.3.2 Connections

The truss structure is connected on one side to the tensile tie and on the other side the compressive strut. All the connection are utilized with UHPC and with prestressed bars. The inspiration to this design is followed by the research of C.K. Cheung in 2002 [T07]. Peak stresses are present in the concrete joint caused by the large compressive forced introduced by the prestressing. Creating a FEM main-model of the superstructure with 1D line-elements modelling the truss and shell elements modelling the compressive strut and the top layer together with modelling the connection as substructure with volume elements (ANSYS) [Figure 7.6]. This analysis is important to verify that the working stresses in the connections meet the ULS and SLS requirements. Furthermore non-linear material properties may be used in this analysis in order to analyse the post-peak behavior of the connection.

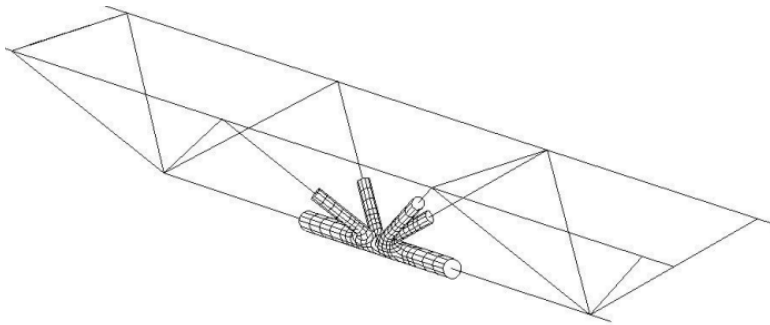


Figure 7.6: Modelling of substructure in ANSYS, [Lecture notes CIE5126 Dr. ir. Richard Pijpers]

7.3.3 Fatigue

Fatigue of the structure occur by repeated traffic loads which cause fluctuating stresses. The fatigue analysis can be described with NEN6723 (Voorschriften beton, Bruggen VBB1995) and CUR-recommendation 37. The slender structural element will be more sensitive to fatigue however using UHPC reinforced with additional fibers will increase fatigue resistance. Also the prestressing will be beneficial to the fatigue resistance. Complete Fatigue analysis is essential for any future research.

Part IV

Lists

A ● References

A.1 Books

- [B01] Designing and Building with UHPFRC – State of the art and development
Francios Toutlemonde and Jacques Resplendino
- [B02] Concrete Structures under Imposed Thermal and Shrinkage Deformations - ED.K
van Breugel 2011
- [B03] Construction Technology of Civil Engineering Projects CT 4170 - November 2013
Prof. Ir. A.Q.C. van der Horst
- [B04] Hoogstandjes, 2004, betontechniek
- [B05] Creep shrinkage and durability mechanicis of concrete – T. Tamabe, K. Sakata, H.
Mihashi, R. Sato, K. Maekawa and H. Nakamura , 2009
- [B06] Significance of Tests and Properties of Concrete and Concrete-making Materials -
Joseph F. Lamond, J. H. Pielert
- [B07] A.H.J. Nijhof (2004); Vezelversterkte Kunststoffen – Mechanica en Ontwerp; Delft
University Press
- [B08] COMPOSITES ORvCONSTRUCTION: Structural Design with FRP Materials -
Lawrence C. Bank 2006
- [B09] G.Parke, N.Hewson (2008); ICE Manual of Bridge Engineering; Thomas Telford
- [B10] Lecture notes CIE3150 Prestressed concrete

[B12] Use of foamed concrete in construction

[B13] Strain Hardening Cement composites: Structural design and performance

[B14] Kracht en Vorm

[B15] High Performance Fiber Reinforced Cement Composites 6 - Gustavo J. Parra-Montesinos

A.2 Papers

[P01] Hogere Sterkte Beton - Ervaringen met sterkteklasse B65 en hoger - Ministerie van Verkeer en Waterstaat

[P02] International Symposium on Ultra High Performance Concrete - Influence of the packing density of fine particles on structure, strength and durability of UHPC , *Thomas Teichmann*

[P03] Durability of structural lightweight concrete - Celik Ozyildirim

[P04] - Holm & Bremner , 2000

[P05] Excellence in Concrete Construction through Innovation - Mukesh C. Limbachiya & HseinY. Kew

[P06] Optimizing the Use of Fly Ash in Concrete - Michael Thomas

[P07] High-performance, high volume fly ash concrete for sustainable development - P. Kumar Mehta

[P08]] The European Guidelines for Self-Compacting Concrete Specification, Production and Use – 2005

[P09] Improvement of Serviceability and Strength of Textile Reinforced -Marcus Hinzen

[P10] Study on stress-strain properties of reactive powder concrete

A.3 Theses

[T01] Hybrid FRP-Lightweight Concrete Sandwich System for Engineering Structures - Erika Schau mann

[T02] Feasibility study on fiber reinforced polymer cylindrical truss bridges for heavy traffic - Mathis Chlosta July 2012

[T03] Creep and shrinkage of high performance lightweight concrete: A multi-scale investigation - Mauricio Lopez

[T04] Feasibility study on heavy-traffic FRP Bascula bridges - J.C.Moen

[T05] UHPFRC Modelling the shear, bending and fatigue behaviour - L.W.H. Bouvy

[T06] Optimisation of a high strength concrete plate bridge

[T07] Detaillering B200 Hefschuiven Stormvloedkering Oosterschelde

A.4 Articles

[A01] [<http://www.uhsb.nl>]

[A02] CEA (Comissariat à l’Energie Atomique – Atomic Energy Agency) [CEA 97] and at CEBTP (Centre d’Études du Bâtiment et d[1]es Travaux Publics – Trade Laboratory for Buildings and Civil Works)

[A04] Concrete science and technology – ED.K van Breugel CIE5110

[A05] <http://www.concretenetwork.com/self-consolidating-concrete/>

[A06] Foamed concrete - Cement Readymix

[A07] <http://theconstructor.org/concrete/types-of-concrete/966/>

[A10] Albstadt-Lautlingen

[A11] <http://www.jeccomposites.com/news/composites-news/textile-reinforced-concrete-high-performance-carbon-fibre-grids>

[A12] Concrete science and technology – ED.K van Breugel CIE5110

[A13] http://www.theconcreteportal.com/react_pow.html

[A14] 3RD international rilem symposium self-compacting concrete

[A15]

<http://www.fhwa.dot.gov/publications/research/infrastructure/structures/05058/03.cfm>

[A16] http://www.theconcreteportal.com/cons_rel.html

[A17] Study On Stress – Strain Behaviour of Hardened Concrete with HVFA, GGBS AND GBS as Partial Replacement Materials- Suvarna Latha Kakara, M V Seshagiri Rao

[A19] Cement – Buigprof staalvezelbeton prof.dr.ir. L. Vandewalle en ir. D. Dupont, Katholieke Universiteit Leuven, departement Burgerlijke Bouwkunde

A.5 Codes

[C01] NEN-EN 1992-1-1 2005

[C02] Building code requirements for structural concrete (ACI 318-95) and commentary (ACI 318R-95)

[C03] NEN 6720 – Belastingen en vervormingen TGB 1990

[C04] NEN-EN 1990, 2002

[C05] NEN-EN 1992-2

[C06] NEN-EN 1991

[C07] Recommendations for Design and Construction of High Performance Fiber Reinforced Cement Composites with Multiply Fine Cracks (HPFRCC)

[C08] NEN-EN 206

[C09] JAP 06

[C10] CUR Aanbeveling 111

[C11] CUR- Aanbeveling 97

[C12] CUR- Aanbeveling 36

[C13] DAFStb-richtlijn

[C14] CNR recommendation

[C15] Model code 2010 art. 5.6 and 7.7

A.6 Witteveen+Bos

[W01] Ontwerpbasis K3.01 – KW 110 VO, UO K3.07 – KW 160

B. List of Tables

Table 1.1: Material choice	6
Table 1.2: Infrastructure objects in main road network Netherland 2012 [Rijkswaterstaat, 2012]	7
Table 2.1: Innovative concrete material	15
Table 2.2: Performance criteria concrete	15
Table 2.3: Existing standards and recommendations ACM (*guidelines).....	17
Table 2.4: Calculation methods used to plot the stress-strain diagram.....	20
Table 2.5.....	24
Table 2.6: Mechanical properties matrix	26
Table 2.7: Summary creep	28
Table 2.8: Shrinkage matrix	29
Table 2.9: Freeze-Thaw	30
Table 2.10: Resistance to aggressive chemical attacks.....	31
Table 2.11.....	32
Table 2.12: Costs overview	34
Table 3.1: Degradation mechanism of bridge components.....	41
Table 3.2: Overview durability	45
Table 4.1: General design specifications KW110 [W01].....	50
Table 4.2: General design specifications KW110 [W01].....	50
Table 4.3 General design specification KW110 [W01]	50
Table 4.4: Material level requirements for bridge design	53
Table 4.5: Cross-sectional level requirements for bridge design.....	53
Table 4.6: Structural level requirements for bridge design	53

Table 4.7: Application of LM1 [Figure 4.5].....	57
Table 4.8: Adjustment factor LM1	57
Table 4.9: LM2 The contact area of LM2 correspond is 0.35*0.6 m.....	58
Table 5.1: Summary design – requirement hybrid bridge deck.....	68
Table 5.2: Characteristic and design load on the bridge deck with girders of h=1.6 m b=0.6 m.....	69
Table 5.3: Important characteristics values of prestressing steel [C10].....	70
Table 5.4: Beam constants.....	72
Table 5.5: Results of multimaterial optimization after 200 iterations	107
Table 5.6: Design principles	130
Table 5.7: Critical parameters K for two hinged arch with tie for f/l=0.2.....	139
Table 5.8: Applied actions	141
Table 5.9: Technical requirements.....	144
Table 5.10: Envelope values 1D model. Negative moment = tension upper fiber, Negative normal force = compression force. Units [kN] [kNm].....	156
Table 5.11: Load Model 1	157
Table 5.12: Internal forces 1D model.....	157
Table 5.13.....	159
Table 6.1: Dimensions of the individual girder	167
Table 6.2: dimensions	170
Table 6.3.....	171
Table 6.4: Dimensions.....	174
Table 6.5: Stresses top fiber midspan compressive strut stage 2.1.....	182
Table 6.6: governing prestressing versus external load combinations	185
Table 6.7: Stress component being controlled.....	186
Table 6.8: POT system VSL ES 12.9mm. [mm]	192
Table 6.9: POT system VSL E 15.7mm. [mm]	192
Table 6.10: Evaluation.....	195
Table 6.11: Forces in kN from FEM analysis of the bridge	198
Table 6.12.....	200
Table 6.13: Working forces at tie – girder connection	203
Table 6.14: comparison prestressing system	217
Table 6.15: Summary applied Y1030H bars for each truss member.	218
Table 6.16.....	226
Table 6.17: Applied shear reinforcement	230

Table 7.1: Overview potential application ACM	245
Table D.1.....	274
Table D.2: Mix design example. Percentage by volume	274
Table D.3 : Nominal costs in the Netherland 2008. [B03, p31].....	278
Table D.4: Mechanical properties	279
Table D.5: Example concrete mix-design [B04]	279
Table D.6: Typical properties [A03]	285
Table D.7: Example concrete mix-design [B04]	285
Table D.8: Tensile strength values [A18].....	285
Table D.9: Shear capacities concrete member	286
Table D.10 : Compressive strength and curing method [P02, P313]	287
Table D.11 : [P02, P317]	288
Table D.12: Mechanical properties [P05, p241]	290
Table D.13: RPC mic design for compressive strength of 200 MPa and 800Mpa [P05, p241].....	290
Table D.14: RCP-600	290
Table D.15: Shear capacities concrete member.....	291
Table D.16: Mechanical properties [T01, P26].....	294
Table D.17: Example mix-design [A04]	294
Table D.18: Shear resistance LWC.....	295
Table D.19: Typical HVFA properties [P06] [T08].....	300
Table D.20: Typical properties foamed concrete	310
Table D.21: Mix design for foam concrete	310
Table D.22: Mechanical properties of different reinforcement fibres [B07, p21]	314
Table D.23: Mechanical properties matrices [B07, p21].....	314
Table D.24: Mechanical properties of different composite based on fiber content of 60% [B07, p21].....	315
Table D.25: 28 days properties [P02, p516]	319
Table D.26: Mix design [P02, p512].....	319
Table D.27 : Mechanical properties SHCC [A20] [B11, p101, p17 , p12].....	323
Table D.28: Mix-design of SHCC [P11]	323
Table D.29: Mechanical properties GC.....	328
Table D.30: Geopolymer Concrete mixture proportions on fly ash-based(s (Wallah and Rangan, 2006).....	328
Table E.1: Governing mechanical properties	333

Table E.2: Governing mechanical properties	334
Table E.3: Governing mechanical properties	336
Table E.4: Overview material properties [Cement Rekenmodel VVUHSVB] [CUR- aanbeveling 111] [AFGC/SETRA].....	339
Table E.5: Governing mechanical properties	340
Table E.6: Governing mechanical properties	341
Table E.7: Governing mechanical properties	344
Table F.1: Load Model 1 conform table 4.3 NEN-1991-2, tandem system with uniform distributed loads (UDL)	348
Table F.2	351
Table F.3: Flexural capacities.....	354
Table F.4: Material properties	356
Table F.5	362

C. List of figures

Figure 1.1: Little Cedar Creek bridge USA 2011, Ductal UHPC waffle deck, girders and joints.....	2
Figure 1.2: Hybrid bridge deck with sandwich structure.....	2
Figure 1.3: Illustration of thesis scope	5
Figure 1.4: Realization concrete bridges in Netherland	8
Figure 2.1: Current practice of mixing concrete [Erix Schlangen, 2012]	14
Figure 2.2: Bi-linear stress-strain diagram for compression and tension [conform EC2]...18	
Figure 2.3: Bi- linear and parabolic stress-strain diagram for compression and tension conform different design codes and experiments.....	19
Figure 2.4: Compressive stress-strain diagram.....	21
Figure 2.5: Compressive stress-strain relationship ACM	21
Figure 2.6: Tensile stress-strain relationship ACM.....	22
Figure 2.7: Upper boundary shear strengths of different concrete types	23
Figure 2.8: Relationship between modulus of elasticity and compressive strength of UHPC according to the CEB-FIP Model Code 1990 [P02, p209].....	24
Figure 2.9: Example of finding the creep factor for RH=80% [Walraven, 2012]	27
Figure 3.1: Degradation causes concrete [CIE5127]	36
Figure 3.2: Uncovered rebars [CIE5127]	36
Figure 3.3: Chlorides as accelerator [CIE5127]	37
Figure 3.4: Carbonation of concrete [CIE5127] [CIE5110]	38
Figure 3.5: Alkali-Silica reaction [CIE5127].....	38

Figure 3.6: Environmental classes of sub and superstructure for typical traffic bridge in the Netherland.....	40
Figure 3.7: Concrete Bridge [B09, p574].....	42
Figure 4.1: Location of objects KW110 and KW160 , interchange Kethelplein in Schiedam [W01].....	48
Figure 4.2: Impression Interchange Kethelplein with objects KW110 and KW160 [W01]	49
Figure 4.3: From top to bottom: Longitudinal cross-section, Top-view and lateral cross-section KW110 [W01].....	51
Figure 4.4: Action on bridges [CIE5127].....	54
Figure 4.5: Application of LM1 [B09, p29].....	56
Figure 4.6: Subdivision of an arbitrary temperature load in components [B02, p18].....	62
Figure 4.7: Effect of deck slab shrinkage on composite section [B09, p32].....	65
Figure 5.1: Prestressed statically determinate beam using a draped tendon anchored in the centroidal axis.....	69
Figure 5.2: prestressing design.....	70
Figure 5.3 Several of cross-section to be accounted for [B10].....	71
Figure 5.4: The AMS rectangular massive beam. L, h, b are variables.....	72
Figure 5.5: M-K diagram as function of girder height.....	74
Figure 5.6: M-K diagram FRC with/without conventional reinforcement [Cement 2010/6].....	Error! Bookmark not defined.
Figure 5.7: Permissible strain as function of member height.....	75
Figure 5.8: Cross-sectional efficiency for different concrete classes.....	76
Figure 5.9: Crack control with prestressed beam [CIE4160].....	77
Figure 5.10: Crack width.....	78
Figure 5.11: Characteristic length [Cement Rekenmodel VVUHSB].....	79
Figure 5.12 stress-crack opening relationship of UHPC.....	79
Figure 5.13: Crack width as function of the applied prestressing.....	80
Figure 5.14: Structural concept.....	81
Figure 5.15: Principle stresses trajectories in uncracked simple supported beam [B03]....	82
Figure 5.16: Stress as a result of uniform dead and live loads in a linear elastic beam [B10].....	83
Figure 5.17: Force flow in cracked concrete.....	83
Figure 5.18: Compressions lines.....	84
Figure 5.19: Shear behavior of simply supported beam.....	85

Figure 5.20: Brittle flexural shearing of beam without shear reinforcement	87
Figure 5.21: Crack pattern at ultimate failure.....	88
Figure 5.22: Behavior nearby support	89
Figure 5.23: Stress-strain diagram according the CUR-recommendation.....	90
Figure 5.24: Optimal bending moment cross-section	92
Figure 5.25: Mechanical schematization of chain and arch [B14]	95
Figure 5.26: construction principles	96
Figure 5.27: Conceptual design arch beam	97
Figure 5.28: The main idea of the load transferring system [B14]	97
Figure 5.29: The arch beam, first considering compression forces and then adding tensile element	98
Figure 5.30: Shear distribution embedded in the design, steel bars covered with SHCC..	98
Figure 5.31: Cross-sections for different longitudinal locations.....	99
Figure 5.32: Using splines to draw the arch within the design domain (C02 continuity) .	99
Figure 5.33: Optimal shapes for normal force, bending moment and shear force [T06, p45]	100
Figure 5.34: Static determined beam with design region $L=20\text{m}$, $h=2.0\text{m}$ and $b=1.2\text{m}$	101
Figure 5.35: The initial problem on the left hand side and the optimal solutions are shown on the right.....	101
Figure 5.36: Topological optimization 3DBeam with target density 80% weight reduction	104
Figure 5.37: Mechanical constraints and loads	105
Figure 5.38: Typical truss structures	108
Figure 5.39: Construction principles UHPC prestressed segmental truss bridge [B01, p210]	109
Figure 5.40: Cross-section of standard segment [B01, p290]	110
Figure 5.41: Concrete truss beam [Javier Mentado-Duran]	111
Figure 5.42: Concrete beam casted into textile formwork designed with topological optimization in ANSYS [C.A.S.T. Manitoba University ,Canada]	111
Figure 5.43: Evolutionary structural optimization in ANSYS using BESO algorithm (Huang , 2006).....	112
Figure 5.44: Variety of truss design with fabric formwork	113
Figure 5.45: Tension element (red), high performance concrete (orange), Strain hardening concrete (green), conventional concrete (blue), fibre reinforced concrete (dark green), and foamed concrete (yellow)	114

Figure 5.46: Multi material Fiber-formed truss with high performance concrete (orange), strain-hardening concrete (green), fiber reinforced concrete (blue) and self-compacting concrete (pink).....	114
Figure 5.47: General load case. Support conditions and initial design domain for BESO algorithm in ANSYS [Diederik Veenendaal, 2008].....	115
Figure 5.48: Result after 13 iterations for BESO run with $E=28.485 \text{ N/mm}^2$, $f_{ck}=28.2 \text{ N/mm}^2$, $f_{ct}=2.98 \text{ N/mm}^2$ including longitudinal reinforcement	115
Figure 5.49: Result after 200 iterations with run of Matlab algorithm with equivalent beam geometry and boundaries	115
Figure 5.50: Modified construction principles hybrid truss.....	116
Figure 5.51: The oriented shaft [www.3dprintcanalhouse.com].....	117
Figure 5.52: Volume of fabric-cast compared to conventional rectangular beam.....	118
Figure 5.53: Tests set up [University of Bath].....	121
Figure 5.54: Tests results [University of Bath]	121
Figure 5.55 Uniform strength prestressing beam [Guyon].....	122
Figure 5.56: Local strengthening of the girder	123
Figure 5.57: Comparison of UHPFRC and ordinary concrete precast prestressed girder bridges, NU I-girder [B01, p333].....	124
Figure 5.58: 3D sketch of the proposed girder	126
Figure 5.59: The cyclic design process where the design progresses to the end-product.	130
Figure 5.60: Global concept [A. Rietsema]	131
Figure 5.61: Massive rectangular girder with compression top layer (bridge deck),	132
Figure 5.62: Zip girder with top compression layer of 200mm [Spanbeton].....	133
Figure 5.63: Plot of the arch center line for $L=50.0\text{m}$ and $f=1.8\text{m}$	135
Figure 5.64: Normal forces (vertical axis) in arch on Figure 5.63 loaded according to LM1 with only uniform load and self-weight.....	135
Figure 5.65: Critical load as function of the constant arch thickness	138
Figure 5.66: for two hinged arch with tie	139
Figure 5.67: Extensional deformation (left) and In-extensional deformation (right)	139
Figure 5.68: Deflection of two-hinged arch loaded with uniform and tendon load with $E=58000 \text{ N/mm}^2$	140
Figure 5.69: Influence support stiffness on horizontal thrust.....	141
Figure 5.70: Bending moments in statically determined beam (red) and in the parabolic arch.....	141

Figure 5.71: Shear forces in a statically determined beam (red) and in the parabolic arch (blue).....	142
Figure 5.72: Normal stresses parabolic arch	142
Figure 5.73: Maximum shear stresses parabolic arch.....	143
Figure 5.74: Rectangular beam with compressive arch.....	143
Figure 5.75: Increasing stiffness with truss members.....	144
Figure 5.76: Proposed cross-section at $x=0.5L$	145
Figure 5.77: Possible realistic cross-sections at $x=0.5L$, with variable compressive arch (red) height $z(x)$	145
Figure 5.78: Side-view arch beam	146
Figure 5.79.....	146
Figure 5.80: max deflection when $F_{TD} \Rightarrow x=0.2*L$	147
Figure 5.81: Deflection as function of the arch for tendon load at $0.2*L$	148
Figure 5.82: Massive arch beam with concrete web (red).....	149
Figure 5.83: Multi-linear optimised beam.....	149
Figure 5.84: Coupling of compressive and tensile arch in a beam	150
Figure 5.85.....	151
Figure 5.86: $TD=30\%$	151
Figure 5.87: $TD=60\%$	151
Figure 5.88: Topological optimizations, the colours are indication of the stress levels in each element.	152
Figure 5.89: Multi-material Matlab analysis. Blue=UHPC, light blue=NSC, green=SHCC, red=steel	152
Figure 5.90: Overview one dimensional models	153
Figure 5.91: location concentrated load	154
Figure 5.92:.....	154
Figure 5.93.....	155
Figure 5.94: Connections	155
Figure 5.95: Rigid connection and hinged connections SCIA model.....	156
Figure 5.96: Illustration of loaded the girder with LM1	157
Figure 5.97: 1D FEM model	157
Figure 5.98: Compressive stresses as function of ratio between member area and reference member.....	158
Figure 5.99: 2D FEM.....	158
Figure 5.100.....	160

Figure 5.101: Sharebroek footbridge	161
Figure 5.102: Design criteria cycle	162
Figure 5.103: Connections of truss elements with POT strads. [B04, p623]	163
Figure 5.104.....	164
Figure 5.105: Reader Dimensioneren van Betonnen Bruggen C. van der Veen, CIE4160	165
Figure 6.1: Multimaterial topological optimization, L=50m h=1.80m. 200 iterations, 50% material reduction.....	167
Figure 6.2: 3D impression, concept version of the girder, the height and span correlate with that of SKK girder [Spanbeton].....	168
Figure 6.3: SLS envelope normal stresses. SKK-1800 girder, L=50.0m	169
Figure 6.4: SLS envelope normal stresses 1D FEM analysis.....	170
Figure 6.5: SLS envelope normal stresses, 2D in plane FEM analysis	171
Figure 6.6.....	172
Figure 6.7: Shear stresses distribution	172
Figure 6.8: Principal tensile stresses trajectories	173
Figure 6.9: Warren truss layout.....	173
Figure 6.10: The Warren T-girder	174
Figure 6.11: Complete bridge deck with width of 11.2m and 50m span. In green the cast in situ top flanges.	174
Figure 6.12: The Warren T-girder	176
Figure 6.13: 3D sketch of the girder	176
Figure 6.14: Four construction phases are modelled.....	178
Figure 6.15: Governing girder no.3 from left have the largest internal forces.....	178
Figure 6.16: PRT strands in red.....	179
Figure 6.17: Deflections due to self-weight of the member	179
Figure 6.18: Unity check tie member during lifting.....	180
Figure 6.19: Capacity PRT strands check	180
Figure 6.20: Acting shear stresses during lifting.....	180
Figure 6.21: Stage 2. Connecting tie member to girder. Stages 2.1 and 2.2.....	181
Figure 6.22: Linear FEM analysis of stage 2 maximum deflection as function of applied prestressing	181
Figure 6.23: Stage 2.2 prestressing the tie member up to full prestressing load	182
Figure 6.24: Coupler [VSL]	183
Figure 6.25: Connections tie – truss and top web - truss	184

Figure 6.26: Linear FEM analysis of stage 4 deflection	186
Figure 6.27: : Max deflection $U_z = 68.4\text{mm}$ for $P_{m0}=1600\text{ kN}$ and self-weight without deck	187
Figure 6.28: Types of shear connectors [CIE4121]	187
Figure 6.29: Shear force n_{xy} [kN/m] for uniform distributed traffic load	188
Figure 6.30: Shear force n_{xy} [kN/m] for ULS	188
Figure 6.31: Left - Balanced design, strands/bars are yielding prior to crushing of concrete, Right – axial loaded truss is cracked before steel is yielding [CIE4160]	189
Figure 6.32: The girder	190
Figure 6.33: Prestressing tendon type E [VSL]	192
Figure 6.34: Dead end anchorage systems for top side of truss member	193
Figure 6.35: Dead end anchorage type P for POT strands of 15.9mm	194
Figure 6.36: Threaded bars	194
Figure 6.37: Anchorage and coupler of threaded bar	195
Figure 6.38: FEM main model	197
Figure 6.39: For $b=420\text{mm}$, Area confined between the black and the red lines is the design space	200
Figure 6.40: Forces distribution in the cross-section, fiber contribution is neglected [CIE4160]	204
Figure 6.41: Tensile normal bending stresses in the tie member as result of self-weight only	207
Figure 6.42: Wedge set losses, anchorage prestressed from left side only	209
Figure 6.43: Joint	211
Figure 6.44: Connection truss members with girder and tensile member	212
Figure 6.45: Conventional reinforced joint, the bars will be anchored with U-shaped hairpins	213
Figure 6.46: Multiple cables	213
Figure 6.47: Cross-section tensile tie space between POT strands will be used for crossing of POT members strands	214
Figure 6.48: Seven identical tie – truss steel joint are required	215
Figure 6.49: Wedge set losses truss member	216
Figure 6.50: The truss members in x-z plane	217
Figure 6.51: Tie – truss joint	219
Figure 6.52: Outer dimensions tie – truss joint	220

Figure 6.53: Bars connected to coupler (red) connected to anchorage bar with total length $L_{b,rd}$ [NEN-1992-1-1 art. 8.4].	220
Figure 6.54: compressive strut-truss connection with straight anchorage bars	221
Figure 6.55: Compression node without ties [NEN 1992-1-1 art 6.5.4]	223
Figure 6.56: Anchorage of 5-15.7mm duct	224
Figure 6.57: Concrete deck $h_{deck}=170mm$	225
Figure 6.58: nxy-max, ULS load class	227
Figure 6.59: shear forces in the compressive strut	228
Figure 6.60: Example duels protruding from web	229
Figure 6.61: ULS web-deck connection shear force in kN/m	229
Figure 6.62: Location of splitting reinforcement individual member (side view)	231
Figure 6.63: Top-view	232
Figure 6.64: Cross-section girder $0 < x < 4.5m$ and $46.5 < x < 50m$	232
Figure 6.65: Strut-Tie model	233
Figure 6.66: Top view	234
Figure 6.67: Girders supports	234
Figure 6.68: Cross-section A-A, reinforcement details	236
Figure 6.69: Cross-section A-A,	236
Figure 6.70: Top-view bridge deck longitudinal reinforcement	236
Figure 6.71: Cross-section A-A, reinforcement details	237
Figure 6.72: Cross-section A-A, reinforcement details	237
Figure 6.73: Reinforcement details truss-tie connection and truss-strut connection	238
Figure 6.74: Reinforcement details cross-sections B-B and C-C	238
Figure 7.1: Topological optimization with Matlab script, 50% material reduction	243
Figure 7.2: Distribution material in superstructure	244
Figure 7.3: The modular girder with 5 structural elements: tensile tie (yellow), compressive strut (blue), truss members (light blue), UHPC thin plate (green), and cast in situ layer (gray)	246
Figure 7.4: [www.Praxis.nl]	248
Figure 7.5: Further dividing the girder into segments with possibility to enlarge the span by adding segments to the midspan.	249
Figure 7.6: Modelling of substructure in ANSYS, [Lecture notes CIE5126 Dr. ir. Richard Pijpers]	250
Figure D.1: Compressive stress-strain curve	275
Figure D.2: Drying shrinkage of hardened concrete with RH=50% [P01, p16]	276

Figure D.3: Environmental class classification [NEN-EN 206-1].....	277
Figure D.4 : Stress-strain curves for different compressive strength [A15]	280
Figure D.5 Creep coefficient as function of the compression strength [A01].....	280
Figure D.6: Tests [B1, p48].....	281
Figure D.7 : Compressive strength progress [P01, p20]	282
Figure D.8: Adiabatic curves [P01, p20]	282
Figure D.9 : vertical axis years [P01, p20]	283
Figure D.10 : Structure costs in millions guilders [B03, p31].....	283
Figure D.11: Typical stress-strain diagrams of UHPFRC.....	286
Figure D.12: Stress-strain curve of axially loaded PRC [P10]	291
Figure D.13: Concrete compressive strength 28 days [A04].....	294
Figure D.14: Stress-strain curve LWC.....	296
Figure D.15: Autogenous shrinkage of LWC [A04].....	297
Figure D.16 Autogenous shrinkage of LWC [A04].....	297
Figure D.17 : Fly ash mix-design properties [P07].....	300
Figure D.18: Strain-stress curve of cylinder under axial load [A17].....	301
Figure D.19: Example mixed design SCC [P08].....	304
Figure D.20: Shear strength versus shear arm ratio for beams without stirrups [B12, p154]	305
Figure D.21: Stress-strain curve of typical SCC	305
Figure D.22: Stress-strain relationships of VC and SCC with different fillers [B12, p34]	306
Figure D.23: Comparison of measured stress-strain curves for SCC and VC mixture [B12, p36].....	306
Figure D.24: Influence of dry density on the compressive strengths of foamed and other lightweight concretes [B12, p70]	311
Figure D.25: Stress-strain curve with strain hardening branch	312
Figure D.26: Stress-strain curve of under tension glass fibers [B08, p337].....	315
Figure D.27: Stress-strain curves for confined and unconfined concrete [B08, p337]	316
Figure D.28: Stress-strain curve of in-plane shear test	320
Figure D.29: Stress-strain curve of TRC with and without short fibers.....	320
Figure D.30: Concept of strain hardening and strain softening under tensile stress [C07]	324
Figure D.31: Strain hardening behavior of SHCC and UHPFRC under direct tension load [PB11].....	324

Figure D.32: Autogenous shrinkage (Wang & Li 2005)	326
<i>Figure D.33: Total primary energy consumption by life cycle stage for and SHCC link slab bridge and</i>	327
Figure D.34: Stress-Strain Relation of Geopolymer Concrete in Compression (Hardjito and Rangan, 2005).....	329
Figure D.35: Effect of Compressive Strength on Creep (Wallah and Rangan 2006)	330
Figure D.36: Total Strain and Drying Shrinkage Strain (Wallah and Rangan, 2006)....	330
Figure D.37: Effect of Curing Time on Compressive Strength of Geopolymer Concrete (Hardjito and Rangan, 2005).....	331
Figure E.1: Assumed tensile and compressive behavior HPFRC [B01,p295]	335
Figure E.2: ULS Stress - strain hardening relationship UHPFRC [CUR-Aanbeveling 111]	337
Figure E.3: ULS Stress – strain softening relationship UHPFRC [CUR-Aanbeveling 111]	337
Figure E.4: Cement 2011-3 Rekenen met VVUHSB.....	339
Figure E.5 Comparison between experimental results and the design stress-strain relationship [C07].....	342
Figure E.6: Compressive strain-strain relationship model SHCC [C07]	343
Figure E.7: Tensile stress-strain relationship model [C07]	343
Figure F.1: Homogenous symmetrical bridge beam	346
Figure F.2: Main actions on carriageway.....	346
Figure F.3: Traffic loads on deck.....	347
Figure F.4: Vertical actions on the bridge (transversal view) B=15.0 m.....	349
Figure F.5: Maximum moment.....	349
Figure F.6: Superposition principle TS load	350
Figure F.7: Governing field moment M_{Ed}	351
Figure F.8 British Standard normal loading curve [B09, p735]	352
Figure F.9: Stress-strain diagrams of (1) concrete (2) prestressing steel (3) reinforcement steel	355
Figure F.10: Design rule prestressed beam [B10].....	357
Figure F.11: ULD design with the theoretical distribution (upper) and the practical distribution (bottom).....	358
Figure F.12: Stress-strain diagram [CUR-111].....	362

Figure F.13: Isostatic 3-points bending test for FRC according to RILEM TC162-TDF [C10]	363
Figure F.14: F-CMOD-curve for plain concrete (left) and F-CMOD-curve for FRC (right)	364
Figure F.15: ULS strain and stresses diagram of FRC [C10].....	366
Figure F.16: Parabolic strain distribution	367
Figure F.17: Stresses and strain distribution in UHPC cross-section with additional steel rebar	368
Figure F.18: Distribution of stress and strain [B13].	369

Part V - Appendix

D. Innovative concrete

D.1 Normal strength concrete (NSC)

D.1.1 Properties

This type of concrete is the most common concrete used in the industry. The NSC is defined as concrete with strength class up to C50/60 which means that $f_{ck,cube} = 60$ N/mm². [Walraven , 2006]. The mechanical properties of NSC is given in Table D.1.

<i>Compression</i> [N/mm ²]	<i>Tension</i> [N/mm ²]	<i>Bending</i> <i>strength</i> [N/mm ²]	<i>E – modulus</i> [N/mm ²]*10 ³	<i>Density</i> [kg/m ³]
≤65	1.6 – 4.1	3-5	27 - 37	2500

Table D.1

<i>Strength</i> <i>class</i>	<i>Cement</i>	<i>w/c</i>	<i>Water</i>	<i>Air void</i>	<i>Gravel</i>	<i>Sand</i> (<250μm)
C20/25	10%	0.53	16%	1-2%	46%	26%

Table D.2: Mix design example. Percentage by volume

D.1.2 Shear strength

The shear capacity of the ordinary concrete is calculated with the empirical relations conform the NEN-EN 1992-1-1 art. 6.2.2. Indication of the shear capacity of ordinary concrete is derived from empirical expression for the upper and lower-bound:

$$v_{min} = 0.035k^{3/2}f_{ck}^{1/2} = 0.035 * 1.51^{3/2} * 35^{1/2} = 0.38 \text{ N/mm}^2$$

Where:

$$k = 1 + \sqrt{\frac{200}{d}}$$

We assume member height h=800mm with 50mm cover → d=750mm. Concrete class C35/45.

$$f_{ck} = 35 \text{ N/mm}^2$$

$$f_{cd} = \frac{\alpha_{cc} f_{ck}}{\alpha_c} = \frac{35}{1.5} = 23.3 \text{ N/mm}^2$$

$$k = 1 + \sqrt{\frac{200}{750}} = 1.51$$

The shear capacity will be calculated for members without shear reinforcement in order to obtain the shear capacity of the concrete. A few assumption will be made which will be valid for concrete classes C12/15 up to C90/50. The design value of the shear resistance is given by (eq. 6.2a NEN-EN1992-1-1) :

$$v_{Rd,c} = [C_{Rd,c} k (100 \sigma_l f_{ck})^{1/3} + k_1 \sigma_{cp}] = [0.12 * 1.51 * (100 * 0.02 * 35)^{1/3} + 0.15 * 0] = 1.51 \text{ N/mm}^2$$

Where:

$\sigma_l = 0.02$ Upper bound longitudinal reinforcement

$C_{Rd,c} = 0.12$ reduction factor shear cracking

$k_1 = 0.15$ reduction factor shear cracking

D.1.3 Stress-strain

The stress-strain curve of concrete conform the EC2 based on parabolic-linear relation. The aggregate is more rigid than the cement paste and will deform less under the same applied stress. However this relation is non-linear due to micro-cracks formation

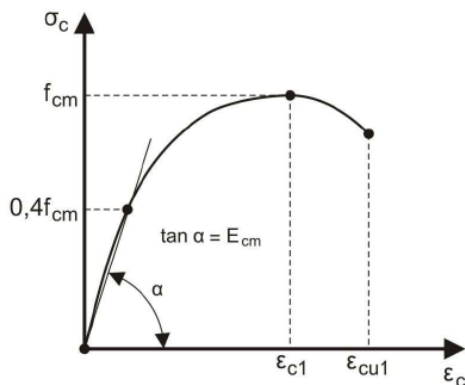


Figure D.1: Compressive stress-strain curve

D.1.4 Creep

It is assumed that the bridge girders are prestressed with a constant mean compressive stress of $7\text{--}8 \text{ N/mm}^2$ for concrete C45/55. Elastic deformation caused by the only the prestressing force is equal to $\epsilon_{el}=8/36000=0.2\cdot 10^{-3}$. The creep deformations caused by prestressing $\epsilon_{cr}=2\cdot 0.2\cdot 10^{-3}$. Global creep factors are from 1.5 and up to 1.4.

D.1.5 Shrinkage

We can assume a shrinkage of $0.2\cdot 10^{-3} \text{ m/m}$

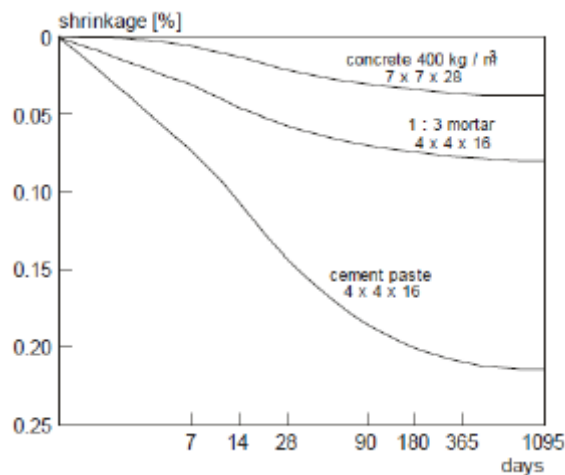


Figure D.2: Drying shrinkage of hardened concrete with RH=50% [P01, p16]

It is commonly assumed that deformation of a prestressed bridge due to creep and shrinkage is 1mm/m of bridge length.

D.1.6 Freeze – thaw

According to the EC2-2 bridges should be in environmental classes XD3. According to EN 1992-1-1 table E.1N, indicative strength class for bridges conform XD3 will be C35/45. The maximal permissible wcf will be 0.45 with minimal cement content 300 kg/m^3 [NEN-EN 206-1]

NEN 8005		NEN-EN 206-1						
Maximum wcf / wbf	Min. cement geh. (kg/m ³)	Geen aantasting	Aantasting wapening			Aantasting beton		
0,70	200	X0						
0,65	260		XC1					
0,60	280			XC2				
0,55	280			XC3				
0,55	300				XD1	XF1	XF2-lucht	XA1
0,50	300		XC4	XD2	XS1	XF3	XF4-lucht	
0,50	320							XA2
0,45	300				XD3	XS2	XF2	
0,45	320					XS3	XF4	
0,45	340							XA3
NEN 6720, tabel 44 ^a		Betondekking c ^a (mm)						
Plaat, wand	—	15	25	30	25	30		
Balk, poer, console	—	25	30	30	35	40		
Kolom	—	30	35	40	35	40		
NEN 6720, tabel 2		Scheurwijdte w (mm)						
Zonder voorspanstaal	—	0,4	0,3	0,2	0,3	0,2		
Met voorspanstaal	—	0,3	0,2	0,1	0,2	0,1		

Figure D.3: Environmental class classification [NEN-EN 206-1]

D.1.7 Compaction

The compaction characteristics of NSC corresponds with the design process of the mix-design. The concrete will be design conform the NEN 8005 where the quantities of the materials, reinforcement design and formwork walls will be taken into account in order to obtain a workable mixture and compact concrete element.

D.1.8 Curing

The curing process of concrete is related to the hydration process of the young concrete. For a NSC the water/cement ratio will be within the recommended values depending on the mix-design, air temperature, evaporation, temperature peaks and temperature drop. These al are balanced during the execution stage of NSC.

D.1.9 Costs

The costs of NSC in viaducts projects is approximately 12% from the total projects costs. The reinforcement costs are 20% and the formwork costs are 22% from the total costs of the viaduct project. For bridge construction (one span) the costs are 10% concrete, 10% reinforcement and 10% formwork. [B03].

The nominal costs of NSC per m³ without formwork costs are:

<i>Material</i> [€/ m ³]	<i>Batching</i> <i>plant</i> [€/ m ³]	<i>Casting at</i> <i>site</i> [€/ m ³]	<i>Reinforcement</i> [€/ m ³]	<i>Total</i> [€/ m ³]
57.8	48	38	139	282.8

Table D.3 : Nominal costs in the Netherland 2008. [B03, p31]

D.2 High strength concrete (HSC)

D.2.1 Properties

This type of concrete differs from NSC in quite few aspects. The properties of this type of concrete are given in Table D.4: [EC2-1-1 table 3.1]

<i>Compression</i> [N/mm ²]	<i>Tension</i> [N/mm ²]	<i>E – modulus</i> [N/mm ²]*10 ³	<i>Density</i> [kg/m ³]
65-105	4.2-5	38-44	2500

Table D.4: Mechanical properties

<i>Strength class</i>	<i>Cement</i> [kg]	<i>w/c</i>	<i>Water</i>	<i>Silica foam</i>	<i>Gravel</i>	<i>Sand</i> (<250µm)
C70/85	20%	0.3	6%	1%	40%	32%

Table D.5: Example concrete mix-design [B04]

D.2.2 Shear stress

Similar to the calculations in D.1.2 also for HSC the Eurocode can be applied. For concrete class C80/95 the lower bound of the shear capacity and the upper bound are given:

$$v_{min} = 0.035k^{3/2}f_{ck}^{1/2} = 0.035 * 1.51^{3/2} * 80^{0.5} = 0.58 \text{ N/mm}^2$$

$$v_{Rd,c} = [C_{Rd,c}k(100\sigma_{lf_{ck}})^{1/3} + k_1\sigma_{cp}] = [0.12 * 1.51 * (100 * 0.02 * 80)^{1/3} + 0.15 * 0] = 0.98 \text{ N/mm}^2$$

D.2.3 Stress-strain curve

The ascending branch of stress-strain is more linear and steeper for HSC. Strain at maximum strength is greater and descending part becomes steeper compared to NSC.

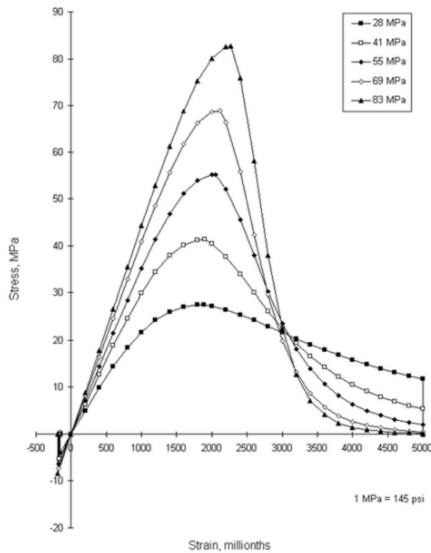


Figure D.4 : Stress-strain curves for different compressive strength [A15]

D.2.4 Creep

In Figure D.5 the creep coefficient as function of the concrete strength class is given. The creep coefficient for HSC with silica foam is 0.8 and 1.0 (long term)

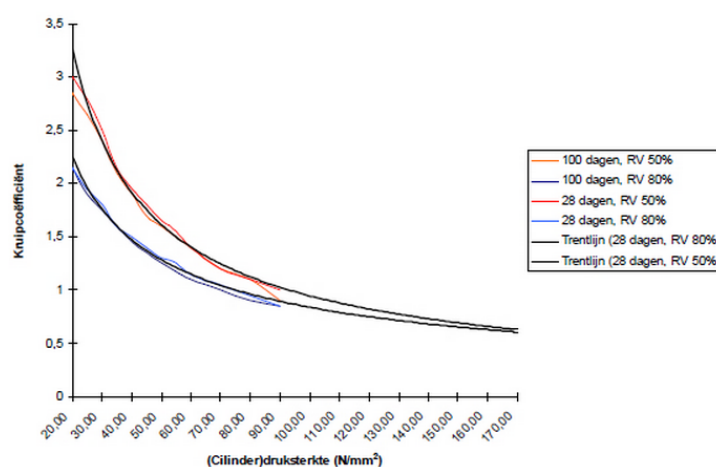


Figure D.5 Creep coefficient as function of the compression strength [A01]

D.2.5 Shrinkage

Unlike NSC, the HSC has a lower w/c ratio, which causes higher autogenous shrinkage, which is by far less significant to NSC. The low w/c ratio is also responsible for a small drying shrinkage. Therefore autogenous shrinkage in HSC is an important factor for cracking especially if the concrete is restrained.

D.2.6 Freeze – thaw

Due to higher density of HSC the influence of freeze-thaw is smaller. The EDF (the Fraench Electricity company) have published design criteria for HSC which say that the resistance to freeze/thaw the losses of compressive strength smaller than 10% after 100 thermal cycles within the range of -20 +20°C. Moreover the Freeze-thaw tests were carried out on Ductal® samples at show that HSC material resist the freeze-thaw effects better than ordinary concrete.

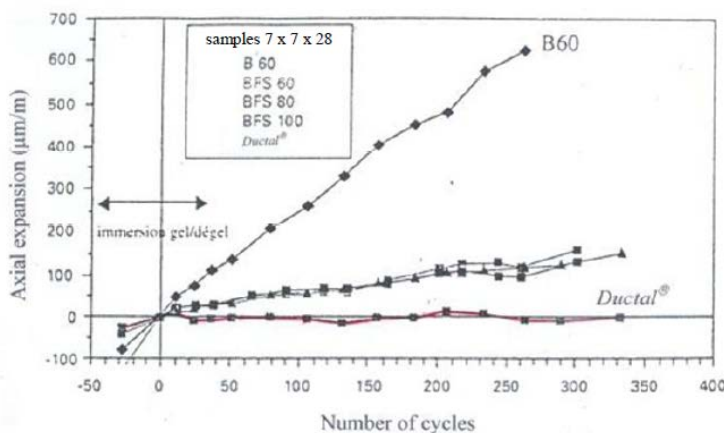


Figure D.6: Tests [B1, p48]

D.2.7 Compaction

The compaction characteristics of HSC corresponds with the design process of the mix-design. The concrete will be design conform the NEN 8005 where the quantities of the materials, reinforcement design and formwork walls will be taken into account. However, large density require vibration of less than a minute around the dense reinforcement.

D.2.8 Curing and finishing

Ramezianipour&Malhotra (1995) stated that “if the potential of concrete with regards to strength and durability is to be fully realized, it is most essential that it be cured adequately.

Special thermal treatment applied during the curing process. The HSC element is being consistently heated to 90 degrees. This treatment increase the durability by preventing drying shrinkage, reduces creep and accelerating maturity (see Figure D.7). Moreover the constructor should consider the heat development during the curing process and the duration of the curing process. (Higher temperature peek).

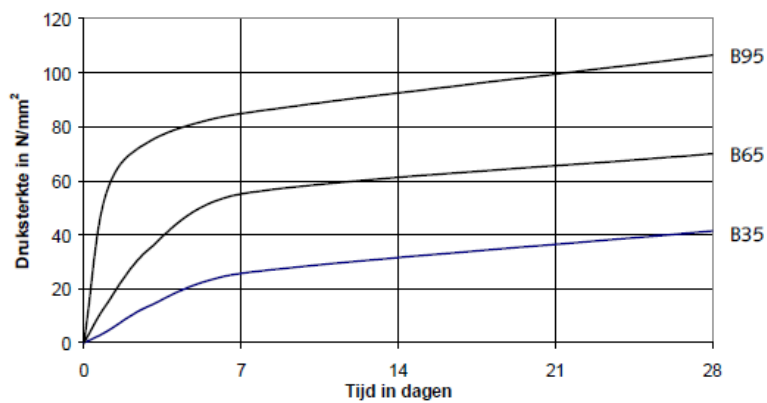


Figure D.7 : Compressive strength progress [P01, p20]

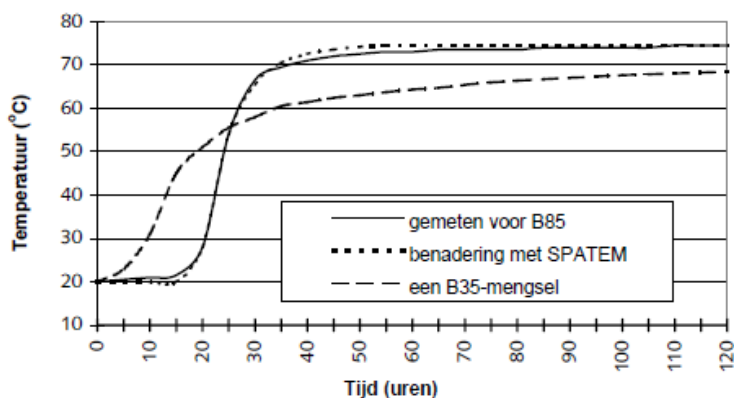


Figure D.8: Adiabatic curves [P01, p20]

D.2.9 Durability

HSC have a better resistance against environmental attacks such as chloride attack, carbonation, alkali-silica reaction ext. Figure D.9 illustrates amount of time in years in which the critical chloride content in rebar (40mm cover) is exceeded.

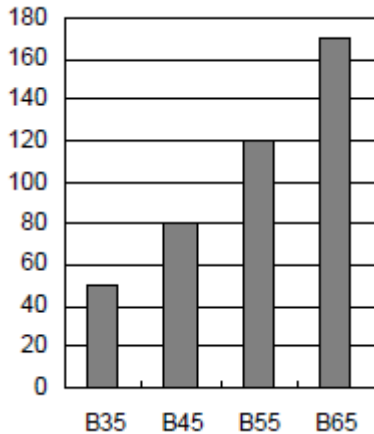


Figure D.9 : vertical axis years [P01, p20]

D.2.10 Costs

The continued rise in steel prices in recent years has changed the economics of the different material options. Long-time durability of HSC is an important costs component. The saving in material usage due to the slender design and light-weight span will reduce the total price during the execution stage. Higher strength class will lead to few percent of saving for standard viaduct design. [2]

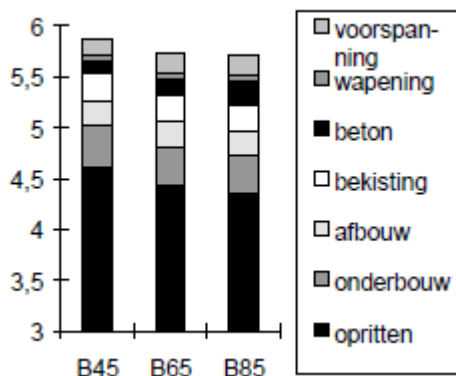


Figure D.10 : Structure costs in millions guilders [B03, p31]

D.2.11 Result

Explanation:

- a. Higher strength values, E-modulus and tensile strength.
- b. Stress-strain curve :: more brittle steeper post-peak behaviour, low w/c ratio,
- c. Higher creep coefficient
- d. Low w/c ratio cause high autogenous shrinkage
- e. Higher resistance due to permeability
- f. Density material
- g. Required heat treatment and heat development during the curing
- h. HSC have a better resistance against environmental attacks
- i. Cheaper alternative

D.3 Ultra – high performance concrete (UHPC)

D.3.1 Properties

<i>Compression</i> [N/mm ²]	<i>Tension</i> [N/mm ²]	<i>Bending</i> <i>strength</i> [N/mm ²]	<i>E – modulus</i> [N/mm ²]*10 ³	<i>Density</i> [kg/m ³]
150-200	5-6.2	25-60	40-70	2800

Table D.6: Typical properties [A03]

<i>Strength</i> <i>class</i>	<i>Cement</i> [kg]	<i>w/c</i>	<i>Water</i> [kg]	<i>Silica</i> <i>foam</i> [kg]	<i>Gravel</i> [kg]	<i>Sand</i> (<250μm) [kg]	<i>Fibers</i> [kg]
C170/200	28%	0.15	6%	9%	0%	41%	6 wt%

Table D.7: Example concrete mix-design [B04]

D.3.2 Shear strength

The Eurocode and the Dutch code provide simple derivation of the shear capacity from the compressive and tensile strength properties. However these empirical expressions are valid for concrete class up to C90/105. Despite this, the theoretical values for the tensile strengths (according to the Eurocode and Dutch code) of concrete class larger than C90/105 are calculated in Table D.8. It is found that these values are much lower than the values obtained in laboratory tests in the University of Kassel, Germany. [A18]

	f_{ck} [N/mm ²]	f_{ctk} [N/mm ²]
Theoretical	170	4.35
In practice	150-250	8.0

Table D.8: Tensile strength values [A18]

<i>Norm</i>	<i>Fibers content</i>	$v_{Rd,c}$ [N/mm^2]
VBC $f_{ctk}=4.35$ N/mm ²	0 vol%	1.74
VBC $f_{ctk}=8$ N/mm ²	0 vol%	3.2
EC2	0 vol%	1.26
AFGC / SETRA	1.6 vol%	8.15

Table D.9: Shear capacities concrete member

Shear tests response of UHPC is conducted by the University of Baroda [P16] for UHPC compressive strength higher than $100 N/mm^2$ found shear strengths between $8-15 N/mm^2$ for fiber content up to 2.5%.

D.3.3 Stress-strain curve

UHPC shows linear elastic behaviour. The failure is completely brittle without the fibers (no descending branch) .

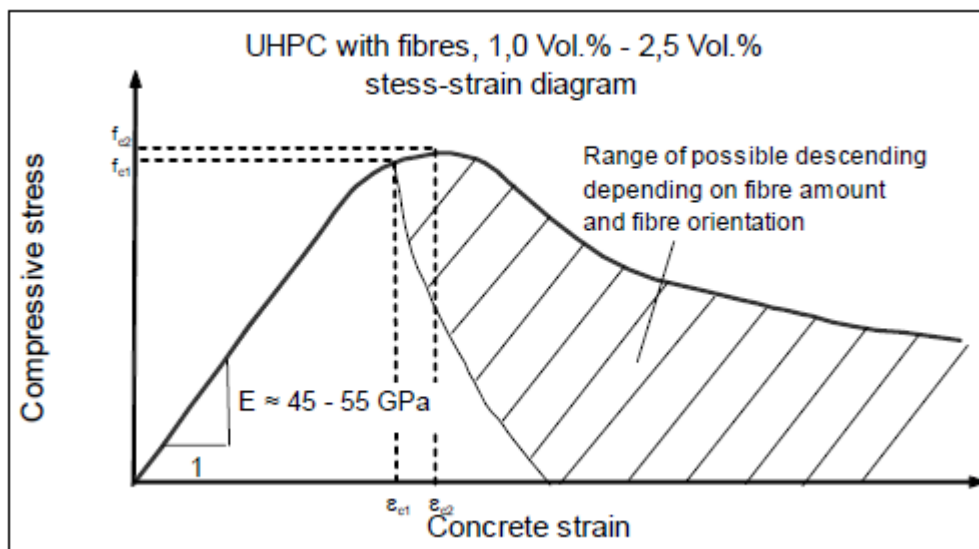


Figure D.11: Typical stress-strain diagrams of UHPFRC

D.3.4 Creep

The UHPC with fibres (UHPFRC) have a creep coefficient just like the HSC between 0.8-1.0. After heat treatment it can decrease dramatically to 0.2-0.5. In a case of post-tensioned girders, heat treatment will reduce the creep strain. Consequently, prestressing

force can be reduced [B01]]. So UHPC is very suitable for precasting due to the low creep and shrinkage effect comparing with NSC.

D.3.5 Shrinkage

Unlike ordinary concrete, the UHPFRC has a very low W/L ratio, which causes very high autogenous shrinkage (about 550 $\mu\text{m}/\text{m}$) and very small drying shrinkage about 150 $\mu\text{m}/\text{m}$ for UHPFRC without heat treatment.

D.3.6 Freeze – thaw

In comparison with conventional concrete (NSC) the UHPC is more durable in the long life-time. It have higher resistance against mechanical abrasions and freeze and thaw stresses as well as a greater impermeability for fluids and gasses.

D.3.7 Compaction

UHPC isn't a self-compacting concrete but it flows extremely well due to the good lubricating effect of the binder.

D.3.8 Curing and finishing

Due to the lack of bleeding water in UHPC the surface can crack if it not protected from drying. Self- desiccation developed within the whole mass of the concrete, while drying begins to develop at the surface of the concrete. To get the wanted high compressive stress the UHPC should not be water cured as much as possible. The standard curing achieve the best end-results [P02].

Table		NC C35	HPC C100	UHPC C200 water cured	UHPC C200 heat cured	RPC C500
compr. Strength after 28d	N/mm ²	40	109	162	213	487
spec. density	g/cm ³	2.36	2.48	2.39	2.39	2.76

Table D.10 : Compressive strength and curing method [P02, P313]

D.3.9 Durability

Just like HSC , the UHPC is durable material thanks to his density and low permeability:

Table		NC C35	HPC C100	UHPC C200	RPC C500
total porosity	vol.-%	15.0	8.3	6.0	2.0
capillary pores	vol.-%	8.3	5.2	1.5	0.8

Table D.11 : [P02, P317]

D.3.10 Costs

High material costs of UHPC is the largest market constraint now on days. The net material costs are about €700/m³.

If such light cross-sections in conjunction with prefabricated segmental construction, external prestressing and dry joints come to application, new or adapted and very fast erection methods in bridge construction are imaginable. These should compensate for the higher material costs. Due to the high durability compared to conventional concrete bridges, the life-span will be increased to 200%, while the costs of maintenance will be halved. Since these aims can be met, the lifecycle costs will decrease by 50%, which leads to low affordability for maintenance over a long lifetime. Last, but not least, these advantages unburden our political economy. [B01, P210].

D.3.11 Result

Explanation:

- a. Higher density, strength, E-modulus
- b. Stress-strain curve: Fibers add ductility and strain-strain curve exhibit strain hardening
- c. Creep is similar to HSC
- d. Autogenous shrinkage is very high
- e. Excellent resistance
- f. Compaction with admixtures
- g. High curing temperature, heat treatment during curing required
- h. Excellent durability
- i. Very costly

D.4 Reactive powder concrete (RPC)

Belongs to the UHPC family of concrete mixture. This type of concrete is described as a fiber-reinforced, super plasticized, silica fume-cement mixture with very low water-cement ratio (W/C) characterized by the presence of very fine quartz sand (0.1-0.5 mm) instead of ordinary aggregate. In fact, this is a concrete without aggregate. [P02, p133]

D.4.1 Properties

<i>Compression</i> [N/mm ²]	<i>Tension</i> [N/mm ²]	<i>Flexural</i> <i>strength</i> [N/mm ²]	<i>E-modulus</i> [10 ³ * N/mm ²]	<i>Density</i> [Kg/m ³]
200-800	45-100	45-140	60-75	2714-2949

Table D.12: Mechanical properties [P05, p241]

<i>RP</i> <i>C</i>	<i>Cemen</i> <i>t</i>	<i>w/c</i>	<i>Wate</i> <i>r</i>	<i>Silic</i> <i>a</i> <i>Fum</i> <i>e</i>	<i>Fine</i> <i>aggregate/sa</i> <i>nd</i>	<i>Amorpho</i> <i>us Silica</i>	<i>Steel</i> <i>fiber</i> <i>s</i>	<i>Superplasticiz</i> <i>er</i>
200	36%	0.1 6	5.6%	8.5%	38%	0.4%	7 vol%	0.5%
600	34%	0.1 8	6.4%	8%	30%	0%	21 vol%	0.65

Table D.13: RPC mic design for compressive strength of 200 MPa and 800Mpa [P05, p241]

D.4.2 Shear strength

The tensile strengths of RPC- 600 is determined in the university of Marche, Italy [P05, p241] by laboratories tests. During the test tensile strength of 100 N/mm² is found with micro-fibers content of vol% (see Table D.13). The shear capacity of the concrete can be calculated with the tensile properties in Table D.14.

	f_{ck} [N/mm ²]	f_{ctk} [N/mm ²]
Theoretical	680	6.3
In practice	No data	45-100

Table D.14: RCP-600

The shear capacities according to different norms are calculated in Table D.15:

<i>Norm</i>	<i>Fibers content</i>	$v_{Rd,c}$ [N/mm^2]
VBC $f_{ctk}=6.3$ N/mm^2	0 vol%	2.5
VBC $f_{ctk}=45-100$ N/mm^2	0 vol%	18-40
EC2	0 vol%	2.00
AFGC / SETRA	21 vol%	39-81

Table D.15: Shear capacities concrete member

The values obtained by the French recommendations deviate from the values originated from the Eurocode. This deviation may be explained by the high fibers content in the specimen.

D.4.3 Stress-strain curve

Just like UHPC the RPC is very rigid and brittle. However adding fibers will improve the ductility.

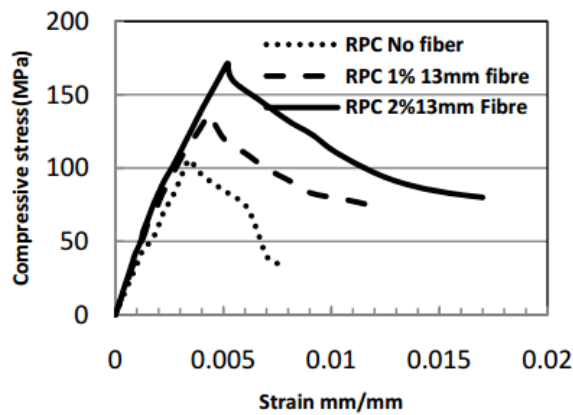


Figure D.12: Stress-strain curve of axially loaded PRC [P10]

D.4.4 Creep

Creep behavior of RPC is similar to the UHPC creep behavior.

D.4.5 Shrinkage

High cement content and low water to binder ratio in UHPC may lead to high autogenous shrinkage, which will induce micro cracks in early ages.

D.4.6 Freeze-thaw

Due to low air entrance of RCP the resistance to freeze and thaw is very high. [A12]

D.4.7 Curing and finishing

Heat curing is required to enhance the wanted design compressive strength of RPC. The curing temperature is between 90 and 400 degrees.

D.4.8 Durability

The durability related characteristics such as carbonation, chloride attack, erosion and air permeability is very high in comparison with NSC. [A12]

D.4.9 Costs

In a typical RPC mixture design, the least costly components of conventional concrete are basically eliminated or replaced by more expensive elements. The mineral component optimization alone results in a substantial increase in cost over and above that of conventional concrete (5 to 10 times higher than HPC). RPC should be used in areas where substantial weight savings can be realized and where some of the remarkable characteristics of the material can be fully utilized [A13]

D.4.10 Result

Explanation:

- a. Very high strength properties
- b. Material is brittle but adding fibers
- c. Similar to UHPC
- d. High autogenous shrinkage
- e. Dense material with high resistance
- f. X
- g. Very high hydration temperature, heat treatment is required
- h. Very durable
- i. Expansive material and production

D.5 Light weight concrete (LWC)

D.5.1 Properties

<i>Compression</i> [N/mm ²]	<i>Tension</i> [N/mm ²]	<i>E - modulus</i> [N/mm ²]*10 ³	<i>Density</i> [kg/m ³]
12-80	2.1-3.2	27-37	800-2150

Table D.16: Mechanical properties [T01, P26]

<i>Strength class</i>	<i>Cement</i> [kg]	<i>w/c</i>	<i>Water</i> [kg]	<i>Liapor</i> 4-8mm [kg]	<i>Gravel</i> [kg]	<i>Sand</i> (<250µm) [kg]
C56/65	17.5%	0.4	6%	6%	36%	32%

Table D.17: Example mix-design [A04]

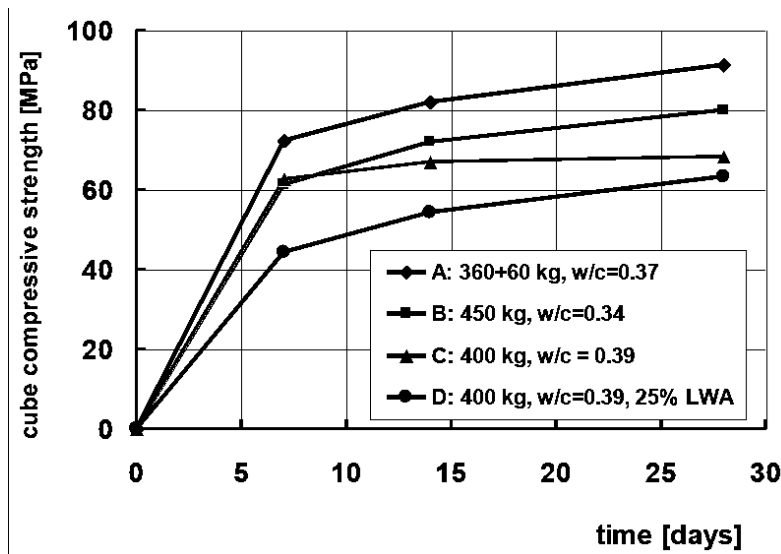


Figure D.13: Concrete compressive strength 28 days [A04]

D.5.2 Shear strength

The shear behavior of light weight concrete without any additional shear reinforcement can be predicted on the basis of the EC2 [C01]. The LWC have a very low shear resistance. A beam consist of LWC will probably fail by shear. The mean value of the LWC shear resistance of LW concrete beams is given in Table D.18. The LW aggregate is classified according to its density according to EC2 art. 11.3.1. The shear resistances in Table D.18 is therefore calculated for the lowest density and the highest density.

<i>Parameter</i>	<i>Description</i>	<i>Expression</i>
$v_{IRD,c}$	Shear strength without stirrups	$[C_{IRD}\eta_1 k(100\sigma_l f_{lck})^{1/3} + k_1\sigma_{cp}] = 0.69 - 0.96 \text{ N/mm}^2$
C_{IRD}	Statistical factor	0.12
k	scale coefficient	$1 + \sqrt{200/d} = 1 + \sqrt{200/750} = 1.51$
σ_l	Steel reinforcement	0.02
η_1	Coefficient of oven-dry density	$0.4 + 0.6\rho/2200$
ρ	Upper limit density	1150 – 2150 kg/m ³

Table D.18: Shear resistance LWC

The American code, the ASI [C02, p146], is used to verify the values in Table D.18. For nonprestressed members without stirrups subjected to shear and flexural the following expression is used:

$$v_c = 2\sqrt{f_{ck}}$$

When f_{ck} should be in psi units. For concrete compressive strength of 5000 pi (35 N/mm²) the shear strength will be 141.5 psi (0.97 N/mm²).

D.5.3 Stress-strain curve

Lower elasticity caused by the LW aggregate.

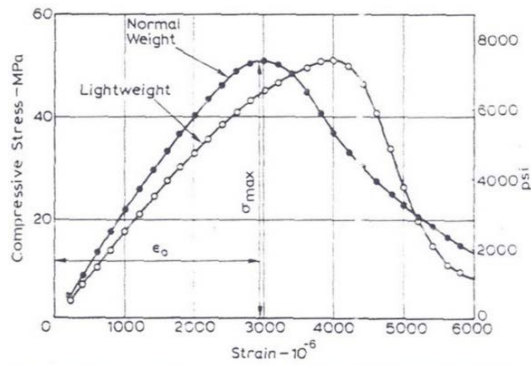


Figure D.14: Stress-strain curve LWC

D.5.4 Creep

Creep of LWC is expected to be larger than creep of NSC. According to Mauricio Lopez [T03] creep of normal weight concrete is on average lower than lightweight concrete at comparable strength. However there are several of LWC mixtures with less creep than their normal weight counterparts. Creep factor for LWC will be around 1.2. [T03].

According to the EC2 art. 11.3.3 [C01, p188] the creep coefficient of lightweight concrete may be assumed equal to the value of normal density concrete multiply by a factor of

$\left(\frac{\rho}{2200}\right)^2$. For densities in order of 1850 kg/m³ the creep factor will be 1.05. 1.05-1.2

D.5.5 Shrinkage

The autogenous shrinkage of LWC is introduced in Figure D.15 where four concrete mixture of strength class C53/B65. The curve of the LWC, curve D shows negligible autogenous strain comparing with the NSC curves.

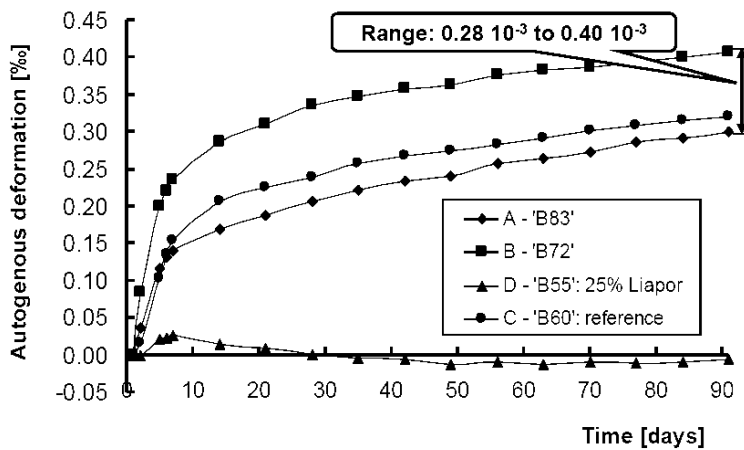


Figure D.15: Autogenous shrinkage of LWC [A04]

However, the drying shrinkage of LWC according to Figure D.16 is higher than NSC. The drying shrinkage is high due to lower stiffness of lightweight aggregate and lower capability of water retention.

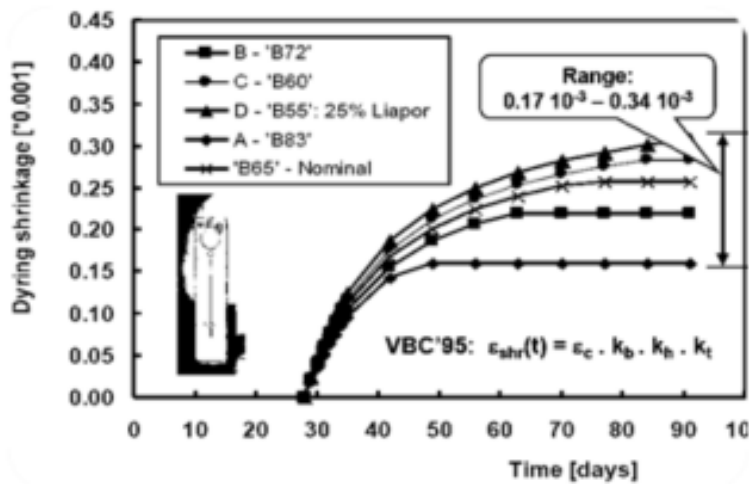


Figure D.16 Autogenous shrinkage of LWC [A04]

D.5.6 Freeze – thaw

It can be generally concluded that LWC have adequate freeze -thaw resistance. According to Hover air-entrance and certain level of strength (w/c ratio) are essential for adequate resistance of freezing and thawing cycles. The recommended minimum strength for concrete exposed to cycles of freezing and thawing for bridge decks is 27 Mpa. [P03]

D.5.7 Compaction

Similar to NSC

D.5.8 Curing and finishing

More complicated than for NSC

D.5.9 Durability

Experience with the LWC shows a durable material with average resistance for carbonations and chloride attack. As mentioned at section 3.4.5, Hover concluded that air-entrance and w/c ratio are essential for the durability. Testing LWC arrived in the conclusion that air retaining lightweight concrete provide good durability results .Tests shows similar behavior of LWC and NSC in bridges infrastructure. [B06, P46].

D.5.10 Costs

Lightweight aggregate concrete includes the following costs benefits:

- Reduction of dead load making savings in foundations and reinforcement
- Saving transporting and handling precast units on site
- Reduction in formwork and propping
- Reduction in manpower

Typical costs of LWC for bridges structures which is forecasted and delivered to the project cost about 21% more than the equivalent ordinary concrete .For cast in-place concrete including formwork, reinforcement, conveying, finishing and curing the LWC will cost 4% more than his equivalent NSC. [P04]

D.5.11 Result

Explanation:

- a. Strength properties are similar
- b. Stress-strain curve: more brittle post peak behavior , lower stiffness due to LWA
- c. Larger creep
- d. Negligible autogenous shrinkage, higher drying shrinkage
- e. LWC have adequate freeze -thaw resistance
- f. Similar
- g. More complex curing than NSC
- h. Similar
- i. More costly

D.6 High volume fly-ash concrete (HVFA)

This type of concrete can also contain steel fibres or lightweight aggregate in addition to the fly-ash. Test results indicated that the use of high volumes of Class F fly ash as a partial replacement of cement in concrete decreased its 28 days compressive, splitting tensile, and flexural strengths, modulus of elasticity, and abrasion resistance of the concrete. [P05, P149]

D.6.1 Properties

<i>Compression</i> [N/mm ²]	<i>Tension</i> [N/mm ²]	<i>Modulus of</i> <i>Elasticity</i>	<i>Density</i> [kg/m ³]
26.7-45	2-4.2	23-30	2350

Table D.19: Typical HVFA properties [P06] [T08]

<i>Class F</i> <i>Fly-ash</i> [kg]	<i>Cement</i> [kg]	<i>w/(c+FA)</i>	<i>Water</i> [kg]	<i>Fibers</i> [kg]	<i>Gravel</i> [kg]	<i>Sand</i> ($<250\mu\text{m}$) [kg]	<i>28 - days</i> <i>Compression</i> [N/mm ²]
35%	11%	0.37	6.3%	0%	50%	26.3%	26.7
55%	7.6%	0.37	6.3%	0%	50%	26.3%	23.1
35%	10.7%	0.37	6.1%	2.4%	49%	25.5%	32
55%	7%	0.37	6.1%	2.4%	49%	25.5%	25

Figure D.17 : Fly ash mix-design properties [P07]

D.6.2 Shear strength

Latest experimental research in the university of Missouri, 2002 [T07] the existing design codes for shear capacity of HVFA beams conservatively predict the shear strength.

Which means that the HVFA beams without stirrups on average are in closer agreement with the design code. [T07, p110]

D.6.3 Stress-strain curve

Stress-strain pattern of the hardened concrete is almost similar to ordinary concrete. It is observed that for higher grades of concrete with increase in stress there was decrease in strain. [A17]

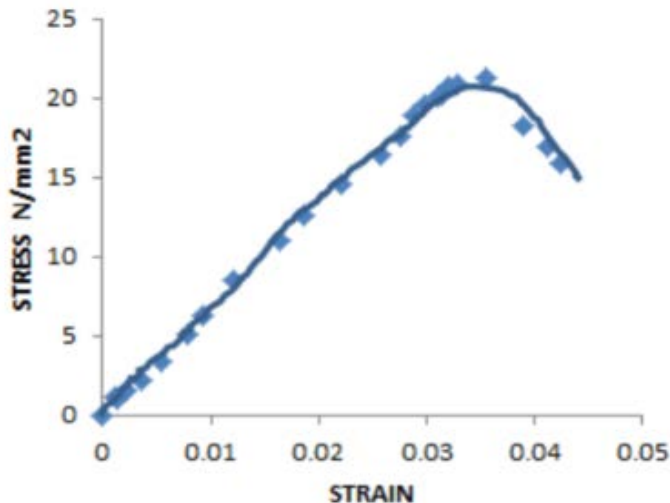


Figure D.18: Strain-stress curve of cylinder under axial load [A17]

D.6.4 Creep

The creep of concrete is influenced by a large number of parameters. The effect of fly ash on creep will depend to some extent on how the effect is measured. For example, if loaded at an early age, fly ash concrete may exhibit higher amounts of creep than Portland cement concrete because it has a lower compressive strength (Lane 1982 and Yuan 1983). However, if concretes are loaded at an age when they have attained the same strength, fly ash concrete will exhibit less creep because of its continued strength gain (Lane 1982 and Ghosh 1981).

Latest studies reveals that the creep of HVFA concrete tends to be lower than Portland cement concrete of the same strength and this has been attributed to the presence of unreacted fly ash (Sivasundaram 1991). It is also likely that the very low water and paste contents attainable in HVFA concrete (and concurrently high aggregate content) play an important role in reducing the creep of concrete with high levels of fly ash. [P06]

D.6.5 Shrinkage

The drying shrinkage of fly-ash concrete is generally less than conventional concrete (Malhotra 2005 and Atis 2003) and this is undoubtedly due to the low amount of water used in producing such a concrete. [P06]

D.6.6 Freeze and Thaw

As mentioned in the previous concrete type, sufficient strength and adequate air-void system. This holds true for fly ash concrete regardless of the fly-ash content. However, studies has shown that it may be less resistant to scaling when subjected to freeze-thaw ((Timms 1956, Gebler 1986, Johnston 1987, Johnston 1994, Whiting 1989, and Afrani 1994). Satisfactory performance may obtained at levels of fly ash up to 30% (Gebler 1986, Gifford 1987, and Bilodeau 1991)

D.6.7 Compaction

The use of good quality fly ash with a high fineness and low carbon content reduces the water demand of concrete and, consequently, the use of fly ash should permit the concrete to be produced at a lower water content when compared to a Portland cement concrete of the same workability of the same workability (Best 1980)

D.6.8 Curing and finishing

Generally fly ash will reduce the rate and amount of bleeding primarily due to the reduced water demand (Gebler 1986). Therefore, the freshly placed concrete should be finished as quickly as possible and immediately protected to prevent plastic shrinkage cracking when the ambient conditions are such that rapid evaporation of surface moisture is likely.

Furthermore, fly-ash have a positive effect on the hydration temperature during the curing process. It reduces the maximum temperature (peek temperature) and therefore have been already used in commercial applications to control the temperature rise in large placement (Mehta 2000, Mehta 2002, and Manmohan 2002). Although, attention for the calcium content in the fly-ash is needed.

D.6.9 Durability

Fly-ash reduces the permeability of the concrete to water and gas. The HVFA concrete will be two times more permeable for chloride than concrete without fly-ashes at curing time of 28 days. However, there is a reversible trend with chloride permeability with increasing fly-ash content by 180 days. [P06]

Alkali-silica reaction can be controlled with Fly-ash class F (low calcium) at moderate rate of replacement (20% to 30%). (Shehata 2000 and Shehata 1999)

Sulphate resistance of HVFA however do not meet the requirements according to the study of Shashiprakash and Thomas (2001).

It has been documented that concrete containing fly ash will carbonate at a similar rate compared with Portland cement concrete of the same 28-day strength (Tsukayama 1980, Lewandowski 1983, Matthews 1984, Nagataki 1986, Hobbs 1988, and Dhir 1989)

D.6.10 Costs

The cost of this HVFA concrete are less than ordinary concrete thanks to the usage of by-product the fly-ash as a replacement of the expansive cement powder.

D.6.11 Result

Explanation:

- a. Similar strength properties as ordinary concrete
- b. Smaller amount of cement is used, stress-strain curve is similar to that of Portland cement concrete
- c. Smaller creep
- d. Less shrinkage
- e. Lower resistant to scaling when subjected to freeze-thaw
- f. Lower water content when compared to a Portland cement concrete of the same workability
- g. Positive effect on the hydration temperature
- h. Increased durability
- i. Cheaper alternative

D.7 Self-compacting concrete (SCC)

D.7.1 Properties

Compressive and tensile strength of SCC with a similar w/c ratio will usually have slightly higher strength than traditional vibrated concrete, due to improved interface between the aggregate and the cement paste.

The modulus of elasticity is influenced by the type and amount of aggregate. SCC have often a higher paste content than traditional concrete which consequently lead to lower E-modulus. The EN 1992-1-1 provide a formula to deal with this.

<i>Cement</i> [kg]	<i>w/c</i>	<i>Water</i> [kg]	<i>Metakaolin</i> [kg]	<i>Sand</i> ($<250\mu\text{m}$) [kg]
32%	0.39	12%	1.7%	53%

Figure D.19: Example mixed design SCC [P08]

D.7.2 Shear strength

Shear capacity of SCC will be lower than for traditionally vibrated concrete and may be therefore insufficient to carry any shear force. While some researchers indicated that the shear capacity of SCC generally was slightly lower than NC, researchers have found that the shear capacity of SCC beams still had sufficient safety margin compared with predicted capacity using existing design equations such as the Eurocode (Burgueño and Bendert 2007, Choulli et al. 2005, Hamilton and Labonte 2005, Hegger et al. 2007, Ozyildirim 2007).

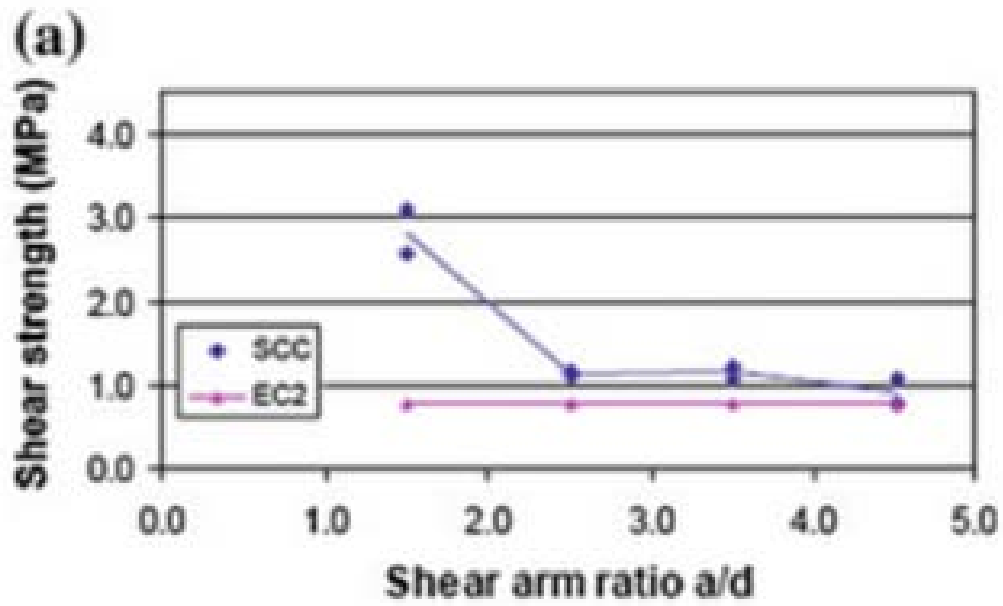


Figure D.20: Shear strength versus shear arm ratio for beams without stirrups [B12, p154]

D.7.3 Stress-strain curve

Stress-strain curve don't have any noticeable change.

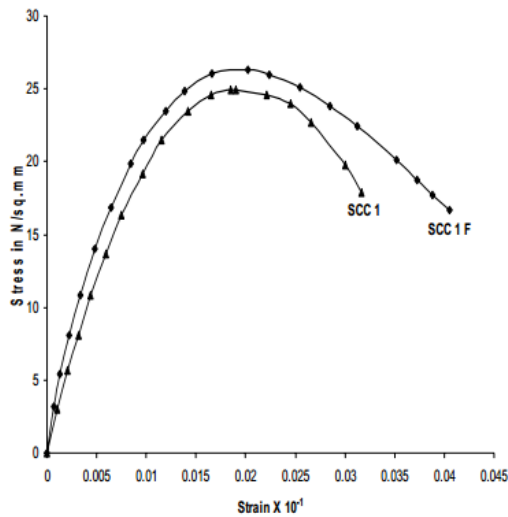


Figure D.21: Stress-strain curve of typical SCC

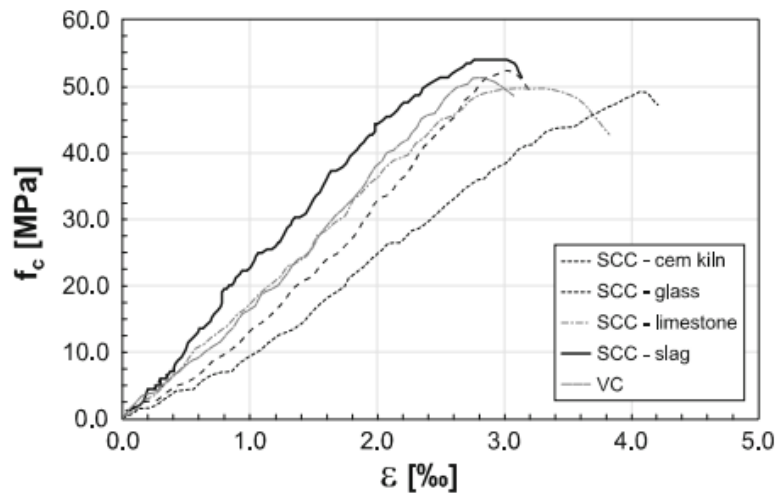


Figure D.22: Stress-strain relationships of VC and SCC with different fillers [B12, p34]

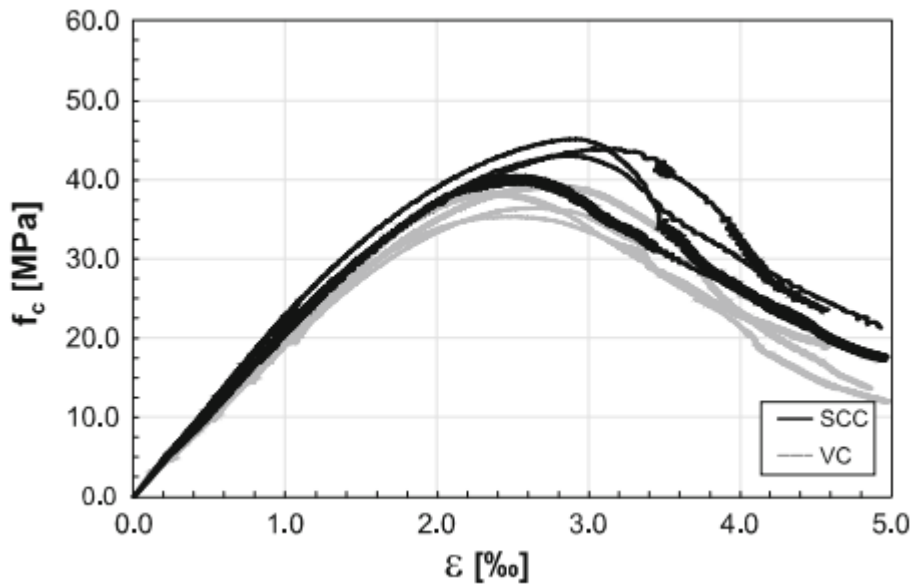


Figure D.23: Comparison of measured stress-strain curves for SCC and VC mixture [B12, p36]

D.7.4 Creep

Creep take place in the cement paste and it's influenced by its porosity (w/c ratio). As aggregate restrain the creep of the cement paste, the higher its volume the higher the E-value of the aggregate, the lower the creep will be.

Due to the higher volume of cement paste, the creep coefficient for SCC may be expected to be higher than for normal concrete of equal strength, but such differences are small and covered by the safe assumptions in the tables and the formulae provided in the Eurocode. [P08]

D.7.5 Shrinkage

The aggregate restrains the shrinkage of the cement paste and so the higher volume of the aggregate and the higher the E-value of the aggregate, the lower the drying shrinkage. The Eurocode gives values for normal concrete which is valid for SCC. Tests performed on creep and shrinkage of different SCC and reference concrete show that [P08] :

- The deformation caused by shrinkage may be higher
- The deformation caused by creep may be lower
- The value for the sum of the deformations due to shrinkage and creep are almost similar

D.7.6 Freeze-thaw

Air entraining admixtures may be used in the production of SCC to improve freeze-thaw durability.

D.7.7 Compaction

The concrete do not require any additional compaction

D.7.8 Curing and finishing

Curing is important for all concrete but especially so for the top-surface of elements made with SCC. These can dry quickly because of the increased quantity of paste, the low water/fines ratio and the lack of bleed water at the surface. So comparing with ordinary concrete plastic shrinkage of SCC is found two times higher. [A14, p584].

Initial curing should therefore commence as soon as practicable after placing and finishing in order to minimise the risk of surface crusting and shrinkage cracks caused by early age moisture evaporation [P08].

D.7.9 Durability

The durability performance of SCC is one of the main reasons to use it as construction material. The resulting of free-vibrated concrete is homogenous compaction of the concrete element. Which result in better durability [P08]

D.7.10 Costs

Some people would ask, "So why don't we use SCC everywhere?" The perception is that it's the cost that prevents wider use of SCC-these mixes use fines and admixtures that can increase the price of a meter of concrete by €10 to €15, although some producers may add a surcharge as high as €30 in comparison with ordinary concrete [A05].

Although the material is more expensive, SCC have benefits such as:

- Productivity Improvements – SCC can increase the speed of construction, improve formed surface finish and thus reduce repair and patching costs, reduce maintenance costs on equipment, and provide faster form and truck turn-around time.
- Reduced labor costs – SCC reduces labor demands and compensates for lack of skilled workers to perform the rigorous work required for quality concrete construction.

D.7.11 Result

- a. Properties are similar. Elasticity modulus is smaller
- b. High w/c factor, No noticeable change in shape of the stress-strain diagram
- c. Lower creep deformation
- d. Higher shrinkage
- e. Similar resistance as for vibrated concrete
- f. No additional compaction is required
- g. Plastic shrinkage during curing is two times higher
- h. Homogenous material
- i. Price per m³ is slightly more expensive

D.8 Foamed concrete (FC)

Concrete for trench reinstatement was conducted in the UK, which led to a further increase in use in this country. Foamed concrete or Cellular concrete, has the following properties: it is lightweight, free flowing and easy to level, it does not require compaction, has good thermal insulation and frost resistance properties, and it is easy to pump, both vertically and horizontally [P05, p3].

D.8.1 Properties

<i>Compression</i> [N/mm ²]	<i>Tension</i> [N/mm ²]	<i>Modulus of elasticity</i> [N/mm ²]	<i>Shear strength</i> [N/mm ²]	<i>Density</i> [kg/m ³]
0.5-10	0.5	23-37	0.01-0.043	400-1600

Table D.20: Typical properties foamed concrete

<i>Cement</i> [kg]	<i>w/c</i>	<i>Air volume</i>	<i>Water</i> [kg]	<i>Foam Agent (ltr)</i>	<i>Sand</i> ($<250\mu\text{m}$) [kg]
40%	0.5-0.6	20%	20%	0.32-1.0	40%

Table D.21: Mix design for foam concrete

The range of the modulus of elasticity given in Table D.20: Typical properties foamed concrete Table D.20 are depended on the air content of the FC specimen. Which according to [C17] vary from 4 to 20%.

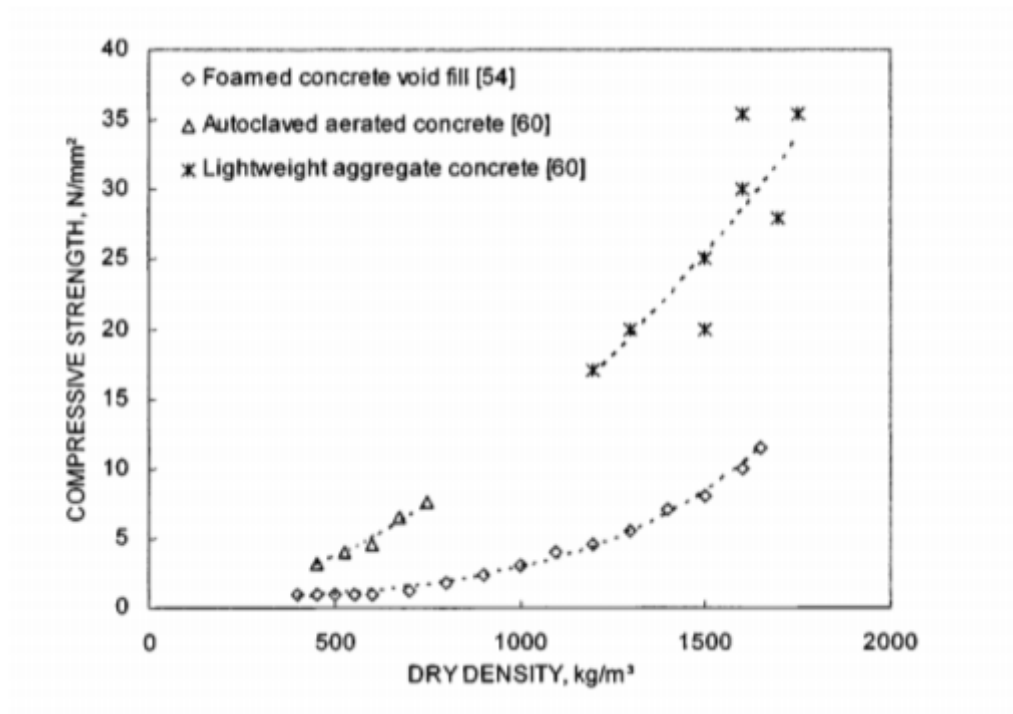


Figure D.24: Influence of dry density on the compressive strengths of foamed and other lightweight concretes [B12, p70]

D.8.2 Shear strength

Very limited data is available on the shear strength capacity of cellular concrete. Tests of cellular concrete beams with cast density ranging from 800 to 1440 kg/m³ have indicated that the shear strength may be estimated using the ACI code requirement for lightweight concrete. [Joseph F.Lamond]. According to the ACI 213R-87

D.8.3 Stress-strain curve

The compressive stress-strain behavior can be divided into three regimes, elastic regime, plateau regime and densification regime. All this happened due to the cracks propagation. Foamed concrete also is one of the brittle materials, but it has the combination of soft and brittle material so it can contain many micro cracks. When loaded in compression these micro cracks will propagated, which will cause the brittle material sample to fail (Zheming Zhu. 1999)

In that case the expression derived in the ASI [C02, p146] will be used as initial indication of the shear capacity.

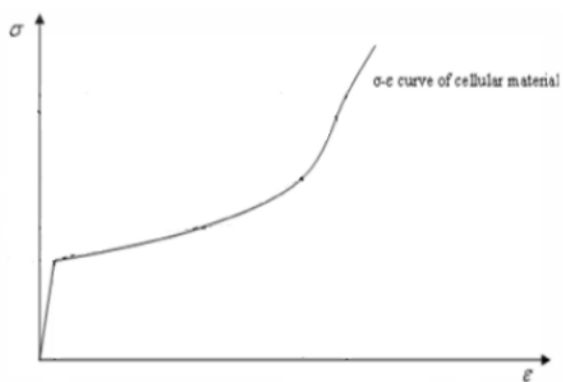


Figure D.25: Stress-strain curve with strain hardening branch

D.8.4 Creep

Based on the results of their research Widmann & Enoekl state that the creep deformation (as measured under constant stress in an air-conditioned room) of foamed concrete is similar to that of normal concrete.

D.8.5 Shrinkage

Foam concrete possesses high drying shrinkage due to the absence of aggregates, i.e., up to 10 times greater than those observed on normal weight concrete. The shrinkage of foam concrete reduces with density which is attributed to the lower paste content affecting the shrinkage in low-density mixes. The drying shrinkage is from 0.07% to 0.3%

D.8.6 Freeze-thaw

The cellular structure of foamed concrete gives it good resistance to the effects of freeze thaw action due to his air-content and high cement content

D.8.7 Compaction

FC is lightweight, free flowing and easy to level, it does not require compaction.

D.8.8 Curing and finishing

Specialist plant (e.g. compactors, vibrators) not needed. Allows controlled discharge into narrow openings. Fully fills void space, including undercut pockets. Entirely surrounds and protect pipelines. [A06]

D.8.9 Durability

Water absorption: Water absorption of foam concrete decreases with a reduction in density, which is attributed to lower paste volume phase and thus to the lower capillary pore volume.

Sorptivity (The moisture transport phenomenon in porous materials) of foam concrete is reported to be lower than the corresponding base mix and the values reduce with an increase in foam volume.

Sulphate resistance of foam concrete, reveals that foam concrete has good resistance to aggressive chemical attack

A study on accelerated carbonation of foam concrete by Jones and McCarthy indicate that lower density concrete appears to carbonate at a relatively higher rate.

D.8.10 Costs

Reduced labour and supervision costs, Cost compares favourably with other fill materials

D.8.11 Result

Explanation:

- a. Low strength values
- b. Stress-strain curve : brittle failure
- c. Similar creep
- d. High drying shrinkage
- e. High air content
- f. No additional compaction is required
- g. Good curing
- h. Good resistance to aggressive chemical attack, sensitive to carbonation
- i. Labour costs, comparable to other filling material

D.9 Polymer modified concrete (PMC)

The type of fibres used as the reinforcement is the basics for classification of FRP composites. There are three types of fibres dominating civil engineering industry: glass, carbon and aramid fibres. In Table D.22 typical properties of FRP composites of interest to the structural designer are listed. Since FRP composite products are anisotropic, properties are reported for the longitudinal direction, the transverse direction, and the shear planes separately, where available.[T03, P75]

D.9.1 Properties

The mechanical properties of the fibers are displayed in Table D.22

<i>Property</i>	<i>Unit</i>	<i>E-Glass</i>	<i>SM-carbon</i>	<i>Aramid</i>
Density	Kg/m ³	2540	1800	1450
E-modulus	10 ³ N/mm ²	70	220-240	130
Tensile strength	10 ³ N/mm ²	1.7-2.7	3.5-4.5	3.0-3.5

Table D.22: Mechanical properties of different reinforcement fibres [B07, p21]

Fibers are of little use unless they are bonded together to make up a structural element that can carry loads. The binder material is normally called a matrix. Matrix materials can be polymers, metals, ceramics or carbon. The main application of these high-tech matrices is the aerospace industry and military [T03, P43].

<i>Property</i>	<i>Unit</i>	<i>Unsaturated Polyester Resin</i>	<i>Epoxy Resin</i>
Density	Kg/m ³	1150-1250	1150-2000
E-modulus	10 ³ N/mm ²	2.4-4.6	3.5
Tensile strength	10 ³ N/mm ²	40-85	50-90

Table D.23: Mechanical properties matrices [B07, p21]

In the table below mechanical properties of different unidirectional reinforced composites are given. These values are based on the characteristic values of the material obtained from specified number of tests [B07, p21].

<i>Property</i>	<i>Unit</i>	<i>FRP E-glas</i>	<i>E FRP SM-carbon</i>	<i>FRP HM-aramid</i>
Density	Kg/m ³	2000	1550	1350
E-modulus	10 ³ N/mm ²	40	130	75
Long. tensile	10 ³ N/mm ²	800	1550	1400
Long. compression	N/mm ²	500	1250	270

Table D.24: Mechanical properties of different composite based on fiber content of 60% [B07, p21]

The FRP is a composite material with two primary raw material , reinforcing fibers and a polymer resin matrix. The fibers content is from 20 to 60% [B08, p40]. The Polymer Resins is a macromolecules material which bind the fibers together.

D.9.2 Stress-strain curve

The stress-strain curve of the fibers under tension shows high tensile strength but brittle failure (see Figure D.26) [B08, p337]. It is interesting to look at an application of FRP in the infrastructure industry. Concrete column confined with FRP wrap subjected to axially load. The stress-strain curve (see Figure D.27). The unconfined column shows decrease in strength when the steel reinforcement yields. Since the FRP jacket is linear to failure, the strength of the confined RC column continues to increase until the FRP wrap fails. In this manner, FRP confining increases the contribution of the concrete in the internal force equilibrium rather than increasing the contribution of steel reinforcing [B08, 338].

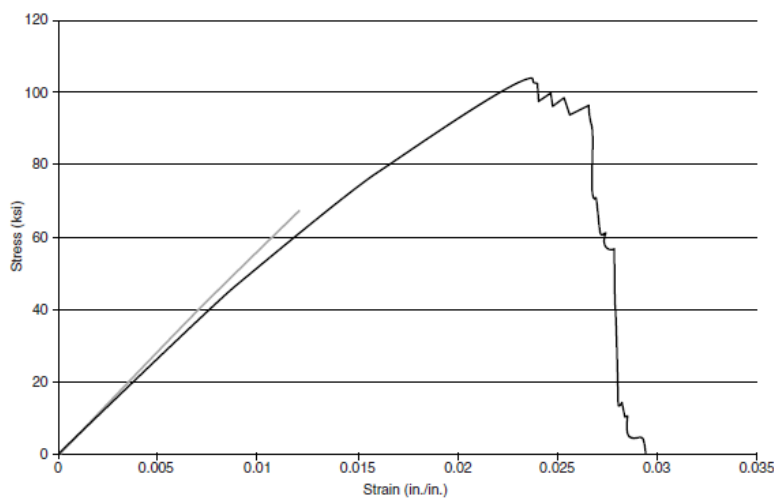


Figure D.26: Stress-strain curve of under tension glass fibers [B08, p337]

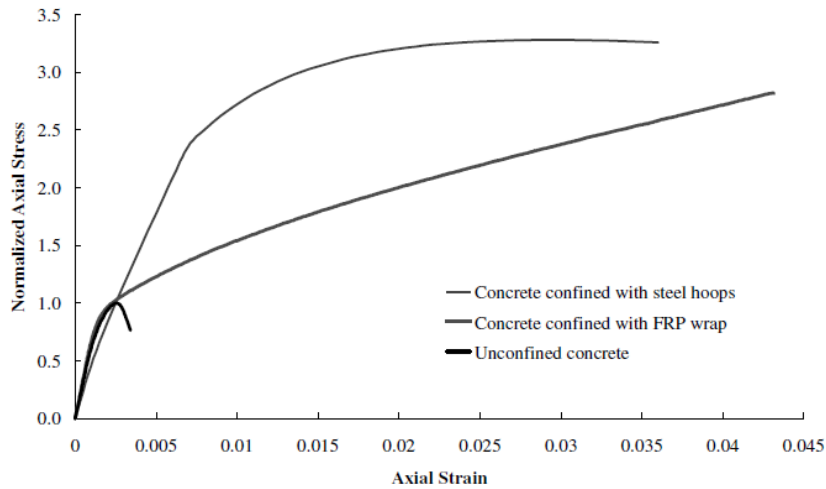


Figure D.27: Stress-strain curves for confined and unconfined concrete [B08, p337]

D.9.3 Creep

Since most fibers exhibit near-to-zero creep, in composites creep is largely dominated by the matrix. It is therefore unlikely that significant creep problems will arise in loading along the fibre direction of the material, while loading in the off-axis direction may result in excessive deformations. [B08, p47]

D.9.4 Shrinkage

The epoxy resin (Unsaturated Polyester Resin) offers high resistance to environmental conditions and behaves less brittle with very low shrinkage during curing. [B08, p47]

D.9.5 Freeze-thaw

Composites do not suffer from corrosion and offer much better resistance to freeze-thaw cycles than traditional materials, elongating the service life of structures up to an estimated 75 years [T04, p25]

D.9.6 Curing and finishing

When the suitable curing agent, catalyst or accelerator is added to this substance, these chains begin to cluster and form a solid, three dimensional structure. Performing this curing process in a controlled environment will dramatically increase the quality of the FRP product [T04, p09]. Curing time is in generally very short due to the prefabrication of the element.

D.9.7 Durability

A major advantage of most composites is that their corrosion-resistance is remarkably better than that of the traditional building materials concrete and steel his is why the general agreement on durability of FRP composites is that their durability is better overall than that of traditional materials. However it is also clear that durability of FRP composites is still an area which does require further research in order to gain a greater understanding of the characteristics over longer periods of time. [B09, p497]

D.9.8 Costs

Currently the production costs of fiber reinforced polymer bridge decks are still higher than conventional concrete or steel decks. However, certain other characteristics, like the corrosion resistance, good fatigue behavior , the long service life, rapid installation, reduced labor costs and minimizes traffic delays can make fiber reinforced decks competitive or even cheaper than traditional decks.

The issue is the raw materials. These are produced at high temperatures in industrialized processes that require highly specialized equipment and control which is very costly.If the production costs can be reduced the future of this material will be promising.

D.9.9 Result

- a. High strength values
- b. Linear-elastic stress-strain behavior up to failure of the fibers, low elasticity of the matrix material. With brittle failure. FRP confined concrete. FRP confined concrete shows.

Since the FRP jacket is linear to failure, the strength of the confined RC column continues to increase until the FRP wrap fails.

- c. Near to zero creep
- d. low shrinkage during curing
- e. Resistance to freeze-thaw
- f. X
- g. Short curing time
- h. High durability
- i. Very high material and production costs

D.10 Textile reinforced UHPC

Slender structural members can be applied due to the very small required cover. Can be applied in the infrastructure sector in bridges (Albstadt-Lautlingen Bridge and Creek Dollnitz bridge) with less steel reinforcement bars. Can be used as lightweight building material for facades. [P02, p512] [A11]

D.10.1 Properties

The bond behavior between the textile and the concrete is important aspect of this type of concrete. The bond behavior can meet the requirements by adding different materials to the mixture.

<i>Compression</i> [N/mm ²]	<i>Tension</i> [N/mm ²]	<i>Flexural</i> <i>strength</i> [N/mm ²]	<i>Shear</i> ⁴ <i>strength</i> [N/mm ²]	<i>E-modulus</i> [10 ³ * N/mm ²]
74-86	4.4-8	5.8-19.4	5	21-35

Table D.25: 28 days properties [P02, p516]

<i>Cement</i>	<i>Fly ash</i>	<i>Silica</i> <i>fume</i>	<i>siliceous fines</i>	<i>siliceous sand</i>	<i>fibers</i>	<i>w/c</i>
25-60%	9-12%	2-12%	26-10%	9-37%	0-3 Vol%	0.36-0.57

Table D.26: Mix design [P02, p512]

D.10.2 Shear strength

The use for TRC is very wide. One application of this material is shear strengthening of RC beam. An experiment conducted in Clermont university of French tried to find the in-plane shear behavior of TRC. Based on new in-plane shear test the ULS shear stress od ca. 5 N/mm² is derived. [T11]

⁴ In plane shear strength [T11]

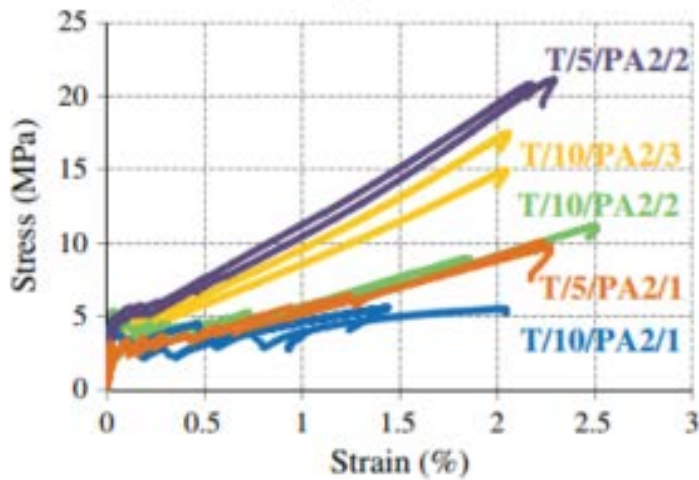


Figure D.28: Stress-strain curve of in-plane shear test

D.10.3 Stress-strain curve

Similar to steel reinforced concrete textile reinforced concrete is able to carry high tensile loads by the use of high strength alkali resistant (AR) glass textiles. However, textile reinforced concrete exhibits a crack formation phase with high strains which is disadvantageous at the verification of serviceability. Furthermore, fine grained concrete and glass, considered individually, show a brittle fracture behavior.

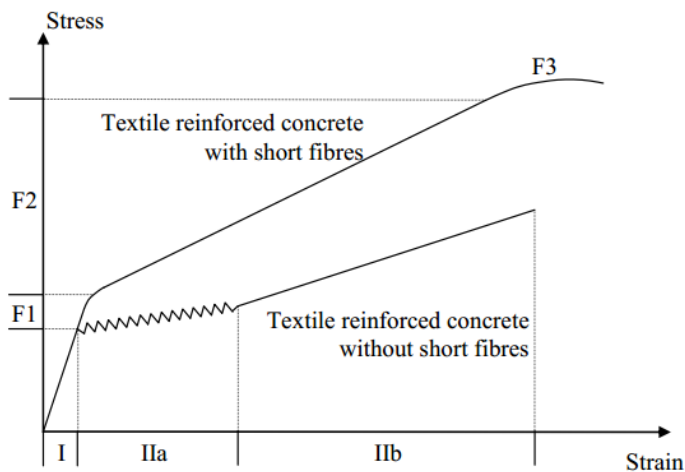


Figure D.29: Stress-strain curve of TRC with and without short fibers

D.10.4 Creep

Investigations regarding creep behaviour and fatigue strength of the fine grained concrete resulted in similar characteristic values as for normal concrete

D.10.5 Shrinkage

The shrinkage measured for the TRC mix-design given in Table D.26 obtain values of 0.84mm/m to 1.88mm/m.

D.10.6 Freeze-thaw

The new footbridge construction had to be given a slender superstructure, it fulfil increased demands regarding freeze-thaw cycles (Albstadt-Lautlingen TRC bridge) [A10]

D.10.7 Durability

Textile have no risk of corrosion, ingress of chloride of carbonation. [A11]

D.10.8 Costs

Just like other innovative concrete materials, also here the raw material costs and the prefabrication costs are higher than conventional reinforced concrete.

D.10.9 Result

Poor Fair Neutral Good Excellent

Explanation:

- a. High compression strength, tensile strength similar to ordinary concrete
- b. Similar to steel reinforced concrete the stress-strain curve
- c. X
- d. X
- e. Fulfil the requirements
- f. X
- g. X
- h. Good Durability
- i. High material costs

D.11 Strain Hardening Cementitious Composites

SHCC is composite concrete with moderate tensile strength and ductility. UHPFRC have high tensile strength, high flexural strength as well as extreme high compressive strength but reach these strengths at moderate strain number. In SHCC cracks are controlled over wide range of strain.

D.11.1 Properties

The mechanical properties of SHCC, also referred to as Engineered Cementitious Composite, are displayed in Table D.27. Compressive strength of SHCC is measured on 100mm cube based on uniaxial test. [A20]

<i>Compression</i> [N/mm ²]	<i>Tension</i> [N/mm ²]	<i>Shear strength</i> [N/mm ²]	<i>E-modulus</i> [10 ⁹ * N/mm ²]
32-60	3-8	5	16-20

Table D.27 : Mechanical properties SHCC [A20] [B11, p101, p17 , p12]

<i>Cement</i>	<i>Fly-ash</i>	<i>Aggregate</i> (<i>fine</i>)	<i>Water</i>	<i>Slag</i>	<i>fibers</i>	<i>w/c</i>
23%	26%	26%	21%	3%	1.5-2.5 Vol%	0.8

Table D.28: Mix-design of SHCC [P11]

In Table D.28 typical mix-design of SHCC is given. All experimental results given in the following sections are based on the specimens with the mass properties in Table D.28.

D.11.2 Stress-strain curve

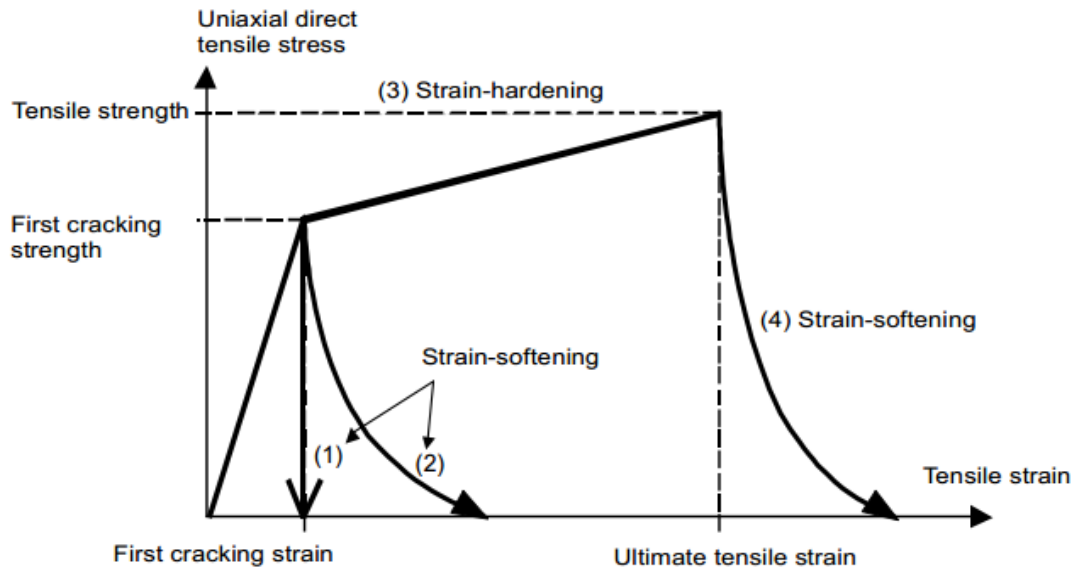


Figure D.30: Concept of strain hardening and strain softening under tensile stress [C07]

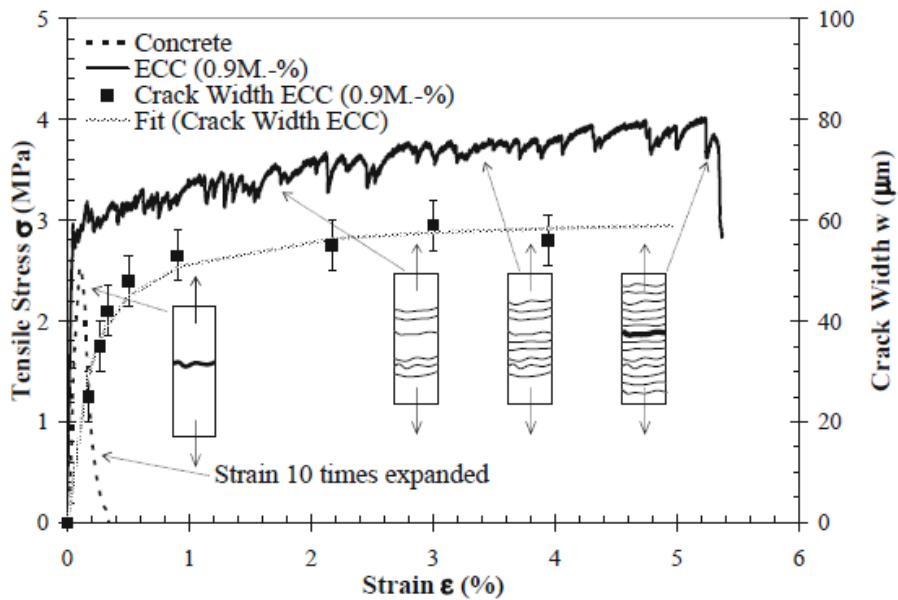


Figure D.31: Strain hardening behavior of SHCC and UHPFRC under direct tension load [PB11]

In plain concrete or mortar, the first crack under direct tension leads to sudden loss of tensile resistance. At crack initiation in FRC, fibres bridge the matrix crack, leading to a reduced rate of strength loss with increased tensile deformation. In SHCC the fibres crossing the first matrix provide sufficiently high resistance that another crack arises in the matrix. This process continues, leading to multiple cracks. (see Figure D.31). The tensile ductility of the SHCC is obtained through balanced fiber and matrix properties, to allow effective crack bridging by the fibers. [A20]

D.11.3 Creep

According to [B10] there is a little information on the creep behavior of SHCC in field of application. However, laboratories tests indicates that the crack control holds the key to understanding and predicting the SHCC short and long term behavior

From a study after the time-deepened behavior of SHCC it is appear that the main creep mechanism are (i) crack initiation, (ii) width evolution of cracks due to fibers pull-out and (iii) matrix creep. In ordinary reinforced concrete high sustained loads will lead to time-depended failure. Tests have been shown that the particular mechanism, fiber creep doesn't have significant contribution in SHCC long-term behavior. The study have also show that uncracked matrix creep is smaller relative to the time-depended deformation of cracked specimens. Which implies that the second creep mechanism is the dominant. A link between single fibre pull-out response (governing creep mechanism) and macroscopic behavior of the composite has been made [P11] .

D.11.4 Shrinkage

According to Weimann & Li (2003) the drying shrinkage of SHCC is in the range of 0.17%-0.25%. This includes the temperature different of 50 degrees which imposed thermal strain of 0.05%. The autogenous shrinkage of SHCC indicates rapid shrinking development of 0.03% at the first two days after casting and 0.06% of autogenous shrinkage 46 days after casting (Weimann & Li ,2005).

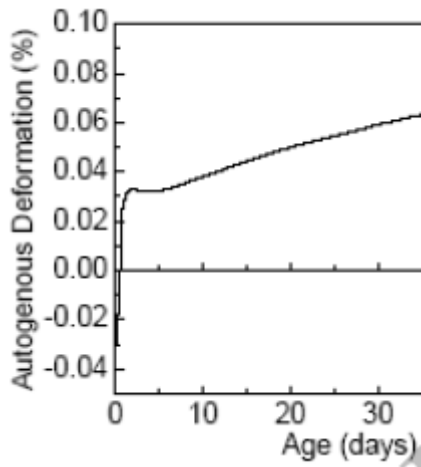


Figure D.32: Autogenous shrinkage (Wang & Li 2005)

D.11.5 Freeze-thaw

Cyclic freezing and thawing is one of the most damaging environmental conditions for concrete. Testing Freeze-thaw was performed by Li et al (2003) with companions series of SHCC and normal concrete specimens. After 14 weeks of freeze-thaw exposure (110 cycles) the normal concrete has been severely deteriorated. However, all SHCC specimen survived 300 cycles with no degradation. This result in a durability factor of 10 for concrete compared to 100 for SHCC. It is noted that the high durability was achieved without deliberate air entrainment into SHCC. [B10, p67]

D.11.6 Curing

The thermal load caused by the heat of hydration has not been enough studied, SHCC required more cement than normal concrete does. Generating more heat of hydration. The heat will cause temperature gap between the inside and outside of construction material leading to crack formation. n. However, it is expected that the replacement of some cement by expanding cement can be effective in reducing the heat.

D.11.7 Durability

The SHCC, material with moderate fibers volume and tight crack control over large strain range archive his durability through crack width limitation. SHCC can resist long-

term moisture and chloride diffusion through this crack control to fine widths. The material has low permeability also during the strain-hardening stage when micro-cracks are present. [B11, p0-38]

These reduced, finely-distributed cracks can provide good resistance to penetration of water and/or aggressive substances from the environment. So applying SHCC is possible to improve durability of RC structures exposed to aggressive environment such as chloride penetration, Alkali aggregate reactions and sulphate attack. [B11, p40]

D.11.8 Costs

This innovative concrete material meets the challenge of sustainable built environment for green infrastructure. The usage of SHCC as bridge replacement element in the USA is resulted in one third reduction in bridge life cycle energy consumption compared to traditional bridge.

Total economic costs are reduced by 15% as result of less maintenance and lower construction traffic congestion. However, due to SHCC high performance and exceptional raw material requirements demand almost double energy consumption per cubic meter SHCC compared with conventional RC. But due to reduction in construction event during the lifetime of the bridge significant energy is saved. [B11, p125]

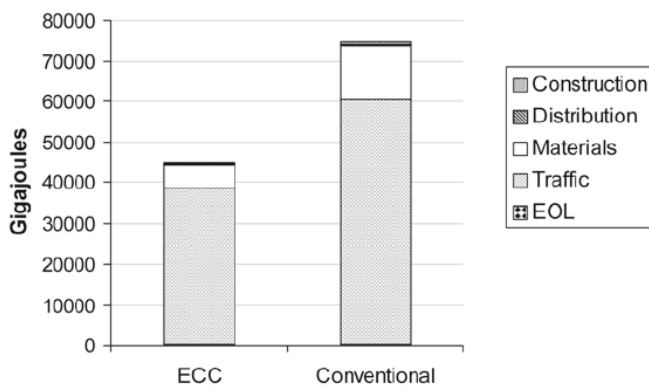


Figure D.33: Total primary energy consumption by life cycle stage for and SHCC link slab bridge and conventional jointed bridge. [B11, p125]

According to Keoleian (2005) [P13] the ECC (referred as SHCC) costs two to three times more per unit volume than conventional concrete. In part, this reflects the higher energy intensity of ECC due to more cement and the addition of fibers in the mixture.

D.12 Geopolymer Concrete (GC)

Non-Portland binder may be used as an alternative to the Portland cement in concrete in order to address the environmental issues.

D.12.1 Properties

<i>Compression</i> [N/mm ²]	<i>Tension</i> [N/mm ²]	<i>Bending</i> <i>strength</i> [N/mm ²]	<i>Shear</i> <i>strength</i> [N/mm ²]	<i>E-modulus</i> [10 ³ * N/mm ²]
30-50	4-5.5	2-3	0.9-1.2	22-29

Table D.29: Mechanical properties GC

<i>Cement</i>	<i>Water</i>	<i>Fly ash</i>	<i>Coarse aggregate</i>	<i>Fine aggregate</i>	<i>Sodium hydroxide solution</i>	<i>Sodium silicate solution</i>	<i>Superplasticizer</i>
0%	0%	17%	53%	23%	1.7%	4.2%	0.3%

Table D.30: Geopolymer Concrete mixture proportions on fly ash-based(s (Wallah and Rangan, 2006)

D.12.2 Shear strength

Chang et al (2007) studied the shear and bond strength of reinforced geopolymer concrete beams. The failure modes and crack patterns observed for reinforced geopolymer concrete beams were similar to those reported in the literature for reinforced Portland cement concrete beams.

The design provisions contained in the American Concrete Institute Building Code ACI318-08 are found to give conservative predictions for the shear strength and bond strength of reinforced geopolymer concrete beams; these design provisions are, therefore, applicable to design of reinforced geopolymer concrete beams. [T08]

D.12.3 Stress-strain curve

The behavior and failure mode of fly ash-based geopolymer concrete in compression is similar to that of Portland cement concrete with a strain peak of 0.0024-0.0026 (Hardjito and Rangan, 2005).

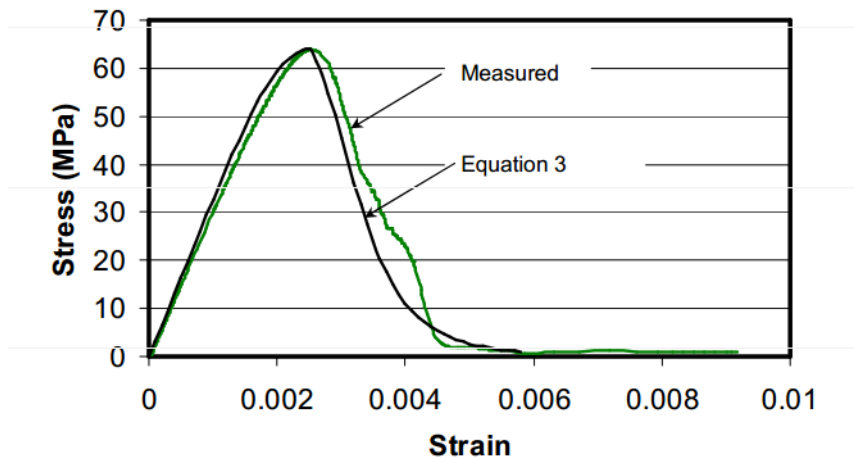


Figure D.34: Stress-Strain Relation of Geopolymer Concrete in Compression (Hardjito and Rangan, 2005)

D.12.4 Creep

Creep behavior of GC was studied for a period of one year by Wallah and Rangan (2006). The results of their study indicate creep coefficient between 0.4 and 0.8 correspond with compressive strength between 40 -67Mpa. This is found by the ratio of creep strain-to-elastic strain after one year of loading.

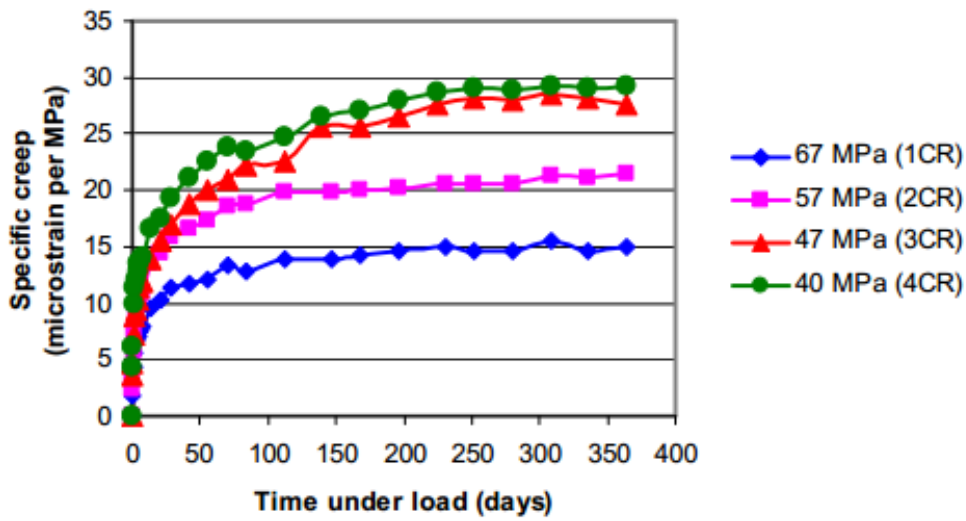


Figure D.35: Effect of Compressive Strength on Creep (Wallah and Rangan 2006)

D.12.5 Shrinkage

Drying shrinkage behavior was also part of the one year study of Wallah and Rangan. The results shows that GC undergoes very little drying shrinkage in the order of about 0.1×10^{-3} after one year. This value is smaller than ordinary concrete with drying shrinkage value of $0.5-0.8 \times 10^{-3}$.

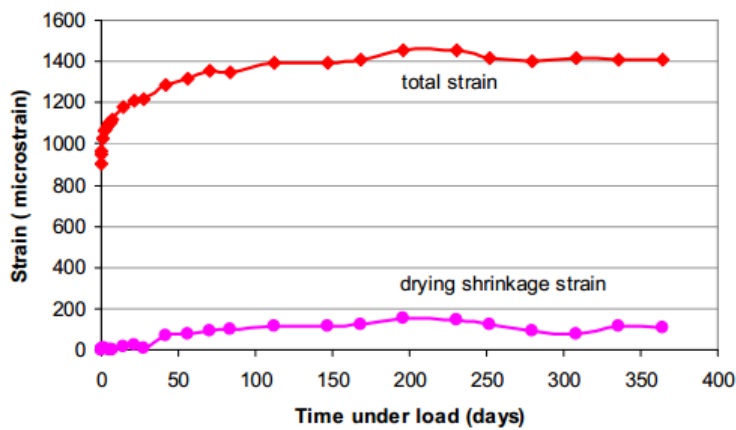


Figure D.36: Total Strain and Drying Shrinkage Strain (Wallah and Rangan, 2006)

D.12.6 Freeze-Thaw

According to the Joseph Davidovits (*Geopolymer Chemistry and Applications*) mass loss smaller than 0.1% and strength loss smaller than 5% is observed after 180 freeze-thaw cycles.

D.12.7 Curing

Both curing time and curing temperature influence the compressive strength of geopolymer concrete. The effect of curing time is illustrated in Figure D.37. h. The rate of increase in strength was rapid up to 24 hours of curing time; beyond 24 hours, the gain in strength is only moderate

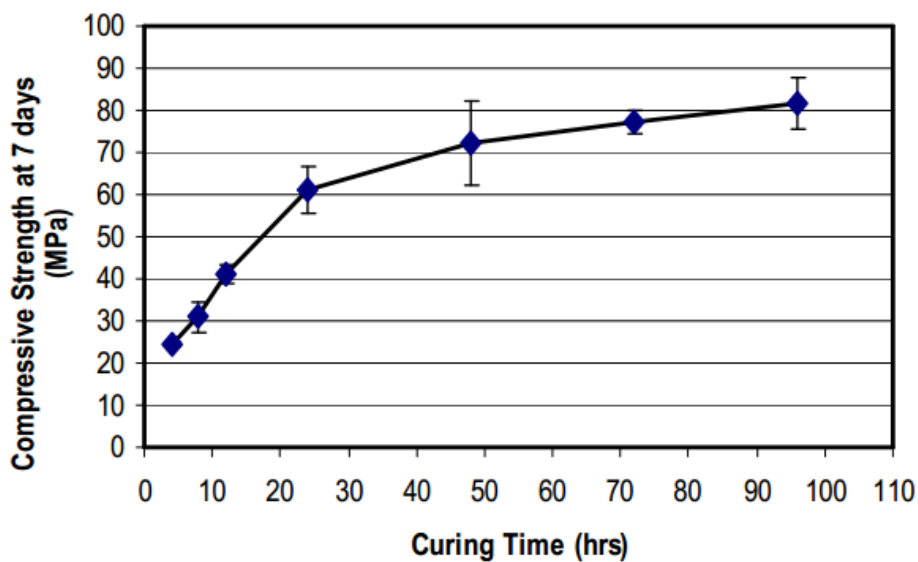


Figure D.37: Effect of Curing Time on Compressive Strength of Geopolymer Concrete (Hardjito and Rangan, 2005)

Moreover, the effect of curing temperature on the compressive strength indicate larger compressive strength for higher curing temperature. (Hardjito and Rangan, 2005). The required heat-curing regime can be manipulated to fit the needs of practical application. Therefore precasting is recommended.

D.12.8 Durability

The GC is a durable material with excellent resistance to chemical attack and shows promise in use of aggressive environment.

D.12.9 Costs

Comparison studies shows that geopolymer concrete can be prepared at comparable cost with that of OPC concrete while they offer huge reduction in carbon dioxide emissions.

E. Stress-strain relationship

The stress-strain curves given in Section 0 is explained in this Appendix.

E.1 Normal strength concrete

This type of concrete is generally defined as conventional concrete up to strength class of C55/67. The stress-strain relation in the graph are taken from the Eurocode (EN-NEN 1992). These compressive strength and strain values are determined with uniaxial compressive test while the tensile strength and strain are determined with 3-points bending test. The Concrete shows very small tensile strain and stress. Moreover the concrete becoming more brittle with increasing stiffness.

<i>Eurocode</i>	<i>Symbol</i>	<i>Value</i>
Characteristic compressive strength	f_{ck}	55 MPa
Bi-linear strain	ϵ_{lc3}	1.8 ‰
Bi-linear strain	ϵ_{luc3}	3.1 ‰
Characteristic tensile strength	$f_{lctk\ 0.05}$	5.5 MPa
Characteristic tensile strain	ϵ_{lct}	0.1 ‰

Table E.1: Governing mechanical properties

E.2 High strength concrete

This type of concrete which still given in the Eurocode (EN-NEN 1992) is valid for concrete classes from C55/67 up to C90/105. The concrete is relatively brittle due to increasing of the stiffness. With upper bound of the tensile strength of 6.6 N/mm².

<i>Eurocode</i>	<i>Symbol</i>	<i>Value</i>
Characteristic compressive strength	f_{ck}	90 MPa
Bi-linear strain	ε_{lc3}	2.3 ‰
Bi-linear strain	ε_{luc3}	2.6 ‰
Characteristic tensile strength	$f_{lctk\ 0.05}$	6.6 MPa
Characteristic tensile strain	ε_{lct}	0.1 ‰

Table E.2: Governing mechanical properties

E.3 Fibre reinforced high strength concrete

Also here the upper bound value is used of C90/105. This type of concrete is still under the regulation of the Eurocode (EN-NEN 1991) but determining the stress-strain diagram will be more complicated due to the steel fibers. For this low concrete class the French guideline (AFGC/SETRA) cannot be used. Also the Dutch guidelines (CUR-Aanbeveling 111) is not suitable for thick beams. Due to lack of experimental data the Canadian Highway bridge design code (CAN-06), Japanese code (JAP 06) and the French recommendation will be combined to simplify the determination of stress-strain curve.

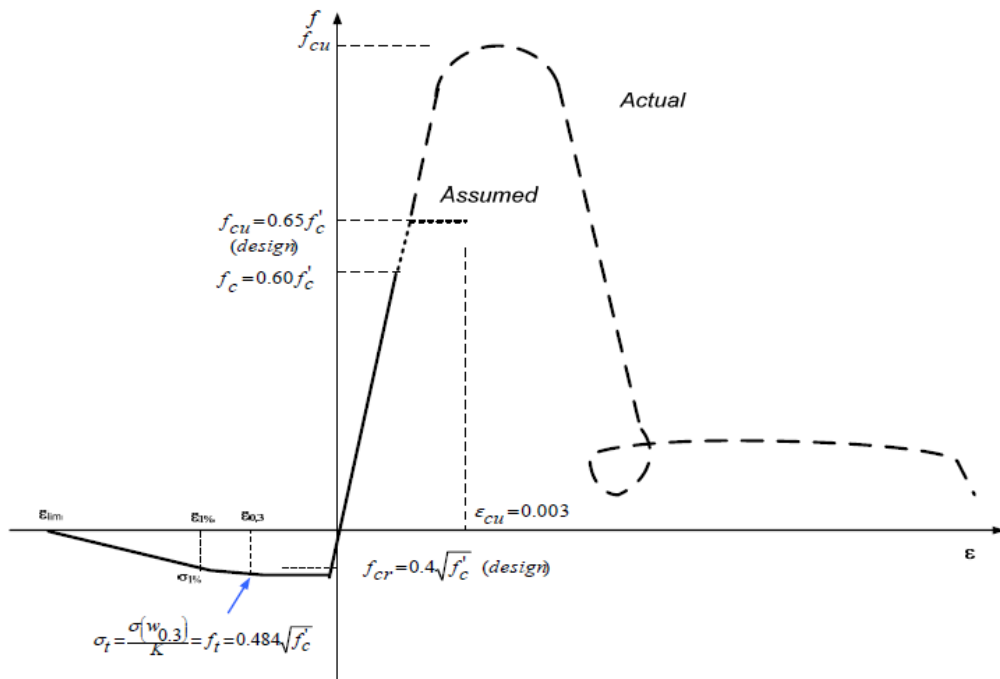


Figure E.1: Assumed tensile and compressive behavior HPFRC [B01,p295]

The governing parameters for the stress-strain diagram:

The design compressive strength $f_{cu} = 0.65 f'_c$

Design tensile strength by first crack $= 0.4 \sqrt{f'_c}$

Design tensile strength by $w=0.30$ mm $f_t = 0.484 \sqrt{f'_c}$

The Characteristic strain by $w=0.30$ mm = +

With $= 0.30$ mm and $= \frac{2}{3} h$

	<i>Eurocode symbol</i>	<i>HPFRC</i>
Compressive strength (f'_c)	f_{ck}	90 MPa
Design compressive strength (f_{cu})	f_{cd}	60 MPa
E-modulus (E_{ij})	E_{cm}	44000 MPa
Bi-linear compressive strength (ε_{cu})	ε_{cu3}	2.60 ‰
Characteristic tensile strength by first crack ()	f_{ctd1}	3.8 MPa
Stain by first crack ()		0.1 ‰
Characteristic strain by $w = 0.30mm$ ()		
Characteristic tensile strength by complete cracking ()	f_{ct2}	4.60 MPa
Limit strain (ε_{lim})		5 - 25 ‰
h	-	1000mm

Table E.3: Governing mechanical properties

E.4 Ultra-high strength fibre reinforced concrete

The properties of this concrete is defined by the French AFGC/SETRA. According to this code the compressive strength will be between 150 - 250 MPa, and contain steel fibers in order to achieve ductile behavior under tension. In this graph the BSI Ductal® UHPFRC will be used in the stress-strain diagram. Testing a 7*7*28 cm prism specimen of BSI200 Ductal® obtained the following results:

Mean direct tensile strength (maximum force divided by sectional area):

10.27 MPa

Standard deviation: 1.19 MPa

Design value: 8 MPa

The stress-strain diagram of UHPFRC is given in the following two figures, the first one is valid for stress-hardening post-cracking behavior and the second figure is valid for post-cracking stress-softening behavior.

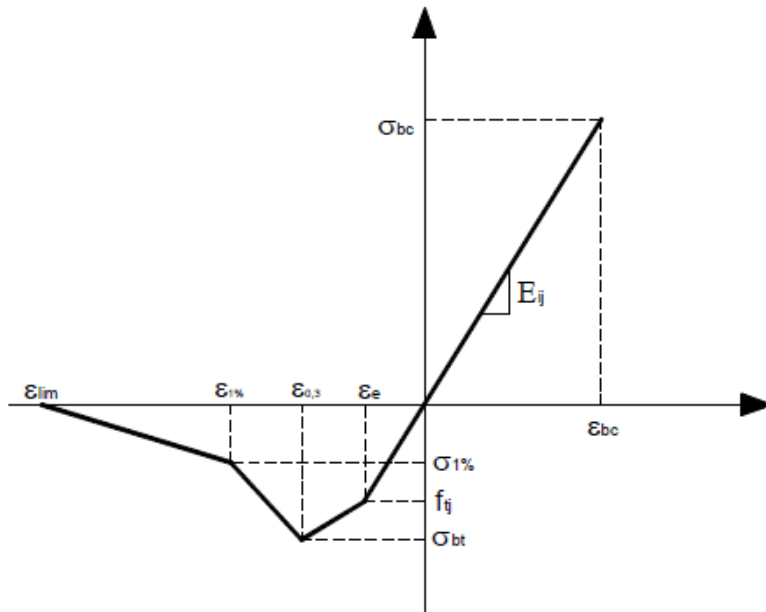


Figure E.2: ULS Stress - strain hardening relationship UHPFRC [CUR-Aanbeveling 111]

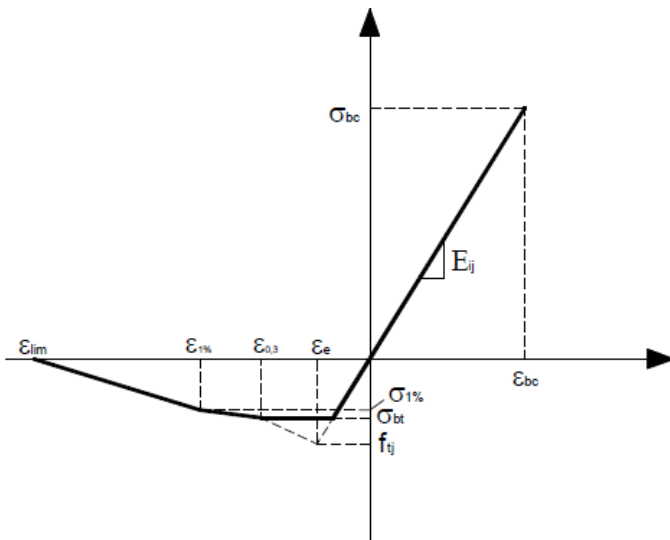


Figure E.3: ULS Stress - strain softening relationship UHPFRC [CUR-Aanbeveling 111]

The failure under compressive and tensile stresses is rather more ductile compared to UHPC without fibers. Of course this depend on the shape, amount and orientation of the fibers.

Minimum percentage fibers for strain-hardening behavior:

100

The governing parameters for the stress-strain diagram:

Ultimate strain by failure = 3 ‰

Stain by first crack

Strain by crack width of 0.3mm

Where = 0.3mm and

Strain by crack width of 1% of the specimen height

Where =0.01h h=height of specimen in mm

Maximum strain =

Where is the fiber length in mm

Characteristic length = h with beam height (h)

The stresses will be calculated with the following expressions:

$$\sigma_{bc} = 0.6 \cdot f_{cj}$$

$$\sigma_{bt} = \frac{\sigma_0}{k}$$

Where σ_0 the characteristic stress for $\varepsilon = \varepsilon_{1\%}$

<i>AFGC/SETRA</i>	<i>Eurocode symbol</i>	<i>UHPFRC</i>
Compressive strength (σ_{bc})	f_{ck}	170 MPa
E-modulus (E_{ij})	E_{cm}	50000 MPa
Characteristic tensile strength by first crack ($\sigma_{w0.30}$)	f_{ctk1}	8.0 MPa
Strain by first crack ($\epsilon_{w0.30}$)		0.160 ‰
Characteristic strain by $w = 0.30\text{mm}$ ($\epsilon_{w0.30}$)		$450/h + 0.160$
Characteristic tensile strength when $w = 0.30\text{mm}$ ($\sigma_{(w0.30)}$)	-	12 MPa
Characteristic tensile strength by complete cracking	f_{ct2}	9.6 MPa
Limit strain (ϵ_{lim})		$4875/h$ (5-25 ‰)
Fiber length (l_f)	-	13mm
h	-	1000mm

Table E.4: Overview material properties [Cement Rekenmodel VVUHSVB] [CUR-aanbeveling 111] [AFGC/SETRA]

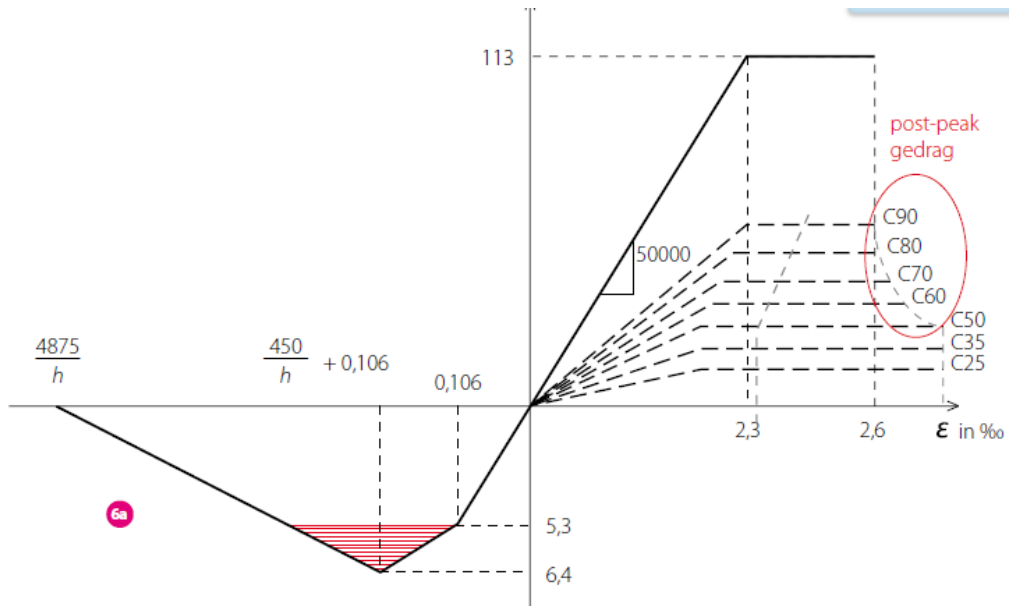


Figure E.4: Cement 2011-3 Rekenen met VVUHSB

E.5 Light weight concrete

The compressive strength of lightweight concrete is mainly determined by the strength and stiffness relationship between the aggregates and the matrix, and by the volume fraction of both. The less stiff aggregate which is usually in the same range of the matrix stiffness will result in different stress-strain curve. The curve is determined by the Eurocode [NEN-EN 1992 Art.11].

The governing parameters for the stress-strain diagram:

$$\text{E-modulus } E_{lc} = \eta_E \cdot E_c \text{ with } \eta_E = \left(\frac{\rho}{2200}\right)^2$$

The LC oven-dry density according to table 11.1 NEN-EN 1992

$$\text{Tensile strength } f_{lctk\ 0.05} = \eta_1 \cdot f_{ctk\ 0.05}$$

$$\text{Where } \eta_1 = 0.40 + 0.60 \frac{\rho}{2200}$$

<i>Eurocode</i>	<i>Symbol</i>	<i>Value</i>
Characteristic compressive strength	f_{lck}	55 MPa
LC oven-dry density	ρ	1740 kg/m ³
Coefficient	η_E	0.62
Coefficient	η_1	0.87
Bi-linear strain	ε_{lc3}	1.8 ‰
Bi-linear strain	ε_{luc3}	2.7 ‰
Characteristic tensile strength	$f_{lctk\ 0.05}$	2.4 MPa
Characteristic tensile strain	ε_{lct}	0.1 ‰

Table E.5: Governing mechanical properties

E.6 High volume fly-ash concrete

Fly-ash concrete based on geopolymer is used to replace the conventional Portland cement. The stress-strain curve represents HVFA concrete type F. Longer curing time will improve the compressive strength. Hardjito and Rangan (2005) published the stress-strain behavior of HVFA concrete.

The governing parameters for the stress-strain diagram:

$$\text{Coefficient } n = 0.8 + \frac{f_{cm}}{17}$$

$$\text{Coefficient } k = 0.67 + \frac{f_{cm}}{62}$$

Where the following expression is used to determine the stress-strain relation (Collins1993) :

$$\sigma_c = f_{cm} \frac{\varepsilon_c}{\varepsilon_{cm}} \frac{n}{n - 1 + \left(\frac{\varepsilon_c}{\varepsilon_{cm}}\right)^{nk}}$$

<i>Parameter</i>		
Strain at peak stress	ε_{cm}	2.5 ‰
Peak compressive strength	f_{cm}	55 MPa
Coefficient	n	4.0353
Coefficient	k	1.5571

Table E.6: Governing mechanical properties

E.7 Foamed concrete

Foamed concrete, also known as Cellular concrete is concrete with high air content (6-70%) which make it ultra-light-weight and workable material but may compromise the compressive strength. The stress-strain relations are determined according to [A27] with mean of three prisms tests. The tests are made for foamed concrete with compressive strength between 8-10 MPa.

E.8 Strain hardening cementitious composite

SHCC shows remarkably high ductility under uniaxial tensile stress and excellent performance distinguished from conventional cementitious materials by multiple cracking and strain hardening behavior. The tensile stress-strain curve proposed by the Japanese recommending is adopted as guideline. The ultimate strain-stress model differ from the experimental model as shown in figure xx

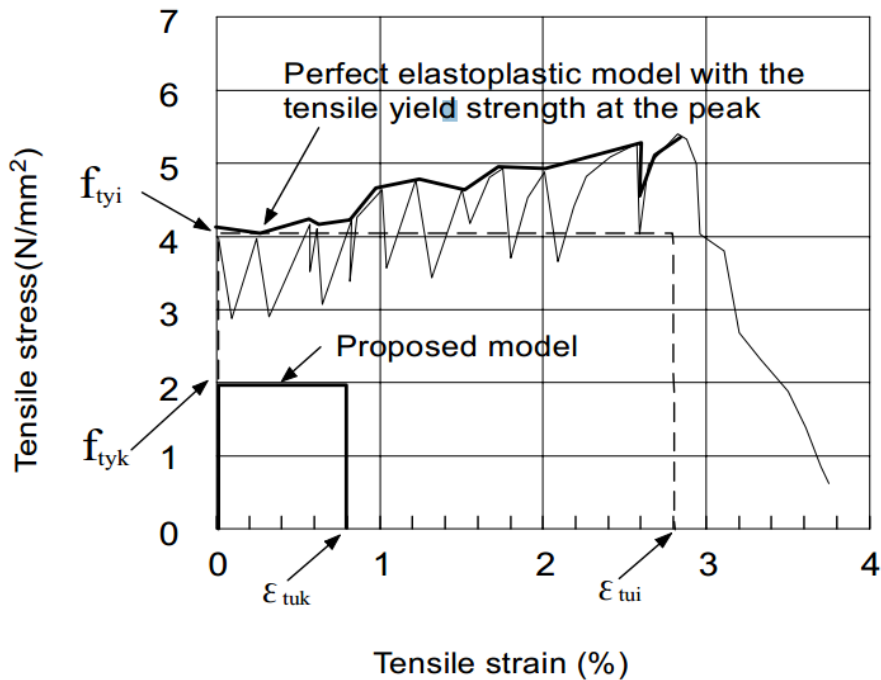


Figure E.5 Comparison between experimental results and the design stress-strain relationship [C07]

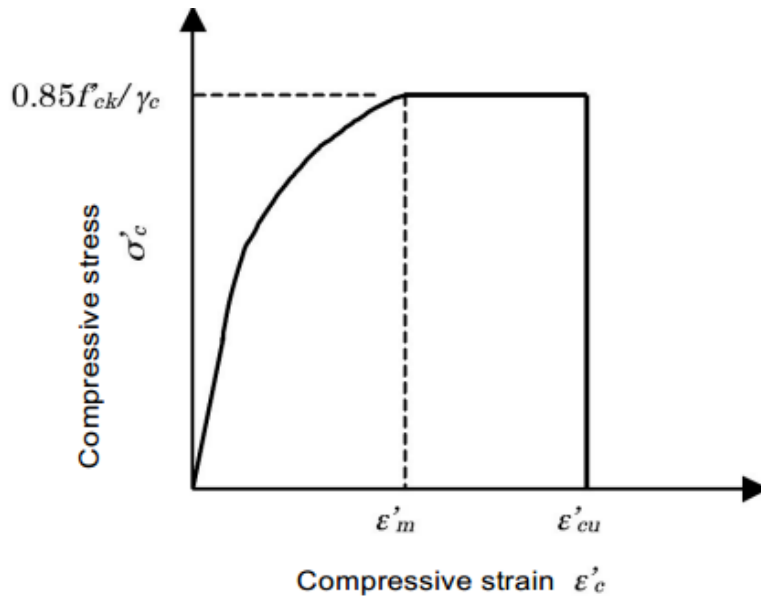


Figure E.6: Compressive strain-strain relationship model SHCC [C07]

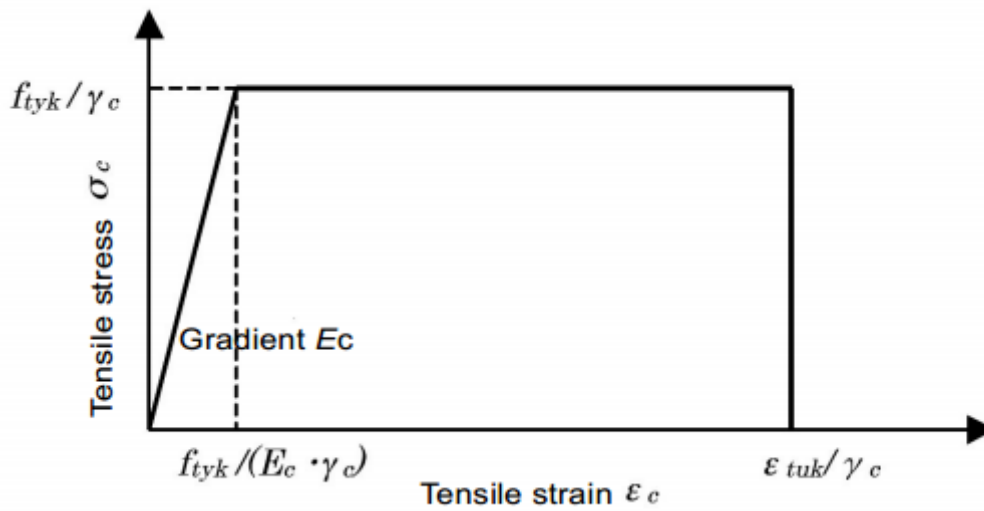


Figure E.7: Tensile stress-strain relationship model [C07]

The governing parameters for the stress-strain diagram:

For the initial curved zone $\sigma_c = 0.85 \frac{f_{ck}}{\gamma_c} \cdot \frac{\epsilon_c}{\epsilon_m} \left(2 - \frac{\epsilon_c}{\epsilon_m} \right)$

Design compressive strength $f_{cd} = 0.85 \frac{f_{ck}}{\gamma_c}$

Design tensile strength $f_{tyd} = \frac{f_{tyk}}{\gamma_c}$

Yielding strain $\epsilon_{c3} = \frac{f_{tyk}}{E_c \cdot \gamma_c}$

Ultimate strain $\epsilon_{cu3} = \frac{\epsilon_{tuk}}{\gamma_c}$

Young's modulus $E_c = 1.77 \cdot 10^4 \cdot \sqrt{\frac{\gamma}{18.5}} \cdot \left(\frac{f_{ck}}{60}\right)^{1/3}$

<i>Parameter</i>	<i>Symbol</i>	<i>Value</i>
Characteristic compressive strength	f_{ck}	55 MPa
Ultimate compressive strength	f_{cd}	36.6 MPa
Strain at maximum compressive stress	ϵ_m	3.0 ‰
Ultimate compressive strain	ϵ_{cu}	3.0 ‰
Characteristic tensile strength	f_{tyk}	2 MPa
Design tensile strength	f_{tyd}	1.3 MPa
Young's modulus	E_c	17000 MPa
Uncracked tensile strain	ϵ_{ct}	0.08
Ultimate tensile strain	ϵ_{ctu}	8

Table E.7: Governing mechanical properties

E.9 Self-compacting concrete

Very little is known about the differences between the stress-strain behavior of SCC and that of CC. The ascending part of the stress-strain curve. When SCC was produced with limestone filler, cement kiln dust or ground granulated blast-furnace slag, the fracture toughness was height than for CC. The strain softening behavior of SCC and CC are comparable for the same compressive strength level. [B12, p34-36]

The tensile behavior and the modulus of elasticity of SCC can be predicted by the expression given in the Eurocode [NEN-EN 1992]

F. Simplified ULS Calculation

F.1 Actions

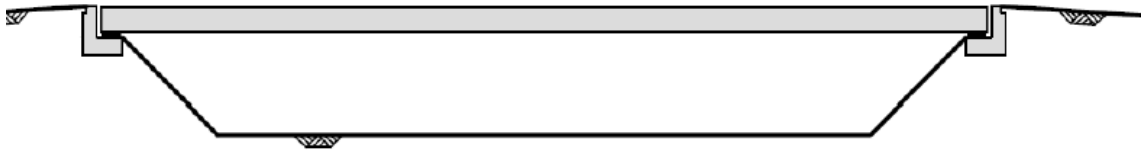


Figure F.1: Homogenous symmetrical bridge beam

In this appendix the actions acting on the bridge carriageway will be derived. The actions are transferred to the beams which transfer the actions to the substructure. The following actions will be accounted for:

		<i>Type</i>	<i>Load group</i>
SW	self-weight	permanent	G
DL	dead load	permanent	G
AS	asphalt	permanent	G
CR	creep and shrinkage	variable	CR
UDL	uniform distributed load	variable	LM1
TS	abnormal load	variable	LM1
TE	temperature	variable	TE

Figure F.2: Main actions on carriageway

F.2 Permanent loads

Self-Weight

The self-weight of the construction will be determined according to the dimensions of the beam which are constant in this simplify analysis. The cross-sectional area is multiplied with the corresponded material density given in Appenix D and the partial load factor ($\gamma_G = 1.2$).

$$q_G = A_c \cdot \rho_c \cdot \gamma_G \quad [kN/m]$$

Dead loads

The assumptions for the derivation of the dead loads are:

- | | | |
|-------------------------------------|----------------------------|---|
| 1. Asphalt deck | 3.91 kN/m ² | (0.17 m*23 kN/m ³) |
| 2. Deck | Variable kN/m ² | ($h * \rho_c$) |
| 3. Stringcourse | 12.5 kN/m ² | (0.3 m*25 kN/m ³ + 5 kN/m ²) |
| 4. Longitudinal line loads on edges | | |
| - Noisebarrier | 9.2 kN/m | |
| - Guardrail | 0.5 kN/m | |
| 5. Safety rails | 1.0 kN/m | |

F.3 Variable loads

Traffic loads

The variable loads acting on the bridge will be limited to the vertical traffic loads according to LM1 and LM2 where LM2 is applicable for local actions on the bridge deck.

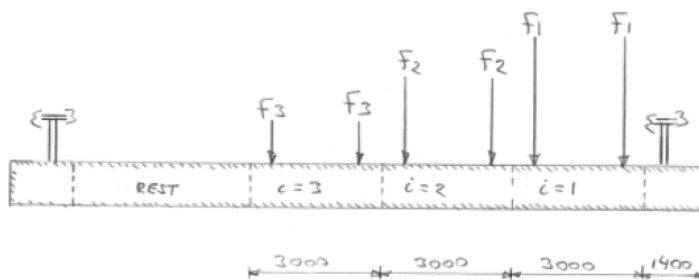


Figure F.3: Traffic loads on deck

	<i>Tandem system [kN]</i>	<i>UDL q_{ik} [kN/m²] * α_{qi}</i>
Lane 1	300	10.35
Lane 2	200	3.5
Lane 3	100	3.5
Other lanes	0	2.5
Remaining area	0	2.5

Table F.1: Load Model 1 conform table 4.3 NEN-1991-2, tandem system with uniform distributed loads (UDL)

6. LM1 UDL

- Lane 1 10.35 kN/m²
- Lane 2 3.5 kN/m²
- Lane 3 3.5 kN/m²
- Restlane 2.5 kN/m²

7. LM1, TS

- Lane 1 2 * 300 kN
- Lane 2 2 * 200 kN
- Lane 3 2 * 100 kN

Loads on stringcourse

The stringcourse is subjected to vertical pedestrian loads of 5 kN/m² on the total width of the stringcourse. Furthermore the self-weight of the stringcourse is accounted for.

F.4 Equivalent UDL load

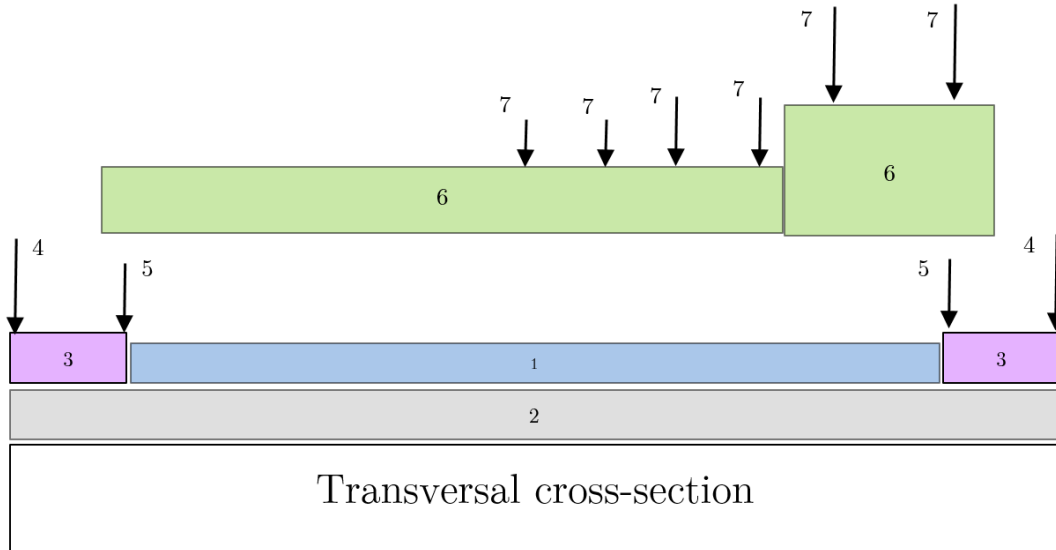
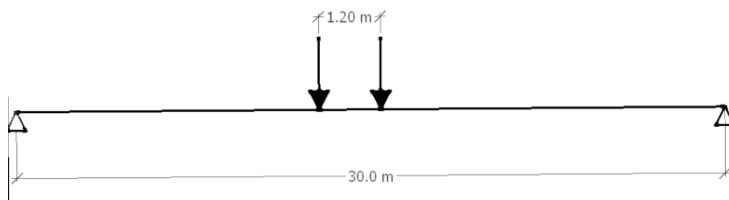


Figure F.4: Vertical actions on the bridge (transversal view) B=15.0 m

The actions on the superstructure according to the NEN-1992-2 which is given in Figure F.4 is calculated in a spreadsheet allowing repeated calculations for different scenarios. The deck is considered as orthotropic which means that the dispersal of the concentrated loads (4, 5 and 7 Figure F.4), associated with LM1 should be taken according to art 4.3.6 NEN-EN 1991-2.

In order to determine the load we model the carriageway with 3 virtual lanes each 3.0 m width. The entire width of the carriageway is subjected to (7) TS load and (6) UDL. The maximum field moment (M_{Ed}) is wanted.

The maximal moment caused by (6) is expressed as equivalent UDL:



$$F * 0.5(L - 1.2) = \frac{1}{8} q_{eq} L^2$$

$$q_{eq,i} = F * \frac{4(L - 1.2)}{L^2} \left[\frac{kN}{m} \right]$$

Figure F.5: Maximum moment

F.4.1 Load dispersal

When the wheel loads on the bridge carriageway falls nearby the supports, shearing will be the governing failure mechanism. The concentrated loads will be spread in the lateral direction with the traditional 45° from the centre of the concentrated load to the supporting point.

F.4.2 Superposition

The concentrated forces over width of the carriageway (b) will be spread over the effective width (b_{eff}). The line load (q_{UDL}) and the self-weight (q_G) will be spread over the effective width (b). The superposition principle applied to find the equivalent UDL is illustrated in Figure F.6 whereby the TS load is decomposed to equal concentrated loads.

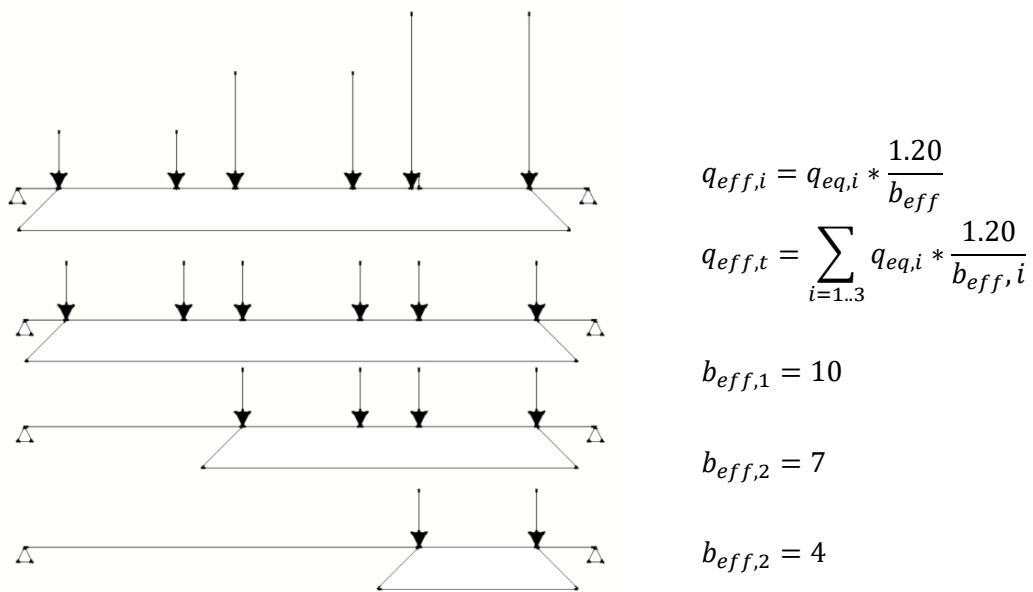


Figure F.6: Superposition principle TS load

Figure F.7: Governing field moment M_{Ed}

The field moment in the longitudinal direction caused by (6) and (7) is calculated for part of the bridge with width of 1.20 m (distance between wheels of vehicle).

<i>Tandem system</i>		
$F_{l,1}$	[kN]	300
$F_{l,2}$	[kN]	200
$F_{l,3}$	[kN]	100
$b_{long,TS}$	[m]	1.2
$b_{trans,TS}$	[m]	2
M_1	[kNm]	4320
M_2	[kNm]	2880
M_3	[kNm]	1440
$b_{eff,1}$	[m]	10
$b_{eff,2}$	[m]	7
$b_{eff,3}$	[m]	4
$q_{eq,1}$	[kN/m]	4.6
$q_{eq,2}$	[kN/m]	4.4
$q_{eq,3}$	[kN/m]	3.8
Uniform distributed load		
Lane 1	[kN/m]	7.61
Lane 2-3	[kN/m]	3.5
Restlane	[kN/m]	3.5
Total live loads governing lane		
$q_{Q,k}$	[kN/m]	20.4
$q_{Q,d}$	[kN/m]	30.7

Table F.2

Verification live loads on governing lane is possible by using the design curve given in the UK code (BD 37/01) which shows more conservative value with deviation of 10% from the calculated value of 30.7 kN/m^2 .

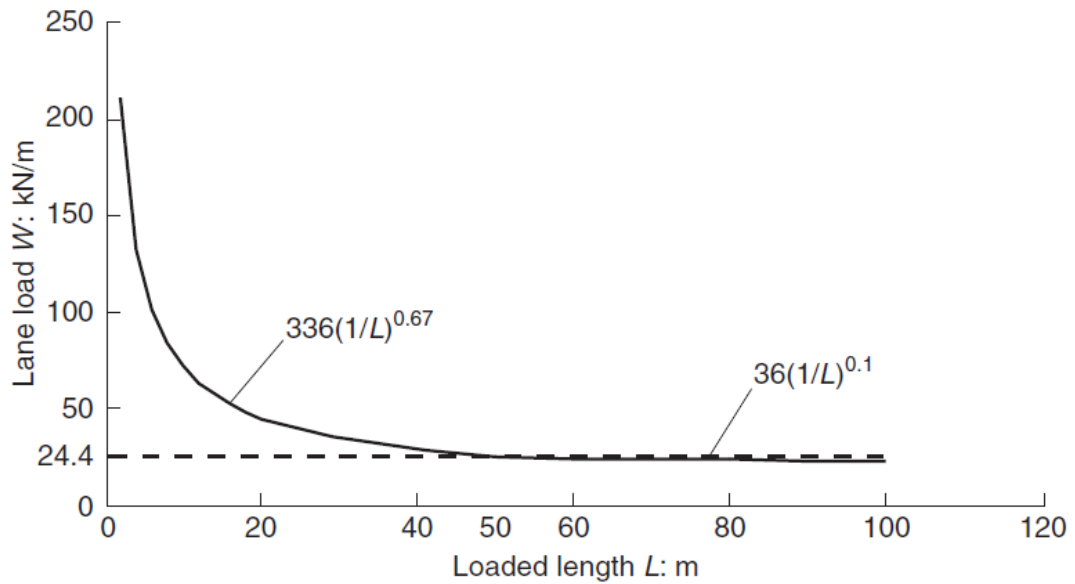


Figure F.8 British Standard normal loading curve [B09, p735]

F.5 Limit state design

Constructions elements will be mainly be subjected to moments, shear and normal forces or combination of those loads. The internal forces will be interpreted to the applied stresses and afterwards these will be verified with the permissible allowable stresses. This will require knowledge about specific material properties (Appendix xx) and stress-strain relations (Appendix xx)

<i>AMS</i>		<i>Unit</i>	<i>Value</i>
NSC-Reinforced	Compressive strength (f_{ck})	N/mm ²	25
	Moment capacity ULS (M_{Rd})	kNm	6388.6
	Prestressing steel (ρ_p)	%	0
	Reinforcement steel (ρ_s)	%	1.40
NSC-Reinforced	Compressive strength (f_{ck})	N/mm ²	50
	Moment capacity ULS (M_{Rd})	kNm	7170
	Prestressing steel (ρ_p)	%	0
	Reinforcement steel (ρ_s)	%	1.40
NSC - Prestressed	Compressive strength (f_{ck})	N/mm ²	50
	Moment capacity ULS (M_{Rd})	kNm	8211
	Prestressing steel (ρ_p)	%	0.50
	Reinforcement steel (ρ_s)	%	0.20
HSC - Prestressed	Compressive strength (f_{ck})	N/mm ²	70
	Moment capacity ULS (M_{Rd})	kNm	6193
	Prestressing steel (ρ_p)	%	0.50
	Reinforcement steel (ρ_s)	%	0.20

HSFRC	Compressive strength (f_{ck})	N/mm ²	70
	Moment capacity ULS (M_{Rd})	kNm	8307.5
	Prestressing steel (ρ_p)	%	0
	Reinforcement steel (ρ_s)	%	1.40
	Fibre content	kg/m ³	25
UHPFRC	Compressive strength (f_{ck})	N/mm ²	170
	Moment capacity ULS (M_{Rd})	kNm	7200
	Prestressing steel (ρ_p)	%	0
	Reinforcement steel (ρ_s)	%	1.40
	Fibre content	kg/m ³	2.5 Vol%
SHCC	Compressive strength (f_{ck})	N/mm ²	50
	Moment capacity ULS (M_{Rd})	kNm	7223
	Prestressing steel (ρ_p)	%	0
	Reinforcement steel (ρ_s)	%	1.30
	Fibre content	kg/m ³	≈ 2.0 Vol%

Table F.3: Flexural capacities

F.5.1 Conventional concrete girder

F.5.1.1 Material properties

The beam will be designed according to the NEN-EN 1992-1 for strength class C55/67. Moment capacity will be derived according to the bi-linear stress-strain diagrams (Figure F.9):

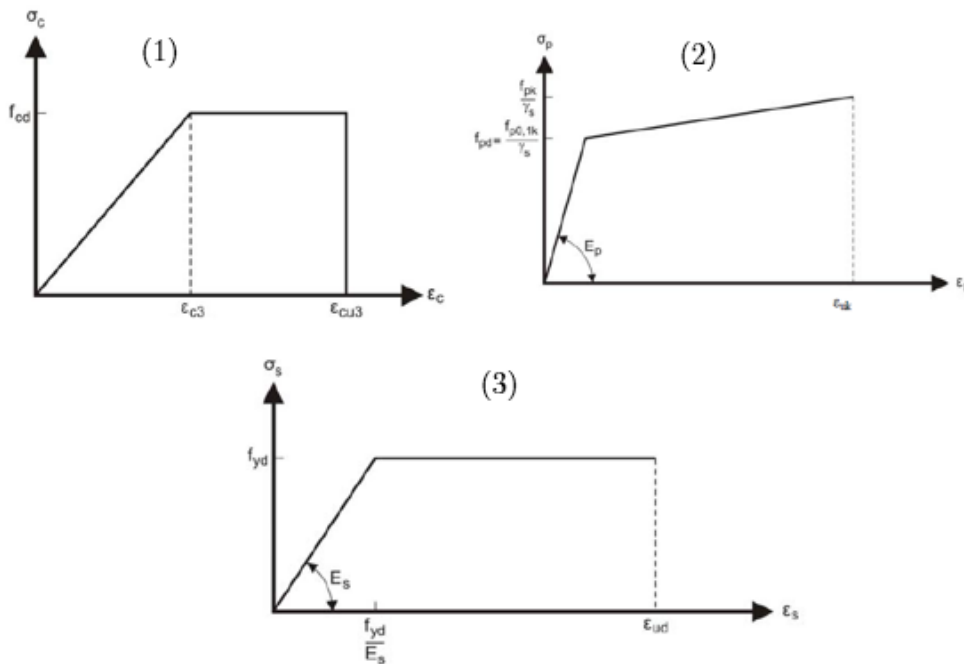


Figure F.9: Stress-strain diagrams of (1) concrete (2) prestressing steel (3) reinforcement steel

The following properties conform the stress-strain diagrams in Figure F.9 are governing for the ULS design:

	<i>Parameter</i>	<i>Value</i>
Concrete	Ultimate strain (ϵ_{cu3})	3.5 ‰
	Ultimate strain (ϵ_{c3})	1.75 ‰
	Sectional area factor (α)	0.75
	Distance factor (β)	0.39
	Design compressive strength (f_{cd})	36.7 MPa
	Mean tensile strength (f_{ctm})	4.2 MPa
Prestressing steel	Tensile strength Y1860S7 (f_{pk})	1860 MPa
	Tensile strength (f_{pk}/γ_s)	1691 MPa
	Design Tensile strength (f_{pd})	1522 MPa
	Ultimate tensile strain (ϵ_{uk})	35 ‰
	Elastic tensile strain (ϵ_k)	7.18 ‰
	Young's modulus (E_p)	195,000 MPa
	Prestressing losses	20 ‰
	Drape (f)	0.88 m
Reinforcement steel	Design tensile strength B500 (f_{yd})	435 MPa
	Young's modulus (E_s)	200,000 MPa
	Yielding strain (ϵ_y)	2.175 ‰

Table F.4: Material properties

F.5.2 Prestressing design

In order to obtain a fast simplified indication of the prestressing effect on the conventional concrete girder and on the high strength beam some design simplification will be introduced. Primarily, the girder dimensions are derived in Figure F.10 for various concrete classes.

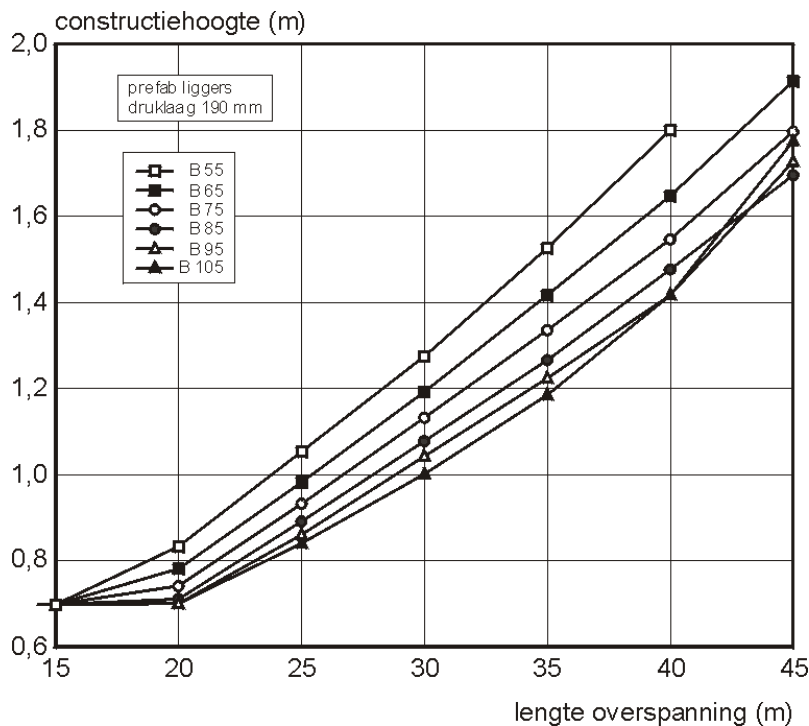


Figure F.10: Design rule prestressed beam [B10]

When the dimensions of the beam are known the ULS moment can be derived. Theoretically, the strain distribution in the height of the girder takes the compression layer into account. The shear plane between the two elements is modeled with bond factor.

F.5.2.2 Flexural capacity

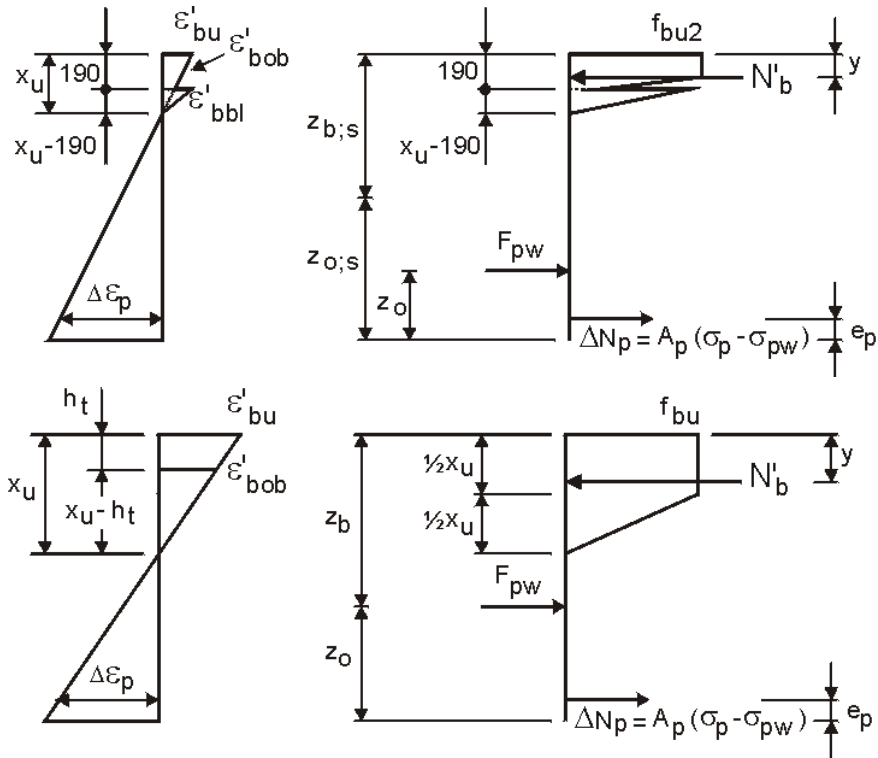


Figure F.11: ULD design with the theoretical distribution (upper) and the practical distribution (bottom)

Where:

- ε_{bu} maximum strain in the upper fibre
- ε_{bob} strain in the bottom fibre
- $\Delta\varepsilon_p$ increasing in prestressing strain
- f_{bu} maximum concrete stress
- F_{pw} active prestressing force
- ΔN_p increasing in prestressing force
- N_s force in reinforcement steel
- y distance between the upper fiber and the concrete compression force

Assuming:

$$\sigma_p = 0.9f_{pu} + \left(\varepsilon_p - \frac{0.9f_{pu}}{E_p} \right) \frac{f_{pu} - 0.9f_{pu}}{\varepsilon_p - \frac{0.9f_{pu}}{E_p}} \quad \text{When: } \varepsilon_p > \frac{0.9f_{pu}}{E_p}$$

The force in the prestressing steel and in the reinforcement bars:

$$N = \Delta N_p + N_s = A_p(\sigma_p - \sigma_{pw}) + A_s \sigma_{su}$$

The force should meet the following:

$$N < N_b - F_{pw} \Rightarrow \Delta N_p + N_s + F_{pw} - N_b < 0$$

If the condition above doesn't met, than higher concrete compression zone should be considered. This is an iterative process for which the optimal X_U will be defined. The ULD flexural capacity is derived with the following equation:

$$M_u = N_c(z_b - y) + A_p(\sigma_p - \sigma_{pw})(z_o - e_p) + A_s \sigma_{su}(z_o - e_s)$$

F.5.2.3 Concrete compression zone

The depth of the concrete compression zone is defined with the following design rule:

$$\frac{X_u}{d} \leq k_{x;\max} = \frac{\varepsilon'_{cu}}{\varepsilon'_{cu} + 7 \cdot 10^{-6} f} - \beta \quad f'_{ck} \geq 105 \text{ N/mm}^2$$

Where:

$$f = 435 \text{ N/mm}^2 \rightarrow \text{Reinforcement}$$

$$f = f_{pu} - \sigma_{pw} \approx 1690 - 1090 = 600 \text{ N/mm}^2 \rightarrow \text{Prestressing}$$

$$d = \frac{d_p A_p \Delta \sigma_{pu} + d_s A_s f_s}{A_p \Delta \sigma_{pu} + A_s f}$$

F.5.2.4 Comparison concrete strength classes

Given the $K_{x,max}$ values and assuming that $\sigma_p=0.95f_{pu}$ the following is found:

C65	$N'_{cu} = 29.25 * X_u$	$K_{x,max} = 0.53$	$\alpha = 0.75$	$\varepsilon'_{cu} = 3.5\text{‰}$
C85	$N'_{cu} = 35.00 * X_u$	$K_{x,max} = 0.50$	$\alpha = 0.70$	$\varepsilon'_{cu} = 3.0\text{‰}$
C105	$N'_{cu} = 37.2 * X_u$	$K_{x,max} = 0.45$	$\alpha = 0.62$	$\varepsilon'_{cu} = 2.5\text{‰}$

The flexural capacity:

$$M_u = z * N'_{cu} = (d - \beta X_u) * N'_{cu}$$

With concentrated concrete forces:

C65	$N'_{bu} = 15.64 * d * b$	100%
C85	$N'_{bu} = 17.85 * d * b$	114%
C105	$N'_{bu} = 16.74 * d * b$	107%

F.5.3 Fiber reinforced girder

Calculating the moment capacity of concrete reinforced with fibers follows from important publications about fibre reinforced concrete [C07] [C09] [C10] [C11] [C12] [C13] [C14] [C15]. The France publications [C07] are focusing on the application of Ductal® concrete of the French supplier Lafarge and applicable for UHPC girders with concrete strength >150 MPa. This is the only document which supply stress-strain diagram for girders. In addition to the French recommendation more articles concerning FRHSC and UHPFRC has been published in the recent years. Some of the publications shares the same recommendation but there is still lack of clarity in the assumptions, approach and results. The Dutch CUR-Aanbeveling [C10] [C11] [C12] is published as guideline for the calculation of FRC limited only to thin slabs and slender elements. The DAfStb-guideline [C13] is a German recommendation applicable for FRC with concrete strength class up to C50/60. Finally the Italian CNR guideline [C14] which the European Model Code is based on [C15].

F.5.3.5 ULS Stress-strain diagram [C10] [C11] [C12]

The basic of the ULS bending moment capacity is possible by using the ideal stress-strain diagram conform CUR-111. Despite the limitation to slender elements there are no restrictions concerning the concrete strength class comparing to the DAfStb guideline with strength limit of C50/60. Therefore for FRHSC the CUR- recommendation is the most suitable in the absent of other appropriate recommendation.

The stress-strain diagram [C10] finds the moment capacity with taking into account the steel fibers contribution which are activated when the concrete starts to crack. The tensile stresses capacity of the steel fibers is depended on the size and fiber content. When maximal tensile strength is reached the first cracks will appear. The second branch of the stress-strain diagram might show strain-softening or strain-hardening behavior depends on the fiber content and fiber size in the concrete mixture.

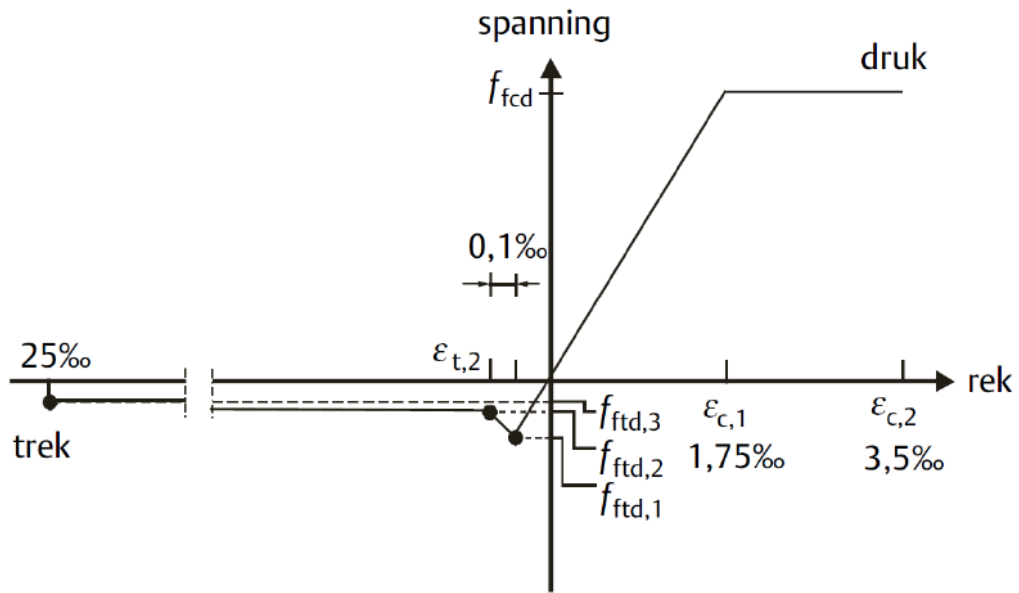


Figure F.12: Stress-strain diagram [CUR-111]

<i>Parameter</i>	<i>Value</i>
$f_{ftd,1}$	3.802 MPa
$f_{ftd,2}$	1.584 MPa
$f_{ftd,3}$	1.542 MPa
$\varepsilon_{t,1}$	0.1305 ‰
$\varepsilon_{t,2}$	0.2305 ‰
$\varepsilon_{t,3}$	25 ‰

Table F.5

Deriving the characteristic material properties with which the maximum moment can be calculated requires to perform uniaxial compressive tests and 3-points bending test according to [C10] with a notch at midspan. The appropriate data from which stress-strain diagram will be derived has been found in the research of prof.dr.ir. L. Vandewalle en ir. D. Dupont [A19].

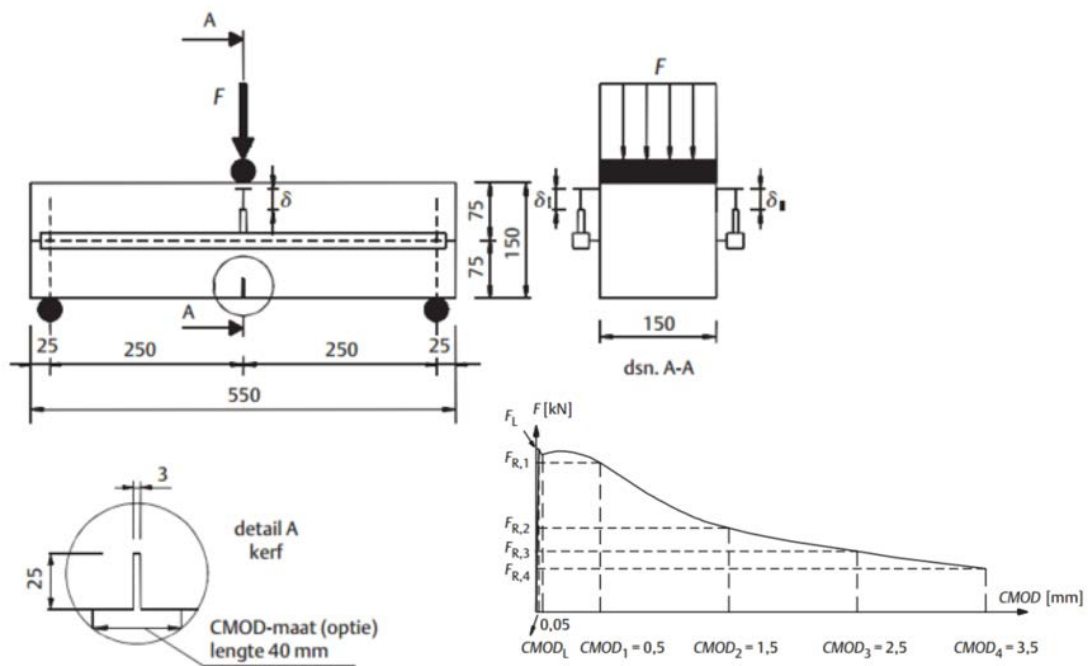


Figure F.13: Isostatic 3-points bending test for FRC according to RILEM TC162-TDF [C10]

The bending test (Figure F.13) data is presented in the CMOD diagram (crack mouth opening displacement) from which the residual test results (in discrete points) are used to derive the post-cracking flexural tensile strength of FRC. The following quantities are determined: ($f_{fct,1}$) proportionality limit, equivalent flexural tensile strengths ($f_{eq,1}, f_{eq,2}$) and residual flexural tensile strength ($f_{R,i}$). The bending tests are available for strength classes C25/30 and C70/85 with steel fibers content of 25, 50 and 75 kg/m³ fibers types RC 80/60 BN, RC 65/60 BN and RC 80/60 BP. The results of the 3-points bending tests is summarized in the diagrams given in Figure F.14 are the mean values of six tests.

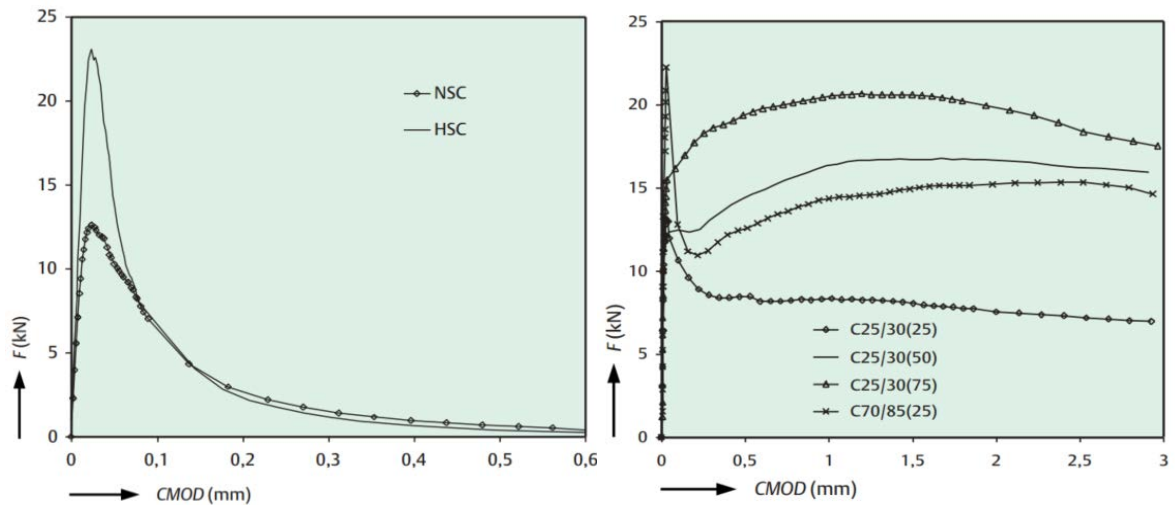


Figure F.14: F-CMOD-curve for plain concrete (left) and F-CMOD-curve for FRC (right) (25) [A19]

The $\sigma - \varepsilon$ curve needed for the determination of moment capacity is the C70/85(25) curve 25 kg/m² fibers content. This is the absolute minimum value of the fibre dosage [Henderick & Supply , 2000]. A maximum value of the fibre dosage is limited by the workability demands and rarely dosage of 70-80 kg/m³ are used.

The mentioned curve in Figure F.14 shows clearly linear-elastic branch up to load level of 22.5 kN. The post-peak behaviour of HSC is significant due to his brittleness. The curve is clearly affected by the present of steel fibers which is accounted for the post-peak strain-hardening branch. The ductility is therefore sufficient with 25 kg/m³ (0.3-1 Vol%) fibers content. If the post-cracking tensile stress must be higher than the cracking tensile strength (strain hardening), fibre dosages up to 5 or 6 Vol% are needed.

The following quantities are governing for the stress-strain diagram [C10] [C12]:

Linear elastic stage

Lower bound design value tensile strength FRC: $f_{ftd,1} = 0.6 \frac{f_{ft,L}}{\gamma_{ft}}$

Fictitious linear flexural tensile strength: $f_{ft,L} = \frac{3F_L L}{2bh_{sp}^2}$ [C12, art 5.2]

which can be approximated with: $f_{ctm,fl} = 0.43(f_{ck,cube} - 10)^{2/3}$

Where:

$F_L = 22.5 \text{ kN}$ load at the limit of proportionality assuming linear-elastic stage according to Figure F.14 C70/85(25) curve

$h_{sp} = 125 \text{ mm}$ height of the remaining ligament in a notched section

$b = 150 \text{ mm}$ width of the specimen

$L = 500 \text{ mm}$ span of specimen

Post-cracking stage

Average residual tensile strength for CMOD1=0.5: $f_{ftd,2} = 0.45 \frac{f_{eq,1}}{\gamma_{ft}}$

Where:

$$f_{eq,1} = \frac{3F_1 L}{2bh_{sp}^2}$$

$F_1 = 12.5 \text{ kN}$ load at CMOD1=0.5

Average residual tensile strength for CMOD4=3.5: $f_{ftd,3} = 0.37 \frac{f_{eq,4}}{\gamma_{ft}}$

Where:

$$f_{eq,3} = \frac{3F_1 L}{2bh_{sp}^2}$$

$F_1 = 14.8 \text{ kN}$ load at CMOD1=3.5

Important [CUR – 111]:

The reduction factors 0.45 and 0.37 for the tensile stresses $f_{ftd,2}$ and $f_{ftd,3}$ are calculated for slender element with height $h \leq 600 \text{ mm}$. Therefore the application of this calculation method is limited and may be incomplete.

F.5.3.6 Maximal moment

The ULS moment for a beam with steel fibers with and without reinforcement calculated based on the $\sigma - \varepsilon$ relations derived in section F.5.3.5.

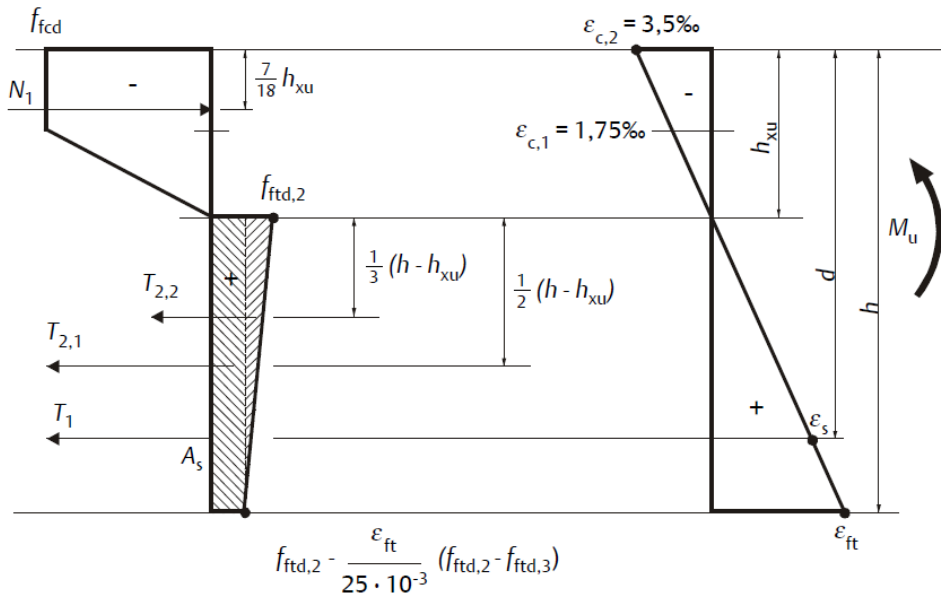


Figure F.15: ULS strain and stresses diagram of FRC [C10]

$$N_1 = 0.75h_{xu}bf_{fcd}$$

$$T_1 = A_s\sigma_s = A_sE_s\varepsilon_s \left(\frac{d - h_{xu}}{h_{xu}} \right) 3.5 * 10^{-3} \leq A_s f_{sy}$$

$$T_{2,1} = b(h - h_{xu}) \left(f_{ftd,2} - \frac{\varepsilon_{ft}}{25 * 10^{-3}} (f_{ftd,2} - f_{ftd,3}) \right)$$

$$T_{2,2} = \frac{1}{2}b(h - h_{xu}) \frac{\varepsilon_{ft}}{25 * 10^{-3}} (f_{ftd,2} - f_{ftd,3})$$

Along the height of the cross-section the strain distribution is rewritten to the stress distribution by the constitutive relations. It is noticed that the stress at the neutral line is not zero while the strain is zero. In the ultimate stress distribution the steel fibers are fully activated in the tensile zone which is cracked. In Figure F.15 linear relation between the strain and the tensile-stress is assumed in order to prevent overestimation of the stresses for small strains.

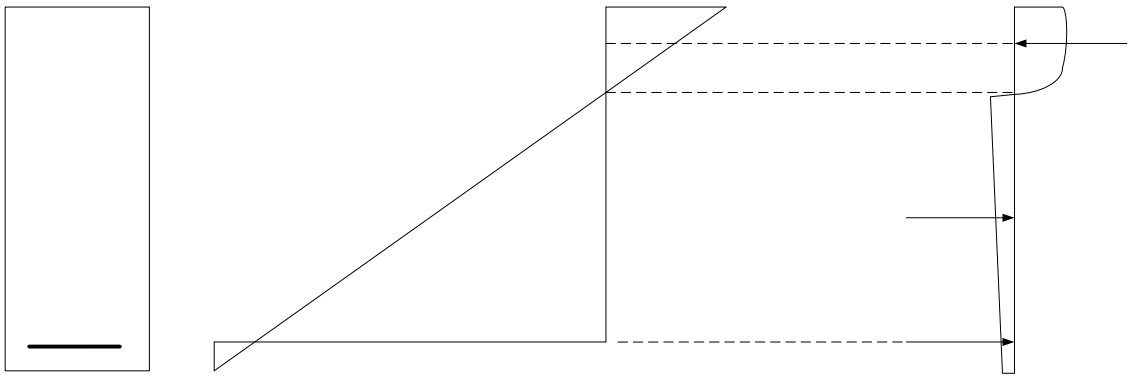


Figure F.16: Parabolic strain distribution

F.5.4 Ultra-High Performance girder

According to the stress-strain diagram derived in [C07] and handled Appendix E.4, the moment capacity can be found. The French norm defines the behavior of the composite beam contain UHPC reinforced with steel fibers and possibly steel rebars. For beam loaded in tension, in the linear elastic phase the fibers are hardly active. The tensile stress will be taken by the concrete matrix. The fibers will be activated with the present of the first cracks. The tensile stress-strain branch is strongly depends on the fiber size and content which will increase the tensile capacity of the composite material. This correspond to strain-hardening behavior. It can easily explained by the stress-strain curve of steel at the long plastic region, between the yielding and the rapture stresses. In the case of strain-softening behavior the tensile stresses will decrease with the formation of the first crack. The moment capacity will be calculated according to [C07]

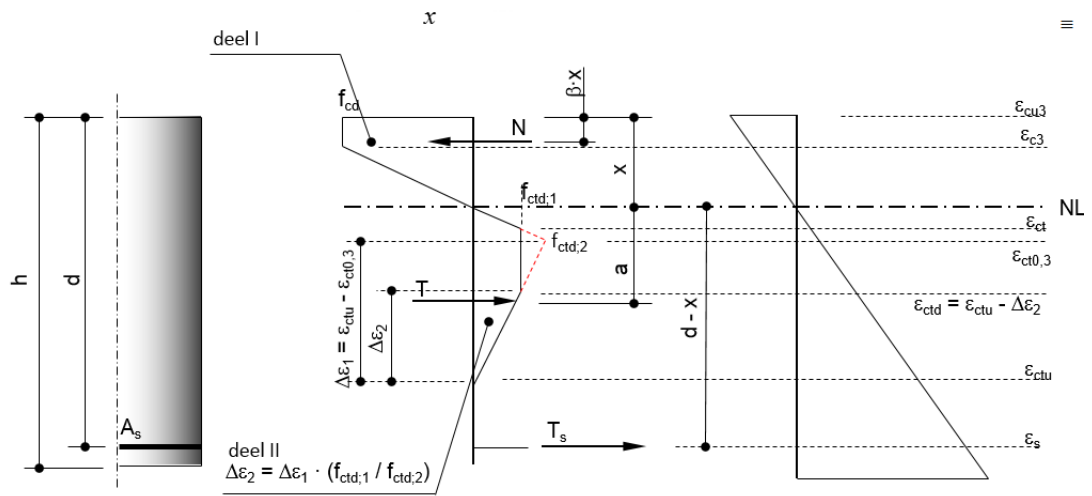


Figure F.17: Stresses and strain distribution in UHPC cross-section with additional steel rebar

F.5.5 Strain-hardening composites beam

Due to its capability of bearing tensile forces after cracking by the bridging effect of fibers, the design of SHCC flexural member will take into account the tensile capacity assuming a perfect elastic-plastic constitutive model [B14], the bi-linear tensile stress-strain diagram (Appendix E.8). The concept of strain and stress distribution having SHCC on the tension side and CC on the rest of the cross-section illustrated in Figure F.18. When used, the SHCC bears the tensile forces reducing the tensile stress of the reinforcement bars. The flexural moment capacity will be calculated according to the compressive and tensile stress-strain curves derived in the JSCE-2008 Recommendations [C13].

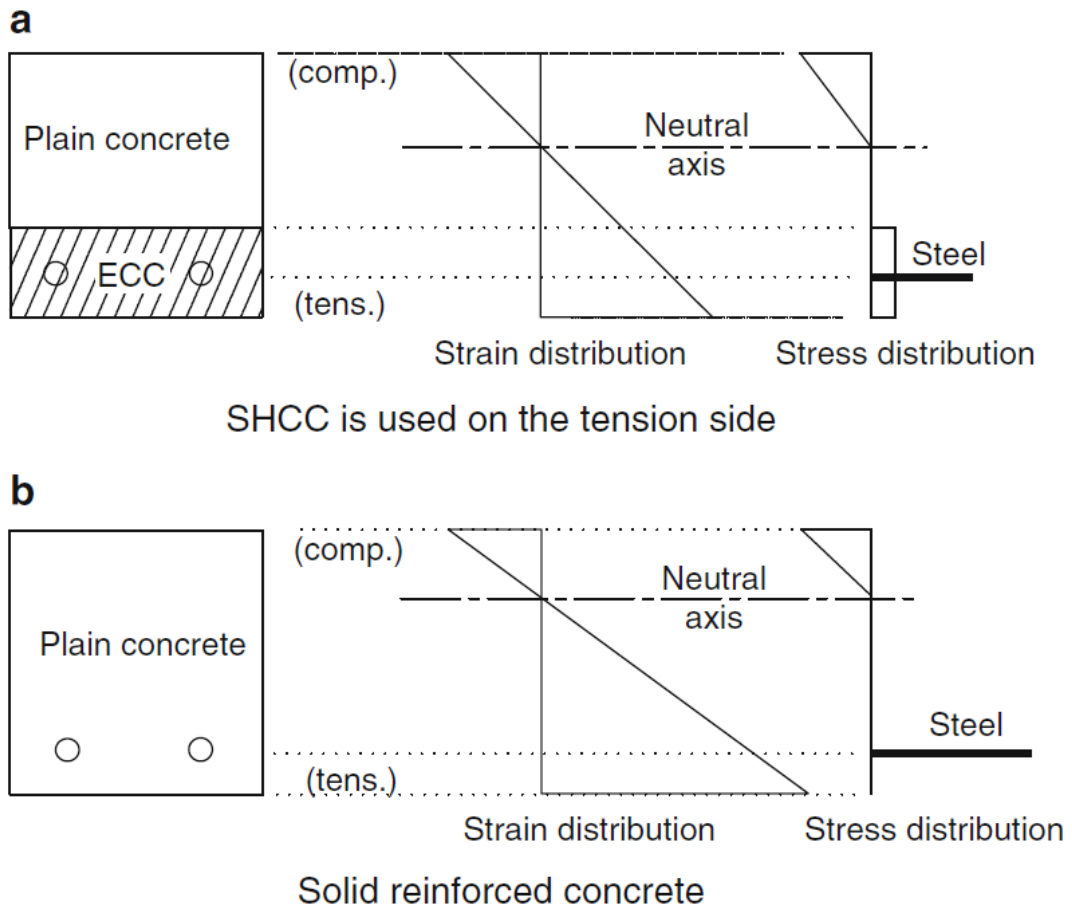


Figure F.18: Distribution of stress and strain [B13].

The following equation are used for a cross-section with SHCC in the tensile side:

$$x = \frac{p_w d f_{yd} + t f_{ty}}{k_1 \beta f'_{cd}}$$

$$M_u = k_1 \beta \left(1 - \frac{\beta}{2}\right) b_w f'_{cd} x^2 + A_s f_{yd} (d - x) + f_{ty} b_w t \left(h - x + \frac{t}{2}\right)$$

With:

x compressive zone

k_1 strength reduction coefficient, generally assumed to be $1 - 0.003 f'_{ck} \leq 0.85$

f_{yd} design yield strength of steel on the tensile side

f_{ty} design tensile yield strength of SHCC

A_s Cross-sectional area of steel on the tension side

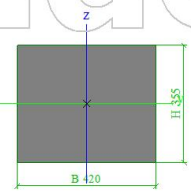
β	$0.52+80\varepsilon'_{cu}$
ε'_{cu}	$\frac{155-f'_{ck}}{30000} \leq 0.0035$
f'_{cd}	design compressive strength of concrete $f'_{cd} \leq 80 \text{ N/mm}^2$
p_w	$A_s/b_w d$
f_{tyk}	Characteristic value of tensile yield strength

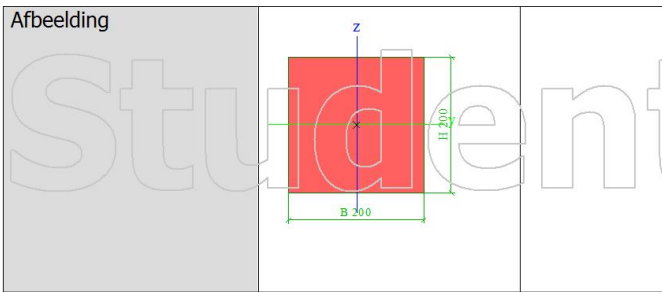
G. Engineering report SCIA

1. Project

Licentienaam	Onbekend
Project	-
Onderdeel	-
Omschrijving	-
Auteur	-
Datum	27. 10. 2015
Constructie	Algemeen XYZ
Aantal knopen :	857
Aantal staven :	117
Aantal platen :	54
Aantal vaste lichamen :	0
Aantal gebruikte doorsneden :	2
Aantal belastingsgevallen :	27
Aantal gebruikte materialen :	4
Gravatieversnelling [m/s ²]	9.810
Nationale norm	NEN

2. Doorsneden

CS1		
Type	Rechthoek	
Uitgebreid	355; 420	
Vorm type	Dikke wanden	
Onderdeelmateriaal	UHPC	
Bouwwijze	beton	
A [m ²]	1.4910e-01	
A _y [m ²], A _z [m ²]	1.2425e-01	1.2425e-01
A _L [m ² /m], A _D [m ² /m]	1.5500e+00	1.5500e+00
C _{y,UCS} [mm], C _{z,UCS} [mm]	210	178
α [deg]	0.00	
I _y [m ⁴], I _z [m ⁴]	1.5659e-03	2.1918e-03
i _y [mm], i _z [mm]	102	121
W _{el,y} [m ³], W _{el,z} [m ³]	8.8218e-03	1.0437e-02
W _{pl,y} [m ³], W _{pl,z} [m ³]	0.0000e+00	0.0000e+00
M _{pl,y,+} [Nm], M _{pl,y,-} [Nm]	0.00e+00	0.00e+00
M _{pl,z,+} [Nm], M _{pl,z,-} [Nm]	0.00e+00	0.00e+00
d _y [mm], d _z [mm]	0	0
I _t [m ⁴], I _w [m ⁶]	3.0798e-03	1.0270e-06
β _y [mm], β _z [mm]	0	0
Afbeelding		
CS3		
Type	Rechthoek	
Uitgebreid	200; 200	
Vorm type	Dikke wanden	
Onderdeelmateriaal	UHPC	
Bouwwijze	Algemeen	
A [m ²]	4.0000e-02	
A _y [m ²], A _z [m ²]	3.3333e-02	3.3333e-02
A _L [m ² /m], A _D [m ² /m]	8.0000e-01	8.0000e-01
C _{y,UCS} [mm], C _{z,UCS} [mm]	100	100
α [deg]	0.00	
I _y [m ⁴], I _z [m ⁴]	1.3333e-04	1.3333e-04
i _y [mm], i _z [mm]	58	58
W _{el,y} [m ³], W _{el,z} [m ³]	1.3333e-03	1.3333e-03
W _{pl,y} [m ³], W _{pl,z} [m ³]	0.0000e+00	0.0000e+00
M _{pl,y,+} [Nm], M _{pl,y,-} [Nm]	0.00e+00	0.00e+00
M _{pl,z,+} [Nm], M _{pl,z,-} [Nm]	0.00e+00	0.00e+00
d _y [mm], d _z [mm]	0	0
I _t [m ⁴], I _w [m ⁶]	2.2445e-04	7.8093e-09
β _y [mm], β _z [mm]	0	0



Verklaring van symbolen	
A	Gebied
A_y	Afschuifoppervlak in hoofd y-richting - Berekend door 2D EEM analyse
A_z	Afschuifoppervlak in hoofd z-richting - Berekend door 2D EEM analyse
A_L	Omtrek per eenheidslengte
A_D	Uithardingsoppervlakte per eenheidslengte
$C_{y,UCS}$	Zwaartepunt coördinaten in Y-richting van het invoer assen systeem
$C_{z,UCS}$	Zwaartepunt coördinaten in Z-richting van het invoer assen systeem
$I_{y,LCS}$	Tweede moment van het gebied rond de YLCS as
$I_{z,LCS}$	Tweede moment van het gebied rond de ZLCS as
$I_{y,ZCS}$	Product moment van het gebied in het LCS systeem
α	Rotatiehoek van het hoofd assen systeem
I_y	Tweede moment van het gebied rond de hoofd y-as
I_z	Tweede moment van het gebied rond de hoofd z-as
i_y	Traagheidsstraal rond de hoofd y-as
i_z	Traagheidsstraal rond de hoofd z-as

Verklaring van symbolen	
$W_{el,y}$	Elastische doorsnede modulus rond de hoofd y-as
$W_{el,z}$	Elastische doorsnede modulus rond de hoofd z-as
$W_{pl,y}$	Plastische doorsnede modulus rond de hoofd y-as
$W_{pl,z}$	Plastische doorsnede modulus rond de hoofd z-as
$M_{pl,y,+}$	Plastisch moment rond de hoofd y-as voor een positief My moment
$M_{pl,y,-}$	Plastisch moment rond de hoofd y-as voor een negatief My moment
$M_{pl,z,+}$	Plastisch moment rond de hoofd z-as voor een positief Mz moment
$M_{pl,z,-}$	Plastisch moment rond de hoofd z-as voor een negatief Mz moment
d_y	Afschuif middencoördinaat in hoofd y-richting gemeten vanaf het zwaartepunt - Berekend door 2D EEM analyse
d_z	Afschuif middencoördinaat in hoofd z-richting gemeten vanaf het zwaartepunt - Berekend door 2D EEM analyse
I_t	Torsie constante - Berekend door 2D EEM analyse
I_w	Welvings constante - Berekend door 2D EEM analyse
β_y	Mono-symmetrische constante rond de hoofd y-as
β_z	Mono-symmetrische constante rond de hoofd z-as

3. Materialen

Steel	
S235	
Thermisch uitz. [m/mK]	0.00
Massa eenheid [kg/m ³]	7850.0
E mod [MPa]	2.1000e+05
Poisson - nu	0.3
Onafhankelijke G-modulus	X
G-mod [MPa]	8.0769e+04
Log. decrement (niet-uniforme demping enkel)	0.025
Therm. exp. (brand) [m/mK]	0.00
Specifieke hitte [J/gK]	6.0000e-01
Thermische geleiding [W/mK]	4.5000e+01
Fu [MPa]	360.0
Fy [MPa]	235.0

Verklaring van symbolen	
Log. decrement (niet-uniforme demping enkel)	Deze materiaal dempingseigenschap is enkel toegepast in het geval van het niet-uniform is demping is geactiveerd voor dynamische analyse (zie project functionaliteit). Gelieve op te merken, dat niet-uniforme demping een specifieke licentie benodigd, welke geen deel uit maakt van het standaard dynamische pakket.

Type	E mod [MPa]	Diameter [mm]	Oppervlak [mm ²]	Fpk (Fpu_rep) [MPa]
Strands 1860 - 12.9	2.0000e+05	12.9	100	1860.0

Concrete NEN 6720

Type	Unit mass [kg/m ³]	E mod [MPa]	Poisson - nu	G mod [MPa]	Karakteristieke kubusdruksterkte (f _{ck}) [MPa]
Naam					Rekenwaarde van de druksterkte (f _b) [MPa]
Concrete C53/65	2500.0	3.8500e+04	0.2	1.6042e+04	65.00 39.00
Concrete UHPC	2500.0	4.7000e+04	0.2	1.9583e+04	180.00 108.00

4. Belastinggevallen

Naam	Omschrijving	Actie type	Lastgroep	Richting	Duur	'Master' belastinggeval
	Spec	Belastingtype				
q-last 1	Standaard	Variabel Statisch	LM1		Kort	Geen
q-last rest	Standaard	Variabel Statisch	LM1		Kort	Geen
TD1	Standaard	Variabel Statisch	LM1		Kort	Geen
TD2	Standaard	Variabel Statisch	LM1		Kort	Geen
TD3	Standaard	Variabel Statisch	LM1		Kort	Geen
TD4	Standaard	Variabel Statisch	LM1		Kort	Geen
TD5	Standaard	Variabel Statisch	LM1		Kort	Geen
TD6	Standaard	Variabel Statisch	LM1		Kort	Geen
TD7	Standaard	Variabel Statisch	LM1		Kort	Geen
TD8	Standaard	Variabel Statisch	LM1		Kort	Geen
TD9	Standaard	Variabel Statisch	LM1		Kort	Geen
TD10	Standaard	Variabel Statisch	LM1		Kort	Geen
TD11	Standaard	Variabel Statisch	LM1		Kort	Geen
TD13	Standaard	Variabel Statisch	LM1		Kort	Geen
TD14	Standaard	Variabel Statisch	LM1		Kort	Geen
TD15	Standaard	Variabel Statisch	LM1		Kort	Geen
TD16	Standaard	Variabel Statisch	LM1		Kort	Geen
TD17	Standaard	Variabel Statisch	LM1		Kort	Geen
TD18	Standaard	Variabel Statisch	LM1		Kort	Geen
TD19	Standaard	Variabel Statisch	LM1		Kort	Geen
TD20	Standaard	Variabel Statisch	LM1		Kort	Geen
TD21	Standaard	Variabel Statisch	LM1		Kort	Geen
Voorspanning trek element		Permanent Voorspanning	LM2			
Voorspanning schijf		Permanent Voorspanning	LM2			
Voorspanning truss		Permanent Voorspanning	LM2			
Eigengewicht		Permanent Eigen gewicht	LG1	-Z		
TDi2	Standaard	Variabel Statisch	LM1		Kort	Geen

5. Belastinggroepen

Naam	Last	Relatie	Coëff.
LG1	Permanent		
LM1	Variabel	Exclusief	0.5
LM2	Permanent		

6. Combinaties

Naam	Omschrijving	Type	Belastingsgevallen	Coëff. [-]
BGT		Omhullende - bruikbaarheid	q-last 1	0.80
			q-last rest	0.80
			TD1	0.80
			TD2	0.80
			TD3	0.80
			TD4	0.80
			TD5	0.80
			TD6	0.80
			TD7	0.80
			TD8	0.80
			TD9	0.80
			TD10	0.80
			TD11	0.80
			TD12	0.80
			TD13	0.80
			TD14	0.80
			TD15	0.80
			TD16	0.80
			TD17	0.80
			TD18	0.80
			TD19	0.80
			TD20	0.80
TD21	0.80			
		Eigengewicht	1.00	
UGT PERM		Omhullende - uiterst	q-last 1	1.25
			q-last rest	1.25
			TD1	1.25
			TD2	1.25
			TD3	1.25
			TD4	1.25
			TD5	1.25
			TD6	1.25
			TD7	1.25
			TD8	1.25
			TD9	1.25
			TD10	1.25
			TD11	1.25
			TD12	1.25
			TD13	1.25
			TD14	1.25
			TD15	1.25
			TD16	1.25
			TD17	1.25
			TD18	1.25
			TD19	1.25
			TD20	1.25
TD21	1.25			
		Eigengewicht	1.40	
UGT GR1A		Omhullende - uiterst	q-last 1	1.50
			q-last rest	1.50
			TD1	1.50
			TD2	1.50
			TD3	1.50
			TD4	1.50
			TD5	1.50
			TD6	1.50
			TD7	1.50
			TD8	1.50
			TD9	1.50
			TD10	1.50
			TD11	1.50
			TD12	1.50
			TD13	1.50
			TD14	1.50
			TD15	1.50
TD16	1.50			
TD17	1.50			

Naam	Omschrijving	Type	Belastingsgevallen	Coëff. [-]
			TD18	1.50
			TD19	1.50
			TD20	1.50
			TD21	1.50
			Eigengewicht	1.25

7. Resultaatklassen

Naam	Lijst
BGT	BGT - Omhullende - bruikbaarheid
UGT	UGT PERM - Omhullende - uiterst
	UGT GR1A - Omhullende - uiterst

Student version

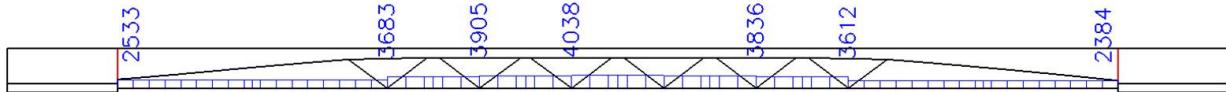
Student version

1. Interne krachten van staven

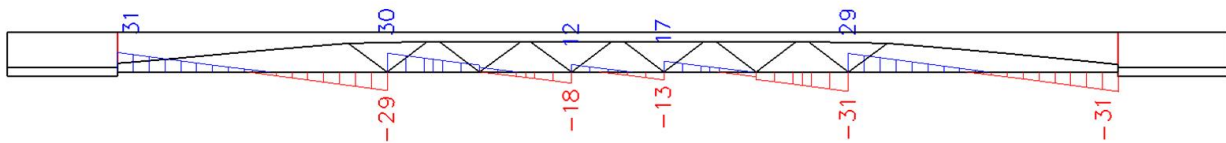
Lineaire berekening, Extreem : Globaal, System : Hoofd
 Selectie : Alle
 Klasse : BGT

StAAF	css	dx [m]	BG	N [kN]	Vy [kN]	Vz [kN]	Mx [kNm]	My [kNm]	Mz [kNm]
S307	CS3 - Rechthoek	2.025	BGT/1	-528	0	-10	0	-8	-1
S297	CS1 - Rechthoek	18.611	BGT/2	2635	0	7	0	24	0
S275	CS3 - Rechthoek	0.000	BGT/3	452	-1	15	-1	-12	0
S280	CS3 - Rechthoek	0.000	BGT/4	478	1	16	0	-12	0
S375	CS1 - Rechthoek	11.056	BGT/5	1026	0	-21	-5	-14	-2
S375	CS1 - Rechthoek	29.944	BGT/5	948	0	22	5	-15	-2
S310	CS1 - Rechthoek	0.000	BGT/5	1319	0	20	-9	0	0
S310	CS1 - Rechthoek	29.944	BGT/5	1244	0	21	9	-5	-4
S297	CS1 - Rechthoek	5.853	BGT/3	1623	0	-1	-2	60	0
S336	CS1 - Rechthoek	11.056	BGT/3	1397	0	-20	-6	-1	-5
S340	CS3 - Rechthoek	1.967	BGT/3	401	1	12	1	15	2

2. Internal forces on member; N UGT

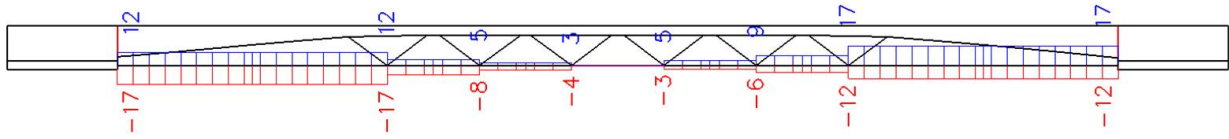


3. Internal forces on member; Vz



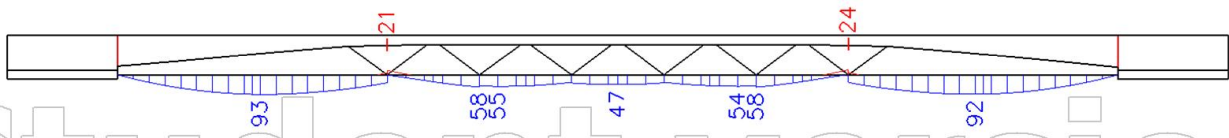
4. Internal forces on member; M_x

Student version



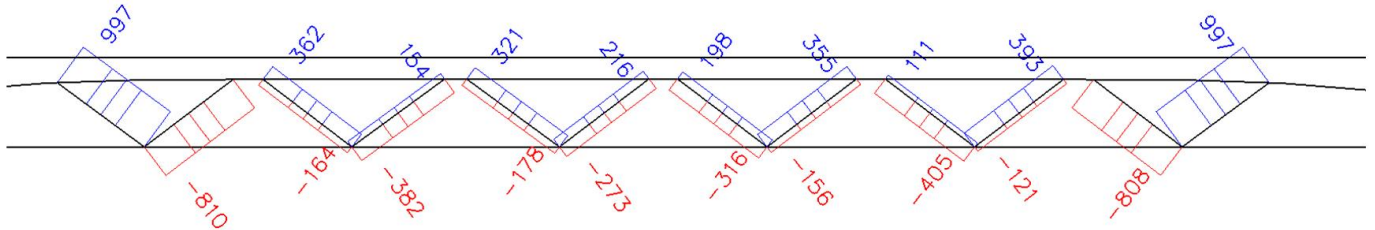
5. Internal forces on member; M_y

Student version



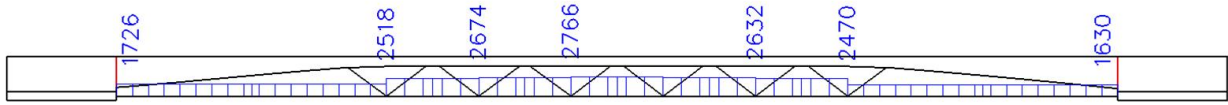
6. Internal forces on member; N

Student version



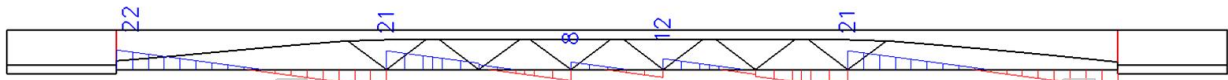
10. Internal forces on member; N

Student version



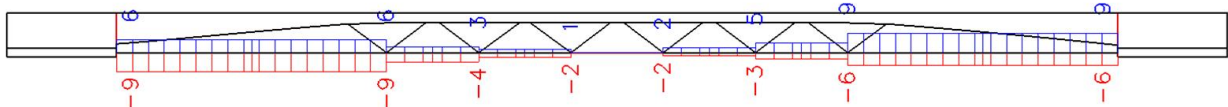
11. Internal forces on member; Vz

Student version



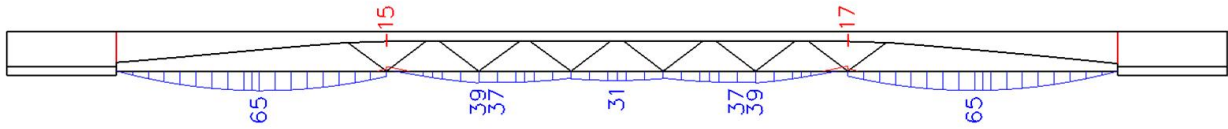
12. Internal forces on member; Mx

Student version



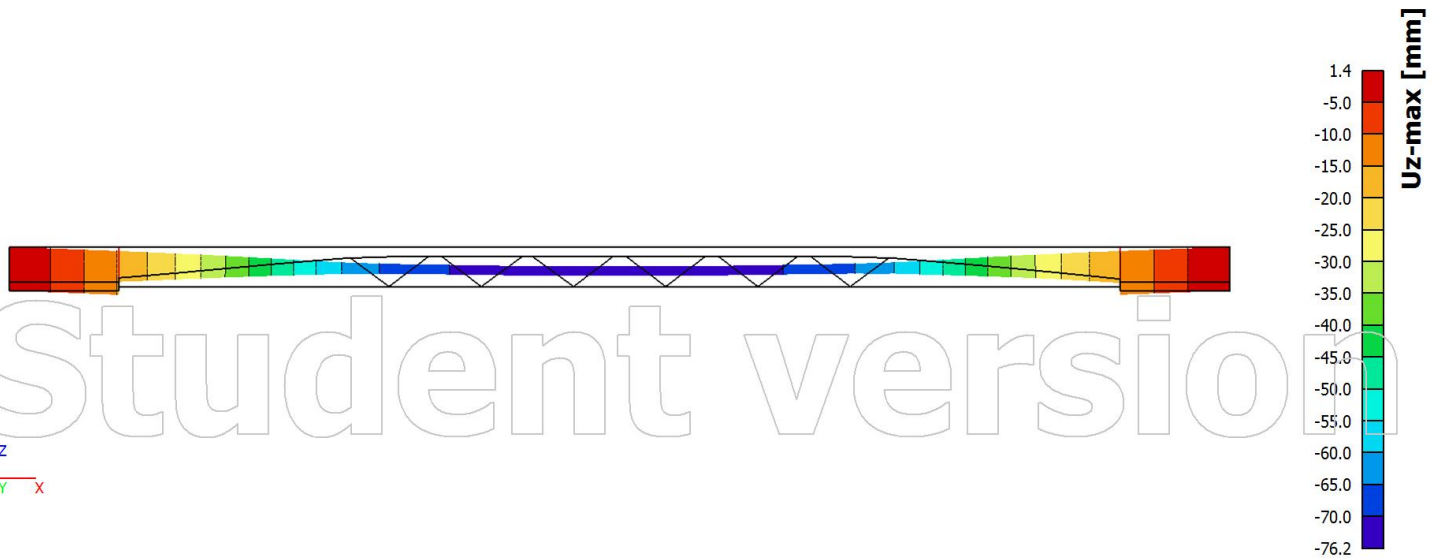
13. Internal forces on member; My

Student version



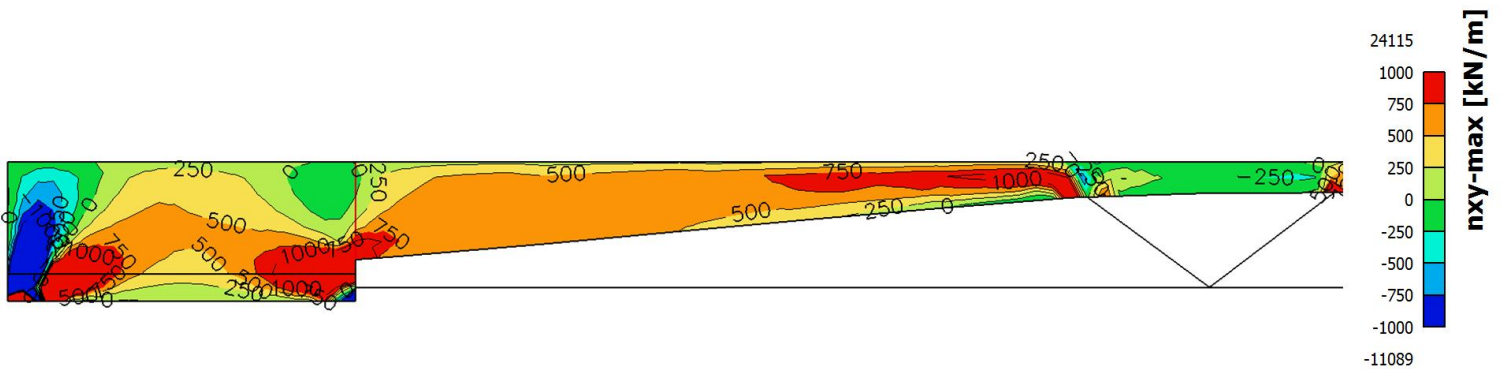
14. Displacement of nodes; Uz

Student version

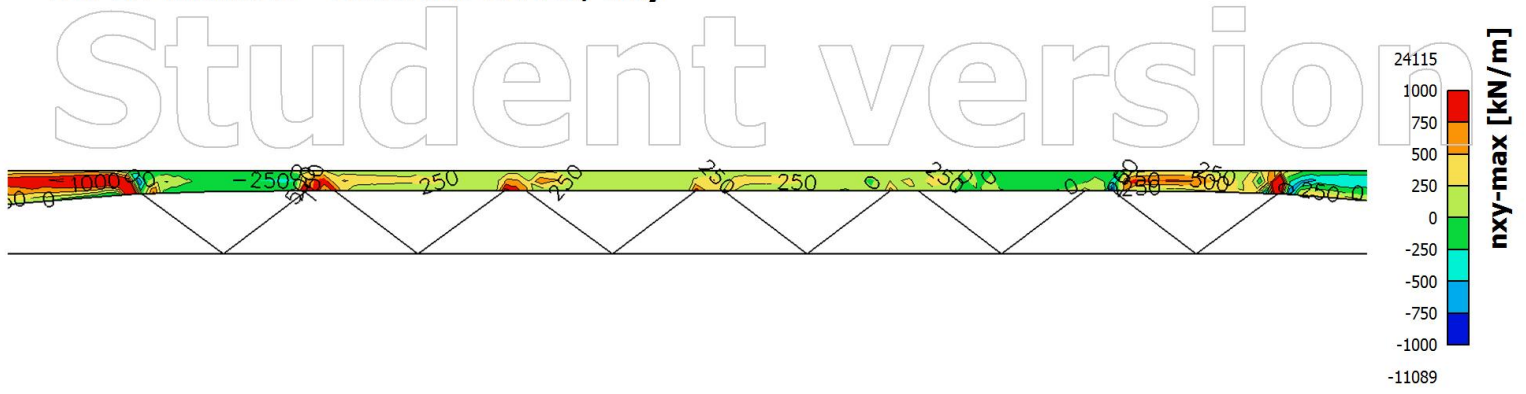


15. 2D member - Internal forces; nxy

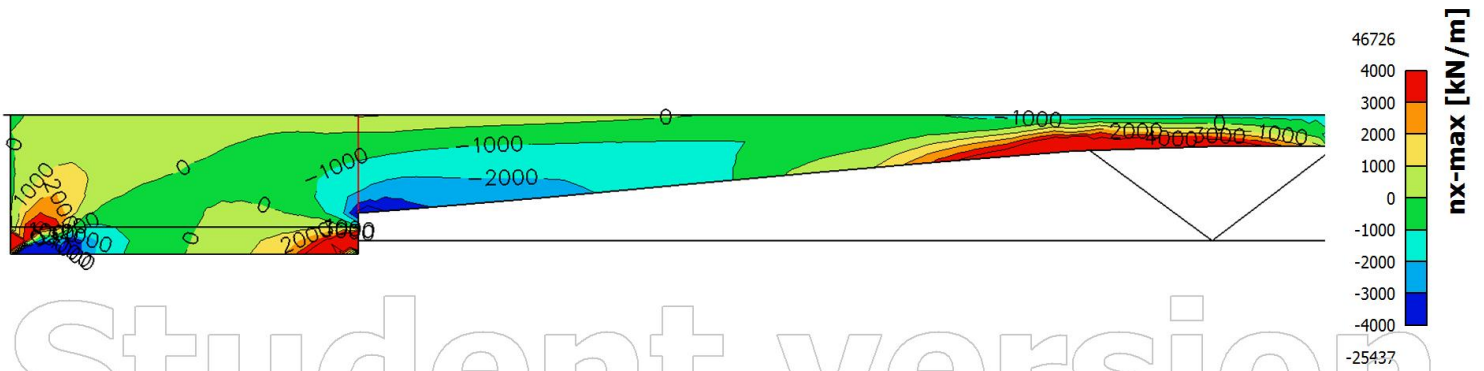
Student version



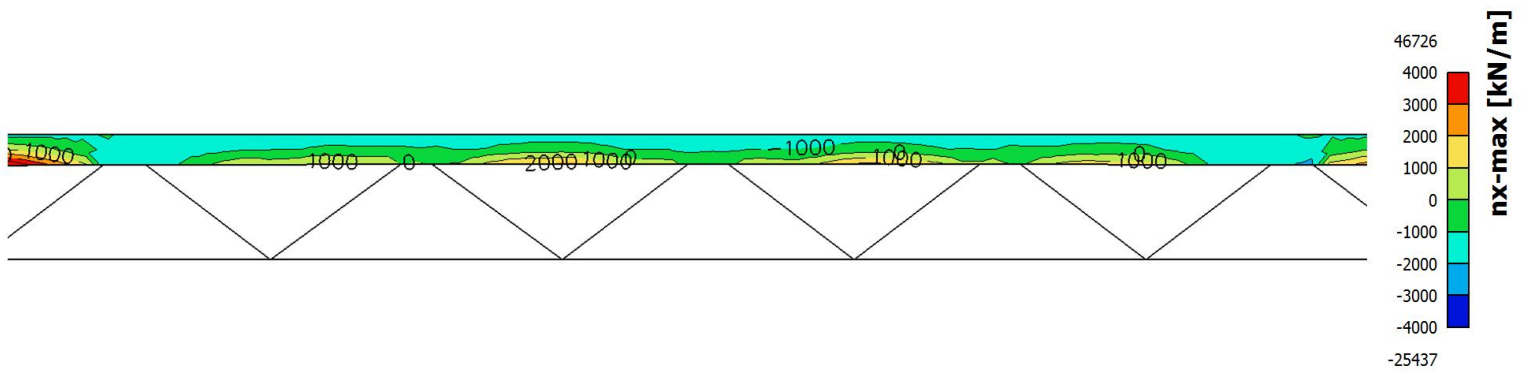
16. 2D member - Internal forces; nxy



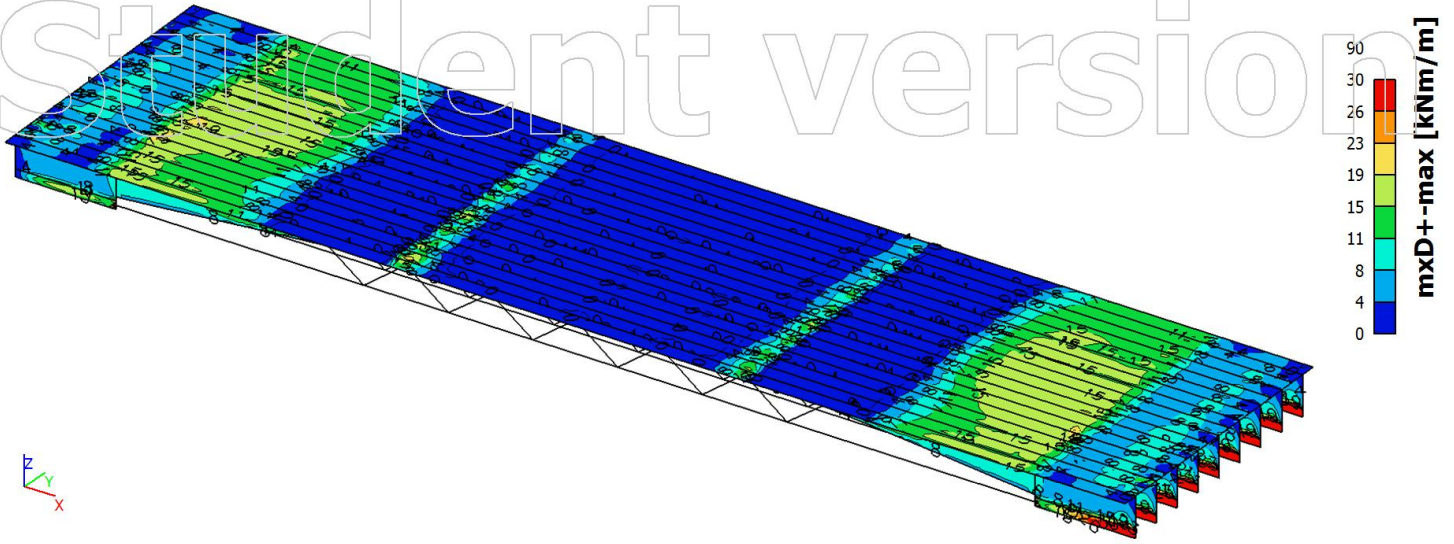
17. 2D member - Internal forces; nx



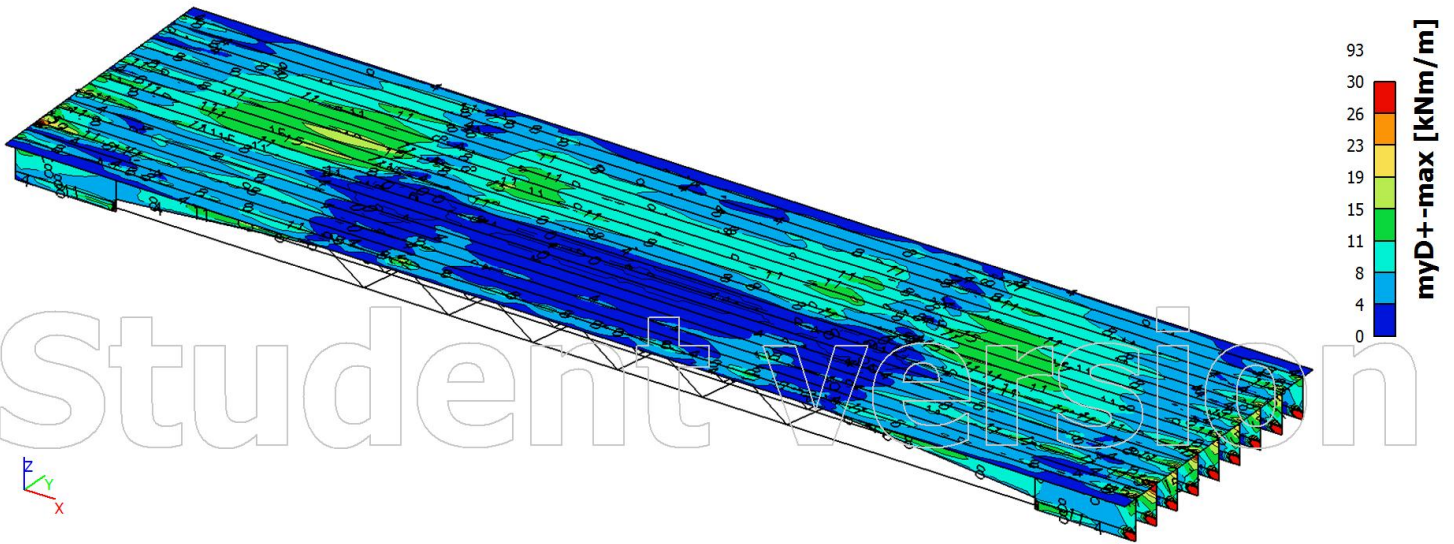
18. 2D member - Internal forces; nx



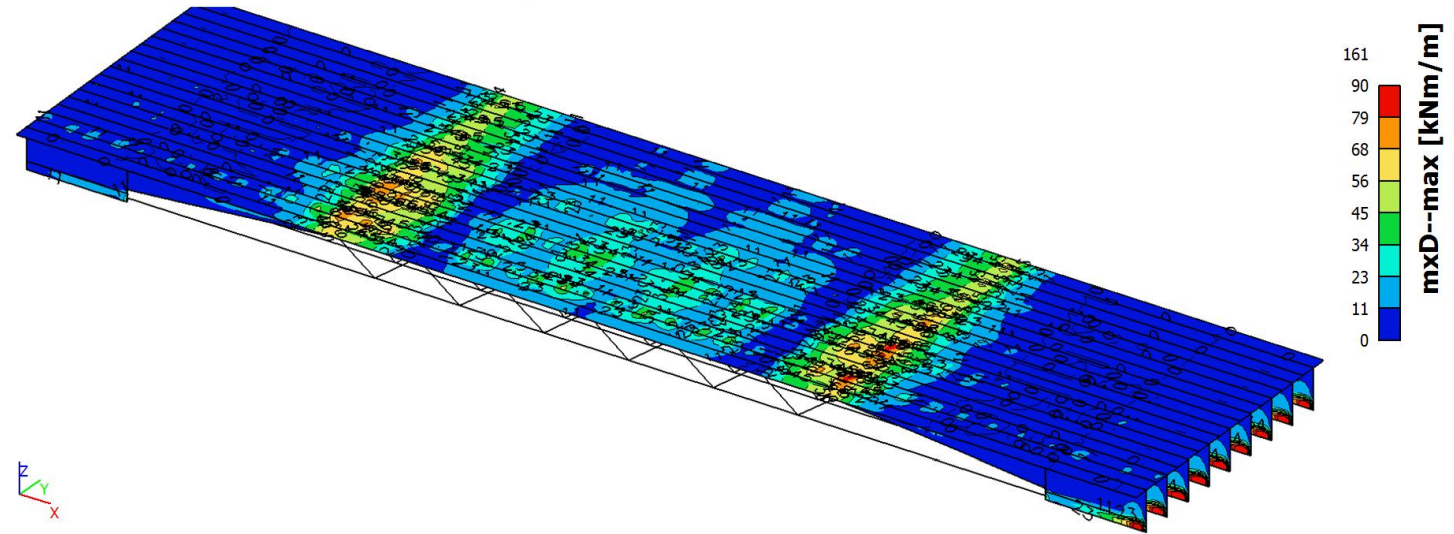
19. 2D member - Internal forces; $mxD+$



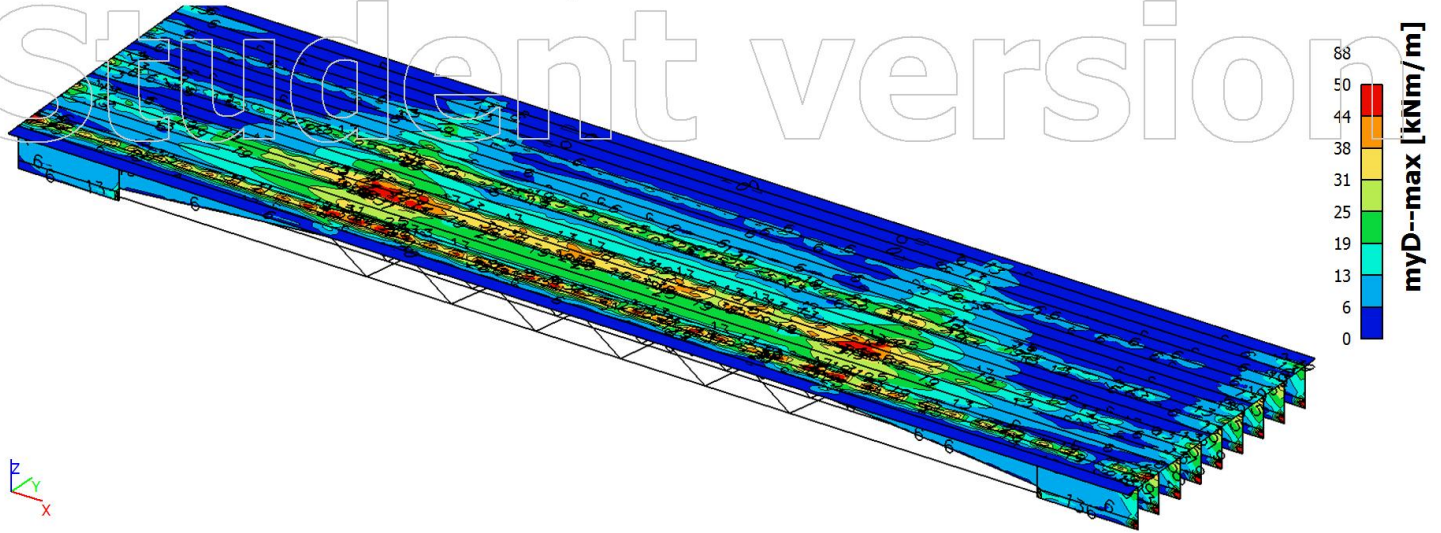
20. 2D member - Internal forces; $myD+$



21. 2D member - Internal forces; $mxD-$



22. 2D member - Internal forces; myD-



Student version

Student version